Characterization of Human Papillomavirus (HPV) Type 16 Capsid-Cell Interactions During Viral Cell Entry

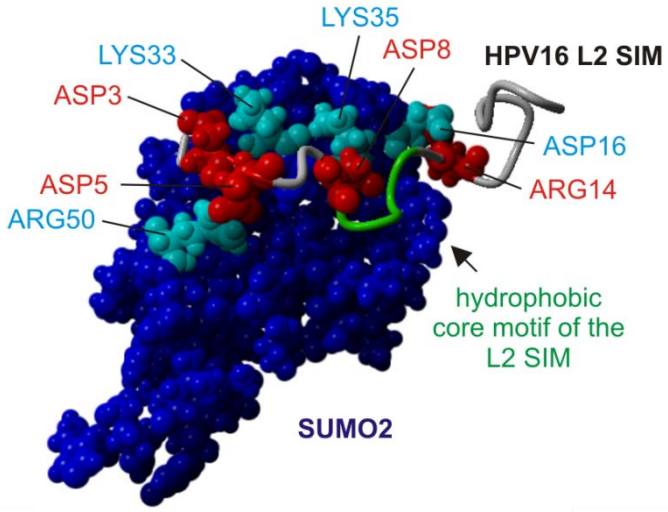

Timo Bund

Max Planck Graduate Center
mit der Johannes Gutenberg-Universität Mainz

Characterization of Human Papillomavirus (HPV) Type 16 Capsid-Cell Interactions During Viral Cell Entry

Timo Bund

Characterization of Human Papillomavirus (HPV) Type 16 Capsid-Cell Interactions During Viral Cell Entry

Timo Bund

Dissertation for the German

Doktor der Naturwissenschaften

Max Planck Graduate Center (MPGC)

Johannes Gutenberg University Mainz

Mainz, Germany, September 2012

Dipl. Biol. Timo Bund

Max Planck Institute for Polymer Research
Ackermannweg 10
55128 Mainz, Germany

bund@mpip-mainz.mpg.de

Der Mensch hat dreierlei Wege klug zu handeln:

durch Nachdenken ist der edelste,

durch Nachahmen der einfachste,

durch Erfahrung der bitterste.

Konfuzius

This work was supported by the Max Planck Graduate Center (MPGC) in cooperation with the Johannes Gutenberg Universität Mainz. Experimental work was performed at the Institute for Medical Microbiology and Hygiene in the workgroup of Dr. Luise Florin under supervision of Dr. Luise Florin and Dr. Gilles Spoden and at the Max Planck Institute for Polymer Research in the workgroup of Prof. Hans Wolfgang Spiess under supervision of PD Dr. Dariush Hinderberger.

Dekan: Prof. Dr. Hans Zischler

1. Proof-Reader: PD Dr. Dariush Hinderberger

2. Proof-Reader: Prof. Dr. Harald Paulsen

3. Proof-Reader: Dr. rer. nat. med. habil. Carsten Lambert

Mainz, September 2012

Max Planck Institute for Polymer Research
Ackermannweg 10
D-55128 Mainz

Contents

1 Introduction and scope of this work 1

1.1 Human papillomaviruses (HPV) 2

1.1.1 Historical review of HPV 2
1.1.2 HPV epidemiology 2
1.1.3 The HPV genome 3
1.1.4 HPV structure 4
1.1.5 The HPV life cycle 5
1.1.6 Virus binding & uptake, and nuclear transport of the viral DNA 7
1.1.7 Manifestation of the viral genome 9
1.1.8 Stimulation of the cell proliferation 10
1.1.9 The vegetative amplification of the genome 11
1.1.10 Viral morphogenesis and release 11
1.1.11 The HPV late protein L2 (HPV16 L2) 12

1.2 The cellular SUMO apparatus 15

1.2.1 SUMO conjugation 18
1.2.2 SUMO interaction 19
1.2.3 Targeting of the cellular SUMO apparatus by human pathogens 20

1.3 Electron Paramagnetic Resonance (EPR) Spectroscopy 23

1.3.1 The history of EPR 23
1.3.2 EPR radicals and site-directed spin labeling (SDSL) 23
1.3.3 EPR spectroscopic methods and their information content 25
1.3.3.1 Continuous wave (CW) EPR 27
1.3.3.2 The electron spin echo (ESE)-detected EPR experiment 28
1.3.3.3 Nanoscale distance measurements with DEER 29

1.4 Motivation and aim 32

2 Materials and methods 33

2.1 Materials 33

2.1.1 Laboratory equipment 33
2.1.2 Chemicals 35
2.1.3 Ready-to-use reagents and kit systems 35
2.1.4 Antibodies 36
2.1.4.1 Primary antibodies 36
2.1.4.2 Secondary antibodies 36
2.1.5 Standard buffers and solutions 37
2.1.6 Enzymes 39

2.1.7 DNA plasmids 39
2.1.7.1 DNA plasmids for L2 and SUMO1/2 protein expression and purification 39
2.1.7.2 DNA plasmids for mammalian 2-hybrid interaction assays 40
2.1.7.3 DNA plasmids for further L2 and SUMO1/2 characterizations 41
2.1.7.4 DNA plasmids for preparation of HPV16 pseudoviruses (PsVs) 41
2.1.8 PCR primers, DNA oligonucleotides, siRNAs 42
2.1.9 Synthetic L2 peptides 43
2.1.10 Cell strains, cultures, and additives 43
2.1.10.1 Mammalian tissue cultures 43
2.1.10.2 Bacteria culture 43
2.1.11 Molecular weight markers 45

2.2 Methods 46

2.2.1 Working with DNA 46
2.2.1.1 Fragmentation of DNA with restriction endonucleases 46
2.2.1.2 Isolation of DNA fragments by agarose gel electrophoresis 46
2.2.1.3 Preparation of DNA from agarose gels 46
2.2.1.4 Ligation of DNA fragments 47
2.2.1.5 Transformation of competent *E. coli* cells 47
2.2.1.6 Plating of *E. coli* cells on LB agar plates 47
2.2.1.7 Preparation of starter bacteria cultures 47
2.2.1.8 Plasmid DNA preparation 48
2.2.1.9 Standard polymerase chain reaction (PCR) 48
2.2.1.10 Mutagenesis PCR 49
2.2.2 Cultivation of human adherent cells 50
2.2.2.1 Cultivation of cell lines 50
2.2.2.2 Cell counting using the Neubauer chamber 50
2.2.2.3 Cultivation of new cells 50
2.2.2.4 Preparation of frozen cell aliquots 51
2.2.2.5 DNA transfection 51
2.2.2.6 siRNA transfection 51
2.2.2.7 Cell harvest 52
2.2.3 Cultivation of *Leishmania tarentolae* 52
2.2.3.1 Cultivation of *Leishmania tarentolae* cell lines 52
2.2.3.2 Cultivation of new cells 53
2.2.3.3 Preparation of frozen cell aliquots 53
2.2.3.4 Transformation of the T7-TR host 54
2.2.3.5 Selection of transgenic LEXSY T7-TR strains 54
2.2.3.6 Expression of recombinant protein 55
2.2.4 Expression of GST or his fusion proteins in *E. coli* 56
2.2.5 Proteinbiochemical methods 56
2.2.5.1 Protein solubilization assay 56
2.2.5.2 Native affinity purification of SUMO1/2-his_6 57
2.2.5.3 Denaturing affinity purification of HPV16 L2 expressed in *L. tarentolae* 57
2.2.5.4 Denaturing affinity purification of HPV16 L2 expressed in human cell lines 57
2.2.5.5 Bradford assay 58
2.2.5.6 SDS PAGE 58
2.2.5.7 Protein staining 59
2.2.5.8 Transfer Blot 60
2.2.5.9 Ponceau S staining 61
2.2.5.10 Immunodetection 61
2.2.5.11 Stripping of blot membranes 62
2.2.5.12 Spin labeling of proteins for EPR measurements 62

2.2.5.13 Fluorescence labeling of the HPV16 L2 SIM peptide 64
2.2.5.14 Characterization of SH group labeling efficiency with the Ellman's reaction 64
2.2.6 Molecular biological methods 65
2.2.6.1 Immunoprecipitation 65
2.2.6.2 SUMO1/2-his$_6$ Pulldown 66
2.2.6.3 SUMO1/2-GST Pulldown 68
2.2.6.4 Ubiquitin pulldown 70
2.2.6.5 Mammalian 2-hybrid assay 70
2.2.7 Virological methods 71
2.2.7.1 Preparation of HPV16 L1/L2 PsVs 71
2.2.7.2 DNA quantification of PsVs based on picoGreen 72
2.2.7.3 Reporter gene assay 72
2.2.7.4 Lactate dehydrogenase (LDH) cytotoxicity assay 73
2.2.7.5 Characterization of PsVs by sucrose gradient ultra centrifugation 74
2.2.7.6 Flow cytometry 75
2.2.7.7 Preparation of HPV16 PsVs for cell binding assays based on CW EPR 76
2.2.8 Microscopic methods 76
2.2.8.1 Immunofluorescence microscopy 76
2.2.8.2 Antibody staining 77
2.2.8.3 EdU staining of PsVs after infection 77
2.2.8.4 Microscopic documentation 78
2.2.9 Biophysical methods 78
2.2.9.1 Electron paramagnetic resonance (EPR) spectroscopy 78
2.2.9.2 Fluorescence Correlation spectroscopy (FCS) 80
2.2.9.3 Fluorescence spectroscopy 81
2.2.9.4 Circular dichroism spectroscopy 82
2.2.9.5 Isothermal titration calorimetry (ITC) 82
2.2.9.6 Molecular dynamics simulation 83

3 Results 84

3.1 Characterization of the interaction of HPV16 L2 with SUMO proteins 85

3.1.1 The HPV16 L2 protein sequence comprises multiple SIMs 85
3.1.2 Three potential SIMs within the L2 protein are conserved for high risk HPVs 86
3.1.3 L2 interacts with SUMO2 in immunoprecipitation 87
3.1.4 L2 lacking the SIM does not interact with SUMO2 88
3.1.5 Wild-type L2 colocalizes with GFP-SUMO1/2 in PML NBs 92
3.1.6 No colocalization of L2 ΔSIM with SUMO1/2 or PML 92
3.1.7 L2 wt and L2 ΔSCM are stabilized by SUMO1/2 after coexpression in HeLa cells 94
3.1.8 No Interaction of L2 and SUMO1/2 in GST-SUMO or SUMO-His pulldowns 95
3.1.9 No interaction of L2 and SUMO in Mammalian-2-Hybrid screening 96
3.1.10 The L2 SIM is also important for ubiquitin interaction of HPV16 L2 97

3.2 Structural and functional analysis of L1/L2 ΔSIM PsVs 98

3.2.1 HPV16 L1/L2 ΔSIM PsVs are noninfectious 98
3.2.2 Correct assembly of L1/L2 ΔSIM PsVs 99
3.2.3 L1/L2 ΔSIM PsVs show a wild-type phenotype in electron microscopy 100
3.2.4 L1/L2 ΔSIM PsVs bind to HeLa and HaCaT cells and are endocytosed 101
3.2.5 No PML-colocalization of DNA or L2 after infection with L1/L2 ΔSIM PsVs 105
3.2.6 No destabilization of L2 after infection with L1/L2 ΔSIM PsVs 107
3.2.7 Overexpression of wild type L2 does not recover infectivity of L1/L2 ΔSIM PsVs 108
3.2.8 Overexpression of GFP-SUMO1/2 enhances infectivity of HPV16 PsVs 109
3.2.9 SUMO2 siRNA knockdown strongly increases infectivity of HPV16 PsVs 109

3.3 Biophysical interaction studies of HPV16 L2 with SUMO1/2 113

3.3.1 Purification of SUMO1/2 protein by native his tag affinity purification....113
3.3.2 Denaturing purification of HPV16 L2 114
3.3.2.1 Full-length and soluble L2 protein after expression in HEK293 cells....114
3.3.2.2 High yield L2 purification under denaturing conditions 118
3.3.2.3 Characterization of affinity purified HPV16 L2 protein 120
3.3.3 Noncovalent interaction of L2 and SUMO1/2 characterized by EPR....123
3.3.3.1 Highly efficient spin labeling of purified SUMO1/2 124
3.3.3.2 SL-SUMO2 seems to self-arrange in SUMO oligomers 125
3.3.3.3 HPV16 L2 interacts with SL-SUMO1/2 126
3.3.3.4 The interaction of L2 with SUMO1/2 is diminished by L2 antibodies 130
3.3.3.5 The L2 labeling positions C22 and C28 are inaccessible for spin labeling 131
3.3.4 No interaction of HPV16 L2 SIM peptides with SUMO1/2 in EPR 133
3.3.5 Interaction of HPV16 L2 SIM peptides with SUMO1/2 in FCS 138
3.3.6 No L2 interaction with SUMO1/2 in isothermal titration calorimetry 139
3.3.7 The L2 SIM peptide attaches to SUMO1 and SUMO2 in MD simulations 140

4 Discussion 143

4.1 Covalent SUMOylation has no effect on assembly and infectivity of L1/L2 PsVs....144
4.2 Two highly conserved SUMO interaction motifs (SIMs) in HPV16 L2....146
4.3 L2 directly interacts with SUMO1/2 proteins 147
4.4 The L2 SIM is crucial for L2 interaction with SUMO proteins 149
4.5 Flanking sequences around the L2 SIM trigger SUMO interaction of L2....150
4.6 The putative L2-SUMO interaction complex based on MD simulation 151
4.7 The challenge of L2 purification and refolding 153
4.8 L1/L2 ΔSIM PsVs are noninfectious despite correct assembly of the L1/L2 capsid....154
4.9 The L2 SIM is not involved in the early steps of HPV16 infection 155
4.10 No PML-colocalization of L2 or viral DNA after infection with L1/L2 ΔSIM PsVs 158
4.11 The L2 SIM at position 284-289 is not regulated by CK2 phosphorylation....159
4.12 SUMO siRNA knockdown affects HPV16 infectivity....160
4.13 Tentative model for regulation of the intrinsic antiviral resistance by HPV16 L2 161

5 Conclusions 166

· **Acknowledgements 168**

· **References 170**

· **List of Abbreviations and Symbols 187**

· **Conferences and Meetings 194**

· **Publications 195**

· **Curriculum Vitae 196**

· **Declaration 199**

1. Introduction and scope of this work

More than 50% of all sexually active adults, both men and women, have come in contact with human papillomaviruses (HPV). In most cases, the viral infection is normally not noticed by the respective person, as it is blocked by the immune system. In some cases, though, malignancies like cervix carcinoma, which represents the most prevalent HPV-based tumor disease, or more unique tumor diseases are evoked. Within the last years, a vaccination against HPV was established, based on seminal efforts in HPV research, which culminated in October 2008, when Harald zur Hausen was awarded with the Nobel Prize for medicine or physiology for elucidating the connection between HPV infection and HPV induced cancer. In this context, the following chapters first describe the onset of HPV research, followed by a detailed characterization of HPVs and infection with HPVs, especially highlighting the high-risk type HPV 16. Then, the focus will be on the HPV16 L2 protein (L=late), one of the two viral capsid proteins of HPV16, and its various eminent interactions with the host cell during viral infection. In this study, small ubiquitin-like modifiers (SUMOs) were identified as important L2 interaction partners. SUMO proteins are ubiquitously and constitutively expressed and establish the very complex host cell SUMO apparatus also involved in viral defense. The SUMO apparatus itself is represented by a smaller pool of free SUMO proteins and a large pool of SUMO monomers or SUMO chains that are covalently or noncovalently linked with multiple SUMO targets, thereby administrating fundamental cellular regulation mechanisms, as will be depicted in detail. Finally, an introduction will be given into the broad range of experiments and experimental techniques, which are used in this thesis for the characterization of the interaction of HPV16 L2 with SUMO.

1.1 Human papillomaviruses (HPV)

1.1.1 Historical review of HPV

The general phenotype of an infection with papillomaviruses (PVs) has been described already 2000 years ago. Nevertheless, the finding that the observed, mostly benign, warts on the skin (papillomas) or mucosa (condylomas) were connected to an infection with viruses was made not until the early 1930s. At that time, it was found that filtered extracts prepared from warts of rabbits, were able to induce lesions on the dermis of other rabbits and that the cottontail rabbit papillomavirus (CRPV) was even carcinogenic for some rabbits (Shope and Hurst 1933). For humans, a connection of viruses with skin and genital warts was first proven in 1949 (skin warts) and 1968 (genital warts), when virus particles were detected by electron microscopy within extracts from the respective tissues. The first molecular biological detection of viral DNAs succeeded in 1977, when DNA stemming from bovine papillomaviruses (BPV) was found in cancer tissue of horses (Lancaster, Olson et al. 1977). Four years later, the first PV-DNA was isolated (de Villiers, Gissmann et al. 1981). The first completely sequenced genome was that of the bovine papilloma virus type 1 (BPV1)(Chen 1982). Within the next years, also the DNAs of HPV types 1, 6, 16, and 18 were sequenced (Danos, Katinka et al. 1982; Dürst, Gissmann et al. 1983; Schwarz, Dürst et al. 1983; Boshart, Gissmann et al. 1984). In radio-labeling experiments based on viral DNA, it was found that most genital carcinomas contained PV-DNA manifesting the close connection of cervix carcinomas and infection with PVs, which contribute to about 99.8% of all cervix carcinomas (Walboomers and Snijders 1999). The HPV types 16 and 18 share a very high prevalence in about 70% of all cervix carcinomas and were therefore classified as high-risk HPV types. They are part of a HPV family, which, nowadays, comprises more than 180 different high- and low-risk HPV types (de Villiers 2004; Calleja-Macias, Kalantari et al. 2005; Bernard 2010). They are found in most mammalians and birds and share an extraordinary specificity concerning the target tissue within their hosts. 90% of the known HPVs are classified as α- or β-papillomaviruses. The rest is characterized as γ-, μ-, or ν-papillomaviruses, which mostly cause cutaneous papillomas or benign condylomas most frequently associated with HPV6 and HPV70 (de Villiers 2004; Nielsen, Iftner et al. 2012).

1.1.2 HPV epidemiology

The infection with HPV is normally not accessible for clinical observation, since, in most cases, the concerning individuals are not aware of the HPV infection. Only sometimes, cutaneous papillomas, or benign condylomas are observed, which heal after several months or years. Thus, HPVs are most often associated with warts on skin and mucosa, but also cervix, penis, or pharynx carcinomas. As

indicated before, the prevalence of a HPV infection of a sexually active adult is remarkably high (60%) (Eckert, Watts et al. 1999; Ho 2002; Cutts, Franceschi et al. 2007). It is even more remarkable that 17.8 % of the 1.9 million cancer incidents worldwide, in 2002, were based on an infectious disease containing a fraction of even 5.2%, which were directly associated to HPV (Parkin 2006). In general, the HPV prevalence is very high in developing countries in Africa and Southeast Asia (83%) (Akogbe, Ajidahun et al. 2012). Based on fundamental efforts in development of vaccines against HPV, since 2006, two commercial vaccines are available. Cervarix™ (GlaxoSmithKline) is a bivalent vaccine targeting the two most relevant HPV high-risk types 16 and 18, which also contains an adjuvant. The tetravalent vaccine Gardasil® (Merck) targets HPV 16 and 18 as well, but additionally, also the low risk types 6 and 11, which are responsible for the majority of cutaneous papillomas. Both vaccines recognize surface loops of the HPV L1 capsid protein in a very HPV type-specific manner and thereby effectively block the HPV infection pathway. The two vaccines provide a long-term and almost 100% protection against infection with HPV16 and 18 (Einstein 2009; Etter, Zimet et al. 2012).

1.1.3 The HPV genome

The HPV genome is represented by a circular, double-stranded DNA with a size of between7,400 and 8,200 base pairs depending on the respective HPV type. In the viruses, the genome is organized together with cellular histones and forms a chromatin-like structure (Howley 2007). The DNA codes for eight viral gene products (Fig. 1.1).

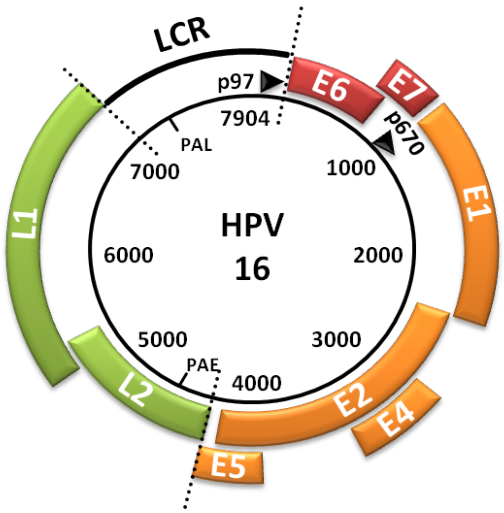

Fig. 1.1: The HPV16 genome. The double stranded, circular HPV16 genome comprises 7904 base pairs and is sub-divided into three major parts, *i*) the long control region (LCR) containing several control elements, *ii*) the early region, and *iii*) the late region. The early region contains the early genes controlled by the early promoter p97 (E6 and E7) or the p670 promoter (E1, E2, E4, E5). The late genes L1 and L2 within the late region are regulated by the p670 promoter. Two different polyadenylation signals are used during transcription: the polyadenylation signal for the early genes, PAE, and the polyadenylation signal for the late genes, PAL. Figure according to Doorbar 2006.

The respective genes are found on all three reading frames. Depending on the function of the respective part of the DNA, the genome is divided into three segments, *i*) the non-coding control region (LCR) with the origin of replication (1 kB), *ii*) the early region (4 kb), *iii*) the late region, which codes for the structure proteins L1 and L2, which build up the viral capsid (L = late, 3kb). The early region comprises the early genes, which encode proteins triggering the amplification of the viral genome and viral expression of genes (E1 and E2), as well as transformation (E6, E7). These proteins are classified as E proteins (E= early) and comprise the proteins E1, E2, E4, E5, E6, and E7. Expression of E6 and E7 is under control of an early promoter (p97 for HPV16), which is constitutively active in non-differentiated suprabasal cells (Hummel, Hudson et al. 1992). The promoter element is part of the LCR region, which is located between the poly-adenylation signal of the late gene L1 and the early gene E6 and regulated by several cellular transcription factors (Sichero, Sobrinho et al. 2012). The expression of the late genes L1 and L2 is regulated by a late promoter element (p670 for HPV16), which is not located within the LCR and activated by differentiation of the keratinocytes. The same promoter element also regulates the transcription of E1, E2, E4, and E5 (Grassmann, Rapp et al. 1996). More recent studies report the existence of two additional promoters for regulation of late genes, one is located 157 nucleotides upstream of P_{97} and the other one in the E5 open reading frame (Milligan, Veerapraditsin et al. 2007). For the late transcription, a total number of 13 mRNAs divided into two pools of late mRNA transcripts was identified. One population of transcripts contains L1 alone, while the other one contains L1 and L2. Alternative splicing leads to the possible expression of four additional late proteins (E6*^*E7, E1^E2C, E6*^E4, and E1^*E4)(Milligan, Veerapraditsin et al. 2007).

1.1.4 HPV structure

Papillomaviruses represent non-enveloped DNA viruses with a diameter of about 52-55 nm. The viral capsid comprises about 360 copies of the major capsid protein L1 and 12-72 copies of the minor capsid protein L2 (Fig. 1.2) (Buck, Cheng et al. 2008).

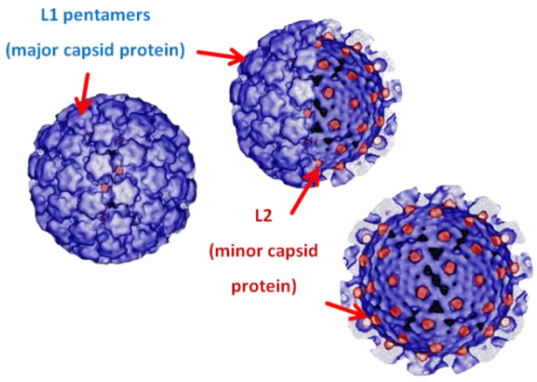

Fig.1.2: 3D-reconstruction of HPV16 capsids. The picture shows single particle 3D-reconstructions of HPV16 capsids assembled from viral L1 (blue) and L2 proteins (red). L1 is arranged in pentamers forming the viral capsomers. The L2 molecules are located beneath the capsomers as shown in the detailed view of the capsid shell on the right (Figure according to Buck et al., 2008; with friendly permission of Benes Trus).

Thereby, five L1 monomers are arranged within homopentamers to build up a L1 capsomer. Up to 72 capsomeres are assembled based on an icosahedral symmetry (triangulation number = 7) to establish the full capsid of the virus (Baker, Newcomb et al. 1991; Belnap and Christensen 1996). Finally, the capsid comprises 12 pentavalent and 60 hexavalent capsomers, meaning that the respective capsomers are located within five or six neighboring capsomers. The L1 protein and, most interestingly, also L1 deletion mutants lacking the first 29 amino acids, feature a very strong tendency for spontaneous formation of capsids (Paintsil 1996; Schäfer 2002). Stabilization of the capsomers is achieved by the formation of intercapsomeric disulfide bridges between neighboring capsomers (Sapp, Fligge et al. 1998; Day 2009; Sapp and Bienkowska-Haba 2009). The L2 molecules are located directly beneath the geometrical center of the L1 pentamers. The interaction of L2 with the L1 capsomers (no interaction of L2 with L1 monomers) is reported to be of noncovalent nature and based on a well-characterized hydrophobic C-terminal L1 binding domain of L2 and an additional L1 binding domain at the N-terminus of the L2 sequence (Volpers 1995; Okun, Day et al. 2001; Finnen, Erickson et al. 2003). L2 incorporation enhances the formation of infectious viruses. In addition, it is discussed whether an L2 network is established within the viral capsid. Direct hints for a L2 network came from fluorescence studies, in which an intermolecular interaction of neighboring L2 N- and C-termini was proposed (Buck, Cheng et al. 2008).

1.1.5 The HPV life cycle

In order to reproduce themselves, viruses established a manifold of interaction and regulation mechanism to take benefit from the host cell. For correct reproduction, the viruses are obliged to infect the virus host, which allows for replication of the viral genome by the cellular replication machinery and for the survival of the virus. A simplified overview of the HPV life cycle is given in **Figure 1.3**.

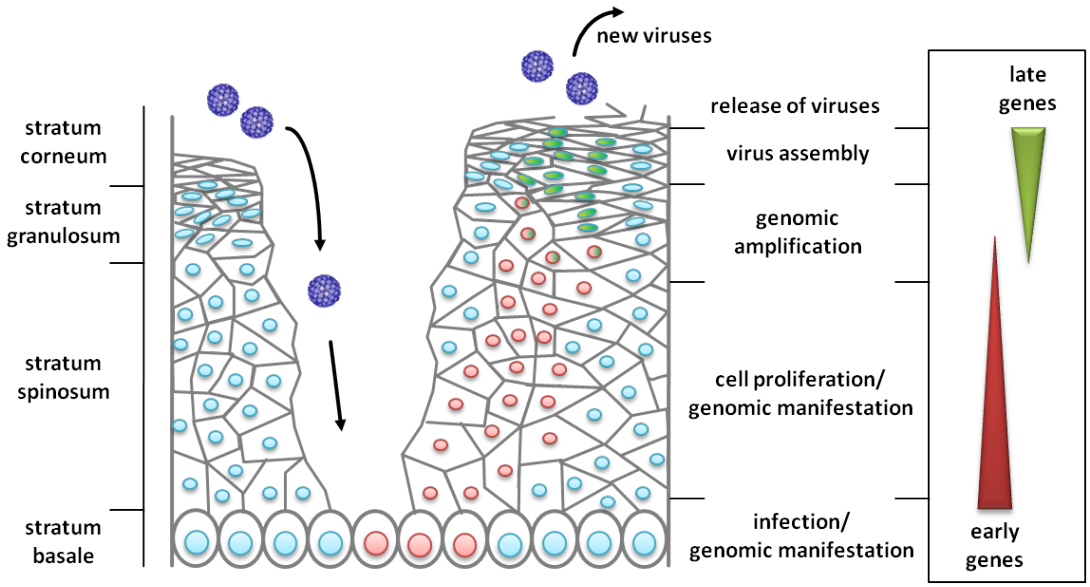

Fig. 1.3: The general infection pathway of HPVs. The HPV replication cycle after infection of epithelial basal cells is schematically illustrated for the respective cell layers. For each step, the characteristic main aspects are highlighted including an overview of viral gene expression. After infection of the epithelial basal cells via microlesions, the viral genome is manifested within the nuclei of the host cells and amplified as episomes. Expression of the early genes E6 and E7 induces the differentiation of the keratinocytes. Then, increased activation of the late promoter results in expression of E1, E2, E4, and E5, which results in enhanced amplification of the viral genome in cells of the late suprabasal layer (stratum spinosum) and granular layer (stratum granulosum). In the top-most layers, the late proteins L1 and L2 are expressed, and, together with viral DNA, assembled into new viral capsids. The mature viruses are finally released by desquamation of the host cells in the stratum corneum.

After infection of basal epithelia cells from skin or mucosa of the host, the replication cycle of the papillomaviruses is closely correlated to the differentiation of the epithelia cells, which are steadily regenerated from basal cells located on top of the basal membrane (Stanley 2012). The differentiation is triggered by several cellular transcription factors, which target the regulation of the early promoter, like e.g. AP-1 proteins, POU-domain proteins, NF-κB proteins, and CCAAT/enhancer binding proteins (Eckert 1997; Ryan 1997; Seitz, Lin et al. 1998; Maytin 1999; Thierry 2009). The viral genome is consecutively replicated to a number of about 20-100 copies per infected basal cell by expression of E1 and E2 (Lambert 1991; Stubenrauch 1999). Meanwhile, the cells are pushed further and form the suprabasal layer (stratum spinosum) and differentiate. This step is mainly driven by expression of E6 and E7 and leads to an enhanced formation of new tissue and therefore also to enhanced productive infection (Stubenrauch 1999). Then, activation of the late promoter induces the expression of the capsid proteins L1 and L2 together with E4. L1 and L2 reach maximum expression levels within the granular layer. Here, the cells partially lose their nuclei and develop a flattened shape. L1 and L2 are assembled into new viral capsids, which are loaded with viral DNA. The new viruses are released during desquamation of the host cells in the stratum corneum (Meyers 1992; Flores 1999).

1.1.6 Virus binding & uptake, and nuclear transport of the viral DNA

The papillomaviruses enter the host organism via micro lesions. At the level of the basal membrane or basal cells, the PVs first bind to a primary receptor molecule, which is represented by heparan sulfate proteoglycans (HSPGs, Fig. 1.4)(Volpers 1995; Joyce 1999; Giroglou, Florin et al. 2001; Culp 2004; Selinka 2007; Johnson 2009; Kines 2009; Broutian 2010; Schiller 2010). HSPGs represent matrix glycans, which are localized in the extracellular matrix (ECM) and on the cell surface of mammalian cells. The high abundance of HSPGs expressed by different host cell tissues can in some cases also result in a primary binding of PVs to non-keratinocytes (Roden, Kirnbauer et al. 1994; Müller, Gissmann et al. 1995; Tiwari, Maus et al. 2012). HSPGs generally function as a kind of cell glue and facilitate internalization of cell-bound ligands (Lindahl 1998). PVs interact with the negatively charged HSPGs via ionic interactions based on positively charged lysine residues of the L1 capsid protein (Knappe 2007; Dasgupta 2011), which can be blocked by incubation with polyanionic or polycationic molecules (Giroglou, Florin et al. 2001; Buck 2006; Selinka 2007; Spoden 2011). As for HPV16, the presence of an additional, non-HSPG binding moiety on the ECM, most likely laminin 332, was reported, since HPV16 binding was not completely inhibited by heparin or enzymatic removal of haparan sulfates (Selinka 2007; Bienkowska-Haba, Williams et al. 2012). The primary binding of the capsid to the HSPGs leads to a conformation change of L1 within the capsids (Selinka 2003; Day 2008b). Then, a conformation change of L2 is induced by the host cell chaperone cyclophilin B (CyPB) and allows for a transfer of the PV to a secondary receptor (Selinka 2003; Schelhaas 2008; Day 2008a; Day 2008b; Bienkowska-Haba, Williams et al. 2012). Recent results show that, during the transfer, the viral particles reside in high molecular weight complexes with HSPGs, including syndecan-1, and bioactive compounds like growth factors (Surviladze, Dziduszko et al. 2012). The nature of the secondary receptor is still under debate. One candidate, α6-integrin, was presented already in 1997 for HPV6 (Evander, Frazer et al. 1997; Culp, Budgeon et al. 2006), but is not necessary for infection of HPV11 and HPV33 (Giroglou, Florin et al. 2001; Shafti-Keramat, Handisurya et al. 2003). Remarkably, a colocalization of HPV16 was observed with tetraspanins (Spoden, Freitag et al. 2008), which drift on cell membranes as compact raft structures forming tetraspanin-enriched micro domains (TEMs) (Sterk 2000; Odintsova 2003; André 2006; Lazo 2007; Spoden, Freitag et al. 2008; Yang 2008). The TEMs allow for binding of HPVs even after very short infection times (<10 min), as was seen in colocalization with the tetraspanins CD63 and CD151 (Spoden, Freitag et al. 2008). Then, the HPVs are internalized via endocytosis (Selinka 2002), which functionally depends on the tetraspanin CD151 for HPV16 (Spoden, Freitag et al. 2008). Since preparation of virus-like particles (VLPs, composed of L1 and L2, no DNA), and pseudoviruses (PsVs, containing reporter DNA) was established, new insights into the binding of the viruses to host cells were achieved. Thus, L2 does not seem to be crucial for viral binding and uptake, although the L2 protein is able to bind to the cell surface and is taken up by

the host cell (Kawana, Kawana et al. 2001; Yang, Day et al. 2003a). It is also known that during cell binding of the viruses, L2 undergoes a cleavage step by furin (or PACE, for Paired basic Amino acid Cleaving Enzyme) recognizing a basic amino acid target sequence of L2 (Arg-X-(Arg/Lys) -Arg'), which gets accessible after binding to HSPGs (Richards, Lowy et al. 2006; Day 2009). Endocytosis of HPV16 viruses does not depend on clathrin, caveolin, or dynamin and may occur via a so far uncharacterized endocytotic pathway supported by tetraspanins and actin (Spoden, Freitag et al. 2008; Schelhaas, Shah et al. 2012). After the disruption of the capsids in the acidified late endosomes (Selinka 2002; Smith 2008b; Schelhaas, Shah et al. 2012), L1 is dissociated from a complex of L2 and the viral DNA by cyclophilins (Bienkowska-Haba, Williams et al. 2012). L2 partly penetrates into the endosomal membrane via its C-terminal transmembrane domain probably enabling interaction with cytoplasmic proteins. L2 interaction with sorting nexin 17, syntaxin 18, and the intramembranous cleaving γ-secretase are putative factors involved in the release of a complex of L2 and the viral DNA into the cytoplasm (Day 2004; Bossis 2005; Kämper, Day et al. 2006; Karanam 2010; Marusic, Ozbun et al. 2012). This step is additionally regulated by protein disulfide isomerases (PDIs). PDIs catalyze the reduction/oxidation and isomerization of disulfide bonds highlighting the role of the two conserved N-terminal cysteines within L2, which are able to form an intramolecular disulfide bond (Campos and Ozbun 2009; Conway 2009; Gambhira 2009). Inhibition of PDIs by bacitracin had no effect on cellular binding and uptake of viruses or lysosomal trafficking, but inhibited the accumulation of the viral DNA at the PML-NBs (Campos, Chapman et al. 2012). In the cytoplasm, the complex of L2 and viral DNA is further transported to the periphery of the nucleus via the motor protein dynein (Florin, Becker et al. 2006; Schneider 2011). Then, the L2-DNA complex is released from the dynein transport complex and transported to the PML NBs, where induction of viral protein expression leads to a very complex reorganization of nuclear structures (Day 1998; Florin 2002b; Day 2004; Jiang and Imperiale 2012).

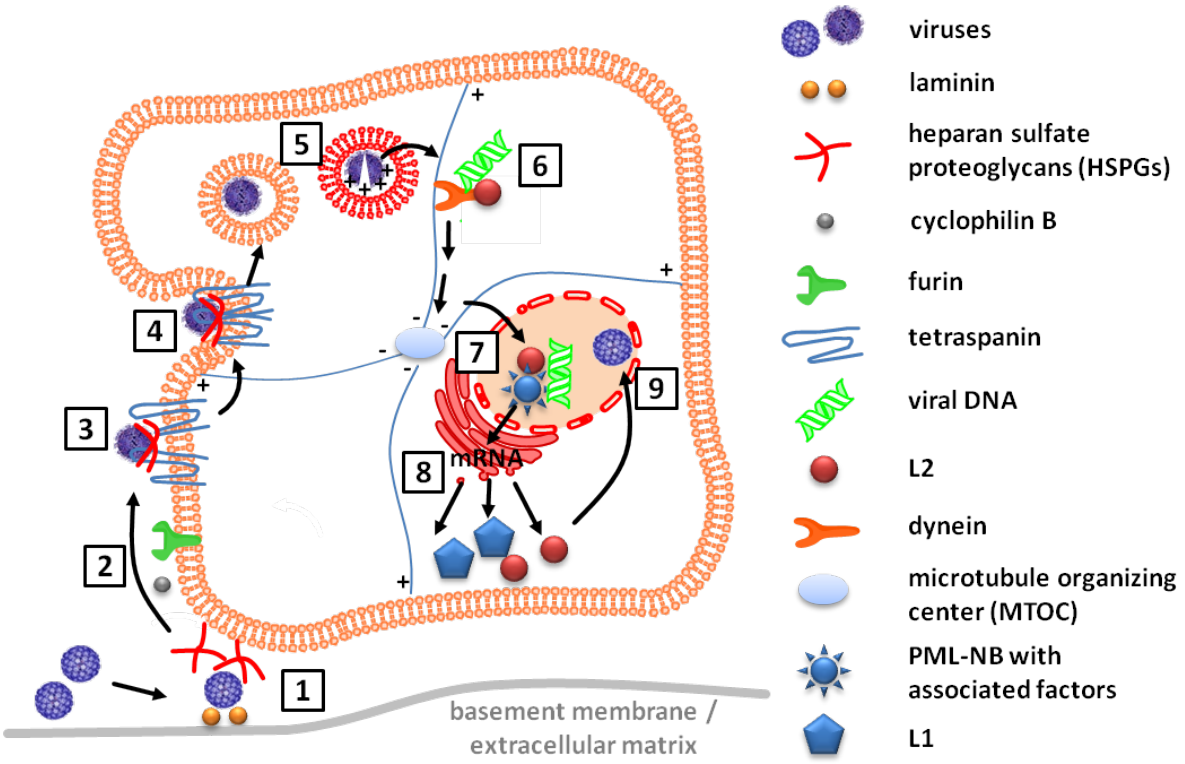

Fig. 1.4: The HPV life cycle. ***1*** The viruses bind to the primary receptor heparan sulfate proteoglycans (HSPGs) of the target cell and laminin 322. ***2*** After a structural rearrangement of L1 by binding to HSPGs, L2 interacts with cyclophilin B, which induces a conformation change of L2 and enables the N-terminus of L2 to be processed by furin. ***3*** The viruses attach to tetraspanin-enriched microdomains (TEMs) representing the secondary receptor. ***4*** Clathrin- and caveolin-independent endocytosis. ***5*** Disassembly of the viral capsids in the acidified late endosomes. A complex of L2 and viral DNA escapes the endosome by interaction with sorting nexin 17, PDIs, γ-secretase, and syntaxin 18. ***6*** The L2-DNA complex interacts with the dynein subunits DYNLT1 and DYNLT3 and is transported to the micrutubuli organizing center (MTOC) near the periphery of the nucleus. ***7*** The L2-DNA complex is released from the dynein transport complex, transported into the nucleus, and accumulates at the PML-NBs. ***8*** During papillomavirus morphogenesis, the late proteins L1 and L2 are expressed upon increased transcription of viral late mRNAs. ***9*** L2 and L1 pentamers are independently transported into the nucleus and assembled into new capsids containing viral DNA. The mature viruses are released from the nucleus by cellular breakdown during desquamination of the host cell.

1.1.7 Manifestation of the viral genome

After the viral DNA is imported into the nucleus, the expression of E1 and E2 triggers the replication and transcription of the viral genome (Chiang, Ustav et al. 1992). E2 plays a key role as viral transcription regulator, which, depending on the HPV type, interacts with various target proteins in the host cell (Muller, Jacob et al. 2012). E2 recognizes four palindromic motifs in the non-coding region of the PV genome (Dell 2003). For low expression levels of E2, only two of the motifs are used, while for high expression levels, all four binding motifs are occupied (Demeret 1998; Hines 1998). E2 dimers bind to the DNA and recruit the E1 protein to the origin of replication. E1 functions as replication initiator protein and binds to the DNA as a dimer recognizing an incomplete palindromic DNA motif via its N-terminal region (Demeret 1998). The origin of replication is located within 60-80 base pairs in the non-coding control region. Then, E2 detaches from the DNA and triggers unwinding of the superhelical DNA, while the recruited E1 proteins form a dihexameric ring structure (Chow

1994). The complex of E1 proteins is stabilized by the heat shock proteins HSP40 and HSP70 (Lee 1999). Finally, E1 associates with the cellular DNA-polymerase primase and the single-strand-DNA-binding protein A (RPA) to recruit the cellular replication machinery to the viral initiation complex (Park 1994; Loo and Melendy 2004). For high E2 expression levels, in a negative feedback regulation, the E2 binding to all four palindromic DNA motifs leads to the detachment of the basal transcription factors Sp1, TFIID, and TBP (TATA-box binding protein) and to a stop of replication (Steger and Corbach 1997). For low E2 expression levels, E2 also controls the expression of E6 and E7 by regulation of the early promoter p97 (Demeret 1998). In general, the replication of the viral genome is synchronized with the cellular replication cycle. Separation of the replicated viral DNAs into the daughter cells after mitosis is performed by anchoring of the viral episomes at the human chromosomes mediated by E2 (You 2004; McBride 2006). E2 also transactivates the SF2/ASF promoter, which is a key factor in the alternative splicing regulation and, thus, directly regulates cellular gene expression and/or expression of an RNA processing factor (Mole, Milligan et al. 2009).

1.1.8 Stimulation of the cell proliferation

The cell proliferation phase is characterized by a strong neoplastic growth of infected cells within the suprabasal layer induced by the expression of the viral proteins E6 and E7. In general, during infection, the viral genome is frequently integrated into the host genome at certain integration sites, which partially disrupt host genes (Schwarz 1985; Baker, Phelps et al. 1987; Schmitz, Driesch et al. 2012). Thereby, only the E6 and E7 genes remain fully functional, which causes increased expression levels of E6 and E7 (Kraus 2006). E6 and E7 inhibit the exit of the cell cycle, which leads to the thickening of the intermediary layer and to the formation of characteristic papillomas (zur Hausen 2000; Munger 2002).

In particular, E6, together with E6AP, binds to the tumor suppressor p53 and induces an ubiquitin dependent degradation of p53. This effects a deregulation of cell division and DNA repair, which are controlled by p53 (Scheffner 1990). As a consequence, the cell division is drastically upregulated and mutations within the DNA are passed on to daughter cells, which finally results in malignancy (Mantovani 1999; Mantovani 2001; Munger K 2006). E6 from high-risk PV types also delays the senescence of the cells based on activation of the catalytic subunit of telomerases (Klingelhutz 1996; Zhang, Tian et al. 2012). The oncogene E7 interacts with several target factors thereby inactivating proteins involved in cell growth (Yu and Munger 2012). This includes the tumor suppressor protein pRb and its relatives p107 and p130 (Zerfass, Schulze et al. 1995), but also cyclin E and A by E7 binding at the p21 and p27 promoter (Arroyo, Bagchi et al. 1993; McIntyre 1996), histone

deacetylases (Brehm 1999; Longworth 2005), components of the AP1 transcription complex (Antinore, Birrer et al. 1996), and the cycline-dependent kinase inhibitors p21 and p27 (Zerfass-Thome 1996; Funk 1997). Both, E6 and E7, comprise DNA binding domains (zinc finger domains) allowing direct regulation as transcription factors.

1.1.9 The vegetative amplification of the genome

For the final assembly of new virus particles, an adequate number of initial viral DNA is necessary for large-scale expression of the viral protein. This threshold level of viral DNA has not been reached at this state of the infection, since the viral genome was only replicated once per cell cycle. During vegetative amplification, the late promoter (p670 for HPV16) is activated allowing that the early proteins E1, E2, E4, and E5 are expressed without a negative feedback regulation based on the E2 expression level. Now, the replication of viral DNA is significantly increased. Thereby, again E1 and E2 trigger replication, while the transmembrane protein E5 localizes in the Golgi apparatus and the endoplasmatic reticulum and interacts with receptors of growth factors like EGF (Conrad, Bubb et al. 1993; Straight, Herman et al. 1995). E5 has several functions, like e.g. transformation of keratinocytes, stimulation of DNA-synthesis, inactivation of other oncogenes, and regulation of signaling pathways (Bouvard 1994; Gu 1995; Valle 1995; Chen 1996; Auvinen 1997; Ganguly 2012). Little is known about the function of E4, but this viral protein seems to be crucial for the viral infection cycle in general, and, in particular, for an arrest of the cell cycle in the G2 phase and therefore resembles an E7 antagonist (Davy, Jackson et al. 2005; Wilson, Fehrmann et al. 2005).

1.1.10 Viral morphogenesis and release

The last step, in which the viral cycle is linked with the host, is represented by the packaging of the viral DNA into the new assembled viral capsids in the cell nuclei of the now fully differentiated epithelia cells. After amplification of the viral genome, first, the expressed L2, and then L1, accumulate within the nuclei at ND-10 bodies (Florin 2002b; Becker, Florin et al. 2004). The regulation mechanism, switching from DNA replication to packaging of the DNA into viral capsids is triggered by specific processing of viral pre-mRNAs (Graham 2008; Schwartz 2008) but also by an E2-induced inhibition of early polyadenylation of late mRNAs resulting in transcripts including also the late genes L1 and L2 (Johansson, Somberg et al. 2012). The assembly of the viral capsids starts with the pentameric arrangement of L1 in the cytoplasm (Fig. 1.4). Then, the L1 pentamers are imported into the nucleus based on the interaction of the C-terminal nuclear localization sequence (NLS) of the L1 protein with the transport-receptor complex Kapα2/Kapβ1, which prevents a premature

cytoplasmic capsid assembly (Nelson 2002; Bird 2008). L2, which is independently imported into the nucleus in association with with Hsc70 (Florin 2004), detaches Sp100 from the nuclear bodies (ND-10) and recruits Daxx to the ND-10 (Florin, Sapp et al. 2002a; Florin 2002b; Becker, Florin et al. 2004). At the ND-10, the viral capsids are assembled and packed with viral DNA. For this step, the C-terminal region of L1 is essential (Schäfer 2002). E2 triggers the transport of the viral DNA towards the ND-10 (Day 1998). L2 is not necessarily needed for the DNA packaging, but seems to increase packing efficiency significantly (Zhao 2000; Buck 2005; Holmgren, Patterson et al. 2005). Finally, the maturation of viruses ends with formation of the characteristic intercapsomeric disulfide bridges, and the mature viruses are released together with the top cell layers, which are gradually desquamated (Campos and Ozbun 2009).

1.1.11 The HPV late protein L2 (HPV16 L2)

The HPV16 L2 protein plays a key role during infection with papillomaviruses. Both, the uptake of viruses and the assembly of new viruses after successful infection directly depend on L2. L2 is a multifactorial protein featuring different regulatory functions after the disassembly of the viral capsids in endosomes. From this step on, L2 represents the only interaction partner accompanying the viral DNA into the nucleus. L2 thereby functions as regulator in endosomal sorting, intracellular membrane passaging, and cytoplasmic and nuclear transport. After that, L2, with its highly specific distribution in the nucleus (PML-NBs) and interaction with transcription factors, might trigger transcription of viral and cellular genes (reviewed in Spoden 2012 (submitted)).

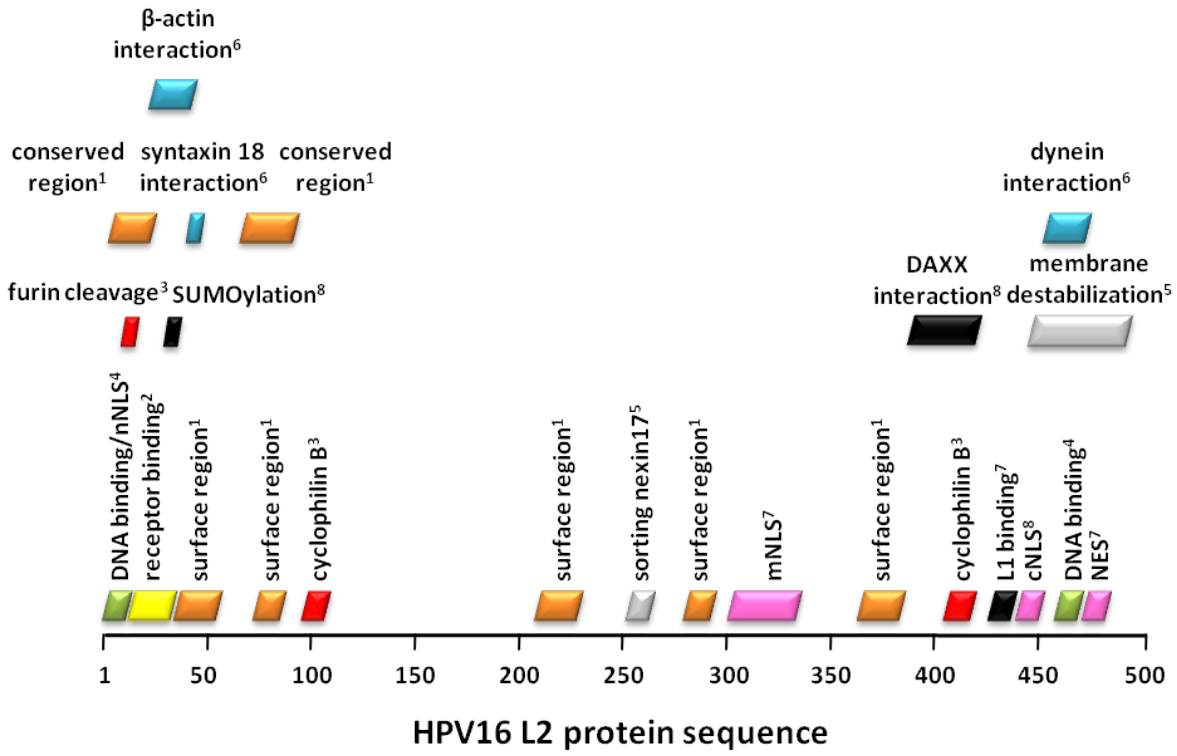

Fig. 1.5: Important sequence motifs within the HPV16 L2 protein sequence. ***1*** Surface exposed L2 regions (orange), 32-51, 69-81, 212-231, 279-291, and 362-381, especially conserved L2 sequence regions (orange), 1-12 and 56-81, described by (Kawana 1998). ***2*** Receptor or cell surface binding site (yellow), 13-31, described by (Roden 2000; Yang, Day et al. 2003a). ***3*** Furin cleavage site (red), 8-11, described by (Richards, Lowy et al. 2006) and cyclophilin B interaction sites (red), 97-103 and 409-417, (Bienkowska-Haba, Williams et al. 2012). ***4*** DNA binding domains (green), 1-13 and 454-462, described by (Bousarghin 2003). ***5*** Membrane destabilizing region (grey), 454-500, (Kämper, Day et al. 2006), sorting nexin17 interaction site (grey), 254-257, (Marusic, Ozbun et al. 2012). ***6*** Syntaxin 18 interaction site (blue), 43-47, described by (Bossis 2005), β-actin interaction site (blue), 25-45, (Yang 2003b), dynein interaction site (blue), 456-461, (Florin, Becker et al. 2006; Schneider 2011). ***7*** Nuclear localization sites (NLS, magenta), nNLS: 8-12, mNLS: 300-330, cNLS: 440-445 (HPV11), described by (Becker 2003; Finnen, Erickson et al. 2003), nuclear export signal (NES, magenta), 462-471, (Becker 2003). ***8*** DAXX interaction sequence (black), 390-420, (Florin 2002b; Becker 2003), L1 binding domain (black), 412-455, (Finnen, Erickson et al. 2003), SUMOylation site (black), 35, (Marusic 2010).

The HPV16 L2 protein comprises 473 amino acids and has a molecular weight of about 52 kDa. Sequence analysis of different HPV types show several strongly conserved regions (aa 1-12 and 56-81, Fig. 1.5, Kawana 1998)). With regard to the protein structure of L2, most of the data is based on single particle reconstruction of L2 monomers within viral capsids together with L1 pentamers by transmission electron microscopy. Thereby, the N-terminal part of L2 at position 60-120 seems to be accessible on the surface of the virus capsids (Liu 1992; Kondo 2007). The N-terminus itself folds back into the capsid (Yang, Day et al. 2003a; Day 2008a). Additional surface exposed regions of L2 were localized at positions 32-51, 69-81, 212-231, 279-291, and 362-381 (Kawana 1998). The ability of L2 to bind to the cell-surface is attributed to a region at position 13-31 (Roden 2000; Yang, Day et al. 2003a). Infection studies with HPV6, 16, and 18 PsVs showed that monoclonal antibodies against a synthetic peptide of the HPV sequence 108-120 blocked infection of VLPs (Kawana 1999; Kawana,

Kawana et al. 2001). Interestingly, the antibody also detects intact HPV16 VLPs, indicating that the L2-antigen is located on the surface of the virions. However, there was no production of neutralizing antibodies after immunization with VLPs containing this peptide (Slupetzky 2007).

After cell binding of the viruses and structural rearrangement of the L1/2 capsid, the N-terminus of L2 is accessible and cleaved by furin based on an interaction sequence at position 9-12 (Richards, Lowy et al. 2006). L2 also interacts with cyclophilin B (interaction sequence 97-103 and 409-417), which induces a conformation change of L2 and is important for endosomal L1/L2 dissociation (Bienkowska-Haba 2009; Bienkowska-Haba, Williams et al. 2012). After endocytosis, the virus capsid is disassembled. The L2 contains two DNA binding domains (aa 1-13 and 454-469, Bousarghin 2003). A complex of L2 and DNA is believed to escape the late endosomes by a membrane destabilizing region of L2 at position 451-464 (Kämper, Day et al. 2006) and a sequence motif (position 254-257) enabling interaction with sorting nexin 17 (Marusic, Ozbun et al. 2012). An interaction site for β-actin at position 25-45 allows for intracellular transport of the L2/DNA complex (Yang 2003b). The cytoplasmic L2 also contains a sequence motif at position 40-44, which enables L2 interaction with the ER receptor syntaxin 18, therefore allowing nuclear entry of the HPV genome (Bossis 2005; Laniosz 2007). In this respect, also two basic sequence regions were identified as classical nuclear localization signals (NLS) at the N-terminus (aa 1-12, nNLS) and the C-terminus of L2 (aa 456-461, cNLS) (Darshan, Lucchi et al. 2004; Mamoor, Onder et al. 2012). In addition to the terminal nuclear localization signals, a non-classical and broader central nuclear localization signal (aa 296-316, mNLS) was characterized, containing four arginines, which were indispensable for nuclear transport of L2 (Mamoor, Onder et al. 2012). In a BPV1 model, L2 is characterized as an adapter between the viral DNA bound at the C-terminal DNA binding side (position 454-462) and karyopherins, which are bound at the N-terminal nuclear localization site of L2, allowing for nuclear import of the viral genome via nuclear pores (Fay 2004). L2 also contains a nuclear export sequence at position 462-471 (Becker 2003).

Additional cytoplasmic interaction partners of L2 are represented by the dynein subunits DYNLT1/Tctex-1 and DYNLT3, which facilitate intracellular transport of the L2/DNA complex (Florin, Becker et al. 2006; Schneider 2011). After the L2-dependent localization of the viral DNA at PML-NBs upon L2 interaction with DAXX (position 390-420, Florin 2002b; Becker 2003), L2 promotes expression of the early genes and may also regulate late gene expression by direct interaction with the viral E2 protein and repression of its transcriptional activation functions. L2 also interacts with the transcription factors TBX2/3 inducing transcriptional repression (Schneider et al. 2012, submitted), and recruits viral E2, L1 and several cellular proteins to the ND-10 (Day 1998; Heino 2000; Florin, Sapp et al. 2002a; Florin 2002b; Becker 2003; Florin 2004). The nuclear import of

expressed L2 depends on the L2 interaction with Hsc70 based on an interaction sequence at position 456-461 (Florin 2004). During HPV morphogenesis, high L2 expression levels result in the loss of detection of the transcriptional transactivator Sp100 (Florin 2002b) and PML-concentration of the transcriptional co-repressor DAXX (Florin 2002b; Becker 2003). Interestingly, PML, SP100, and DAXX are usually modified by the small ubiquitin-like modifier SUMO (Zhong 2000a; Van Damme 2010). SUMOylation was also reported for HPV16 L2 at position 35 (Marusic 2010). The SUMO modification of L2 results in L2 stabilization, inhibits the interaction of SUMOylated L2 with L1, and increases the general SUMOylation level of cellular proteins.

1.2 The cellular SUMO apparatus

The human genome comprises about 30,000 genes, which is a comparably small number with regard to the complexity of the human organism. It was noticed early that the number of genes allowing expression of the respective proteins was by far not enough for formation of the complex tissue structures, network and signaling systems and the regulation of the whole system from the single cell stage to an adult human. The idea that one gene codes for one mRNA and finally one protein, which then fulfills one special function was abandoned very soon. Even on level of the genes, it was discovered that mechanisms like alternative splicing already lead to the expression of several modified forms of a protein group. Then, it was found that even fully translated proteins can be subjected to further modification, termed post translational modification (PTM). These PTMs lead to a modified function of the target protein, like e.g. alternative protein-protein interaction, different localization, or modification of the activity of the target protein. In most cases, specific amino acids of the fully synthesized target proteins are modified by various molecules like phosphate, acetate, lipids, or sugars. In some special cases, the target proteins are even modified with complete polypeptides in reversible as well as in non-reversible interaction. Conjugation of target proteins with ubiquitin (ubiquitination) generally, but not always, targets the ubiquitinated protein for degradation by the 26S proteasome (Hofmann 2001; Weissman 2011) Thereby, ubiquitin is usually attached to lysine side chains of the target proteins resulting in ‘branched’ ubiquitin-protein conjugates (Hochstrasser 1996).

Within the last decades, a large number of proteins was discovered sharing a high sequence similarity with ubiquitin. They were termed ubiquitin-domain proteins (UDPs), which are not conjugated to other proteins, or ubiquitin-like modifiers (UBLs), which are able to conjugate with target proteins and thereby alter the function of target proteins (Hochstrasser 2000; Jentsch 2000; Ohsumi 2001). One group of UBLs is represented by the SUMO proteins (small ubiquitin-like

modifiers). SUMO proteins are found in all eukaryotic kingdoms and share a very high conservation from yeast to humans (Hanania 1999). In invertebrates, only a single SUMO gene exists (SMT3), while for vertebrates four SUMO genes were identified: SUMO1, SUMO2/3, and SUMO4 (Kamitani 1998). The founding member SUMO1 is also known as PIC-1, sentrin, or GMP1 (Boddy 1996; Matunis 1996; Okura 1996). Human SUMO1 shares a ~50% sequence identity with the homologues SUMO2/3 and with SMT3. The two homologues SUMO2 and SUMO3 share a 97% sequence identity. The function of SUMO4 is still under debate (Guo 2004; Owerbach 2005). Although the SUMO proteins posses only a limited overall primary sequence homology to ubiquitin (18%), they nevertheless feature the characteristic ubiquitin-fold tertiary structure with a tightly packed globular fold with β-sheets wrapping around one α-helix (Fig. 1.6)(Bayer 1998).

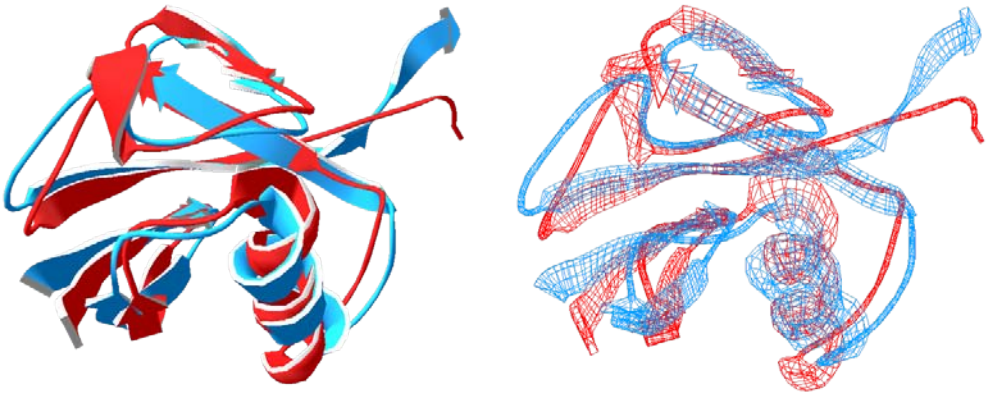

Fig. 1.6: Structure homology of SUMO1 and ubiquitin. Although SUMO proteins only share a primary sequence homology of about 18% with ubiquitin, there is a very high structural homology of the backbones of SUMO1 (blue) and ubiquitin (red) in structural alignments underlining the relationship of the two proteins. The homology modeling was performed with the Swiss-PdbViewer 4.0.1 based on the pdb structures '1Z5S' (SUMO1) and '3UGB' (ubiquitin).

SUMO proteins also differ from ubiquitin by addition of a family-specific, unstructured amino terminal extension of up to 22 residues, which probably serves as a further interaction interface. The majority of SUMO1 exists in the conjugated form, while SUMO2/3 normally exists as free monomers, which can be rapidly recruited for conjugation after cellular stress. Consistent with the difference of the primary sequences, SUMO1 and SUMO2/3 are bound to distinct substrates. The covalent SUMO conjugation to target substrates is also termed SUMOylation and is described for a very large number of SUMO target proteins (Seeler 2003). The SUMO targets or substrates can be found in almost all protein families including proteins regulating the genome integrity/structure, transcription factors and cofactors, nuclear pore proteins, signal transduction proteins, proteins located at the nuclear bodies, but also cytoplasmic and, most interestingly, viral proteins. SUMO2 and 3, but not SUMO1,

comprise an internal SUMOylation site allowing formation of poly-SUMO chains, usually as a stress response, with SUMO1 as possible chain end (Saitoh 2000; Johnson 2004; Vertegaal 2010).

In addition to the covalent SUMOylation, which is methodically comparable to ubiquitination, a noncovalent modification of several SUMO interaction partners has been discovered recently (Kerscher 2007). While the covalent SUMO conjugation depends on a SUMO conjugation motif (SCM, Fig. 1.7, A), the noncovalent interaction is induced via a SUMO interacting motif (SIM) within the target protein (Fig. 1.4, B) and is also included in regulation of SUMOylation. Both types of SUMO modification of target molecules are described separately in the following sections. In general, it seems clear that the possible interplay of both SUMOylation and SUMO interaction dramatically expands the regulatory potential of the SUMO apparatus dramatically, since one SUMO may be covalently bound to one target protein via a SCM, while it targets another protein via SIM-based interaction (Gareau 2010, Fig. 1.7). This could also be one plausible reason for the fact that so many SUMO-regulated cellular mechanisms are described, although only a very small number of direct SUMO conjugates has been reported so far. This phenomenon is termed the SUMO enigma.

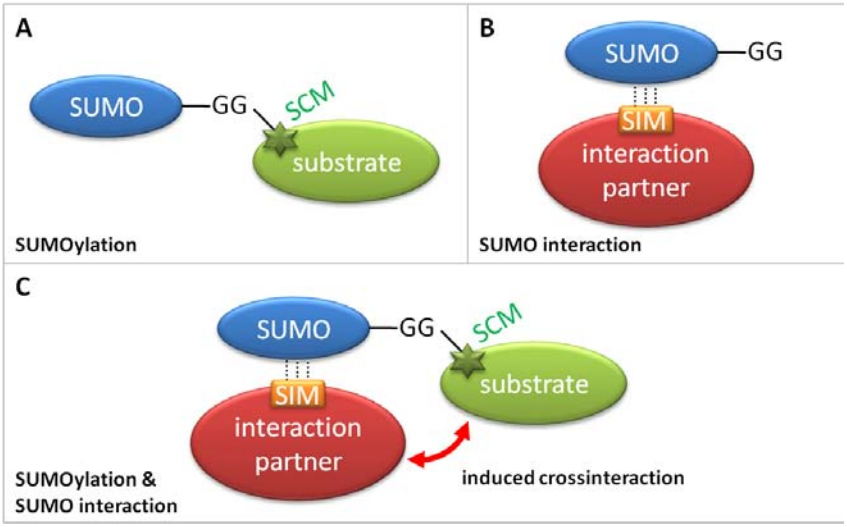

Fig. 1.7: Overview of the different SUMO modification mechanism of SUMO targets. ***A*** During SUMOylation, the SUMO substrate is covalently attached to the C-terminal double glycine of the mature SUMO. The attachment is based on the formation of an isopeptide bond between an acceptor lysine (K) in the conserved SUMO conjugating motif (SCM) of the SUMO substrate and the C-terminal double glycine motif of the mature SUMO proteins. ***B*** SUMO interaction describes the noncovalent interaction of a SUMO target with SUMO via SUMO interacting motifs (SIMs) featuring a (V/I/L) X (V/I/L) (V/I/L) consensus motif. ***C*** Combination of SUMOylation and SUMO interaction may induce crossinteraction between SUMO substrates and SUMO interaction partners.

1.2.1 SUMO conjugation

The SUMOylation pathway involves the covalent attachment of SUMO to a substrate by formation of an isopeptide bond linking the C-terminal carboxyl group of the SUMO with an ε-amino group of an acceptor lysine residue (Johnson 2004; Kerscher 2006; Capili 2007; Geiss-Friedlander 2007) (Fig. 1.8).

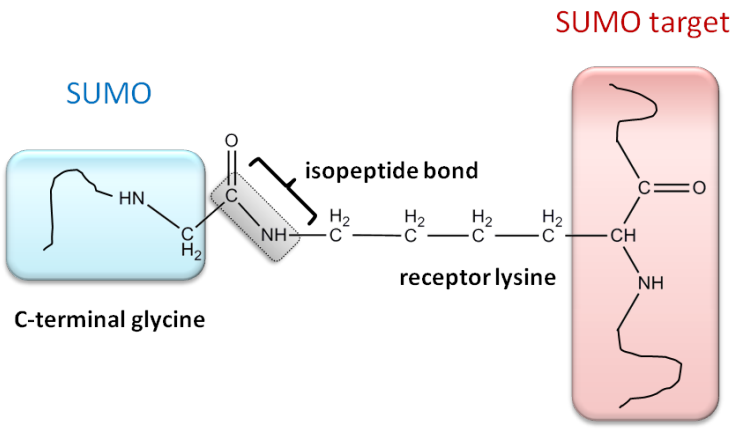

Fig. 1.8: SUMOylated proteins. Schematic view of the isopeptide bond between the carboxy group at the C-terminal end of the double-glycine motif of the mature SUMO and the ε-amino group of the receptor lysine within the SUMO target molecules (SUMO substrates).

Before the conjugation is performed, in analogy to ubiquitin or other UBLs, the immature SUMO proteins are subjected to an activation step by cleavage by SUMO-specific proteases (SUSPs) to generate the mature SUMO form. Mature SUMO proteins feature a C-terminal double-glycine motif required for efficient adenylation by a heterodimeric SUMO E1 enzyme (note that the E1/E2/E3 enzymes involved in SUMOylation are not related to the early (E-) genes of HPVs). The SUMO adenylate is linked to a conserved cysteine on a SUMO E1 protein to establish an E1~SUMO thioester and then further transferred to a conserved cysteine of a SUMO E2 protein (Ubc9) generating an E2~SUMO thioester, which can already be transferred to the receptor lysine residues of some of the SUMO substrates. However, in most cases, an E3 protein ligase catalyzes this process in a two step reaction to promote specificity and improve the release of SUMO from the E2~SUMO complex for transfer to the SUMO substrates (Reverter 2005; Hoeller 2007). Compared to ubiquitination, which is based on several E2 enzymes and hundreds of E3 enzymes, the substrate specificity during SUMOylation only depends on one E2 and a few E3 enzymes. Examples of proteins with an E3 ligase function, which mostly also contain SIMs, are the Ran-binding protein 2, protein inhibitor of STAT (PIAS) proteins, and the polycomb protein 2 (Pc2) (Pichler 2002; Seeler 2003; Rytinki 2009; Merrill, Melhuish et al. 2010). The SUMO conjugation can be reversed by deconjugation of SUMO from the substrates by the same SUMO-specific proteases (SUSPs) involved in maturation of the SUMO proteins (Mukhopadhyay 2007). The specificity of SUMO proteases arises from the distinct

subcellular localization of the proteases, which also feature specificity for some of the SUMO substrates as well as SUMO isoforms (Gong 2000; Kim 2000; Nishida 2000).

For SUMOylation of the SUMO target, a ψKX(D/E) consensus motif (SUMO conjugation motif, SCM) within the substrate region containing the acceptor lysine was identified (ψ denotes a large hydrophobic residue (Rodriguez 2001)). The SCM is mostly localized at rather exposed positions in extended loops or intrinsically disordered regions. The residues of the motif directly interact with the Ubc9 of the SUMO E2 Ubc9 complex (Sampson 2001). Therefore, the short motif adopts an extended conformation enabling the acceptor lysine to fit into a hydrophobic groove of Ubc9, while electrostatic and hydrogen bonding between Ubc9 and the neighboring residues around the lysine mediate recognition of the sequence motif by E2 surface residues (Bernier-Villamor 2002; Lin 2002). This interaction is necessary to center the substrate within the active site of E2 and results in an increased rate of catalysis linking SUMO with the SUMO substrates (Yunus 2006).

In some cases, SUMOylation depends on extended consensus motifs containing additional elements. The respective consensus motifs are described as phosphorylation-dependent SUMO motifs (PDSMs, mostly ψKX(D/E)XXSP) or negatively charged amino acid-dependent SUMO motifs (NDSMs) (Yamashita 2004; Shalizi 2006; Yang 2006). Phosphorylation generally seems to enhance SUMOylation, as was found for phosphorylation of heat shock factors after induction of cell stress (Hietakangas 2003). The enhancing effect is based on an interaction of the phosphorylated serine of the SUMO target with a basic patch on the E2 surface (Mohideen 2009). NDSMs comprise C-terminal negatively charged residues. Akin to the phospohrylated serines in PDSMs, here, the negatively charged residues interact with the basic patch on the E2 (Yang 2006).

1.2.2 SUMO interaction

The noncovalent interaction between SUMO and SUMO substrates is mediated by the SIM, as was initially identified by two-hybrid screening and biophysical studies (Minty 2000; Song 2004; Hannich 2005; Kerscher 2007). The known SIMs share a hydrophobic core with a (V/I/L) X (V/I/L) (V/I/L) consensus motif flanked by acidic residues. The interaction is facilitated by an induced parallel or antiparallel β-strand conformation of the SIM region, which extends the β-sheet of the SUMO interaction surface and directs the hydrophobic core of the SIM into a hydrophobic pocket on the SUMO surface stabilized by H-bonding (Song 2005). The acidic residues apparently serve as first interaction platform and determine the polarity of the SIM-SUMO complex based on H-bonding or electrostatic interaction with conserved basic residues on the SUMO surface. Most SIMs, e.g. the SIMs of the base excision repair enzyme thymine DNA glycosylase (TD), promyelocytic leukaemia

protein (PML), or the transcription factor DAXX show no specificity for a particular SUMO isoform (Bernardi 2007; Geiss-Friedlander 2007; Kerscher 2007), but some do, like e.g. the ubiquitin-specific protease 25 (USP25) and the transcription regulators MCAF1 and COREST1 (Sekiyama 2008; Ouyang 2009). The majority of SIM structures were analyzed in complexes with SUMO, so most molecular determinants of the SIM enabling SUMO specificity remain unknown.

In some cases, SIM-mediated SUMO interaction is enhanced by phosphorylation of special serine residues, which are located c-terminally of the phospho-SIM (Stehmeier 2009). Usually, the serines are phosphorylated by the ubiquitously expressed and constitutively active casein kinase 2 (CK2), as was reported exemplarily for PML and PIAS proteins (Duncan 2008). The phosphorylated serines, now featuring a net negative charge due to the phosphate group, are believed to interact with basic residues on the SUMO surface (Stehmeier 2009).

1.2.3 Targeting of the cellular SUMO apparatus by human pathogens

Viruses and pathogens are obliged to escape or endure antiviral defense to facilitate productive infection. Besides antibody and cell-regulated acquired immunity and interferon mediated innate immunity, the viruses are also opposed to the so called intrinsic immunity as the first antiviral defense barrier. It is not very surprising that over long time periods, also viruses and other pathogens, with their very fast developing genomes, evolved multiple strategies to exploit the cellular SUMO apparatus. In general, the hot spot for interaction of the viruses with the host cell SUMO system seems to be represented by the PML-NBs (Day 1998; Everett 2001; Florin 2002b; Everett 2007; Tavalai 2008; Van Damme 2011). The PML-NBs are mainly comprised of PML and the chromatin organizer Sp100, which are both SUMOylated and recruit several antiviral factors like the transcription repressor DAXX, and the tumor repressors Rb and p53 to the PML-NBs (Swindle 1999; Zhong 2000a; Zhong 2000b; Day 2004; Shih 2007). The PML (promyelocytic leukemia) protein is the major component of PML-NBs and exists in at least seven isoforms which are essential for formation of PML-NBs and function as growth and transformation suppressors (Le, Yang et al. 1996). Sp100 (speckled protein of 100 kDa) is also a permanent PML-NB component participating in chromatin remodeling and designated as transcription regulator (Seeler, Marchio et al. 1998; Bottomley, Collard et al. 2001). Multifunctional DAXX (death domain-associated protein 6) represents a transcription corepressor recruiting transcriptional repressors like histone deacetylase 1 (HADAC1), HADAC2, DNA methyltransferase 1 (DNMT1), or ATRX (α-thalassaemia/mental retardation syndrome X-linked)(Li, Leo et al. 2000; Hollenbach, McPherson et al. 2002; Xue, Gibbons et al. 2003; Ishov, Vladimirova et al. 2004; Muromoto, Sugiyama et al. 2004). The assembly of PML-components in PML-NBs is involved in

apoptosis, regulation of transcription and antigen targeting and represents the innate antiviral defense barrier, which represses viral replication in the host. In most cases, in the early phase of infection, the viruses manage to associate, modulate, or even destroy the PML-NBs or degrade PML-associated factors, which finally leads to a deactivation of the antiviral function of PML-NBs and is best analyzed for adenoviruses and herpesviruses (Wimmer 2012). A collection of results indicating an interaction of a large collection of proteins expressed in pathogens with the cellular SUMO apparatus is given in **Table 1.1**.

As for papillomaviridae, it is known that the viral E1 and E2 proteins interact with Ubc9 and are SUMOylated (Yasugi 1997; Rangasamy 2000a). E1 SUMOylation seems to be regulated by the protein inhibitor of STAT (PIAS) family of E3 ligases. HPV E2 is SUMOylated *in vitro* and *in vivo* with a preference for SUMO-2/3 conjugation in vivo. Thereby, an exogenous overexpression of SUMO-2/3 with Ubc9 significantly stabilizes E2 protein levels, whereas there is no stabilization with SUMO1 (Wu 2007; Wu 2009). E2 stabilization does not depend on covalent attachment of SUMO-2/3 to the viral protein, since inactivation of the predominantly modified lysine residue does not lead to a modified stabilization level. One can conclude that in these systems, stabilization is not triggered by simple competition between ubiquitin and SUMO for covalent attachment sites, but rather by a regulation based on SUMOylated secondary targets.

Also the HPV16 L2 is covalently modified by SUMO1 and, preferentially, by SUMO2/3 at lysine 35, which leads to stabilization of L2 (Marusic 2010). In this context, remarkably, only non-SUMOylated L2 can interact with the major capsid protein L1. For HPV16, the viral L2 protein seems to induce a short-lived change in the general SUMOylation status of host cell proteins by specifically upregulating endogenous SUMO-2/3 modification. Intriguingly, just during keratinocyte differentiation, expression of SUMO-2/3 and Ubc9 is significantly upregulated, whereas SUMO-1 levels remain unaltered (Deyrieux 2007). It seems that the level of viral E2 and L2 protein effectively modifies the levels of the host cell SUMOylation enzymes, which are directly coupled with the differentiation process in infected skin keratinocytes and antiviral defense.

With regard to noncovalent interaction of pathogenic proteins with SUMO, 2-hybrid experiments identified a bit more than a handful of viral proteins interacting with SUMO (Wimmer 2012). From this selection, four viral proteins, ICP0 of the herpes simplex virus (Boutell 2011), ORF61 of the varicella zoster virus (Wang, Oliver et al. 2011), IE2 of the human cytomegalovirus (Kim 2010), and E3L of the vaccinia virus (Gonzalez-Santamaria, Campagna et al. 2011) were able to interact with SUMO via one or more SIMs.

Table 1.1: A selection of pathogens interacting with the cellular SUMO apparatus.

Family	Pathogen	Protein	Features	References
Adenoviridae	avian adenovirus chicken embryo lethal orphan CELO	Gam-1	de-regulation of SUMOylation	(Chiocca 2002; Colombo 2002)
	human adenovirus HAdV5	E1A, E1B	interaction with Ubc9, affects polySUMOylation, SUMO substrate	(Hateboer 1996; Endter 2001; Endter 2005; Yousef 2010)
Herpesviridae	α-Herpesviridae: herpes simplex virus HSV-1	ICP0	links SUMOylation with ubiquitin-dependent protein turnover, SUMO interaction	(Boutell 2011)
	α-Herpesviridae: varicella-zoster virus VZV	ORF61	links SUMOylation with ubiquitin-dependent protein turnover, SUMO interaction	(Kyratsous 2009; Reichelt 2011; Wang, Oliver et al. 2011)
	β-Herpesviridae: human cytomegalovirus HCMV	IE1 IE2	SUMO substrate SUMO substrate, SUMO interaction	(Spengler 2002; Sadanari 2005; Kim 2010)
	γ-Herpesviridae: Epstein Barr virus EBV	Zta, Rta	SUMO substrate	(Adamson 2001; Hagemeier 2010; Murata 2010)
	γ-Herpesviridae: Kaposi's sarcoma-associated herpesvirus KSHV	B-bZIP, Lana2	SUMO substrate	(Izumiya 2005)
Papillomaviridae	human and bovine papillomavirus HPV and BPV	vE1, vE2	SUMO substrate, interaction with Ubc9	(Yasugi 1997; Rangasamy 2000a; Rangasamy 2000b)
	HPV16	L2	SUMO substrate	(Marusic 2010)
Poxviridae	vaccinia virus VV	E3L A40R	SUMO substrate, SUMO interaction SUMO substrate	(Rogan 2000; Palacios 2005; Gonzalez-Santamaria, Campagna et al. 2011)
RNA viruses	Bunyviridae: Hantaan virus HTNV, Tula virus TULV, Seuol virus SEOV	N, NP	SUMO interaction	(Kaukinen 2003; Lee 2003; Maeda 2003)
	Coronaviridae: Severe acute respiratory sydrome SARS-CoV	N	SUMO substrate, interaction with Ubc9	(Li 2005)
	Filoviridae: Ebola Zaire Virus EBOV	VP35	induces SUMOylation	(Chang 2007)
	Flaviridae: Dengue virus DENV	env	interaction with Ubc9	(Chiu 2007)
	Orthomyxoviridae: Influenza Virus	NS1, PB1, M1, NS2	SUMO substrate	(Pal 2010; Pal 2011; Wu 2011; Xu, Klenk et al. 2011)
	Paramyxoviridae: Parainfluenzavirus PIV5	P	SUMO substrate	(Sun 2011)
	Picornaviridae: Enterovirus EV71	3C	SUMO substrate	(Chen 2011)
	Retroviridae: Human immunodefiency virus HIV-1	p6 (gag) IN	SUMO substrate, SUMO interaction, interaction with Ubc9 SUMO substrate	(Gurer 2005; Jaber 2009; Zamborlini, Coiffic et al. 2011)
	Retroviridae: Human T-cell leukemia virus HTLV-1	Tax	SUMO substrate	(Lamsoul, Lodewick et al. 2005; Kfoury, Setterblad et al. 2011)
Extra/intracellular bacteria	Yersinia spec	Yops	SENP-like	(Cornelis 2001)
	Lysteria monozytogenes	LLO	Ubc9 modulation/degradation	(Citro 2010; Ribet, Hamon et al. 2010)
	Clostridium perfringens	PFO	Ubc9 modulation/degradation	(Citro 2010; Ribet, Hamon et al. 2010)
	Streptococcus pneumoniae	PLO	Ubc9 modulation/degradation	(Citro 2010; Ribet, Hamon et al. 2010)

1.3 Electron Paramagnetic Resonance (EPR) Spectroscopy

1.3.1 The history of EPR

Electron paramagnetic resonance (EPR) spectroscopy today represents a powerful tool for investigation of molecular structure and dynamics, as well as of the local distribution of paramagnetic centers (Schweiger 2001). Since its discovery in Kazan in 1944, EPR spectroscopy developed from a discipline for studying basic physical properties of condensed matter to a sophisticated and acknowledged research method for addressing a very broad collection of problems which emerge in most different research fields. Thus, over years, EPR spectroscopy manifested its place as a very special technique in material science and biophysics, which can also be attributed to three major benefits within the last four decades: *i)* the seminal work of Freed and others to theoretically describe the EPR effect in context of the analysis of molecular dynamics (Goldman 1972; Hwang 1975; Schneider 1989), *ii)* the onset of pulse EPR spectroscopy (Milov 1984; Höfer 1986), and *iii)* the possibility to perform distance measurements in the biophysically relevant range between 1 and 8 nm (Milov 1984; Martin 1998; Pannier 2000; Jeschke 2002). For biophysicists, EPR is a powerful alternative or complement to neutron scattering, nuclear magnetic resonance (NMR), or Mößbauer spectroscopy, which allow comparable investigations.

In general, the EPR method is based on the interaction of an electron spin of a paramagnetic center with an external magnetic field B_0. Since naturally occurring paramagnetic systems are relatively seldom (examples are complexes of proteins with paramagnetic transition metals like e.g. Cu^{2+}, Co^{2+}, $Ni^{1/3+}$, Mn^{2+}, Fe^{3+} (Calle 2006)), without further efforts, the research field of EPR would be rather limited. However, just this limitation, the lack of naturally abundant paramagnetic species, simultaneously allows for the very promising artificial introduction of paramagnetic species into EPR samples. The apparent disadvantage leads to a very high specificity of EPR towards covalently attached spin labels or noncovalently introduced spin probes compared with e.g. NMR on ^{1}H-nuclei (Kocherginsky 1995; Hubbell 2000).

In the following section, the reader is familiarized with most common theoretical aspects of EPR and with the experimental EPR techniques, which were used here, with special focus on the respective problems addressed by each EPR technique. For a more detailed introduction to these techniques, the reader is referred to Atherton (1993) and Schweiger (2001).

1.3.2 EPR radicals and site-directed spin labeling (SDSL)

For EPR experiments, in general, the correct choice of the respective spin label or spin probe is of highest importance to extract a maximum of information from EPR measurements. For interaction studies including covalently attached spin labels to target proteins, common nitroxide radicals like

PROXYL IAA (3-(2-iodoacetamido)-PROXYL) or MTSSL (1-Oxyl-2,2,5,5-tetramethylpyrroline-3-methyl) were used (Fig. 1.9).

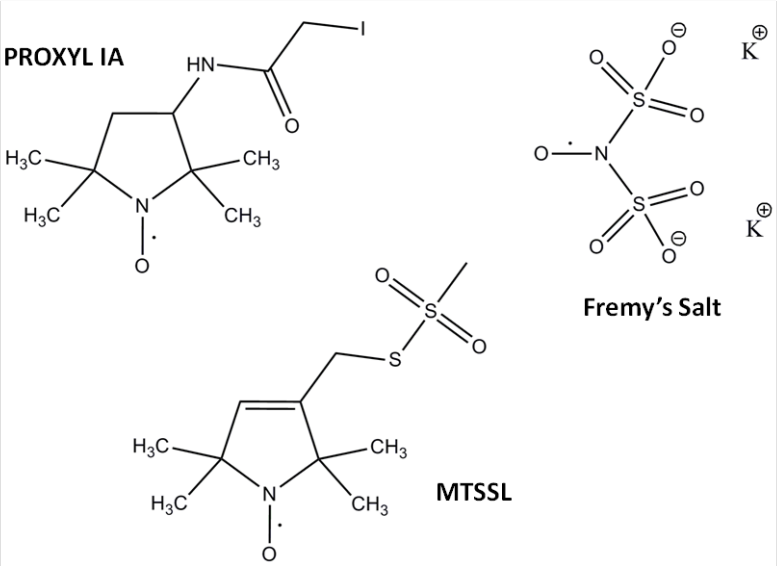

Fig. 1.9: Chemical structure of the EPR spin probes used in this study. Chemical structure of common nitroxide spin probes: PROXYL IAA (3-(2-iodoacetamido)-PROXYL), MTSSL (1-Oxyl-2,2,5,5-tetramethylpyrroline-3-methyl), and Fremy's Salt (potassium nitrosodisulfonate, NDS).

The spin probes were covalently attached to the target proteins by site-directed spin labeling (SDSL) based on the presence of sulfhydryle (SH) groups, which occur within the amino acid side groups of cysteines contained within the target protein (Berliner 1982). An example is given for the covalent attachment of the most common spin label MTSSL to a cysteine side group of a protein (Fig. 1.10).

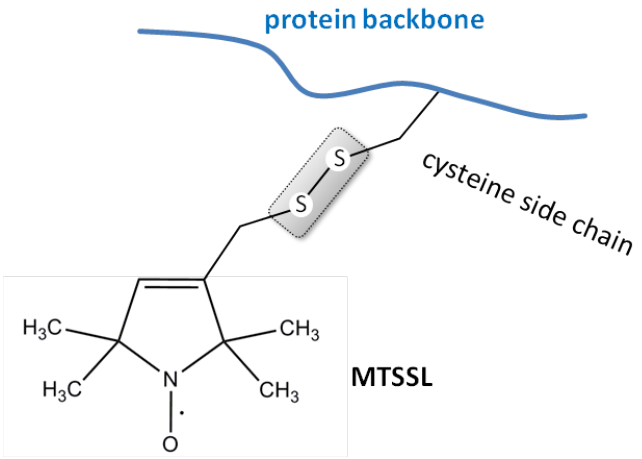

Fig. 1.10: Chemical structure for the attachment of MTSSL to a target protein. The stable radical MTSSL is covalently attached to a receptor cysteine. Thereby, a disulfide bond is generated between the label and the sulfhydryl group of the cysteine.

In principle, intrinsically abundant cysteines can be labeled as well as artificially introduced cysteins. Mutation experiments, which allow the insertion of cysteines at almost every position within the protein, therefore enable selective labeling throughout the whole primary sequence of the protein. In brief, the labeling reaction includes reduction of the target protein to prepare free and accessible sulfhydryl (SH) groups. In a one step reaction, the label is covalently attached to the reduced SH groups of the target protein by incubation of the sample protein with the respective spin label.

For EPR experiments based on electrostatic interaction of the spin probe with HPV16 viruses, Fremy's Salt (NDS) was used (Fig. 1.9). Here, the electrostatic interaction of the negatively charged NDS ions with stretches of several closely neighbored positively charged amino acids (arginines and lysines) within the target L1 and L2 capsid proteins of HPV16 pseudoviruses results in rather defined loci with a very high concentration of paramagnetic FS ions. Thus, FS can be noncovalently "attached" to positively charged amino acid patches of the target molecules. L2 comprises two patches of positively charged amino acids, which are represented by the nNLS and the cNLS at the N- and C-termini of the protein. L1 comprises only one stretch of positively charged amino acids at its C-terminus.

1.3.3 EPR spectroscopic methods and their information content

Characterization of the spin label is routinely performed based on continuous wave (CW) EPR at any temperature and on echo-detected (ED) EPR at low temperatures. The measurements give a fingerprint of the radical including especially electronic but also geometric information about the radical center (Fig. 1.11).

Based on determination of the rotational motion by simulation of CW EPR, detailed information about molecular dynamics of the labeled molecule is accessible in the range of 10 ps - 1 µs. In a straightforward application, the change (or non-change) in rotational mobility can be used to prove (or rule out) whether a target molecule is attached to membranes or whether there is an interaction of two proteins (Beier and Steinhoff 2006; Musse, Boggs et al. 2006; Volkov, Dockter et al. 2009; Homchaudhuri L. 2010; Haimann, Akdogan et al. 2011; Kattnig, Bund et al. 2012). Furthermore, CW EPR spectra, also in combination with ED EPR measurement characterizing the T_2 relaxation time, report on the immediate chemical environment (polarity, proticity) in the range of several solvation layers (up to 2 nm) around the paramagnetic center (Plato 2002; Junk, Jonas et al. 2008). Also information about closely located, dipolar coupled nuclei (mostly N or P atoms) can be obtained (Bund, Boggs et al. 2010).

Additional pulse EPR measurements expand the accessible information content to a further extent. With hyperfine sublevel correlation (HYSCORE) spectroscopy and pulse electron-nuclear double

resonance (ENDOR), hyperfine couplings with surrounding magnetically active nuclei are detected and geometrically characterized, since the measurements are performed in frozen solution (Schweiger 2001).

One of the main achievements is represented by the establishment of a pulse method detecting dipole couplings between the unpaired electron spins of the spin labels, allowing for biophysical structure determination (Milov 1984; Martin 1998; Pannier 2000; Jeschke 2002; Schiemann, Piton et al. 2007; Schiemann and Prisner 2007; Schiemann, Cekan et al. 2009). In this context, double electron-electron resonance (DEER) allows distance measurements via the ω_{dd} r^{-3} dependence (ω_{dd} = dipolar coupling frequency, r = interspin distance). The limited EPR frequency range allows for a detectable range of DEER distances between 1.5 – 8 nm.

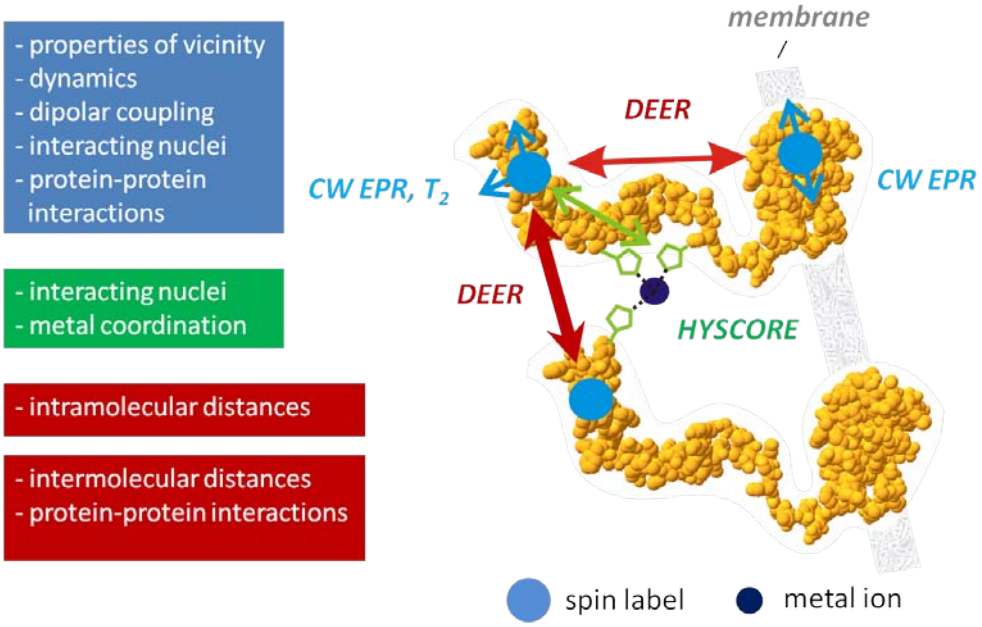

Fig. 1.11: Schematic summary of the information content of EPR spectroscopic methods on nitroxide radicals. CW EPR measurements (together with T_2 detection in ESE experiments) deliver information about the direct vicinity of the spin label, including dipolar coupling to neighboring nuclei, but also dynamics of the label. Thus, e.g. membrane anchoring or protein-protein interactions can be addressed. The accessibility of the spin label to solvent molecules even allows for identification of helical regions. With pulsed EPR techniques like HYSCORE, information about potential nuclei, which interact with the spin label, can be obtained. Examples are special nitrogen nuclei involved in metal coordination or the protein backbone. DEER measurements allow for biophysical structure determination. With DEER, both intramolecular distances between two spin labels within the same molecule as well as intermolecular distances between different molecules containing only one spin label can be measured, allowing protein interaction screening as well as protein folding experiments.

1.3.3.1 Continuous wave (CW) EPR

In liquid solution, the description of nitroxide radicals by the general anisotropic spin Hamilton operator is only based on the electron-Zeeman interaction and the hyperfine coupling to the magnetic ^{14}N nucleus (I = 1)(Atherton 1993). The fast motion of the spin probe results in an averaging of the g- and hyperfine (A-) tensors to isotropic values and the resonance condition for the irradiated microwave is described by:

$$\Delta E_{nit} = \hbar\omega_S = g\beta_e B_0 + a_{iso} m_I$$

Thus, the interaction with the nitrogen (I = 1) leads to three allowed transitions and the typical three-line nitroxide spectrum (Fig. 1.12).

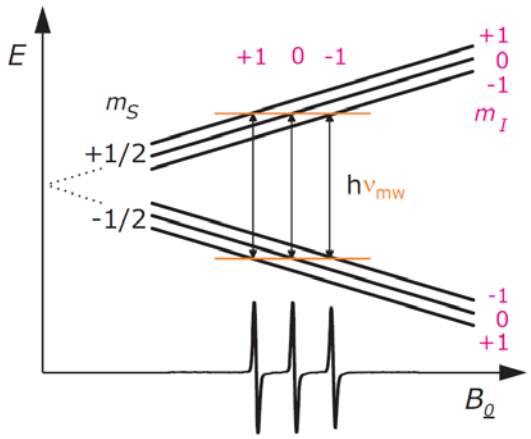

Fig. 1.12: Splitting of the energy levels of a free electron spin in a magnetic field. The arrows indicate the allowed transitions excited by the micro wave.

The effect of rotational motion and chemical environment on X-band CW EPR spectra is now explained in detail. The rotational correlation time τ_c represents a measure for the rotational diffusion of the spin probe molecules and can roughly be categorized in the following regimes: *i*) fast motion ($\tau_c \leq 100$ ps), *ii*) intermediate motion (100 ns > τ_c > 1 ns), and, *iii*) rigid limit ($\tau_c \geq 1$ µs, Fig. 1.13, A). In general, the rotational motion can be isotropic or anisotropic. The latter case is very often observed when spin labels are attached to larger molecules.

The nitroxide spectra are also influenced by effects based on the local environment of the paramagnetic centers. **Figure 1.13 B** depicts the basic principal axis system of electron-Zeeman and hyperfine tensors to describe the spectra. The electronic structure of the nitroxide is directly changed by different levels of polarity and/or proticity (pH, Fig. 1.13, C). The formation of H-bonds in polar

surrounding leads to an increased electron spin density at the nitrogen π-orbital (Fig. 1.11, D). This is reflected by changes of the hyperfine coupling parameter a_{iso} :

$$a_{iso}\,(\text{hydrophilic/polar}) > a_{iso}(\text{hydrophobic/apolar})$$

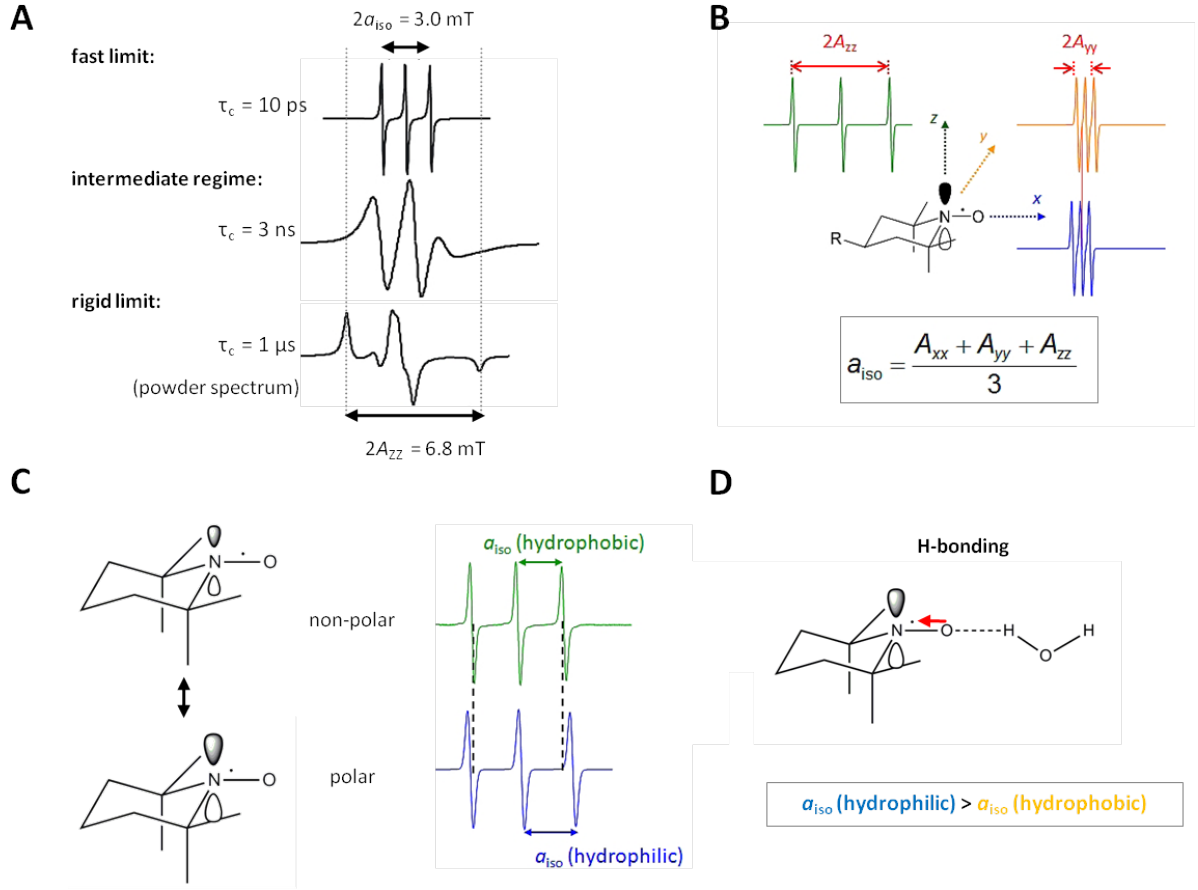

Fig. 1.13: Information from nitroxide CW EPR spectra. ***A*** The effect of rotational dynamics on CW EPR spectra: *i*) fast rotation with τ_c~10 ps leading to the typical, averaged three-line spectrum. The isotropic g_{iso} represents the center of the central line. The spacing between the lines is dominated by a_{iso}, *ii*) intermediate motion with 100 ns > τ_c >1 ns, and *iii*) rigid limit with τ_c ~1 µs. ***B*** Principal axis system of electron-Zeeman and hyperfine tensors (collinear). ***C*** Influence of the chemical environment on CW EPR spectra. Hydrophilic or polar molecular surroundings lead to an increased electron spin density at the nitroxide ^{14}N nucleus and an increased a_{iso} and line splitting compared with hydrophobic and non-polar environments. ***D*** H-bonding in polar/hydrophilic environments (Figure based on Hinderberger, 2011).

1.3.3.2 The electron spin echo (ESE)-detected EPR experiment

One of the simplest pulse EPR experiments is based on detection of the primary echo, which describes the re-appearance of magnetization of the initial magnetization after a pulse sequence of (π/2)-τ-(π)-τ-*echo*. Based on this sequence, ESE-detected EPR is a technique where the pulse sequence is repeated at every magnetic field position during a sweep of the magnetic field (Fig. 1.14,

A). Finally, the echo intensity is plotted against the magnetic field to give the standard ESE-detected EPR spectrum depicted in **Fig. 1.14, B**.

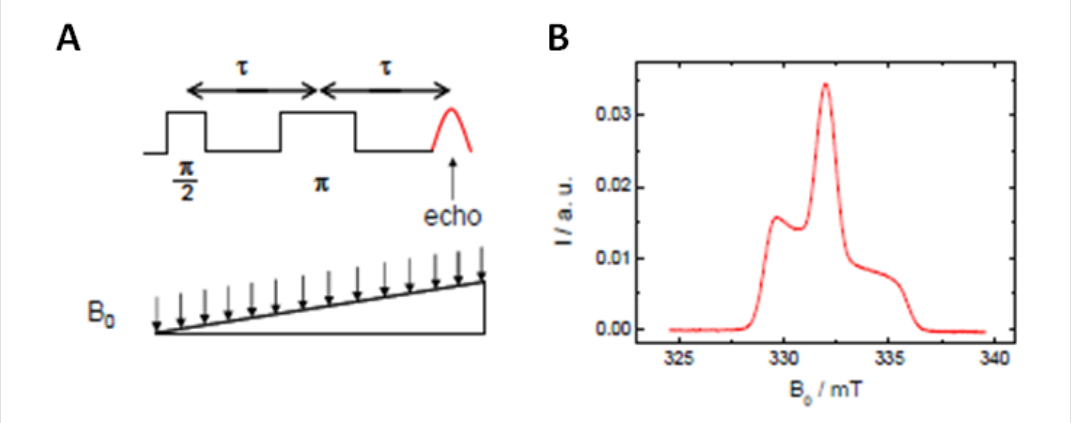

Fig. 1.14: ***A*** ESE pulse sequence with sweep of the magnetic field B_0 and the pulse interval time τ. ***B*** Typical ESE-detected EPR spectrum.

1.3.3.3 Nanoscale distance measurements with DEER

In this type of pulse EPR measurements, the double electron-electron resonance (DEER) effect of the dipole interaction between two spins is used to deduce information about the distance distribution between electron spins in a system based on the r^{-3} dependence of the dipolar coupling frequency ω_{DD} (Martin 1998; Pannier 2000; Jeschke 2002). One of the pulse EPR experiments, in which the dipolar coupling effects are efficiently isolated from other effects in the spin system, is the 4-pulse double electron-electron resonance (DEER) experiment described in the following. The pulse scheme of the typical 4-pulse DEER method is illustrated in **Fig. 1.15, A**.

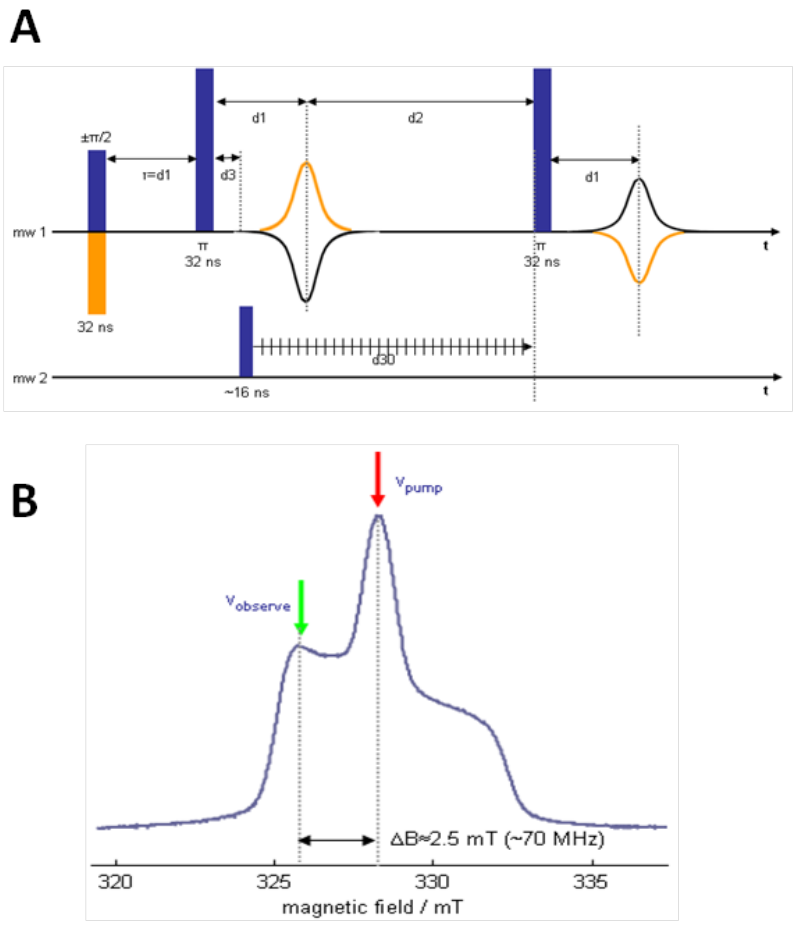

Fig. 1.15. ***A*** DEER pulse sequence including the characteristic measurement parameters. ***B*** Excitation (ν_{pump}) /observation ($\nu_{observe}$) positions in the echo-detected EPR spectra selected for 4-pulse DEER experiments.

Thereby, detection of the refocused echo is used, which bears the advantage of a dead time-free detection, and was actually developed in Mainz (Martin 1998). The echo intensity of the refocused echo is recorded as a function of the pump pulse position d2. The resulting spectrum contains the information of the dipolar coupling of the two spins. In a more detailed view, observer and pump spins are manipulated separately from each other by selection of two different microwave frequencies depicted in **Fig. 1.15, B**. Here, an 'observer' experiment with a refocused echo is performed on spins 'A' with frequency mw1 ($\nu_{observe}$), while on spins 'B' a π (pump) pulse is applied with the resonance frequency mw2 ($\nu_{observe}$). The irradiation time of the pump-pulse is varied between the position of the primary echo (which is not detected, but dephases again) and the last π-pulse of the observer sequence. Spins 'B' are thus inverted by the π-pulse. This results in a changed magnetic field at the position of the 'A' spins. Therefore, the precession of the 'A' spins changes and magnetization features a phase difference of $\Delta\phi_{DD} = \omega_{DD}t$. Finally, the intensity of the refocused echo is recorded as a function of the pump pulse position d2.

Extraction of distance data from this experiment is based on the equation for the dipolar coupling

$$\omega_{DD} = \frac{\mu_0 g_1 g_2 \beta_e^2}{4\pi\hbar} \frac{1}{r_{12}^3}.$$

The distance range that is accessible by DEER measurements is limited at the lower end to ~ 1.5 nm by the technical excitation bandwidth of the mw pulse generators at X-band frequencies. Spins, which are closer than 1.5 nm feature stronger dipolar couplings with frequencies > 35 MHz, which significantly exceed the excitation bandwidth (but can often be detected in broadenings of the low-temperature CW EPR spectra). The limitation at the upper end is directly determined by the dipolar evolution time and allows for detection of a theoretical maximum distance of ~ 8 nm with common EPR spectrometers. Larger distances only contribute to the homogeneous background signal. A typical, background-corrected DEER time trace and the resulting distance distribution are shown in **Fig. 1.16, A** and **B**, respectively. The modulation depth is defined as the depth of the intramolecular oscillation after background correction and is a direct measure of the number of interacting spins.

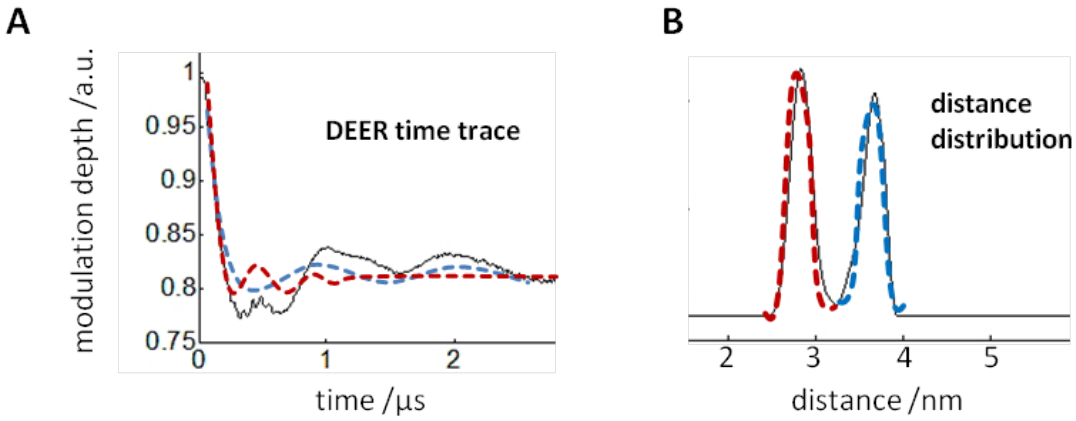

Fig. 1.16: *A* DEER time trace after removal of the experimental background obtained for a mixture of two rigid nitroxide biradicals. The measured spectrum (black) contains contributions of two oscillations with different dipoar frequency ω_{DD}. ***B*** The corresponding distance distribution is obtained after direct intergral transformation of the time trace in *A* and shows two peaks correlated to the two dipolar coupling frequencies. Note that a higher dipolar coupling frequency is correlated to shorter distance in the distance distribution.

1.4 Motivation and Aim

The minor capsid protein L2 of the human papillomavirus (HPV) type 16 fulfills a multiplicity of important functions during the HPV16 life cycle including interaction with furin during cell binding of the HPVs, facilitation of viral disassembly, endosomal escape, and transport of the L2-DNA complex towards the PML-NBs, but also regulation of transcription of viral proteins in late infection phase and stabilization of the freshly assembled L1/L2 capsids just before release of new HPVs after succesfull infection. However, little is known about the interaction of L2 with cellular factors just after nuclear entry of the L2-DNA complex, which represents a key situation in counteracting antiviral defense systems bundled in PML-NBs of the target cell, but at the same time taking benefit from the host replication machinery by colocalization with the same PML-NBs to establish viral replication.

The aim of this work was to unravel the complex L2 interaction mechanism with cellular target proteins, which regulates the transport of the viral DNA into subnuclear structures known as PML-NBs, replication of viral DNA, viral transcription, and also morphogenesis of new viral particles. An additional challenge was to purify the HPV16 L2 protein and to establish new experimental methods, to characterize HPV infection and, in particular, to make the model system of a virus accessible to a very special technique like electron paramagnetic resonance (EPR) spectroscopy. Thereby, the special focus was on the interaction of HPV16 L2 with one of the most abundant proteins in PML-NBs, the small ubiquitin-like modifiers (SUMOs). SUMOs are indispensible for functionality of a number of PML-NB associated cellular factors featuring also antiviral functions but also play a role to establish infectivity for some viruses. Also, L2 interacts with the host SUMO apparatus, as we were able to reproduce covalent SUMOylation of L2, which was reported before, but additionally identified a noncovalent interaction of L2 with SUMO proteins, which is based on a conserved SUMO-interacting motif (SIM) at L2 position 286-289. The identified SIM was indispensible for infectivity for HPV16 L1/L2 PsVs. Although PsVs lacking the SIM did not show any detectable aberrations in cell binding and endocytosis, there was no nuclear transport of the L2-DNA complex and no colocalization of L2 or DNA with PML-NBs, explaining the complete loss of infectivity of SIM deficient PsVs. However, the L2 SIM seems to be crucial for additional tasks of L2 in the context of PML NBs, which most obviously include regulation of the activity of several PML-NB-associated host factors involved in viral defense and viral replication, as it was already observed for DAXX or Sp100.

2. Materials and methods

2.1 Materials

2.1.1 Laboratory equipment

Tab. 2.1: Laboratory equipment.

equipment	**type**	**manufacturer**
analytical balance	Mettler AE 100	Mettler
blot chamber	Trans Blot Cell	BioRad
centrifuge	Sorvall RC-5B	Du Pont instruments
centrifuge	Megafuge 1.0	Heraeus
centrifuge	Laborfuge 400R	Heraeus
centrifuge	Biofuge Pico	Heraeus
centrifuge	Biofuge fresco	Heraeus
electric pipettes	Pipetus®-akku	Hirschmann Laborgeräte
electrophoresis chamber (DNA)	n.a.	LMS GmBH Labortechnik
electrophoresis chamber (protein)	n.a.	BRL Life Technologies
ELISA reader	Multiscan RC models 351	Thermo Labsystems
FACS	FACScan	Becton Dickinson
fluoeescence microscope	Axiovert 200M	ZEISS
gel documentation	Transillumination BioDocAnalyze	Biometra
heat block (rotation)	Thermomixer Comfort	Eppendorf
heat block (static)	Blockthermostat BT1303	HLC
incubator (cell culture)	Heraeus 6000	Heraeus
incubator (*E. coli*)	n.a.	WTC Binder
laboratory balance	BL1500S	Sartorius
light microscope	Wilovert S AFL	Hund Wetzlar
luffing incubator	Rocky	Heraeus

luminometer (plate format)	Tristar LB941	Berthold Technologies
luminometer (tube format)	Lumat LB9507	Berthold Technologies
magnetic stirrer/heater	IKAMAG REC-G	Janke & Kunkel
micro wave	Micromat	AEG
pH-meter	pH Level 2	InoLab
pipettes	P10, P20, P100, P200, P1000	GISLON
power supply (DNA gels)	Gene Power Supply GPS200/400	Pharmacia
power supply (protein blotting)	PowerPack P25	Biometra
power supply (protein blotting)	PHERO-stab.500	Biotec-Fischer
power supply (protein gels)	ECPS3000/150	Pharmacia
power supply (protein gels)	Standard Powerpack P25	Biometra
rotor	SW40, SW55, SW60, 70Ti	Beckmann
rotor	GS 3, GSA, HB-4	Du Pont Instruments
shaking device	Certomat R	B.Braun
shaking device	Certomat HK	B.Braun
shaking device (over head)	Reax2	Heidolph
shaking incubator	Certomat	Sartorius
sonifier	Sonifier 250	Branson
sterile flow	NU-440-400E (Class II)	Biological safety cabinets
thermocycleer	T-Gradient	Biometra
ultra centrifuge	L8-70M	Beckmann
UV transilluminator	TFX-35-MC	Vilber Lourmat
vortexer	MS1 Minishaker	JK
water bath	W12D	Peter Huber GmbH

EPR CW-spectrometer (X-band):

- MiniScope MS200 with TE102 rectangular resonator, *mt* magnettech GmbH Analysemesstechnik, Berlin;

- Temperature Controller HO2, *mt* magnettech GmbH Analysemesstechnik, Berlin;

- Frequency Counter Model 3200, XL-Microwave Inc. Oakland (CA) USA.

EPR pulse-spectrometer (X-band):

- Bruker Elexsys 580 EPR spectrometer with a Bruker Flexline split-ring resonator ER 4118X_MS3, Bruker biospin GmbH, Wikingerstraße 13, Mühlburg, Karlsruhe, Germany;

- Closed cycle cryostat, ARS AF204, customized for CW and pulse EPR, ARS, Macungie, PA, USA;

- Temperature controller, Lake Shore Cryotronics, Inc., 575 McCorkle Blvd, Westerville, OH 43082-8888, USA;

- Frequency counter & X-band magnet, Bruker biospin GmbH, Wikingerstraße 13, Mühlburg, Karlsruhe, Germany;

- Vacuum pump, Pfeiffer Vacuum GmbH, Berliner Straße 43, 35614 Asslar, Germany.

All plastics laboratory materials were purchased from Falcon/Beckton Dickinson, Greiner, or Sarstedt. Glass ware was obtained from Schott. Further lab equipment is listed in **Tab. 2.2**.

2.1.2 Chemicals

Standard chemicals were purchased from Acros, Alexis Biochemicals, AppliChem, Becton Dickinson, Fluka, GE Healthcare, Gibco BRL, Invitrogen, Merck, Pharmacia-LKB Biotechnology, Roche, Roth, Serva or Sigma Aldrich. Dialysis membranes were purchased from Millipore and nitrocellulose membranes from Schleicher & Schüll. Concentratrors were purchased from Sartorius.

2.1.3 Ready-to-use reagents and kit systems

Tab. 2.2: Ready-to-use reagents and kit systems.

product	vendor	description
3-(2-iodoacetamido)-PROXYL	Acros	EPR label for site-directed spin labeling (SDSL)
5,5'-dithiobis-(2-nitrobenzoic acid), DTNB	Thermo Scientific	quantification of thiols
BioRad Protein Assay	BioRad	protein quatification
BODIPY®507/545IA	Invitrogen	fluorescence labeling
Cell Culture Lysis Reagent	Promega	cell lysis reagent
Click-iT® EdU Imaging Kit	Invitrogen	Edu staining for immunofluorescence
cOmplete protease inhibitor	Roche	protease inhibitor tablets
Cytotoxicity Detection KIT^{PLUS} (LDH)	Roche	cytotoxicity assay
Fluoprep	bioMérieux	fixation reagent for preparation of microscopic slides
Glutathione Sepharose^{TM} 4B	GE Healthcare	protein purification
His60 Ni Superflow resin	Clontech	protein purification
Hoechst 33342	Sigma Aldrich	DNA staining
jetPEI^{TM}	Polyplus transfection^{TM}	DNA transfection
JetPEI^{TM} DNA transfection reagent	Polyplus transfection^{TM}	DNA transfection
KOD hot start DNA polymerase	Novagen	PCR polymerase
Lipofectamine^{TM} 2000	Invitrogen	DNA transfection
Lipofectamine^{TM} RNAiMAX	Invitrogen	RNA transfection
Mammalian 2-Hybrid Assay Kit	Stratagene	mammalian protein interaction screening
MATra-A Reagent	IBA GmbH	RNA transfection

methanetiosulfonate spin label (MTSSL)	Alexis Biochemicals	EPR label for site-directed spin labeling (SDSL)
NucleoBond® Xtra Midi	Macherey und Nagel	plasmid DNA preparation from *E. coli*
peqGOLD Gel Extraction Kit	Peqlab	preparation from DNA from agarose gels, PCR or restrictions
peqGOLD Plasmid Miniprep KitI	Peqlab	plasmid DNA preparation from *E. coli*
peqGOLD Pwo Polymerase	Peqlab	PCR polymerase
Protein A/G PLUS Agarose	Santa Cruz Biotechnology	immuno precipitation
PureProteome™ Magnetic Beads	Millipore	immuno precipitation
Quant-iT™ PicoGreen®	Invitrogen	DNA quantification
ubiquitin agarose	Sigma Aldrich	ubiquitin binding assay
Western Lightning™ Plus-ECL	Perkin Elmer Inc.	Western Blot detection (ECL)
β-Gal Triggering Reagent	p.j.k	substrate for luminescence measurements
β-Gal-Juice PLUS	p.j.k	substrate for luminescence measurements

2.1.4 Antibodies

2.1.4.1 Primary antibodies

Tab.2.3: Primary antibodies.

antibody	species	clone/specification	dilution	manufacturer
anti-FLAG	mouse monoclonal	M2	WB 1:10000	Sigma Aldrich
anti-Gal4	rabbit monoclonal	A-712	WB 1:2000	Santa Cruz Biotechnology
anti-GFP	mouse monoclonal	Jl-8	WB 1:10000	Clontech
anti-HIS	mouse monoclonal	MMS-156R	WB 1:5000	Covance
anti-L1	mouse monoclonal	33L1-7	IF 1:10	M. Sapp
anti-L1	rabbit monoclonal	K75	IF 1:400, WB 1:1000	M. Sapp
anti-L1	mouse monoclonal	16L1312F	WB 1:300	M. Sapp
anti-L2	mouse monoclonal	33L2-1	IF 1:500, WB 1:300	M. Sapp
anti-PML	rabbit polyclonal	SC5621	IF 1:500	Santa Cruz Biotechnology
anti-SUMO	rabbit monoclonal	A-712	WB 1:250-1:500	Boston Biochem
anti-β-actin	mouse monoclonal	AC-15	WB 1:10000	Sigma Aldrich
anti-γ-tubulin	rabbit monoclonal	T3195	WB 1:10000	Sigma Aldrich

2.1.4.2 Secondary antibodies

Tab.2.4: Secondary antibodies for immunofluorescence microscopy.

antibody	species	conjugate	dilution	manufacturer
anti-mouse	goat	Alexa Fluor 488	1:400	Invitrogen
		Alexa Fluor 546	1:400	
		Alexa Fluor 647	1:125	
anti-rabbit	goat	Alexa Fluor 488	1:250	Invitrogen
		Alexa Fluor 546	1:250	
		Alexa Fluor 647	1:125	

Tab.2.5: Secondary antibodies for Western Blot.

antibody	species	conjugate	dilution	manufacturer
anti-mouse	goat	horseradish peroxydase	1:5000	Dianova
anti-rabbit	goat	horseradish peroxydase	1:10000	Dianova
anti-goat	rabbit	horseradish peroxydase	1:8000	Dianova

2.1.5 Standard buffers and solutions

DNA loading dye, 10 x:

0.42% (w/v) xylene cyanol

0.2% (w/v) OrangeG

50% (v/v) glycerole

SDS-PAGE protein loading dye, 1 x:

(based on Lämmli)

50 mM Tris pH 6.8

2% (w/v) SDS

20% (v/v) glycerol

0.1% (w/v) bromphenole blue

5% (v/v) β-mercaptoethanol

SDS-PAGE protein loading dye, 5 x:

250 mM Tris HCl pH 6.8

8% (w/v) SDS

30% (v/v) glycerol

0.2% (w/v) bromphenole blue

10% (v/v) β-mercaptoethanol

SDS-PAGE running buffer, 10 x:

0.25 M Tris pH 8.0

1.92 M glycin

1% (w/v) SDS

SDS-PAGE solution A:	30% (v/v) acrylamid
(based on Lämmli)	0.8% (v/v) bisacrylamide
SDS-PAGE solution B:	1.5 M Tris-HCl ph 8.8
(based on Lämmli)	0.4% (w/v) SDS
SDS-PAGE solution C:	0.5 M Tris-HCl ph 6.8
(based on Lämmli)	0.4% (w/v) SDS
TAE buffer, 10 x, pH 8.0:	400 mM Tris
(for DNA agarose gels)	200 mM sodium acetate
	10 mM EDTA
Western Blot transfer buffer:	25 mM Tris
	192 mM glycin
	20% (v/v) methanol
PBS/Tween:	1 x PBS
	0.1% (v/v) Tween 20
Stripping buffer:	62.5 mM Tris HCl pH 6.8
(for nitrocellulose membranes)	2% (w/v) SDS
	0.1 M β-mercaptoethanol

Ponceau S protein stain: 0.1% (w/v) Ponceau S

3% (v/v) trichloro acetic acid

2.1.6 Enzymes

Enzymes used for standard restriction of DNA were purchased from New England Biolabs and used according to the manufacturer's protocol. T4-DNA ligase was purchased from Fermentas. Benzonase® and Lysonase™ were purchased from Sigma Aldrich and Novagen.

2.1.7 DNA plasmids

2.1.7.1 DNA plasmids for L2 and SUMO1/2 protein expression and purification

Tab.2.6: DNA plasmids for HPV16 L2 and SUMO1/2 protein expression and purification.

vector	expression type	resistance	purification method	induction type	vector origin
pLexsyI-neo2-L2 his6	mammalian	Ampicillin	C-term His-tag, his beads	Tetracyclin	vector was provided by G. Spoden
pLexsyI-neo2 his10 L2 wt (codonopt)	*L. tarentolae*	Neomycin	N-term His-tag, his beads	Tetracyclin	16L2 was isolated by NdeI/KpnI-HF restriction from pcDNA3.1 NdeI L2 and inserted into the NdeI/KpnI-HF restricted target vector pLexsyI-nleo2 his10 (codonopt), which was produced by insertion of the BglII/NcoI isolated DNA fragment from pLexsyI-bleo2 his10 (codonopt) into the BglII/NcoI restricted target vector pLexsyI-neo2
pLexsyI-bleo2 his10 L2 wt (codonopt)	*L. tarentolae*	Bleomycin	N-term His-tag, his beads	Tetracyclin	16L2 was isolated by NdeI/KpnI-HF restriction from pcDNA3.1 NdeI L2 and inserted into the NdeI/KpnI-HF restricted target vector pLexsyI-bleo2 his10 (codonopt), which was produced with DNA oligos containing a codonoptimized BglII-10xhis-NdeI-NcoI sequence
pet28a pro SUMO1	*E. coli*	Kanamycin	C-term His-tag, his beads	IPTG	purchased via addgene.com, ID25101, Mikolajczyk et al.
pet28a pro SUMO2	*E. coli*	Kanamycin	C-term His-tag, his beads	IPTG	purchased via addgene.com, ID25102, Mikolajczyk et al.
pGEX-6p-1 SUMO1	*E. coli*	Ampicillin	GST-tag, glutathione beads	IPTG	SUMO1 was isolated by BamHI/XhoI restriction from pEGFP-CI-SUMO1 and inserted into the BamHI/XhoI restricted target vector pGEX-6p-1
pGEX-6p-1 SUMO2	*E. coli*	Ampicillin	GST-tag, glutathione beads	IPTG	SUMO2 was isolated by BglII/NotI restriction from pLexsy SUMO2 and inserted into the BamHI/XhoI restricted target vector pGEX-6p-1
pet19b L2 wt	*E. coli*	Ampicillin	N-term His-tag, his beads	IPTG	16L2 was isolated by NdeI/XhoI restriction from pcDNA3.1 NdeI L2 and inserted into the NdeI/XhoI restricted, de-phosphorylated target vector pet19br
pcDNA3.1 Hygro (-) his10 L2 wt	mammalian	Ampicillin	N-term His-tag, his beads	constitutive	10xhis16L2 fragment was isolated by BglII/KpnI restriction from pLexsyI-neo2 his10 L2 wt (codonopt) and inserted into the BamHI-HF/KpnI-HF restricted target vector pcDNA3.1 Hygro (-)

pcDNA3.1 (+) L2 wt his6	mammalian	Ampicillin	C-term His-tag, his beads	constitutive	L2-his_6 was isolated with BglII/NotI restriction from pLexsyI-neo2-L2 his6 inserted into a BglII/NotI restricted pCMV-HA target vector. Then, L2-his6 was isolated by EcoRI/NotI restriction and inserted into the EcoRI/NotI restricted target vector pcDNA3.1 (+)
pcDNA3.1 (+) L2 C22S his6	mammalian	Ampicillin	C-term His-tag, his beads	constitutive	vector was produced by mutagenesis PCR based on pcDNA3.1 (+) L2 wt his6
pcDNA3.1 (+) L2 C28S his6	mammalian	Ampicillin	C-term His-tag, his beads	constitutive	vector was produced by mutagenesis PCR based on pcDNA3.1 (+) L2 wt his6
pGEX-6p-1 16 L2 wt	*E. coli*	Ampicillin	GST-tag, glutathione beads	IPTG	A BamHI-16L2-EcoRI DNA fragment produced by PCR based on the pUF 16L2 vector was restricted with BamHI/EcoRI and inserted into the BamHI/EcoRI restricted target vector pGEX-6p-1

2.1.7.2 DNA plasmids for mammalian 2-hybrid interaction assays

Tab. 2.7: DNA plasmids for mammalian 2-hybrid interaction assays.

vector	resistance	characteristics	vector origin
pAD-SV40T	Ampicillin	positive interaction with p53	original vector
pAD-TRAF	Ampicillin	negative interaction wiith p53	original vector
pBD-p53	Ampicillin	positive interaction with SV40T	original vector
pCMV AD	Ampicillin	original vector for expression of the prey protein	original vector
pCMV AD-16L2 wt	Ampicillin	expression of HPV16 L2 as prey protein	L2 was isolated by EcoRI/NotI restriction from pCMV HA 16L2 and inserted into the EcoRI/NotI restricted target vector pCMV AD
pCMV AD-SUMO1	Ampicillin	expression of SUMO2 as prey protein	vector was provided by G. Spoden
pCMV AD-SUMO2	Ampicillin	expression of SUMO2 as prey protein	vector was provided by G. Spoden
pCMV BD	Ampicillin	original vector for expression of the bait protein	original vector
pCMV BD-16L2 wt	Ampicillin	expression of HPV16 L2 as bait protein	vector was provided by G. Spoden
pCMV BD-SUMO1	Ampicillin	expression of SUMO1 as bait protein	vector was provided by G. Spoden
pCMV BD-SUMO1 ΔGG	Ampicillin	expression of SUMO1 ΔGG-stop as bait protein	SUMO1 ΔGG was produced by PCR restricted with BamHI/PstI and inserted into the BamHI/PstI restricted target vector pCMV BDS
pCMV BD-SUMO2	Ampicillin	expression of SUMO2 as bait protein	SUMO2 was isolated by NotI/BamHI restriction from pCMV AD SUMO2 and inserted into the NotI/BamHI restricted target vector pCMV BD
pCMV BD-SUMO2 ΔGG	Ampicillin	expression of SUMO2 ΔGG-stop as bait protein	SUMO2 ΔGG was produced by PCR restricted with BamHI/PstI and inserted into the BamHI/PstI restricted target vector pCMV BDS
pFR-Luc	Ampicillin	luciferase expressing reporter plasmid	original vector

2.1.7.3 DNA plasmids for further L2 and SUMO1/2 characterization

Tab. 2.8: DNA plasmids for further HPV16 L2 and SUMO1/2 characterization.

vector	resistance	characteristics	vector origin
pEGFP CI	Kanamycin	expression of GFP protein in mammalian cells	original vector
pEGFP CI SUMO1	Kanamycin	expression of GFP-SUMO1 fusion protein in mammalian cells	vector was provided by G. Spoden
pEGFP CI SUMO1 ΔGG	Kanamycin	expression of GFP-SUMO1 ΔGG fusion protein in mammalian cells	SUMO1 ΔGG was isolated by BamHI/PstI restriction from pCMV BD SUMO2 and inserted into the BglII/PstI restricted target vector pEGFP CI
pEGFP CI SUMO2	Kanamycin	expression of GFP-SUMO2 fusion protein in mammalian cells	vector was provided by G. Spoden
pEGFP CI SUMO2 ΔGG	Kanamycin	expression of GFP-SUMO2 ΔGG- fusion protein in mammalian cells	SUMO2 ΔGG was isolated by BamHI/PstI restriction from pCMV BD SUMO2 and inserted into the BglII/PstI restricted target vector pEGFP CI
pUF AAV #893 16L2 K35R	Ampicillin	expression of HPV16 L2 K35R in mammalian cells	vector was provided by G. Spoden
pUF AAV #893 16L2 wt	Ampicillin	expression of HPV16 L2 wt in mammalian cells	original vector, Leder et al., 2001
pcDNA 3.1 (+) 16L2 wt	Ampicillin	expression of HPV16 L2 wt in mammalian cells	vector was provided by G. Spoden
pcDNA 3.1 Hygro (-)	Ampicillin	original vector used to adjust DNA to a faixed total amount	original vector
pcDNA 3.1 Hygro (-) 16L2 K35R (ΔSCM)	Ampicillin	expression of HPV16 L2 K35R (ΔSCM) in mammalian cells	vector was produced by mutagenesis PCR based on pcDNA 3.1 Hygro (-) 16L2 wt
pcDNA 3.1 Hygro (-) 16L2 wt	Ampicillin	expression of HPV16 L2 wt in mammalian cells	vector was provided by G. Spoden
pcDNA3.1 (+)	Ampicillin	original vector used to adjust DNA to a faixed total amount	original vector
pcDNA 3.1 Hygro (-) 16L2 286-9AAAA (ΔSIM)	Ampicillin	expression of HPV16 L2 286-9AAAA (ΔSIM) in mammalian cells	vector was produced by mutagenesis PCR based on pcDNA 3.1 Hygro (-) 16L2 wt
pcDNA 3.1 Hygro (-) 16L2 295/6AA (ΔPHOS)	Ampicillin	expression of HPV16 L2 TS296/6AA in mammalian cells	vector was produced by mutagenesis PCR based on pcDNA 3.1 Hygro (-) 16L2 wt

2.1.7.4 DNA plasmids for preparation of HPV16 pseudoviruses (PsVs)

Tab. 2.9: DNA plasmids for preparation of HPV16 pseudo virions (PsVs).

vector	resistance	characteristics	vector origin
pSHELL 16L1/L2 286-9AAAA (ΔSIM)	Ampicillin	expression of HPV16 16L1/L2 286-9AAAA (ΔSIM)	L2 ΔSIM was isolated by NheI/EcoRV restriction from pcDNA 3.1 Hygro (-) 16L2 286-9AAAA (ΔSIM) and inserted into the XbaI/EcoRV restricted target vector pSHELL 16L1/L2 wt
pSHELL 16L1/L2 K35R (ΔSCM)	Ampicillin	expression of HPV16 16L1/L2 K35R	L2 ΔSCM was isolated by NheI/EcoRV restriction from pcDNA 3.1 Hygro (-) 16L2 K35R (ΔSCM) and inserted into the XbaI/EcoRV restricted target vector pSHELL 16L1/L2 wt
pSHELL 16L1/L2 TS295/6AA (ΔPHOS)	Ampicillin	expression of HPV16 16L1/L2 TS295/6AA (ΔPHOS)	L2 ΔPHOS was isolated by NheI/EcoRV restriction from pcDNA 3.1 Hygro (-) 16L2 295/6AA (ΔPHOS) and inserted into the XbaI/EcoRV restricted target vector pSHELL 16L1/L2 wt

pSHELL 16L1/L2 wt	Ampicillin	expression of HPV16 16L1/L2 wt	original vector
pUF3 AAV #893 16L1 wt	Ampicillin	expression of HPV16 L1 wt	original vector, Leder et al., 2001
pcDNA 3.1 (+) Luciferase	Ampicillin	luciferase expression	original vector, Schneider et al., 2011

2.1.8 PCR primers, DNA oligonucleotides, siRNAs

Tab. 2.10: Mutagenesis primers, sequencing primers, DNA oligonucleotides, and siRNAs. DNA or RNA oligonucleotides were purchased from Sigma, biomers, or eurofins.

mutagenesis primers	**sequence**
16 L2 3'-Stop KpnI	5'-TTT GGT ACC TCA GGC GGC CAG GCT CAC GTC-3'
16 L2 K35R forward	5'-GCA CAG GCC CGC CCT GGC GGC GAG GAG GAC CGG CAT CAG G-3'
16 L2 K35R reverse	5'-CCT GAT GCC GGT CCT CCT CGC CGC CAG GGC GGG CCT GTG C-3'
L2 C22S forward	5'-CTG TAC AAG ACC AGC AAG CAG GCC GG-3'
L2 C22S reverse	5'-CTG GGT GGC GCT GGC CCT CTT GGT CC-3'
L2 C28S forward	5'-CAG GCC GGC ACC AGC CCC CCC GAC ATC-3'
L2 C28S reverse	5'-CTT GCA GGT CTT GTA CAG CTG GGT GG-3'
L2 ΔPHOS forward	5'-G CAC AGG CCC GCC CTG GCG GCG AGG AGG ACC GGC ATC AGG-3'
L2 ΔPHOS reverse	5'-CCT GAT GCC GGT CCT CCT CGC CGC CAG GGC GGG CCT GTG C-3'
L2 ΔSIM forward	5'-CGA CCC CGA CTT CCT GGA CGC CGC CGC CGC CCA CAG GCC CGC CCT GAC C -3'
L2 ΔSIM reverse	5'-GGT CAG GGC GGG CCT GTG GGC GGC GGC GGC GTC CAG GAA GTC GGG GTC G-3'
NdeI-16 L2his forward	5'-ATT CAT ATG AGG CAC AAG AGG AGC GCC-3'
SUMO1 ΔGG forward	5'-ATT GGA TCC ATG TCT GAC CAG GAG GCA AAA C-3'
SUMO1 ΔGG reverse	5'-AGC CTG CAG TCA CGT TTG TTC CTG ATA AAC TTC AAT C-3'
SUMO2 ΔGG forward	5'-ATT GGA TCC ATG GCC GAC GAA AAG CCC AAG G-3'
SUMO2 ΔGG reverse	5'-AGC CTG CAG TCA CGT CTG TTG GAA CAC ATC-3'
sequencing primers	**sequence**
BGH reverse	5'-TAG AAG GCA CAG TCG AGG-3'
CMV forward	5'-CGC AAA TGG GCG GTA GGC GTG-3'
pGEX reverse	5'-CCG GGA GCT GCA TGT GTC AGA GG-3'
pMK1-5' pUF3 forward	5'-AAG CTG CGG AAT TGT ACC CG-3'-3'
pUF reverse	5'-ACA GAT GGC TGG CAA CTA GAA GG-3'
T7 forward	5'-AAT ACG ACT CAC TAT AGG-3'
oligonucleotides	**sequence**
his_{10}-L2 forward	5'-GA TCT GCC ATG GGC CAC CAC CAC CAC CAC CAC CAC CAC CAC CAC AGC AGC GGC CAC ATC GAC GAC GAC GAC AAG CAT ATG C-3'
his_{10}-L2 reverse	5'-CA TGG CAT ATG CTT GTC GTC GTC GTC GAT GTG GCC GCT GCT GTG GTG GTG GTG GTG GTG GTG GTG GTG GCC CAT GGC A-3'
siRNAs	**sequence**
SUMO1 siRNA	CAAAGAAUCAUACUGUCAAtt
SUMO2 siRNA #1	GUUGGAAAUGGAGGAUGAAtt
SUMO2 siRNA #1	GAGGCAUACACCACUUAGUtt
luciferase siRNA (GL3)	CUUACGCUGAGUACUUCGAtt
control siRNA	AllStars Negative Control siRNA (Quiagen)

2.1.9 Synthetic L2 peptides

The synthetic L2 SIM peptides used for this work were purchased from GenScript (USA). Quantity was about 1-4 mg with >95% purity, N-terminal acetylation, and C-terminal amidation.

Tab. 2.11: Synthetic L2 SIM peptides.

name	sequence
L2 SIMCys	APDPDF**LDIVAL**HRPA**C**TSRRT
L2 SIM	APDPDF**LDIVAL**HRPALTSRRT
L2 CysSIM	I**C**PDPDF**LDIVAL**HRPALTSRRT

2.1.10 Cell strains, cultures, and additives

2.1.10.1 Mammalian tissue cultures

HeLa: Human cervix carcinoma cell line, HPV18 positive (Scherer, Syverton et al. 1953).

HaCaT: Human, spontaneously immortalized epithelial cell line (Boukamp, Petrussevska et al. 1988).

HEK293/T/TT: Cell line derived from the human embryonic kidney cell line 293, without or with one or two copies of the large T-Antigen from SV40 (Graham, Smiley et al. 1977; Pear, Nolan et al. 1993; Buck 2004).

Tab. 2.12: Human cell culture additives.

product	manufacturer	characteristics
0.05% Trypsin/0.02% EDTA	Gibco	detachment of cells
Ciprofloxacin (2 mg/ml)	Fresenius Kabi	cell medium additive
Dulbecco's Modified Eagle Medium (DMEM)	Gibco	cell culture medium
fetal calf serum (FCS)	Gibco	cell medium additive
Hygromyvin B	Roth	selection antibioticum for HEK293TT cells
nonessential amino acids (100 x)	PAA Laboratories	cell medium additive
Penicillin/Streptomycin	Invitrogen	cultivation antibiotics

2.1.10.2 Bacteria culture

Tab. 2.13: Bacteria strains.

strain	resistances	special features	manufacturer
Bl21-CodonPlus(DE3)-RIL	Cam	Cam: for rare codons additional plasmid	Novagen
NEB 5-alpha chemically competent cells	-	for cloning experiments and DNA preparation	New England Biolabs
rosetta 2 DE3	Cam	Cam: for rare codons additional plasmid, 2: codon bias	Novagen

rosetta-gami 2 DE3	Tet, Str, Cam	Cam: for rare codons additional plasmid, Tet: selectible S-S bonds, 2: codon bias	Novagen
rosetta-gamiB DE3	Kan, Tet, Cam	Cam: for rare codons additional plasmid, Tet: selectible S-S bonds, B: expression control	Novagen
SoluBL21	-	specialized for soluble protein expression	Genlantis
TG1 Phage Display Electrocompetent Cells	-	for cloning experiments and protein expresssion	Lucigen
XL10-Gold Ultracompetent cells	-	for large vector cloning experiments and DNA preparation	Stratagene

E. coli strains were routineously cultivated in LB (Luria Bertani) medium. For solid growth media, 1.5% (w/v) agar was added before preparation of the plates.

LB (Luria Bertani) medium:

0.5% (w/v) yeast extract

1% (w/v) trypton

1% (w/v(NaCl

pH 7.0

low salt LB medium:

0.5% (w/v) yeast extract

1% (w/v) trypton

0.5% (w/v(NaCl

pH 7.0

2.1.11 Molecular weight markers

DNA was routineously characterized on agarose gels using the GeneRuler™ 1 kB DNA Ladder (Fermentas) (Fig. 2.1).

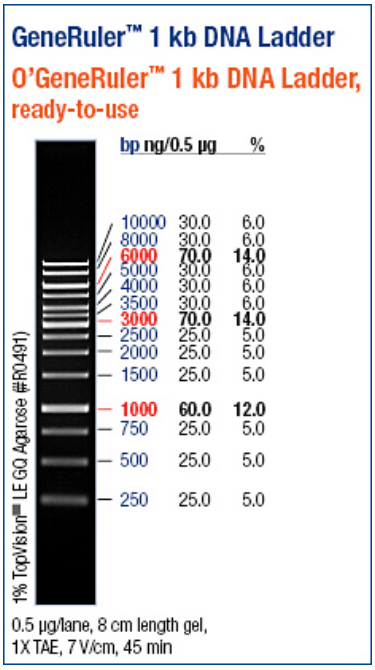

Fig. 2.1: DNA ladder for agarose gelelectrophoresis (GeneRuler™ 1 kB DNA Ladder, Fermentas).

For protein SDS-PAGE the *Page Ruler™ Prestained Protein Ladder* was used (Fermentas, Fig. 2.2).

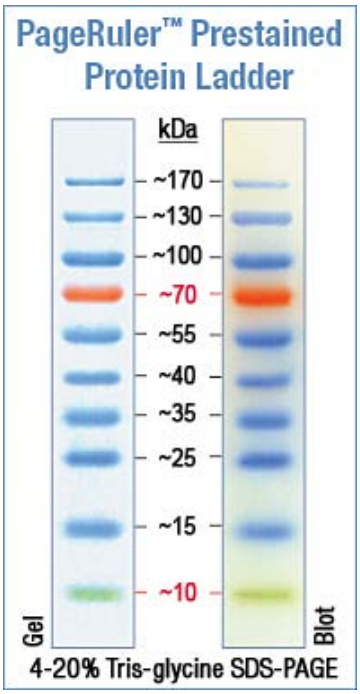

Fig. 2.2: Prestained protein ladder for SDS-PAGE (*Page Ruler™ Prestained Protein Ladder*, Fermentas).

2.2 Methods

2.2.1 Working with DNA

2.2.1.1 Fragmentation of DNA with restriction endonucleases

A typical amount of 1 to 5 µg DNA was mixed with ultra pure water, reaction buffer, BSA, and the restriction endonuclease(s) and incubated for 1-2 h at 37 °C or the temperature of maximum enzymatic activity (Table 2.14).

Tab. 2.14: Reaction mix for enzymatic DNA restriction.

DNA	**target**	**insert**
sample volume	20 µl	40 µl
DNA	1 µg	5 µg
10 x reaction buffer	2 µl	4 µl
BSA (1 mg/ml)	2 µl	4 µl
enzyme	2 µl max	4 µl max
H_2O	ad 20 µl	ad 40 µl

2.2.1.2 Isolation of DNA fragments by agarose gel electrophoresis

After DNA restriction with restriction endonucleases or to check DNA plasmids, the DNA was diluted in an appropriate volume of H_2O, mixed with 10 x loading dye, and loaded onto 0.8-2.5% (w/v) agarose gels (containing about 0.5 µg/ml ethidium bromide) prepared with TAE buffer. The gels were run at 90 V (10 V per cm agarose gel).

TAE buffer:

40 mM Tris

20 mM acetic acid

1 mM EDTA.

2.2.1.3 Preparation of DNA from agarose gels

The isolation of DNA products from agarose gels was performed with a peqGOLD Gel Extraction Kit according to the manufacturer's protocol.

2.2.1.4 Ligation of DNA fragments

The DNA fragments were mixed with T4 DNA ligase reaction buffer and T4 DNA ligase and incubated for 1 h at 37 °C, over night at 16 °C, or over the weekend at 4 °C. The reaction was stopped and the enzyme was inactivated by incubation for 15 min at 65 °C.

Tab. 2.15: T4 DNA ligation.

DNA	45 µl (gel isolated DNA)
10 x ligase buffer	5 µl
T4 DNA ligase	5 µl

2.2.1.5 Transformation of competent *E. coli* cells

50-100 µl chemically competent *E. coli* cells were thawed on ice and mixed with 20-30 µl of the pre-cooled and inactivated DNA ligation mix. The DNA content should not exceed about 200 ng DNA. The sample was incubated for 30 min on ice followed by a 30 - 60 s heat shock at 42 °C depending on the sample volume. The sample volume was filled up with LB medium to give a final volume of 1 ml and incubated for 1 h at 37 °C.

2.2.1.6 Plating of *E. coli* cells on LB agar plates

After transformation or longer storage of *E. coli* cultures, aliquots or the whole transformation mix were transferred onto LB agar plates (LB/ 1.5% (w/v) agar) containing antibiotics for selection (Table 2.16). Small culture aliquots (up to 100 µl) were directly applied onto the plate. To apply larger amounts of cells, the culture was centrifuged for one min at 6,000 g. The cell pellet was resuspended in residual 50-100 µl culture medium and applied onto the plate. The plates were incubated bottom up at 37 °C over night.

Tab. 2.16: Selection antibiotics used for *E. coli* cultures/agar plates.

antibiotics	ampicillin	kanamycin	tetracyclin	chloramphenicol	streptomycin
final concentration	100 µg/ml	50 µg/ml	12.5 µg/ml	34 µg/ml	50 µg/ml

2.2.1.7 Preparation of starter bacteria cultures

After transformation of *E. coli* cells and plating on LB agar plates, single bacteria colonies were used to inoculate starter bacteria cultures. After cultivation for 10-16 hours at 37 °C, the cultures

produced enough cell material for DNA plasmid preparation or to inoculate large scale bacteria cultures for expression of recombinant proteins.

2.2.1.8 Plasmid DNA preparation

Mini plasmid DNA preparations for characterization of DNA by restriction enzymes were performed with a peqGOLD Plasmid Miniprep Kit according to the manufacturer's protocol based on starter cultures, which were incubated over night at 37 °C. Midi scale plasmid DNA preparations were performed with a NucleoBond® Xtra Midi kit (Macherey und Nagel) based on 100-200 ml cultures, which were prepared by 1:1000 dilution of starter cultures, and incubated over night at 37 °C. After incubation, the cells were centrifuged at 6,000 g. Cell lysis and DNA isolation were performed according to the manufacturer's protocol. The amount of isolated DNA (A_{260}) and purity (A_{260}/A_{280}) was determined with a UV spectrophotometer.

2.2.1.9 Standard polymerase chain reaction (PCR)

PCR reactions were prepared according to a standard protocol in thin walled PCR tubes (Tab. 2.17).

Tab. 2.17: Standard PCR reaction mix for amplification of target DNA.

PCR component	**amount**
template DNA	100 ng
forward and reverse primer (10 µM or 10 pmol/µl)	1.5 µl
dNTP mix (10 mM)	1 µl
10 x PCR buffer	5 µl
Pwo polymerase	1 µl
H_2O	ad 50 µl

The PCR was performed according to a standard thermocycler protocol (Tab. 2.18).

Tab.2.18: Thermocycler program for standard PCR amplification of target DNA.

time	temperature	step	
5 min	95 °C	denaturation	
1 min	95 °C	denaturation	30-40 x
1 min	T_m-5 °C	annealing	
30 s - 120 s/Kb	65-72 °C	elongation	
5 min	65-72 °C	final elongation	

2.2.1.10 Mutagenesis PCR

Mutagenesis PCR was performed to selectively introduce DNA mutations into a DNA region of interest. Here, the usage of two complementary DNA primers containing the mutation(s) leads to a replication of the entire DNA plasmid and insertion of the mutations into the replicated DNA. Mutagenesis PCR was performed based on the peqGOLD Pwo-DNA-Polymerase kit, the Phusion® Site-Directed Mutagenesis Kit (Finnzymes, ThermoScientific), or the Stratagene Pfu DNA polymerase kit (Tab. 2.19).

.

Tab.2.19: Mutagenesis PCR reaction mix.

PCR component	**amount**
10 x PCR buffer	5 µl
dsDNA template	5-50 ng
forward and reverse primer (10 µM or 10 pmol/µl)	1.5 µl
dNTP mix (10 mM)	1 µl
Pfu Turbo DNA polymerase	1 µl
H_2O	ad 50 µl

The reaction protocol was changed according to the specificities of a mutagenesis PCR. Here, less final DNA is needed, since no subcloning steps are needed afterwards and the number of repeated steps is lowered to 20. In contrast, the elongation time has to be expanded because the whole plasmid is replicated during PCR (Tab. 2.20).

Tab.2.20: Thermocycler program for mutagenesis PCR.

time	temperature	step	
5 min	95 °C	denaturation	
1 min	95 °C	denaturation	20 x
45 s	52-60 °C	annealing	
2 min/Kb	68 °C	elongation	
5 min	65-72 °C	final elongation	

After the PCR, the template DNA was digested by DpnI restriction for 3 h at 37 °C. Finally, 2-5 µl DNA were transformed into 100 µl competent *E. coli* cells (NEB-5-alpha).

2.2.2 Cultivation of human adherent cells

2.2.2.1 Cultivation of cell lines

Human HeLa, HaCaT, HEK293, HEK293T, and HEK293TT cells were used. Cell cultivation was always performed under sterile conditions. Cell incubation was performed at 37 °C and 5% CO_2. The cells were cultivated in single layer flasks in Dulbecco's modified Eagle Medium (DMEM) containing nonessential amino acids, 10% (v/v) fetal bovine serum (FCS), and Pen/Strep (Roth). For improved selection of HEK293TT cells, 200 µg/ml Hygromycin B were added to the medium once a week. Passaging of the adherent and confluent cells was performed by removal of the cell medium and a washing step with PBS/2.5 mM EDTA. Incubation with 0.05% Trypsin/0.02% EDTA (2-10 min, 37 °C) was used for detachment of the cells. Then, the cells were resuspended in an adequate amount of cell medium for trypsin neutralization and separated by repeated pipetting. Finally, the cells were either transferred into new cell medium for further cultivation or counted for precise plating for following experiments.

2.2.2.2 Cell counting using the Neubauer chamber

Cell counting was performed with 10 µl of freshly detached and separated cells in a Neubauer chamber. The sum of the cells of the four large squares was divided by 400 to obtain the cell concentration in millions of cells/ml.

2.2.2.3 Cultivation of new cells

After 30 to about 50 passages, some cell lines develop significantly slower growth speed and/or differences in morphology. In order to establish maximum constant conditions for the experiments, new cells were used after 2-3 months of cell cultivation. Therefore, cell stocks, which were stored in cryo vials in liquid nitrogen in 90% FCS/10% DMSO, were thawed as quickly as possible and mixed with DMEM/10% FCS to get a final volume of about 10 ml. Then, the cells were centrifuged for 5-10 min at 300 g at RT. The supernatant containing the toxic DMSO was discarded. The remaining cell pellet was resuspended in DMEM/10% FCS and transferred into a cultivation flask containing additional culture medium for further cultivation.

2.2.2.4 Preparation of frozen cell aliquots

The following protocol was used for preparation of five cell stocks from one big culture flask. For storage of cell stocks, freshly cultivated cells were brought to a late logarithmic growth phase (about 70-80% confluency) in a large culture flask. Then, the cells were detached and separated as described before. The cells were taken up in DMEM/10% FCS and centrifuged 5-10 min at 300 g and RT. The supernatant was discarded and the cells were resuspended in 5 ml pre cooled 90% FCS/10% DMSO. Afterwards, 1 ml aliquots of the cell suspension were transferred into cryovials. The vials were stored for three days in freeze boxes containing isopropanol at -80 °C to guarantee a slow and linear decrease of temperature. Finally, the vials were transferred into liquid nitrogen storage dewars.

2.2.2.5 DNA transfection

For (co-) transfection of DNAs into mammalian tissue cells, different standard transfection kits were used. HeLa and HEK293(T) cells were transfected with Lipofectamine 2000 (LF2000). DNA transfection was performed according to the manufacturer's protocol. Briefly, the appropriate amount of LF2000 (75% of the recommended amount was used) was incubated with DMEM for 5 min. The DNA was also pre-diluted and incubated in DMEM. After addition of the LF2000 to the DNA solution, the mixture was incubated for 20 min at RT. Meanwhile, the cell medium was changed. Then, the transfection mixture was applied onto the cells. After 4 h, the culture medium was changed again. Protein expression was allowed to proceed for 24 h until the cells were harvested or another working step was performed. HEK293TT and HaCaT cells were transfected with MaTra transfection reagent. Analog to transfections with Lipofectamine 2000, separate mixtures of MaTra reagent and DNA in DMEM were prepared and incubated for 5 min. Then, the mixtures were unified and incubated for 20 min. After a medium change, the transfection mixture was added onto the cells and the cell flask was placed on magnet plates for 15 min at RT followed by standard incubation at 37 °C. An optional medium change was performed 5 h post transfection.

2.2.2.6 siRNA transfection

For siRNA-based knockdown experiments, specific double stranded siRNAs (20-25 nucleotides) were used for degradation of the mRNA of the corresponding protein of interest. Therefore, transfection of siRNAs was performed with Lipofectamine RNAiMAX according to the manufacturer's protocol. Briefly, siRNA and Lipofectamine RNAiMAX were prepared in separate tubes together with DMEM. Then, the preparations were mixed and incubated for 15 min at RT. Meanwhile, a medium change

was performed. Hereafter, the transfection mixtures were added onto the cells and transfection was performed for 24-48 h. The final siRNA concentration was adjusted to 30 nM. For standard siRNA transfection, 50,000-100,000 cells (HeLa and HaCat) were cultivated in 24-well format. Depletion of the target proteins was characterized by immunodetection or with fluorescence measurements for GFP-fused protein targets.

2.2.2.7 Cell harvest

The cell medium was discarded and the cells were washed with PBS/2.5 mM EDTA. Then, 0.05% Trypsin/0.02% EDTA (2-10 min, 37 °C) was used for detachment of the cells. Hereafter, a fourfold excess of DMEM/10% FCS was used for neutralization of the trypsin. The cells were centrifuged for 5-10 min at 300 g at 4 °C. The supernatant was discarded and the cells were resuspended in 10 ml PBS containing protease inhibitors. After an additional centrifugation for 5-10 min at 300 g at 4 °C, the supernatant was discarded again and the cell pellet was frozen for at least 1 h at -80 °C until follow up experiments were performed.

2.2.3 Cultivation of *Leishmania tarentolae*

Expression of recombinant HPV16 L2 protein was partly performed with the LEXSinduce2 Eucaryotic Protein Expression kit (Jena Biosciences) based on *Leishmania tarentolae*. The system combines the features of eukaryotic protein expression and modification machinery with prokaryotic robustness. The system offers high success rates for protein expression, large-scale compatibility, and mammalian-type post translation modifications (PTMs) like e.g. N-glycosylation. The following chapters describe the experimental outline for recombinant protein expression based on the LEXSY system.

2.2.3.1 Cultivation of *Leishmania tarentolae* cell lines

For this work, the *L. tarentolae* original strain T7-TR was used. The aerobic LEXYSY host and expression strains were cultivated in the dark at 26 °C as suspension culture in LEXSY BHI complex medium. For cultivation, hemin was added as well as penicillin and streptomycin to inhibit bacterial infections. Maintenance of T7 polymerase and TET repressor genes was achieved by addition of LEXSY NTC and hygromycin. For preparation of standard growth medium, 500 ml LEXSY BHI medium were prepared by dissolving 18.5 g LEXSY BHI powder in 500 ml H_2O and autoclaving for 15 min at 121 °C. Then, 2.5 ml Pen-Strep (200 x stock), 1 ml Hemin (500 x stock), 500 µl LEXSY NTC (1000 x

stock), and 1 ml Hygromycin (1000 x stock) were added. For selection of recombinants, bleomycin (100 µg/ml) or neomycin (50 µg/ml) was added from 1000 x stock solutions. Thereafter, the cells were cultivated as continuous suspension culture with regular dilutions of 1:5 to 1:20. Best results were achieved by 1:10 dilutions of 10 ml cell cultures on Monday, Wednesday, and Friday with ventilated tissue culture flasks. Large-scale cultivation was performed in Erlenmeyer flasks in an incubator at approximately 140 rpm (culture volumes: 50-1000 ml).

Standard BHI growth medium:

3.7% (w/v) LEXSY BHI powder

50 units/ml penicillin and streptomycin

5 µg/ml hemin

100 µg/ml LEXSY NTC

100 µg/ml LEXSY hygromycin

2.2.3.2 Cultivation of new cells

After long-term storage of *L. tarentolae* glycerol stocks at -80 °C, the cryo-vials were thawed on ice. Then the entire content was transferred into 10 ml fresh LEXSY BHI medium with appropriate antibiotics. The culture was centrifuged for 5 min at 2,000 g and the pellet was resuspended in 5-10 ml BHI medium for further cultivation. First dilution was performed when the culture got turbid or after maximal four days.

2.2.3.3 Preparation of frozen cell aliquots

The LEXSY strains were stored at -80 °C in 20% (v/v) glycerol. For preparation of six glycerol stocks 2.4 ml autoclaved glycerol (80% (v/v)) were mixed with 7.2 ml LEXSY suspension culture from mid growth phase (4-8 x 10^7 cell/ml, OD_{600} ≈1.2-1.8) in a 15 ml tube. Then, 1.6 ml aliquots were transferred into 2 ml cryo tubes and incubated for 10 min at RT, then for 1 h on ice, over night at -20 °C, and, finally stored at -80 °C.

2.2.3.4 Transformation of the T7-TR host

For transformation of the LEXSY T7-TR host cells with the respective LEXSY expression plasmids, a T7-TR culture was diluted 1:3 the day before transfection. On the day of transfection, the OD was checked (optimal OD_{600} ≈ 1.4) and the cells were centrifuged for 5 min at 2000 g at RT. Half of the supernatant was removed and the pellet was resuspended in the residual medium. The cells were incubated on ice for 10 min. Meanwhile, about 3-8 µg DNA of the SwaI restricted and gel isolated expression fragment were pre-incubated in tubes on ice in a total volume of 50 µl H_2O. Then, 350 µl aliquots of the cell suspension were transferred into the DNA tubes, pipetted up and down 3-4 times and further transferred into precooled electroporation cuvettes (d=2 mm) without formation of air bubbles. The outer surface of the cuvettes was dried and eletroporation was performed at 450 V and 450 µF with pulse times of about 5-6 ms. After electroporation, the cuvettes were incubated on ice for 10 min. Finally, the transformations were transferred into 5-10 ml fresh LEXSY BHI medium with a Pasteur pipette and incubated over night at 26 °C.

2.2.3.5 Selection of transgenic LEXSY T7-TR strains

In this work, clonal selection was used for establishment of expression strains. Therefore, 1-4 aliquots à 2 ml of the overnight culture after T7-TR transformation were centrifuged for 5 min at 2,000 g at 20 °C. The cell pellet was resuspended in 50-100 µl of residual medium before the cells were spread carefully on autoclaved nitrocellulose filters placed on top of freshly prepared LEXSY BHI agar plates supplemented with the respective selection antibiotics. The plates were sealed with parafilm and incubated bottom up at 26 °C. After 5-8 days, small colonies appeared and were grown until they reached diameters of about 2 mm after 2-3 additional days. Then, about 200 µl selective growth medium were inoculated with cell material (inoculation with sterile pipette tips) and incubated for 1-2 days at 26 °C in 96-well plates. The cell clones were expanded into 6-, 12-or 24-well cultures. Meanwhile, aliquots of the cell clones were grown to check expression of the target protein after induction with tetracycline (10 µg/ml) and expression for at least 48 h. For immunodetection of the target protein, the tetracycline induced cell suspensions were centrifuged for 5 min at 2000 g before the cell pellets were resuspended in 2.5 x SDS-PAGE loading dye and prepared for SDS-PAGE. Strains with maximal expression of the target protein were expanded to 10 ml cultures and used for large-scale protein expression or cryoconservation.

preparation of BHI agar plates (2 plates):

prepare 25 ml medium

17.75 ml 2xLEXSY BHI

5 ml inactivated FCS

2 ml 1M Hepes pH 7.4

250 µl penstrep

100 µl hemin

100 µl hygromycin

50 µl NTC

50 µl selective antiobiotics (bleomycin or neomycin)

The mixture was incubated at 37 °C. Meanwhile, 2% (w/v) BACTO-Agar (DIFCO) was melted in the micro-wave and kept at 55 °C (10 min). For plating, 25 ml agar was mixed with the 25 ml BHI medium and 25 ml were distributed per plate. After solidification, the plates were dried for 10 min and sterile nitrocellulose membranes were applied onto the BHI agar. Then, the plates were ready for clonal selection of the T7-TR transformations.

2.2.3.6 Expression of recombinant protein

For large scale expression of recombinant protein from *L. tarentoae,* 90 ml BHI medium containing selection antibiotics were inoculated with 10 ml of the respective expression strain. At the point of inoculation, protein expression was induced by addition of 10 µg/ml tetracycline. The culture was cultivated for 48 h at 28 °C at 140 rpm in an Erlenmeyer flask. Then, the culture was diluted 1:10 into 900 ml BHI medium containing 10 µg/ml tetracycline (with antibiotics). After additional 48 h of cultivation at 28 °C at 140 rpm, the cell suspension was centrifuged in a Sorvall GSH rotor for 10 min at 2000 g and 20 °C. The cell pellets were resuspended in 1xPBS and aliquoted into 15 ml tubes for long term storage of frozen cell pellets.

2.2.4 Expression of GST or his fusion proteins in *E. coli*

Production of GST or His fusion proteins for protein pulldown assays or affinity purifications was performed with the *E. coli* expression system. For expression of recombinant proteins, the target expression vector was introduced into *E. coli* protein expression strains (Rosetta 2(DE3)) based on the standard transformation protocol presented above. Then, a 5 ml over night starter culture (LB medium with antibiotics) was inoculated with a single colony. The overnight culture was expanded to 200 ml and incubated at 37 °C until the OD_{600} was about 0.6-1. Hereafter, 800 ml LB medium were added and protein expression was induced by addition of 1 mM Isopropyl-β-D-thiogalactopyranosid (IPTG). Protein expression was allowed to proceed for 4 h at 28 °C for GST-SUMO1/2 and for 16 h at 16 °C for SUMO1/2-his_6. The cultures were centrifuged for 20 min at 4 °C and 6,000 g. The supernatants were discarded and the pellets resolubilized in cold PBS and divided into aliquots resembling 100 ml cell culture. After an additional centrifugation step, the cell pellets were frozen at -80 °C for further applications.

2.2.5 Proteinbiochemical methods

In this section, standard assays to analyze protein solubilization and purification are described as well as follow up experiments for characterization of affinity purified proteins and protein pulldown assays.

2.2.5.1 Protein solubilization assay

To characterize solubilization of HPV16 L2 expressed in different protein expression systems the respective cells were harvested according to the standard protocols described above. Lysis of the harvested cell pellets was performed by sonication in the respective lysis buffers on ice (at least 5 x 20 s, 30% duty cyle, 30% output) followed by incubation for at least 20 min at 4 °C. The lysis buffers contained well defined amounts of detergents, reduction agents, and salt to stabilize the target protein, and were compatible with optional follow-up affinity purification of proteins. To test protein solubility, the cell lysates were centrifuged for 10 min at 10,000 g and 4 °C. The supernatants were subjected to ultracentrifugation for 1 h at 100,000 g and 4 °C in a 70Ti rotor. The pellet was resuspended in a 10% volume (with respect to the total volume of lysate) 2.5 x SDS-PAGE loading dye. For SDS-PAGE and immunodetection, comparable amounts of the resuspended pellet and the supernatant were characterized to compare the fraction of soluble L2 protein in the UZ supernatant with the amount of insoluble L2 protein in the UZ pellet.

2.2.5.2 Native affinity purification of SUMO1/2-his$_6$

For medium-scale SUMO1/2-his$_6$ purification, 100 ml culture pellets of SUMO1-his$_6$ or SUMO2-his$_6$ expressed in the *E. coli* were thawed on ice and lysed in 4 ml his lysis buffer (20 mM Tris pH 8.0, 500 mM NaCl, 5 mM imidazole, protease inhibitors: aprotinin, leupeptin, pepstatin (all 0.1 µg/ml), phenylmethylsulfonylfluorid (PMSF, 0.2 µM)), sodium fluoride (NaF,0.2 µM)). After sonication on ice (5 x 20 s, 30% duty cycle, 30% output, large top piece), the lysate was incubated for 30 min (wheel, 4 °C). Then, the lysate was centrifuged for 20 min at 22,000 g at 4 °C. For the subsequent affinity purification based on Ni-NTA beads, 200 µl Ni-NTA slurry (Clontech) were washed with 300 µl H_2O, equilibrated with 500 µl his lysis buffer in gravity columns (BioRad), and loaded with the lysate. The flowthrough was applied onto the column for a second time. The column was washed with 10 ml his wash buffer (20 mM Tris pH 8.0, 500 mM NaCl, 35 mM imidazole). Protein elution was performed with 800 µl elution buffer (20 mM Tris pH 8.0, 500 mM NaCl, 350 mM imidazole).

2.2.5.3 Denaturing affinity purification of HPV16 L2 expressed in *L. tarentolae*

For HPV16 L2 purification from *L. tarentolae*, denaturing his affinity purification was used. Therefore the cells of a 50 ml culture were resuspended in 3.5 ml 1xPBS pH 7.4/ 500 mM NaCl/ 1% Triton X-100. The cells were lysed by sonication (4 x 1 min with 1 min breaks on ice, 30% output, 30% duty cycle, large sonication tip) and incubated for 20 min at 4 °C. Then ultra centrifugation was performed for 1 h at 100,000 g and 4 °C. The pellet was resuspended in 6 M guanidine HCl pH 8.0 containing 10 mM imidazole by sonication. Then, the lysate was incubated with Ni NTA agarose (Clontech) for 2.5 h at RT in the purification column. The residual buffer was discarded by gravity flow and the beads were washed with 5 ml 6 m Guanidine HCl pH 8.0/ 30 mM imidazole. For elution of the target protein, 800 µl 8 M Guanidine HCl pH 4.6/500 mM imidazole were added. The protein content was determined by Bradford assaying and SDS-PAGE with 1:10 dilutions of the protein solutions due to the incompatibility of concentrated guanidine HCl solutions with SDS-PAGE.

2.2.5.4 Denaturing affinity purification of HPV16 L2 expressed in human cell lines

Large scale L2 preparation was based on denaturing affinity purification of a L2-his fusion proteins. Therefore, a cell pellet obtained after L2 expression in two or three 15 cm plates HEK293 or HEK293T cells was thawed on ice and resuspended in 3.5 ml lysis buffer. After sonication (5 x 20 s, 30% duty cycle, 30% output, large sonication tip), the lysate was incubated for 30 min at 4 °C in siliconized tubes. Then the lysate was centrifuged for 1 h at 100,000 and 4 °C in an SW60 rotor. The supernatant was discarded and the pellet was resuspended in 1.5 ml 6 M guanidine HCl (10 mM imidazole) after

one freeze-thaw cycle and sonication. The lysate was centrifuged for 20 min at 22,000 g and RT and the supernatant was used for denaturing purification. Therefore, 200 µl Ni-NTA beads slurry (Clontech) were washed in a polypropylene column (BioRad) with three volumes H_2O and equilibrated with five volumes guanidine HCl pH 8.0 before the cleared lysate was applied onto the column. The flowthrough was applied onto the column, again. Then, the column was washed with 100 column volumes of guanidine HCl pH 8.0/ 35 mM imidazole. Finally, the target protein was eluted with 800 µl guanidine HCl pH 8.0/500 mM imidazole.

Lysis buffer:

500 mM NaCl

1% (w/v) Triton X-100

1 mM DTT

50 mM Tris HCl, pH 8.0

2.2.5.5 Bradford assay

Protein quantification was routinely performed based on a Bradford protein quantification kit (BioRad). Therefore, 5 µl protein solution were added to 795 µl H_2O. 200 µl ready-to-use Bradford reagent were added and the mixture was incubated for 10 min at RT. Finally, the OD_{595} was determined and protein concentration was calculated according to calibration curves obtained with BSA. Additionally, protein concentration was checked with a Nanodrop (ND1000) device based on the theoretical extinction coefficients of the target proteins (in cm^{-1} M^{-1}, L2: 0.647, SUMO1/2: 0.25, L2 SIM peptides: 0.046).

2.2.5.6 SDS PAGE

For protein characterization by Coomassie staining or immunodetection, the proteins have to be separated according to their molecular weight. This was done by SDS PAGE (sodium dodecylsulfate polyacrylamid gel electrophoresis)(Laemmli 1970). One-dimensional separation of proteins is thereby realized under denaturating conditions in a gel system containing an upper stuffer gel and a lower separation gel. The separation of the proteins theoretically only depends on the molecular weight of the proteins without larger contributions of intrinsic protein charges. For standard SDS-PAGE, gels

with a diameter of 1 mm were prepared. First, the separation gel was cast and covered with 1 ml isopropanol to provide a planar gel boundary. After polymerization, the ispropanol was discarded, and the stuffer gel solution was applied on top of the separation gel together with the gel-comb. After polymerization, the gels were either directly used or stored under wet atmosphere at 4 °C.

separation gel:	**stuffer gel:**
10-12% (w/v) acrylamid	5% (w/v) acrylamid
1% (w/v) SDS	0.1% (w/v) SDS
1% (w/v) APS	0.8% (w/v) APS
0.05% (w/v) TEMED	0.04% (w/v) TEMED
pH 8.8	pH 6.8

Before SDS-PAGE, the protein solutions were mixed with protein loading buffer and heated for 5-10 min at 95 °C. A maximum volume of 100 µl was applied onto the gels. The gels were run at 200 V/ 75 mA for 3-4 h or 60 V/ 12 mA overnight in 1x running buffer. After SDS-PAGE, the gels were subjected either to protein staining (Coomassie, DirectRed81) or transfer blotting.

For nondenaturing PAGE (known as clear-native PAGE or CN-PAGE), gel and sample preparation were identical with the protocol for SDS-PAGE, but all involved buffers were prepared without SDS and reducing agents.

2.2.5.7 Protein staining

Staining of proteins was performed based on Coomassie Acid-Blue R-250 or Direct Red 81 proteins staining (Achilonu and Goldring 2010). The gels were incubated for at least 30 min with the protein dye solutions. Then the gel was destained for several hours until background staining was minimized and the protein bands of interest were clearly visible. For documentation, the gel was scanned either directly or after gel drying on a membrane paper. Therefore, the gel was incubated for 1 h in 6% glycerol (v/v) in H_2O, placed onto a membrane paper, and dried under vacuum on a 58 °C incubator.

staining solution:

50% (v/v) ethanol

10% (v/v) acetic acid

1.5 µmol/ml Direct Red 81 or Coomassie Acid-Blue R-250

destaining solution:

50% (v/v) ethanol

10% (v/v) acetic acid

Also colloidal Coomassie blue (CCB) protein staining was used, which allows more sensitive protein staining without the use of destainers (Kang 2002).

colloidal Coomassie blue (CCB):

10 % (v/v) ethanol

2% (v/v) phosphoric acid

0.02% (w/v) Coomassie Acid-Blue G250

5% (w/v) aluminum sulfate

2.2.5.8 Transfer Blot

In order to perform immunodetection, the proteins, which were seperated by SDS-PAGE, were transferred onto nitrocellulose or polyvinylidenfluorid (PVDF) membranes. Therefore, semi-dry transfer blotting was performed and the proteins from the gels were transferred onto the blot membrane by an electric field, which was applied adjacent to the gel and the membrane. Briefly, the gel was placed onto the blot membrane and both of them were packed between additional blot paper and sponges. The sandwich was placed into the transfer chamber and transfer was performed at 400 mA for 2-3 h or at 150 mA over night in transfer buffer. After transfer blotting, the membranes

were stained with Ponceau S for visualization of gel bands and were either directly used for immunodetection or dried for long term storage.

2.2.5.9 Ponceau S staining

The proteins, which were transferred onto the blot membranes by transfer blotting, were stained with Ponceau S in order to get a first measure of the protein amount and the position of the specific target bands on the gel e.g. when cutting of the blot membrane was necessary. Therefore, the membrane was incubated for 30-60 s with Ponceau S solution. Then, the membrane was washed with H_2O to visualize red protein bands. For further processing of the blot membranes, the Ponceau S stain was discarded by incubation of the membrane in 1xPBS for several minutes and the membranes were ready for characterization by immunodetection. Ponceau S stained membranes can also be dried and stored. For further processing, the dried membranes were re-soaked in transfer buffer.

2.2.5.10 Immunodetection

Immunodetection was performed to characterize protein amounts in the lower nanogram or picogram range. This method is based on a combination of a primary, very target specific antibody and a secondary antibody, which is coupled to horseradish peroxidase (HRP). The primary antibody specifically binds to an antigen of the protein of interest, while the secondary antibody recognizes an antigen of the primary antibody with a very high affinity, which dramatically lowers the detection limit. In brief, the blot membranes were incubated with 1xPBS/5% (w/v) low-fat milk for 1 h on a shaker to reduce nonspecific antibody binding by blocking of the membrane. After that, the solution was discarded and the membrane was incubated for 1 h with the first antibody, which was diluted in 1xPBS/5% (w/v) low-fat milk. Then, four washing steps, each 10 min, were performed with 1xPBS/0.1% (v/v) Tween-20. After that, the secondary antibody was applied according to the recommended dilution in 1xPBS/5% (w/v) low-fat milk for 1 h on a shaker. Finally, four washing steps, each 10 min, with 1xPBS/0.1% (v/v) Tween-20 and two additional washing steps in 1xPBS were performed. Then, the blot membranes were incubated for 2 min in a 1:1 mixture of the enhanced cheminuminescence (ECL) reagents A and B (Perkin Elmer, Western Lightning™ detection). Documentation of the ECL reaction on light sensitive films (GE Healthcare) was performed in a development chamber for several seconds up to 2-3 days before the films were developed, fixed, and ready for visual characterization. The membranes were washed with 1xPBS and either dried for long-term storage or treated with new antibodies for additional immunodetections.

2.2.5.11 Stripping of blot membranes

In many cases, it is necessary to detach antibodies, which were bound to the membrane during immunoblotting, from membranes to allow binding of new antibodies for another immunodetection experiment. This is of special importance, when the primary antibodies share the same secondary antibody or if the position of the target proteins on the blot is more or less identical. In order to remove the "old" antibodies, the membranes were washed with 1xPBS or transfer buffer and then incubated with 62.5 µM Tris pH 6.8/2 % (w/v) SDS/0.8 % (v/v) β-mercaptoethanol for 1 h at 55 °C. Then, a first washing step with 1xPBS/0.1% (v/v) Tween-20 was performed for 10 min at 22 °C followed by two additional washing steps at RT. After that, standard procedure for immunodetection was performed and the membranes were blocked with 1xPBS/5% (w/v) low-fat milk before the new primary antibody was applied.

2.2.5.12 Spin labeling of proteins for EPR measurements

For preparation of EPR samples, in the site-directed spin labeling (SDSL) reaction, the respective spin label molecules were covalently attached to one or more sulfhydryl groups within the protein of interest. In brief, for spin labeling of purified proteins, first, the appropriate amount of protein was prepared in low retention 1.5 ml tubes. According to the protein characteristics, a first reduction step with DTT or TCEP was performed to break potential intra- or intermolecular disulfide bonds and to reduce the target sulfhydryle groups for SDSL. Then, an excess of spin label molecules was added and the labeling reaction was performed for 2-24 h. After that, excess label was removed and the protein solution was concentrated to obtain the desired concentration of spin labeled protein for EPR measurements.

For preparation of SL-SUMO1/2, 1.5 mg SUMO1 or SUMO2 (520 µM) were incubated with a tenfold molar excess of TCEP for 2 h at RT. Then, the sample was divided into two aliquots à 125 µl in order to perform two different washing protocols. Aliquot A was incubated with a fivefold excess of Proxyl IAA and aliquot B with a 20 fold excess of Proxyl IAA for 2 h at RT in the dark. Preparation A was then washed with 5 ml SL buffer in a concentrator (MWCO 5,000) and finally adjusted to a volume of 250 µl (260 µM). Preparation B was applied onto pre-equilibrated PD10 columns according to the manufacturer's protocol. Based on size exclusion chromatography, excess salt (imidazole) and excess label molecules were separated from the target protein. The protein content of the elution fractions was determined by Bradford Assay. Finally, the three protein containing peak fractions were pooled and applied on concentrators to adjust the sample volume to 250 µl followed by protein quantification. Both preparation methods led to successful removal of excess spin label.

Labeling of the HPV16 L2 SIM peptide was performed with 0.25 mg SIM peptide (200 µM). Optional reduction was achieved with a tenfold molecular excess of TCEP and incubation for 2 h at RT. Then, a fivefold excess of Proxyl IAA was added and the sample was incubated for 2 h at RT in the dark. After that, the labeling reactions were washed and concentrated in concentrators (MWCO 2,000) and brought to a final volume of 250 ml followed by protein quantification.

For labeling of full length HPV16 L2, different labeling techniques were performed. An overview is given in **Figure 2.3**. First, denaturing, non-denaturing or high salt buffer conditions were used for experimental setup. Then, the reduction step was modified. Labeling was performed with either no reduction at all or reduction with TCEP or DTT followed by subsequent removal of DTT by dialysis or buffer exchange in concentrators (no removal needed after reduction with TCEP). For the labeling step itself, the incubation times were modified (2-24 h at RT or 4 °C). Also the final buffer exchange (removal of excess spin label) and sample concentration step was modified. Both, mini column size exclusion chromatography as well as concentrators, were tested. Finally, the samples were concentrated in concentrators (MWCO 25,000) or by lyophilization. Labeling was testes with PROXYL IAA as well as with MTSL.

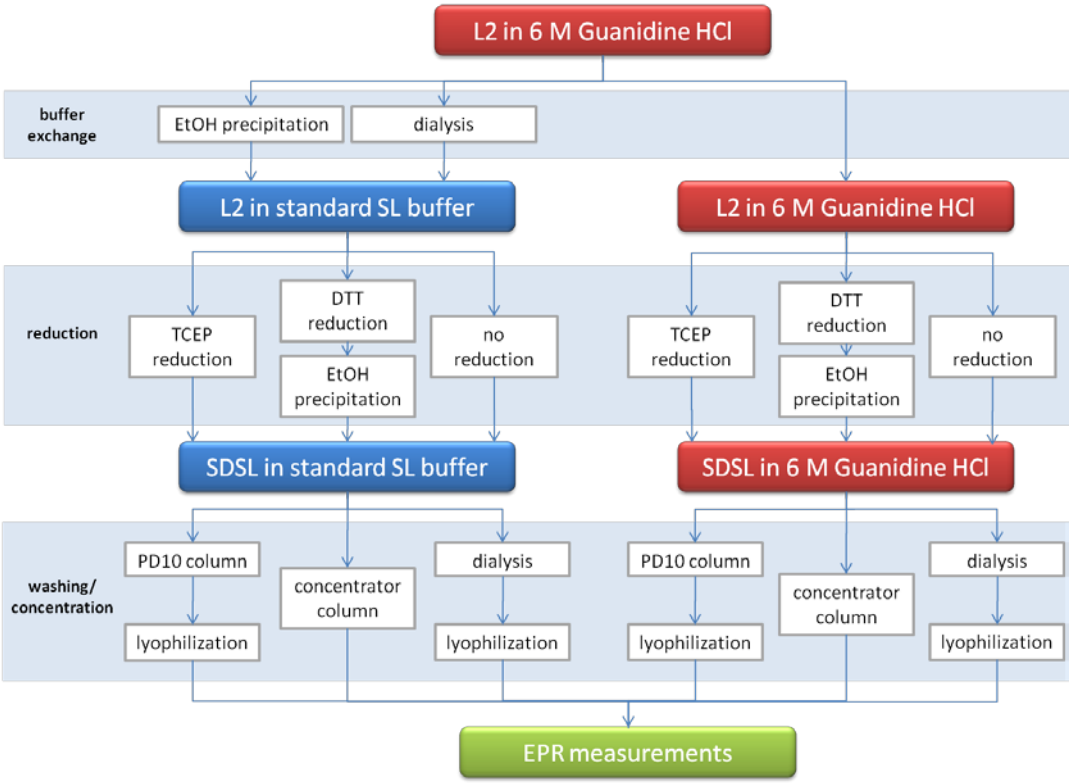

Fig. 2.3: HPV16 L2 labeling procedures. Most major labeling parameters were widely modified to allow L2 labeling. Thereby, different combinations of L2 preparation for labeling, reduction, the labeling reaction itself, as well as final washing and concentration steps were tested.

2.2.5.13 Fluorescence labeling of HPV16 L2 SIM peptides

Fluorescence labeling for FCS measurements was comparable with spin labeling of HPV16 L2 SIM peptides. Since the experimental molar target concentrations are in the nano molar scale for fluorescence labeling (micro molar scale for spin labeling), smaller amounts of the L2 peptide, reduction agent, and fluorescent label were used. In a 50 µl preparation, about 100 µg L2 SIM peptide were reduced with a tenfold excess of TCEP for 1.5 h. Then, a threefold molar excess of fluorescence label (BODIPY®507/545 IA) was used to perform the labeling reaction at RT in the dark over night. Excess label was removed by excessive washing with labeling buffer in concentrators (MWCO 2,000). Finally, the peptide concentration was adjusted to about 500 nM. In a last step, the protein was diluted in labeling buffer to get the final experimental concentration of about 100 nM for FCS measurements. For characterization of the L2 SIM interaction with SUMO1/2, a fivefold excess of affinity purified SUMO1 or SUMO2 was added before FCS measurements were performed.

2.2.5.14 Characterization of SH group labeling efficiency with the Ellman's reaction

In general, the efficiency of SH group based molecular labeling reactions can be characterized based on the Ellmann's reaction. Thereby, the Ellmann's reagent (5,5'-dithiobis-(2-nitrobenzoic acid), DTNB) reacts with free and reduced sulfhydryl groups and the disulfide bond within DTNB is cleaved to give 2-nitro-5-thiobenzoate (NTB^- ,Fig. 2.4). Then, NTB^- ionizes to NTB^{2-}, which can be photometrically detected at 412 nm. In contrast, if the SH groups are already covalently linked with the labeling molecules, no interaction of DTNB with the SH groups occurs. Therefore, also no NTB^- or NTB^{2-} is formed and there is no absorption at 412 nm. For characterization of labeling efficiency, 10 µl aliquots of the labeling reaction were photometrically analyzed together with negative controls lacking the respective labeling molecules after addition of 990 µl DTNB working solution and incubation for 5 min at RT. The DTNB working solution was prepared by addition of 50 µl DTNB stock solution, 100 µl 1 M Tris pH 8.0, and 840 µl H_2O per sample.

Fig. 2.4: Ellman's reaction. The Ellman's reagent (5,5'-dithiobis-(2-nitrobenzoic acid), DTNB) reacts with free thiol groups. Dissociation of the disulfide group gives rise to 2-nitro-5-thiobenzoate (NTB^-), which ionizes to NTB^{2-} and can be photometrically detected at 412 nm.

DTNB stock solution:

50 mM sodium acetate

2 mM DTNB

in H_2O

2.2.6 Molecular biological methods

2.2.6.1 Immunoprecipitation

Potential (direct and indirect) interactions of L2 and SUMO targets were characterized by immunoprecipitation of one protein and co-immunoprecipitation of the potential interaction partner. For immunoprecipitation experiments, the target proteins were coexpressed in HeLa cells in 6 cm plates as described before. After cell harvest, the frozen cell pellets were thawed on ice and 1 ml lysis buffer (50 mM Tris pH 7.5, 300-500 mM NaCl, 0.1-1% (v/v) Triton X-100) was added. The cells were lysed by sonication (3 x 20 s, small sonication tip, 30% output, 30% duty cycle) on ice. Then, the lysate was incubated for 20 min at 4 °C on an overhead rotator. After that, the protein specific pulldown experiments were performed and are described in the following.

Ip of 3xFLAG-L2 and Co-IP of GFP-SUMO1/2

The lysates containing 3xFLAG-L2 and SUMO1/2 protein were incubated with 3 µg monoclonal anti-FLAG antibody for 1 h at 4 °C. Then, 50 µl Protein A/G-Agarose beads (Santa Cruz Biotechnologies) were added. The mixture was again incubated for 1 h at 4 °C. The beads were centrifuged for 3 min at 600 g at 4 °C and then washed with 250 µl washing buffer (50 mM Tris pH 7.5, 150-300 mM NaCl, 0.1-0.5% (v/v) Triton X-100, 0.1% (w/v) Na-Deoxycholate, 0.01-0.05% (w/v) SDS). The washing step was repeated additional two times until the beads were finally incubated and boiled with 75 µl 2.5 x SDS loading dye for 10 min at 95 °C.

IP of GFP-SUMO1/2 and Co-IP of L2 wt, L2 ΔSIM, L2 ΔPHOS, L2 ΔSCM

For GFP-precipitation of lysates containing L2 wt, L2 ΔSIM, L2 ΔPHOS, L2 ΔSCM, and GFP-SUMO1/2, before immunoprecipitation, an additional preclearing was performed. Thus, 45 µl Protein A/G-Agarose were added and the lysates followed by incubation at 4 °C for 45 min. Preclearing was used

to minimize nonspecific binding of L2 protein to the Protein A/G-Agarose beads in subsequent immunoprecipication. After incubation, the precleared lysate was transferred into a new tube and a lysate control was stored for SDS-PAGE. The remaining lysate was incubated with about 5 µg highly specific anti-GFP antibodies (JI-8) for 45 min at 4 °C. After addition of 45 µl Protein A/G-Agarose beads, the samples were incubated for additional 45 min at 4 °C. Then, as described before, the beads were centrifuged for 3 min at 600 g at 4 °C and washed with 250 µl washing buffer. The washing step was repeated twice until the beads were incubated and boiled with 75 µl 2.5 x SDS loading dye for 10 min at 95 °C.

IP of L2 wt, L2 ΔSIM, L2 ΔPHOS, L2 ΔSCM and Co-IP of GFP-SUMO1/2

Precipitation of L2 was performed with lysates containing L2 wt, L2 ΔSIM, L2 ΔPHOS, L2 ΔSCM, and GFP-SUMO1/2. Before immunoprecipitation, an additional preclearing was performed. 45 µl Protein A/G-Agarose beads were added and the lysates followed by incubation at 4 °C for 45 min. After incubation, the precleared lysate was transferred into a new tube and a lysate control was stored for SDS-PAGE. The remaining lysate was incubated with 45 µl highly specific anti-L2 antibody (L2-1) for 1.5 h at 4 °C. After addition of 45 µl Protein A/G-Agarose beads, the samples were incubated for additional 45 min at 4 °C. As described before, the beads were centrifuged for 3 min at 600 g at 4 °C and washed with 250 µl washing buffer. The washing step was repeated twice until the beads were incubated and boiled with 75 µl 2.5 x SDS loading dye for 10 min at 95 °C.

2.2.6.2 SUMO1/2-his$_6$ Pulldown

For SUMO1/2-his$_6$ pulldown experiments, 100 ml culture pellets of SUMO1-his$_6$ or SUMO2-his$_6$ expressed in the *E. coli* strain Rosetta 2 (DE3) were thawed on ice an lysed in 4 ml his lysis buffer. After sonication on ice (5 x 20 s, 30% duty cycle, 30% output, large top piece), the lysates were incubated for 30 min (wheel, 4 °C). Then, the lysates were centrifuged for 20 min at 22,000 g at 4 °C. Meanwhile, 100 µl Ni-NTA slurry (Clontech) was washed with 200 µl H_2O and centrifuged for 3 min at 600 g. The supernatant was discarded and the beads were incubated with 200 µl his lysis buffer. After centrifugation, the supernatant was discarded again. Then, each 10% of the centrifuged SUMO1/2-his$_6$ lysates were incubated with the washed and equilibrated Ni-NTA beads in siliconized tubes. After 10 minutes, the samples were centrifuged for 3 min at 600 g and 4 °C. The supernatant was discarded. 1 ml his wash buffer was added and the sample was centrifuged again for 3 min at 600 g and 4 °C. This step was repeated two times, until, finally, 400 µl his interaction buffer were

added. After that, a Bradford Assay was performed in order to quantify the amount of purified, Ni-NTA coupled SUMO1-his_6 or SUMO2-his_6 protein. The samples were stored at 4 °C for further processing.

His lysis buffer:

20 mM Tris pH 8.0

500 mM NaCl

5 mM imidazole

protease inhibitors

His wash buffer:

20 mM Tris pH 8.0

500 mM NaCl

35 mM imidazole

protease inhibitors

Meanwhile, a cell pellet obtained after expression HPV16 L2 wt protein in HeLa cells for 24 h on six 6 cm dishes, was thawed on ice. 3 ml lysis buffer were added before sonication was performed on ice (5 x 20 s, 30% duty cycle, 30% output, large top piece). The lysate was incubated for 30 min at 4 °C (wheel) and then centrifuged for 20 min at 13,000 g and 4 °C. 50 µl lysate were taken as a control. The lysate was divided into three 1 ml aliquots and 50 µl washed his-beads were added. The samples were incubated for 1 h at 4 °C (wheel) for preclearing and then centrifuged for 3 min at 600 g. The cleared supernatant was isolated, stored at 4 °C, and a 50 µl lysate control were taken.

For the following his-pulldown experiments, 8 µg Ni-NTA coupled SUMO1- or SUMO2-his_6 protein were added to the precleared L2 samples. After incubation for 3 h at 4 °C, 50 µl washed his beads were added. Then, the samples were centrifuged (3 min, 600 g, 4 °C) and the supernatant was discarded before 1 ml wash buffer was added. This step was repeated additional two times. After the last centrifugation, the supernatant was discarded and the beads were boiled with 75 µl 2.5 x SDS-

PAGE loading buffer for 10 min and frozen before the samples were characterized by immunodetection.

Lysis buffer:

20 mM Tris pH 8.0

500 mM NaCl

1% (v/v) Triton X-100

protease inhibitors

2.2.6.3 SUMO1/2-GST Pulldown

GST, GST-SUMO1, and GST-SUMO2 cell pellets were thawed on ice and resuspended in 4 ml GST interaction buffer. The cells were lysed by sonication on ice (5 x 20 s, 100% duty cycle, 30% output). The cell lysate was incubated for 20 min at 4 °C (wheel). Meanwhile, 200 µl glutathione sepharose 4B beads (per cell pellet) were incubated with 1 ml PBS on ice for 30-60 min and centrifuged at 600 g. The supernatant was discarded and beads stored on ice for further application. The cell lysate was centrifuged for 15 min at 4,800 x g and 4 °C. The supernatant was transferred into 1.5 ml tubes and centrifuged again for 20 min at 22,000 g at 4 °C. Then, the supernatant was added to the washed glutathione sepharose beads in 15 ml tubes and incubated for 2-3 h at 4 °C (wheel). After incubation, the beads were washed with 5 ml GST interaction buffer followed by a 3 min centrifugation at 600 g and 4 °C. This step was repeated twice before the beads were transferred into 1.5 ml tubes together with 1 ml GST interaction buffer. Finally, a Bradford Assay was performed for quantification of the amount of purified and precipitated GST, GST-SUMO1, and GST SUMO2.

GST interaction buffer:

1 x PBS

0.5% (w/v) Triton X-100

1 mM DTT

protease inhibitors

During preparation of GST proteins, three cell pellets obtained upon expression of HPV16 L2 wt in HeLa cells for 24 h in 6 cm plates were thawed on ice. 1.2 ml lysis buffer were added before sonication was performed on ice (5 x 20 s, 30% duty cycle, 30% output, large top piece). The lysate was incubated for 20 min at 4 °C (wheel) and then centrifuged for 20 min at 13,000 g and 4 °C. The supernatants were collected in one tube and 60 µl lysate were taken as a control.

Lysis buffer:

1 x PBS

0.5% (w/v) Triton X-100

1 mM DTT

protease inhibitors

For the following GST-pulldown experiments, 8 µg GST-SUMO1/2 or GST protein alone were added to 1 ml L2 lysate and incubated for 2 h at 4 °C. Then 40 µl additional, washed glutathione sepharose beads were added to the samples, which were then centrifuged for 3 min at 600 g and 4 °C. The supernatant was discarded and 1 ml wash buffer was added. The washing step was repeated four times. After the last step, the beads were boiled in 75 µl 2.5 x SDS-PAGE loading buffer.

GST wash buffer:

1 x PBS

500 mM NaCl

1% (w/v) Triton X-100

1 mM DTT

0.5% (w/v) sodium deoxycholate

0.2% (w/v) SDS

protease inhibitors

2.2.6.4 Ubiquitin pulldown

For identification of potential L2-ubiquitin interaction by coprecipitation experiments, ubiquitin pulldown assays were performed based on ubiquitin agarose beads. Therefore, HPV16 L2 and L2 ΔSIM was overexpressed in HeLa cells in 6 cm plates for 24 h. The cells were harvested and lysed. The lysates were incubated with 300 µl equilibrated ubiquitin agarose beads for 1.5 h at RT on a shaking device and then washed three times with 500 µl Tris pH 7.5/ 300 mM NaCl/1% (v/v) Triton X-100 including 3 min centrifugation steps at 600 g and 4 °C. After final centrifugation, the samples were boiled in 60 µl 2.5x SDS-PAGE loading buffer followed by characterization of co-precipitated L2 by immunodetection.

2.2.6.5 Mammalian 2-hybrid assay

In this work, also a mammalian 2-hybrid assay (Stratagene) was used to identify a potential interaction of HPV16 L2 with SUMO proteins. The kit is based on the expression of two fusion proteins. One fusion protein is composed of the first interaction partner together with an activation domain (AD), while the second fusion protein comprises the second interaction partner together with a DNA binding domain (BD). If activation domain and DNA binding domain get in close contact due to interaction of the respective fusion partners, expression of a luciferase reporter gene (*Photinus pyralis*, lat. for American firefly) is activated, which can be photometrically detected.

In order to perform mammalian 2-hybrid assays, first, the corresponding DNA plasmids were constructed for cotransfection and coexpression of the HPV16 L2 or SUMO1/2 fusion proteins in HeLa cells. In a first experiment, SUMO1 or SUMO2 fusion proteins containing an activation domain were coexpressed together with L2 fusion proteins containing a binding domain. *Vice versa*, in a second experiment, also SUMO1/2 fusion proteins containing a DNA binding domain were coexpressed together with L2 fusion proteins containing an activation domain.

In brief, each three DNA plasmids were transfected into HeLa cells (80-120,000, 12-well plates): *i):* pBD-Sumo1/2, pAD-L2, pFR-luciferase or *ii):* pBD-L2, pAD-SUMO1/2, pFR-luciferase. After protein expression for 24 h, the cells were washed with PBS and lysed with Cell Culture Lysis Reagent (Promega) as described above. The lysate was centrifuged and 100 µl were used for luciferase assays (15 s measurement time) on the LB941 luminometer (Berthold). The experimental setup also contained a positive control (transfection of pAD-SV40 with pBD-p53) and negative controls (transfection of pAD-L2 with pBD or pAD-TRAF with pBD-p53).

2.2.7 Virological methods

2.2.7.1 Preparation of HPV16 L1/L2 PsVs

The preparation of HPV16 pseudovirions (PsVs) was performed based on the protocol of Buck *et al*., 2004. The protocol allows for a high-yield production of intact L1/L2 capsids containing a marker DNA plasmid. In this work, both wild type L1/L2 PsVs assembled from wild-type L1 and L2 proteins were prepared, as well as mutant L1/L2 PsVs containing mutant forms of the HPV16 L2 protein. In addition, also PsVs, in which the incorporated viral DNA was labeled with 5-ethynyl-2´-deoxyuridine (Edu), were prepared. PsVs prepared this way allow for labeling of the viral DNA with an AlexaFluor488 fluorescence label, which specifically binds to Edu molecules attached to the viral DNA and allows for characterization of the localization of the viral DNA in fluorescence microscopic experiments after PsV infection. The protocols for standard PsV preparation are accessible online at the homepage of the National Cancer Institut, U.S. National Institutes of Health (http://home.ccr.cancer.gov/Lco/).

For preparation of PsVs, HEK293TT cells were transfected (MATra) with HPV16 L1/L2 plasmids (pSHELL 16L1/L2 or pUF 16L1) and the reporter plasmid (pcDNA 3.1 (+) Luciferase). After 48 h of protein expression, the cells were detached with PBS/2.5 mM EDTA and 0.05% Trypsin/0.02% EDTA, neutralized with DMEM/10% FCS, and centrifuged for 7 min at 300 g at RT as described before. The pellets were resolubilized in PBS/9.5 mM $MgCl_2$ and centrifuged again for 7 min at 300 g at RT. The cell pellets were resolubilized in about 700 µl PBS/9.5 mM $MgCl_2$ and transferred into new siliconized tubes. Then, 0.5% (v/v) Brij58 and 0.1-0.5% (v/v) Benzonase were added for solubilization of L1/L2 proteins and to digest nonincorporated DNA. Maturation of PsVs was perfomed by incubation of the samples for 24 h at 37 °C with repeated mixing. The samples were cooled on ice and brought to a final NaCl concentration of 0.85 M NaCl to stop Benzonase activity and aggregation of the pseudoviruses. After 10 min on ice, the preparations were centrifuged for 10 min at 2000 g and applied onto an Optiprep® ultracentrifugation gradient for purification of the PsVs. Therefore, Optiprep® gradients were prepared by dilution of a 60% (w/v) Iodixanol solution with PBS/9.5 mM $MgCl_2$/0.85 M NaCl in 27%, 33%, and 39% (v/v) solutions. For preparation of the gradients, 1.4 ml of the Optiprep® solutions were pipetted onto each other in SW55 ultra centrifugation tubes starting with the 39% solution. The gradients were incubated for 1 h at RT, frozen at -20°C, and rethawed in order to be carefully loaded with the cleared lysates. Then, ultra centrifugation was performed for 4 h at 50,000 rpm and 16 °C with a SW55 rotor. After that, 300 µl fractions were taken starting from the top of the gradients and stored at 4 °C until the fractions were characterized by infection assays or immunodetection of the L1/L2 content. Then, 1-3 peak fractions were pooled and 100 µl aliquots were frozen at -20 °C for long term storage.

For preparation of HPV16 L1/L2 PsVs suited for detection of viral DNA in immunofluorescence microscopy, the standard preparation protocol was modified according to Ishii *et al.*, 2010. After DNA transfection for 6 h, 100 µM 5-ethynyl-2'-deoxyuridine (EdU) were added to the cell medium (Ishii, Tanaka et al. 2010). After that, the preparation protocol was identical to the preparation of standard PsVs described above.

2.2.7.2 DNA quantification of PsVs based on picoGreen

As a control for infection assays and for further PsV-based experiments, the reporter DNA content of the PsVs was determined based on the Quant-iT^{TM} PicoGreen® (Invitrogen) DNA detection kit. Knowing the DNA content of the respective PsV preparation, the amount of the respective PsVs used for follow-up experiments was adjusted to guarantee a fixed total amount of reporter plasmid DNA. The assay relies on the high affinity binding of a fluorescent marker molecule to double stranded DNA. DNA quantification was performed on a fluorescence plate reader.

Therefore, 150 µl of a 1:200 dilution of PicoGreen in 1xTE were prepared on a black surface 96-well plate. Then, 1-5 µl PsVs were added. For absolute quantification of DNA, a concentration row containing pcDNA3.1 (+) control plasmid DNA (100 ng, 10 ng, 1 ng, 0.1 ng per 150 µl) was applied onto the plate. The plate was incubated for 10 min at RT in the dark. Then, the fluorescence was measured in a plate reader (excitation at 480 nm, emission at 520 nm). Absolute quantification of DNA was achieved by comparison of the detected fluorescence intensities with intensities obtained for the DNA concentration row.

2.2.7.3 Reporter gene assay

Infectivity of pseudoviruses was routinely characterized based on luciferase reporter gene assays after infection of target cells with PsVs. In this assay, a successful infection of the cells by PsVs leads to expression of luciferase, which is an oxido reductase that catalyzes the decarboxylation of luciferin in the presence of ATP and Mg^{2+} under emission of light with an emission maximum at 560 nm.

For standard Luciferease assays, 25,000-50,000 HeLa or HaCaT cells were cultivated for 24 h in 24-well plates. Then, about 1-5 µl PsVs were added onto the cells after a medium change. The cells were infected for 24 h. Afterwards, the cells were washed with PBS and lysis of the cells was performed with 250 µl 1 x Cell Culture Lysis Reagent (Promega). Cells were detached and further lysed by scraping with pipette tips followed by incubation for 15 min at RT. Then, the lysate was centrifuged for 2 min at 13,200 g. 100-150 µl cell lysate were prepared on 96-well plates for luciferase measurements with the Tristar LB941 luminometer (Berthold). For the measurements, 50 µl luciferase substrate buffer were automatically added to the lysates. After automatic mixing and incubation for 5 s, the light emission based on the luciferase activity was measured for 5-20 s.

Luciferase substrate buffer:	50 mM Tris/HCl pH 7.8
	15 mM $MgSO_4$
	20 mM DTT
	0.5 mM EDTA
	0.5 mM Luciferin
	0.5 mM Coenzyme A
	0.5 mM ATP

2.2.7.4 Lactate dehydrogenase (LDH) cytotoxicity assay

Quantification of cells and characterization of cell vitality was performed with LDH cytotoxicity assays (Roche Cytotoxicity Detection Kit^{PLUS}) in parallel with the corresponding reporter gene assays or other experiments. For LDH assays, the same cell lysates (prepared with 1xCell Culture Lysis Reagent (Promega)) as for luciferase reporter gene assays were used. The kit system is based on the detection of the activity of lactate dehydrogenase (Fig 2.5). First, LDH catalyzes the oxidation of lactate to pyruvate with reduction of NAD^+ to $NADH+H^+$. In a second step, the buffer substrate tetrazolium (faint yellow) is reduced to formazan (red) by the free reduction equivalents $NADH+H^+$. The formation of formazan is quantified by photo absorption at 590 nm.

Therefore, 10 µl cell lysate were prepared in a 96-well plate. Then, 100 µl catalysator/dye solution were added and the solution was incubated for 10 min at RT in the dark. The reaction was stopped

with 50 µl stop solution mix. Finally, absorption at 590 nm was detected on a Tristar LB941 plate reader (Berthold).

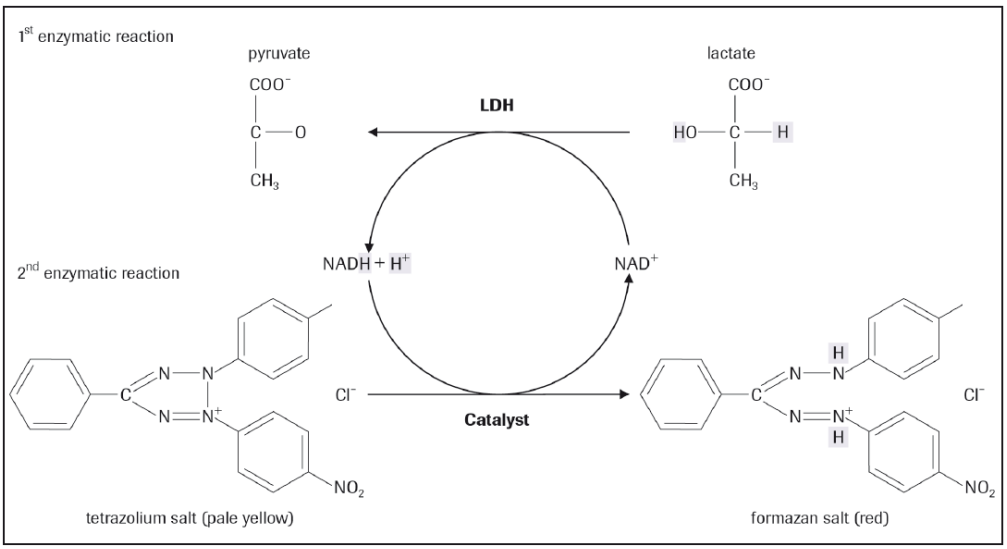

Fig. 2.5: LDH cytotoxicity assay. The lactate dehydrogenase (LDH) catalyzes the oxidation of lactate to pyruvate under reduction of NAD^+ to $NADH+H^+$. In parallel, the free reduction equivalents $NADH+H^+$ reduce the buffer substrate tetrazolium (faint yellow) to formazan (red), which can be photometrically quantified at 590 nm (source: www.roche-applied-science.com)

2.2.7.5 Characterization of PsVs by sucrose gradient ultra centrifugation

After preparation and purification of HPV16 L1/L2 pseudovirions (PsVs), the PsVs were further characterized by sucrose gradient ultra centrifugation based on previous experimental protocols (Becker, Florin et al. 2004; Florin 2004). This was done in order to reassure that only intact capsids and no larger amounts of capsomers, nonincorporated L1/L2, or broken virus debris were used for further experiments. Therefore, 9 ml sucrose gradients (10-60% (w/v) sucrose) were prepared containing 5 µg/ml BSA for stabilization of PsVs. Then, 300 µl L1/L2 PsVs were mixed with 2.7 ml 1xPBS (1:10 dilution) containing 5 µg/ml BSA and applied onto the gradients. Ultra centrifugation was performed for 150 min at 4 °C and 36,000 rpm in a SW40 rotor. After that, 700 µl fractions were collected from top of the gradient and the peak fractions were determined by immunodetection of the L1/L2 content and infection assays.

2.2.7.6 Flow cytometry

Flow cytometry was performed to characterize the ability of mutant HPV16 PsVs to attach to the cell surface of human target cells (HeLa and HaCaT), and also to characterize PsV uptake by endocytosis. For characterization of virus binding, about 200,000 HeLa or 250,000 HaCaT cells were cultivated for 24 h in 12-well plates, washed with PBS/EDTA, and detached by trypsination (100 µl). After 20 min, 400 µl DMEM/FCS were added and the cells were transferred into silikonized tubes. The cells were centrifuged for 5 min at 300 g at RT and resuspended in 600 µl DMEM/FCS. Then, infection with normalized amounts of PsVs (at least 1 µl) was performed for 15 min. The cells were transferred into 3 ml DMEM in 15 ml tubes and centrifuged for 5 min at 300 g at RT. The supernatant was discarded, the cells resuspended in 400 µl PBS, and transferred into 3 ml PBS in FACS tubes. For L1 antibody staining, the cells in the FACS tubes were centrifuged for 5 min at 300 g at 4 °C. The supernatant was discarded and the primary L1 antibody (L1 K75, 1:500) was added in 200 µl PBS/0.5% (v/v) and incubation was performed for 30 min at 4 °C. Then, 4 ml PBS/0.5% (v/v) FCS were added and the cells were centrifuged for 5 min at 300 g at 4 °C. The supernatant was discarded and the secondary fluorescence antibody (AlexaFluor488 anti rabbit, 1:250) was added in 250 µl PBS/0.5% (v/v) FCS and incubated for 30 min at 4 °C. 4 ml (v/v) FCS were added, the cells centrifuged for a last time at 300 g, 4 °C for 5 min and finally resuspended in 300 µl PBS/0.5% (v/v) FCS for analysis by flow cytometry on a Becton Dickinson FACScan device.

To characterize endocytosis of PsVs, 200,000 HeLa or 250,000 HaCaT cells were infected with normalized amounts of PsVs, transferred into 3 ml DMEM in 15 ml tubes and centrifuged for 5 min at 300 g at RT. The supernatant was discarded and the cells were resuspended in 3 ml DMEM and plated on 12-well plates. This time, the infected cells were incubated for 24 hours to allow endocytosis of PsVs. Then, again, L1 antibody staining was performed to allow flow cytometrical detection of residual PsVs on the cell surface, which were possibly not endocytosed due to L2 mutations of the L1/L2 PsVs. Thus, high fluorescence intensities would indicate that the corresponding L1/L2 PsVs were not endocytosed by the target cells, as the fluorescence-labeled L1 would be still accessible to antibody detection, while low fluorescence intensities would indicate successful endocytosis of PsVs and L1 inaccessibility for L1 antibodies, since the PsVs were already taken up. In control experiments, equal amounts of noninfected cells were treated only with the respective primary and secondary antibodies or the secondary antibody, alone, to quantify the level of background fluorescence. All measurements were performed with three individual parallel samples.

2.2.7.7 Preparation of HPV16 PsVs for cell binding assays based on CW EPR

Cell binding of HPV16 PsVs to target cells was characterized based on Fremy's salt as a molecular marker, which could give an indirect measure for the binding of viruses to target cells. Therefore, PsVs were incubated with Fremy's salt, which theoretically attaches to the positively charged L1 and L2 amino acid patches of HPV16 PsVs. By doing so, the marker molecules get in close contact to each other and a very high local concentration of Fremy's salt ions is established. In this milieu, each two Fremy's salt ions react with each other in a disproportionation reaction the molecules lose their paramagnetic properties, leading to a continuous decay of the EPR signal intensity. Addition of cells or heparin as potential binding partners of PsVs in *in vitro* experiments could significantly change the decay of the EPR signal intensity delivering important information about cell binding of the PsVs and structural rearrangement of the L1/L2 capsid.

The general amount of PsVs used for the experiment was adjusted to reach an equimolar amount of positively charged L1/L2 amino acid patches when compared with NDS concentrations (100 µM). Further more, the amount of the different PsVs types was adjusted to reach comparable L1/L2 and DNA levels. The PsVs were washed with 6 ml 1 x PBS in concentrators (MWCO 50,000). Meanwhile, HaCaT cells were harvested and washed with 12 ml 1 x PBS for three times to remove DMEM cell medium, which interferes with later EPR measurements. About 2.5 mio cells were finally resuspended in 1 x PBS and stored on ice for further application. The washed PsVs were adjusted to a final volume of about 30-60 µl. Fremy's salt was added to the samples to give a final concentration of about 100 µM and the preparations were divided into three aliquots. At this time, the interaction partners were added to the different PsV aliquots. 5 µl heparin solution and about 10,000-100,000 cells were used for time dependent cell adhesion experiments. The preparations were mixed and transferred into 1.5 mm glass capillaries. Then, time dependent CW EPR measurements were performed at 16 °C.

2.2.8 Microscopic methods

2.2.8.1 Immunofluorescence microscopy

Immunofluorescence microscopy represents a very powerful tool for investigation of cellular localization and potential *in vivo* interaction of proteins. In this work, both, endogenous proteins of host cells, as well as transiently over-expressed proteins or viral proteins introduced into the cells by PsV infection, were used for characterization.

2.2.8.2 Antibody staining

For characterization of proteins by immunofluorescence microscopy, HeLa or HaCat cells (80,000-180,000) were cultivated on coverslips for 24 h and transfected with LF2000 (HeLa) or JetPEI (HaCaT) for transient expression of proteins for additional 24 h. The cells were washed with PBS (containing protease inhibitors) and then fixed and permeabilized with ice-cold methanol for 10-30 min (<2 min for cells containing over-expressed GFP fusion proteins). After that, the cells were washed three times with PBS and blocked with PBS/1% (w/v) BSA for 30-60 min at RT. Then, the incubation mix was completely discarded from the coverslips and the primary antibody was applied onto the cells in 50 µl PBS/1% (w/v) BSA for 1 h according to the manufacturer's guidelines (Tab.2.3). Incubation of the cells with the antibody was performed for 1 h in a wet chamber at 37 °C. Then, the cells were washed three times with PBS to remove residual antibody and the cells were again blocked for 15 min with PBS/1% (w/v) BSA at RT. After that, the secondary fluorescence antibody was applied onto the cells in 50 µl PBS/1% (w/v) BSA containing the DNA stain Hoechst 33341 in a dilution of about 1:10,000 and incubated for 30-45 min at 37 °C in a wet chamber. Finally, the cells were washed three times with PBS/1% (w/v) BSA, three times with PBS and dried. Subsequently, the coverslips were placed onto a droplet of Fluoprep (bioMérieux) prepared on a microscope slide for fixation. The slides were dried in the dark and the stored at 4 °C until microscopic analysis was performed.

2.2.8.3 EdU staining of PsVs after infection

For immunofluorescence microscopic characterization of viral DNA after infection, PsVs containing the DNA marker molecule 5-ethynyl-2´-deoxyuridine (EdU) were used. In order to stain the viral DNA after PsV infection, the antibody staining procedure contained an additional step based on the Click-iT® EdU Imaging Kit (Invitrogen). In brief, the cells were washed in PBS and fixed/permeabilized in methanol for 30 min. The cells were washed three times in PBS and blocked in PBS/1% (w/v) BSA. Then, in a first reaction a fluorescence antibody (AlexaFluor®488) was covalently linked to the EdU DNA stain in a freshly-prepared solution containing 430 µl 1x Click-iT® reaction buffer, 20 µl $CuSO_4$, 1.2 µl AlexaFluor®488 azide, and 50 µl reaction buffer additive (in this order). The reaction was incubated for 1 h at RT in the dark. From this step on, the cells were treated like cells for standard antibody staining after methanol fixation. Thus, after the Click-iT® reaction solution was discarded, the cells were washed in PBS and blocked again with PBS/1% (w/v) BSA. Then, the primary antibody was added. After washing steps and additional blocking the secondary antibody was applied. The cells were washed, the coverslips were dried and fixed on microscopic slides as described before.

2.2.8.4 Microscopic documentation

The imaging of antibody stained microscopic slides was performed on a Zeiss Axiovert 200 M microscope and a Zeiss Axiocam digital camera. Digital analysis was based on the Axiovision Software 4.7. After iterative fast deconvolution of the z-stack images, the final images were exported in *.tif format and further revised with the CorelDraw Graphics Suite X4.

Quantification of colocalization of viral DNA with PML or L2 with PML after infection with wild-type or mutant HPV16 PsVs was performed by taking fluorescence pictures with fixed exposure times for each detection channel. The pictures were taken as single layer picture focused on PML bodies without any changes of brightness and contrast. For further analysis, the pixel-by-pixel colocalization module was used to determine the channel intensity boundaries for correct report of colocalizing pixels. These boundaries were kept fixed for colocalization analysis of about 80-100 nuclei for each PsV type. Therefore, the cell nuclei were marked with selection tools and the corresponding level of colocalization was tabulated. For analysis, the %-PML colocalization of viral DNA or L2 per nucleus was determined as well as the %-PML colocalization of viral DNA or L2 per total amount of viral DNA or L2.

2.2.9 Biophysical methods

2.2.9.1 Electron paramagnetic resonance (EPR) spectroscopy

In this work, EPR measurements were performed to characterize direct HPV16 L2 *in vitro* interaction with SUMO1/2 or cell binding of HPV16 pseudovirions. For L2 interaction screening with SUMO1/2, continuous wave (CW) EPR measurements were performed as well as pulsed-EPR measurements like electron spin echo (ESE) detected EPR experiments and double electron-electron resonance (DEER) experiments. Cell binding of PsVs was characterized by CW EPR measurements based on Fremy's Salt.

CW EPR measurements

In CW EPR measurements, the efficiency of site-directed spin labeling of purified HPV16 L2 and SUMO1/2 protein as well as HPV16 SIM peptides was characterized. CW EPR experiments were also used to characterize a potential interaction of HPV16 L2 with SUMO1/2. The structural region where the spin labeld was attached to the target molecules was classified by an empirical plot of the inverse of the second moment ($<H^2>^{-1}$) *vs.* the inverse of the central linewidth (ΔH_0^{-1}) (Mchaourab 1996; Isas 2002). $<H^2>^{-1}$ was obtained after simulation of the spectra based on the first moment <H>

(geometrical center of the spectrum) and the second moment $\langle H^2 \rangle$ (spectral breadth) with homewritten Matlab® software.

$$\langle H \rangle = \frac{\int B\, S(B) dB}{\int s(B) dB}$$

$$\langle H^2 \rangle = \frac{\int (B - \langle H \rangle)^2 S(B) db}{\int S(B) dB}$$

ΔH_0^{-1} was directly read from the experimental spectra. Additionally, the binding of PsVs on the surface of HaCaT host cells was studied in time dependent experiments by passive observation of Fremy's Salt degradation.

CW EPR measurements were performed on a MiniScope MS200 spectrometer. Standard measurements were performed at 5 °C for interaction assays and characterization of spin labeling with a modulation amplitude of 1500 mG and 12 dB attenuation (4096 data points, 30 s sweep time). The spectral sweep, as well as video gain and number of scans, were adjusted according to the characteristics of each spectrum. Minimum sample volumes were about 15-30 µl with spin label concentrations of at least 100 µM. Measurements including Fremy's Salt were performed at 16 °C with a modulation amplitude of 150 mG.

Pulse EPR measurements

Pulse EPR measurements, particularly DEER measurements, were performed in order to get additional information about potential protein-protein interaction by measuring the distance between the labels attached to the two interaction partners. DEER measurements also help to characterize proteins in terms of potential protein self-aggregation, e.g. via disulfide bridging. In this work, ESE measurements and DEER measurements were performed on a Bruker Elexsys 580 EPR spectrometer at 50 K in 3 mm quartz capillaries. Sample volumes were at least 40 µl with spin label concentration > 100 µM.

ESE-detected measurements were performed using the Hahn echo sequence π/2-τ- π -τ- echo and a 1.8 mT field sweep. The interpulse delay timeτ was fixed to 200 ns and pulse lengths were 16 ns for the π/2 pulse and 32 ns for the π pulse. The integration gate length was set to 100 ns.

DEER experiments were performed with a $\pi/2(\nu_{observer})$- τ_1-$\pi(\nu_{observer})$-t'- $\pi(\nu_{pump})$-(τ_1+ τ_2-t')-$\pi(\nu_{observer})$-τ_2-*echo* pulse sequence with a [(+x)-(-x)] phase cycle applied to the π/2 pulse. The time t' was incremented in steps of 8 ns. The time τ_1=200 ns was kept constant. τ_2 was set to 1.5 µs. The dipolar evolution time is defined as t= t'- τ_1. Data analysis was performed for t>0 ns. The pump frequency

(ν_{pump}) was set to the center of the resonator dip that coincides with the maximum of the nitroxide EPR spectrum, whereas the observer frequency ($\nu_{observer}$) was set to ν_{pump}+70 MHz and coincided with the low field local maximum of the spectrum for standard nitroxide labels (shoulder position in Fig. 2.6). The observer pulse lengths were 32 ns for both π/2 and π pulses. The π pump pulse length was 12 ns. The width of the integrator gate was 32 ns.

The measurement time of DEER experiments typically was around 4 hours for standard measurements and up to 96 hours for long time measurements.

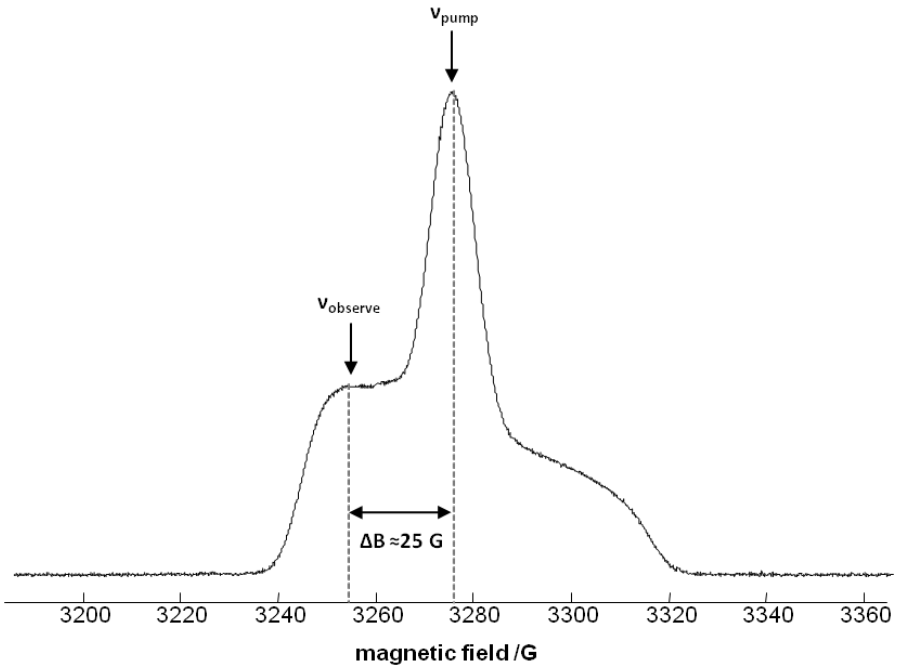

Fig. 2.6: Spin selection in DEER experiments: Selection of observer and pump spins is based on different frequencies for observer and pump pulses. The correlating positions within the ESE spectrum are indicated by arrows for ν_{pump} and $\nu_{observe}$. The difference of about 70 MHz resembles the difference ΔB between the spectral maximum and the low field local maximum of the spectrum (25 G).

2.2.9.2 Fluorescence Correlation spectroscopy (FCS)

Fluorescence correlation spectroscopy is based on detecting and analyzing the fluorescence light emitted by chromophores diffusing through a small and fixed observation volume element *V*, usually formed by a laser focused into the sample of interest using confocal optics. From the measured temporal fluctuations of the fluorescence intensity, *δI(t),* an autocorrelation function

$$G(\tau) = 1 + \frac{\langle \delta I(t) \delta I(t+\tau) \rangle}{\langle I(t) \rangle^2}$$

corresponding to the probability that a chromophore inside the volume *V* at time *t* will be still inside *V* at time t + τ was evaluated. The measured autocorrelation function shows a decay related to the free 3D diffusion and can be fitted to the so-called biophysical model function

$$G(\tau) = 1 + \frac{1}{N^*}\left(1 + \frac{\tau}{\tau_D}\right)^{-1}\left(1 + \frac{\tau}{S^2\tau_D}\right)^{-1/2}$$

where N^* is the average number of fluorescent molecules in the observation volume *V*, τ_D is the lateral diffusion time that a molecule stays in this volume, and $S=z_0/r_0$ is the ratio of axial to radial dimensions of *V* (*S*≈6 in our experiment). If the hydrodynamic radius R_H of a molecule is much smaller than the detection volume ($R_H << r_0$), the diffusion coefficient *D* can be determined from the diffusion time τ_D as . Based on this, the hydrodynamic radii of the molecules can be calculated from the Stokes-Einstein relation

$$R_H = \frac{k_B T}{6\pi\eta D}$$

where k_B is Boltzmann's constant, *T* is the temperature and η is the viscosity of the solution.

FCS measurements were performed at RT at a commercial FCS setup (Zeiss, Germany) consisting of the module ConfoCor 2 and an inverted microscope model Axiovert 200. A Zeiss C-Apochromat 40x/1.2 W water immersion objective was used. The BODIPY®507/545 IA fluorescence label was excited with an Argon laser at λ=488 nm and emission was collected after filtering with a LP560 long pass filter. For detection, avalanche photodiodes were used to enable single-photon counting. An eight-well, polystyrene-chambered cover-glass (Laboratory-Tek, Nalge Nunc International) was used as sample cell.

2.2.9.3 Fluorescence spectroscopy

Fluorescency spectroscopy with proteins is based on the fluorescence of intrinsic tryptophan, tyrosine, and phenylalanine residues. The total fluorescence intensity is dominated by the tryptophan fluorescence, which features a much higher fluorescence quantum efficiency than that of the two other amino acids. Another reason is that there is resonance energy transfer from proximal phenylalanine to tyrosine and from tyrosine to tryptophan (Tab. 2.21). In this study, fluorescence spectroscopy was used to estimate the purity of affinity purified HPV16 L2 protein. Since L2 does not contain any intrinsic tryptophan residues, the detection of tryptophan fluorescence in the spectrum represents a direct hint for background proteins containing tryptophan. Measurements were

performed with 600 µl of a 100 nM protein solution on a spectrofluorometer F777 (Jasco, Tokyo, Japan), with excitation at 295 nm (1.5 nm bandwidth). The fluorescence spectrum was recorded from 240-440 nm.

Tab.2.21: Fluorescence characteristics of tryptophan, tyrosine, and phenylalanine.

		absorption		fluorescence	
	lifetime /ns	wavelength /nm	absorptivity	wavelength/nm	quantum yield
tryptophan	2.6	280	5,600	348	0.20
tyrosine	3.6	274	1,400	303	0.14
phenylalanine	6.4	257	200	282	0.04

2.2.9.4 Circular dichroism spectroscopy

The optical activity of protein to flip circular polarized light around its axis delivers direct information about the secondary structure of the target protein. With CD measurements, the content of α-helical structures, β-sheets, as well as random coiled structures within the target protein, can be addressed. CD measurements were performed on a CARY 61 (Cary, Monrovia, CA, USA) CD spectrometer in a 2 mm µl quartz cuvette. Protein concentration was about 10 µM. The CD measurements were performed with a fixed excitation wave length of 220 nm.

2.2.9.5 Isothermal titration calorimetry (ITC)

Isothermal titration calorimetry was performed to further characterize the interaction of HPV16 L2 with SUMO1/2 and to gain thermodynamic parameters to describe the interaction of proteins. Therefore, binding of one molecular species to another species is characterized by titration and gives direct information about the binding constant, stoichiometry, and energetics. Measurements were performed on a MCS isothermal titration calorimeter from MicroCal (Northampton, MA, USA). To characterize binding of SUMO2 by L2 protein, SUMO2 was injected (18 x 20 µl, 300 µM) into a cell with 1.3 ml of HPV16 L2 solution (5 µM) at 15 °C (interaction buffer: in 50 mM Tris pH 7.5/300 mM NaCl). For characterization of the interaction of SUMO1 with the HPV16 L2 SIM peptides, SUMO1 (300 µM) was injected (5 x 20 µl, 300 µM) into a cell with 1.3 ml 20 µM L2 SIM peptide (interaction buffer: 50 mM Tris pH 7.5/150 mM NaCl).

2.2.9.6 Molecular dynamics simulation

Molecular dynamics simulation was performed with the YASARA software (YASARA Biosciences) for professional structure modeling of the potential attachment of L2 SIM peptides to SUMO1 or SUMO2. Therefore, the L2 peptide sequences were manually edited and implemented into a simulation cell together with the crystal-structures of SUMO1 or SUMO2 from known complexes with SIM containing SUMO targets. The L2 peptide was brought into close vicinity of the interaction surface of the SUMO1/2 molecules and the system was equilibarated for 5-12 ns with the simulation parameters given in **Table 2.22**. Then, simulation was continued by taking snap-shots each 12,500 simulation steps. The simulated model data was characterized by determination of the root-mean-square deviation (RMSD) of the respective L2 SIM peptides within the respective SUMO1/2 interaction complex.

Tab. 2.22: Simulation parameters for Yasara MD simulations.

parameter	selection/specification
simulation cell	5.0 A around all atoms
cell boundaries	periodic walls
force field	Amber03
pH	7.5
temperature	298 K
simulation snapshots	every 12,500 simulation steps

3. Results

In this work, the interaction of the HPV16 late protein L2 with the small ubiquitin-like modifier (SUMO) was characterized with a broad selection of methods. L2 sequence analysis revealed a *bona fide* SUMO interacting motif (SIM) at position 284-289, which might enable noncovalent interaction of L2 with SUMO. In immunoprecipitation experiments it was found that L2 interacts with SUMO2, while no interaction was found between L2 and SUMO1. In electron paramagnetic resonance (EPR) spectroscopic measurements with affinity purified proteins, L2 interacted with SUMO1 and SUMO2. Coexpression of L2 with SUMO1 and SUMO2 led to a significant stabilization of wild-type L2. Furthermore, overexpressed L2 and SUMO1/2 colocalized at PML-NBs in immunofluorescence microscopy. For L2 lacking the SIM, there was no interaction with SUMO, and additionally also no colocalization with SUMO in PML-NBs. In order to characterize the physiologic relevance of the SIM-based interaction of L2 with SUMO, HPV16 L1/L2 pseudoviruses (PsVs) containing mutant L2 were prepared and subjected to cell binding and infection assays. The lack of the L2 SIM did not affect cell binding, but lead to a complete loss of infectivity compared to wild-type L1/L2 PsVs. Then, the subcellular localization of wild-type and mutant L2, as well as localization of the viral DNA, was characterized by fluorescence microscopy after infection with L1/L2 PsVs. Infection with wild-type L1/L2 PsVs resulted in a strong colocalization of L2 and viral DNA in the PML-NBs of the host cells. Remarkably, almost no PML-NB-colocalization of L2 (and viral DNA) was observed after infection with mutant L1/L2 ΔSIM PsVs. Our data suggest that the identified L2 SIM is important for the interaction of L2 with SUMO in the PML-NBs. This most probably also includes L2 interaction with SUMOylated proteins at the PNL-NBs.

3.1 Characterization of the interaction of HPV16 L2 with SUMO proteins

3.1.1 The HVP16 L2 protein sequence comprises multiple SIMs

In general, there are two ways in which SUMO proteins can interact with target molecules: *i)* SUMOylation based on covalent SUMO modification and *ii)* SUMO interaction via SUMO interacting motifs (SIMs). With regard to HPV16 L2 as SUMO target, it is already known that L2 is SUMOylated by SUMO1/2/3 at the L2 K35 lysine residue, which leads to a stabilization of L2 (Marusic 2010). A SIM-based interaction of L2 with SUMO has not been described yet. Remarkably, SIM-based SUMO interaction has already been reported for a very large number of target proteins including several viral proteins, which are functionally comparable to HPV16 L2. We searched for SIMs within the L2 protein sequence and identified 9 potential SIMs which meet the criteria of the classical SIM consensus sequence (V/I/L)-(V/I/L)-X-(V/I/L) or (V/I/L)-X-(V/I/L)-X-(V/I/L) (Fig. 3.1) (Minty 2000; Song 2004; Hannich 2005; Song 2005; Kerscher 2007).

Fig. 3.1: Sequence alignment of potential SIMs within the HPV16 L2 protein sequence. Nine potential SIMs were identified based on the classical SIM sequence (V/I/L)-(V/I/L)-X-(V/I/L) or (V/I/L)-X-(V/I/L)-X-(V/I/L). The hydrophobic core of the potential SIMs is highlighted in the black frame. At L2 sequence positions 105-109, 284-289, and 428-431, two SIMs overlap with each other resulting in a double SIM. SIMs are frequently flanked by negatively charged amino acids (red) and/or phosphorylation sites. Potential phosphorylation sites within the L2 sequence were identified using the NetPhos 2.0 prediction server and underlined for clarity. Positively charged amino acids are shown in blue, negatively charged amino acids in red, the hydrophobic core amino acids of the classical SIM in green, and all other amino acids in yellow.

Three potential SIMs represent double SIM sequences (positions 105-109, 284-289, and 428-431), in which two SIMs overlap with each other sharing at least two of the hydrophobic core amino acids. Further characteristics of a SIM include the presence of neighboring negatively charged amino acids, which induce a first docking of the SIM at the SUMO interaction surface. Additionally, phosphorylation sites play an important role in the SIM mediated SUMO interaction. Therefore, potential serine, threonine, and tyrosine phosphorylation sites were identified (analysis via NetPhos 2.0 Server, http://www.cbs.dtu.dk) (Blom 1999). Both, negatively charged amino acids and a potential casein kinase 2 (CK2) phosphorylation site were identified in the direct neighborhood of all potential SIMs. Thus, for further evaluation of the integrity of the potential SIMs, the conservation of the SIMs within the L2 sequences of the different HPV high risk types was checked.

3.1.2 Three potential SIMs within the L2 protein are conserved for high risk HPVs

Specific sequence motifs, like e.g. protein interaction sequences or localization signals, often share a very high amino acid conservation between related proteins. The amino acid conservation of the identified SIMs was characterized based on an L2 sequence alignment of high-risk HPV L2 proteins (Fig. 3.2).

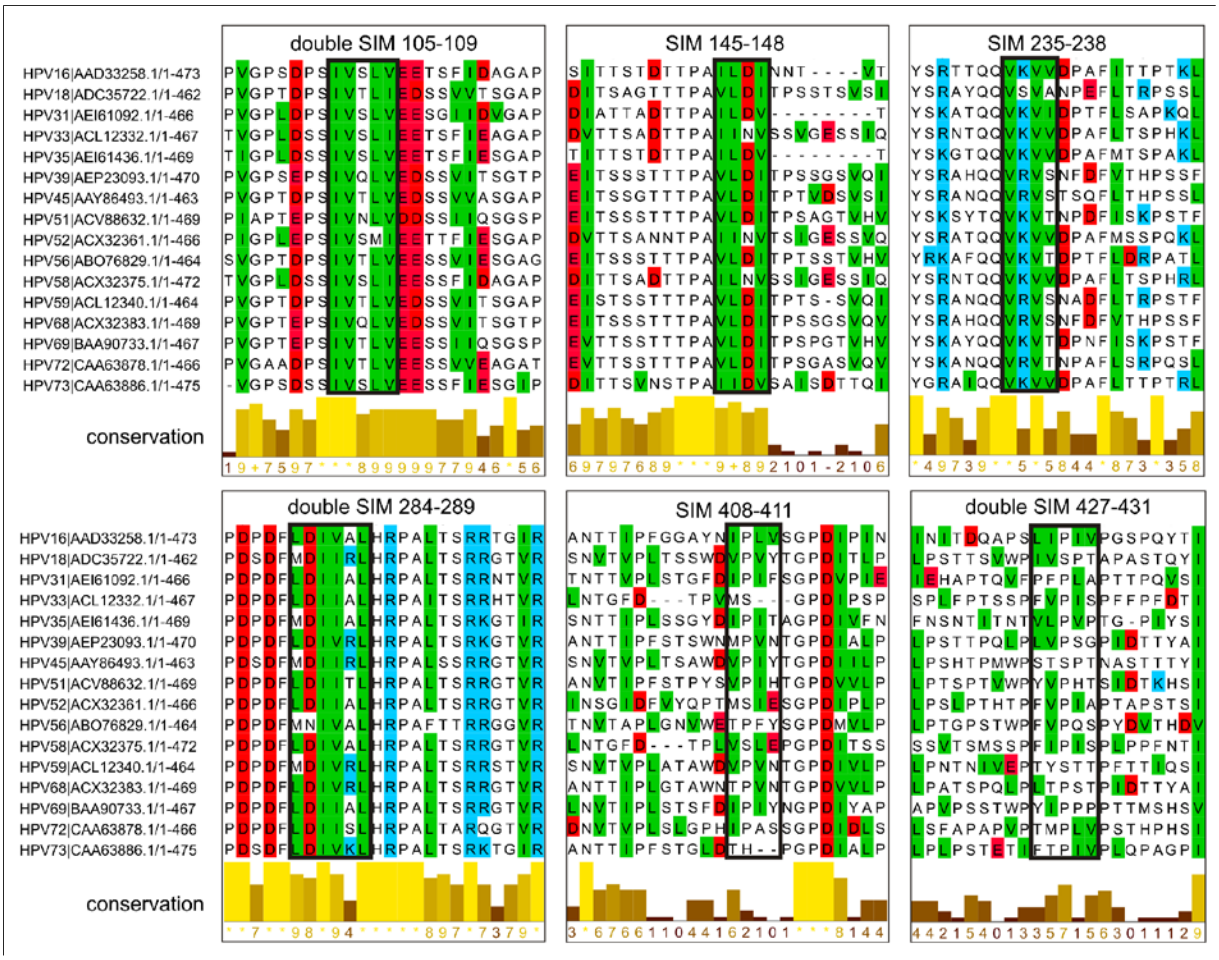

Fig. 3.2: Sequence alignment of L2 in different high-risk HPV types. Only medium or no conservation is observed for the hydrophobic core of the potential SIMs at positions 235-238, 408-411, and 427-431. The potential SIMs at positions 105-109, 145-148, and 284-289 share a very high conservation of the hydrophobic core residues. The complete sequence region around the potential double SIM at L2 position 284-289 is highly conserved. 100% sequence conservation is found for the most promising IVAL motif of the potential SIM at position 286-289. Additionally, an almost 100% conservation was found for flanking negatively charged amino acids (red) as well as the potential CK2 phosphorylation site at position 295/6 (TS). Hydrophobic core amino acids of the classical SIM are shown in green, negatively charged amino acids in red, and positively charged amino acids in blue. The multiple sequence alignment was performed with ClustalW2 (http://www.ebi.ac.uk) (Larkin 2007; Goujon 2010) and edited with Jalview (http://www.jalview.org) (Waterhouse, Procter et al. 2009).

For the potential SIMs at position 408-411, 427-430, and 428-431, no significant conservation of the hydrophobic core was observed. A slightly better conservation of the core region was observed for the potential SIM at position 235-238, but here the charged, flanking amino acids and potential phosporylation sites were not conserved. As for the SIMs/double SIMs at positions 105-109, 145-148, and 284-289, a high conservation of the core hydrophobic amino acids, as well as the flanking

charged amino acids and phospohorylation sites, was observed. The highest level of conservation for the whole amino acid region containing a potential SIM was found for the double SIM at position 284-289. This potential double SIM region fulfills all requirements of a classical SIM and thus resembles a *bona fide* SIM. For simplification, the double SIM at position 284-289 will be referred to as L2 SIM throughout this work. Nevertheless, also the potential double SIM at position 105-109 features a very high level of conservation.

3.1.3 L2 interacts with SUMO2 in immunoprecipitation

The interaction of HPV16 L2 with SUMO1/2 was characterized based on different interaction experiments. First, immunoprecipitation was used to elucidate a potential interaction of L2 with SUMO1 or SUMO2. Therefore, 3xFLAG-L2 was coexpressed together with GFP-SUMO1, GFP-SUMO2, or GFP as control in HeLa cells. After immunoprecipitation of 3xFLAG-L2, coprecipitation of GFP was analyzed by immunodetection (Fig. 3.3). Coprecipitation was only observed for GFP-SUMO2 (lane 6), while there was no coprecipitation of GFP or GFP-SUMO1 (lanes 4 and 5). Interestingly, in the lysate controls (lanes 1-3) and IPs (lanes 4-6), an increased amount of L2 was detected after coexpression with GFP-SUMO1 and -2 as compared with the GFP control. This might result from a stabilization of L2 by GFP-SUMO1 and even stronger by GFP-SUMO2.

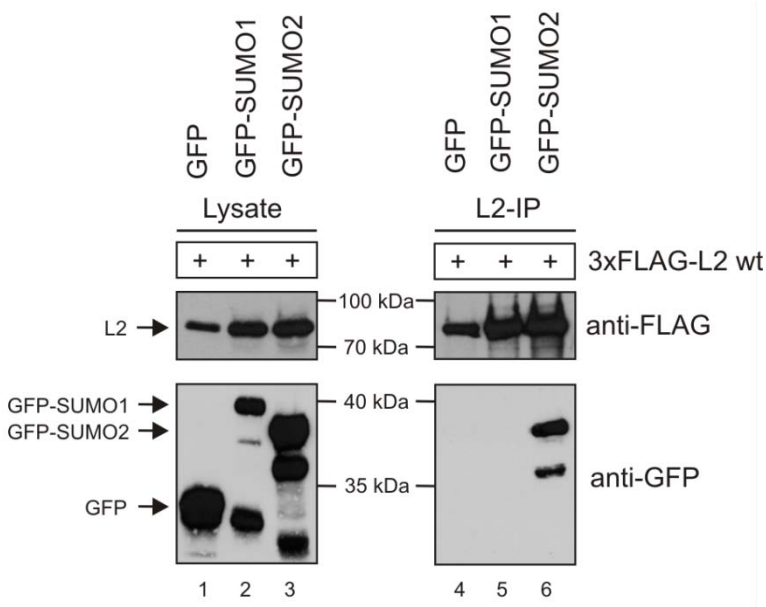

Fig. 3.3: L2 interacts with GFP-SUMO2 in immunoprecipitation. HeLa cells were transiently cotransfected with 3xFLAG-L2 together with GFP, GFP-SUMO1, or GFP-SUMO2. After 24 h, the expressed proteins were analyzed by immunodetection with anti-FLAG (detection of 3xFLAG-L2) or anti-GFP antibodies (lanes 1-3). Residual lysate was subjected to immunoprecipitation of 3xFLAG-L2 with an anti-FLAG antibody. Coprecipitation of GFP was analyzed with an anti-GFP antibody (JI-8) and was only observed for GFP-SUMO2 (lane 6). There was no co-precipitated GFP (lane 4) or GFP-SUMO1 (lane 5). An increasing amount of L2 was observed after coexpression with GFP-SUMO1 and GFP-SUMO2 compared to coexpression with GFP, indicating L2 stabilization by GFP-SUMO1 and especially GFP-SUMO2.

3.1.4 L2 lacking the SIM does not interact with SUMO2

For further characterization of the L2 interaction with SUMO, different L2 mutants were created (Fig. 3.4). In order to check whether the identified SIM at L2 position 284-289 is responsible for the SIM-based L2 interaction with SUMO2, the amino acids 284-289 of the hydrophobic core of the SIMs were mutated to alanines (Fig. 3.4, B). This L2 mutant was termed L2 ΔSIM. To investigate the influence of L2 SUMOylation on the L2 interaction with GFP-SUMO2, the lysine at position 35 within the SUMO conjugation motif (SCM), which was reported to be the target for SUMOylation (Marusic 2010), was changed to arginine (K35R, Fig 3.4, A). The L2 ΔSCM mutant lacks the SCM and is not able to be covalently modified by SUMO (Marusic 2010). A further L2 mutant, L2 ΔPHOS, was created to characterize the influence of phosphorylation of a potential casein kinase 2 (CK2) phosphorylation site located in the direct vicinity of the double SIM on protein interaction (Fig. 3.4, C). In this L2 mutant, the phosphorylation receptors threonine and serine (L2 position 295/6) were replaced by alanines to inhibit potential phosphorylation.

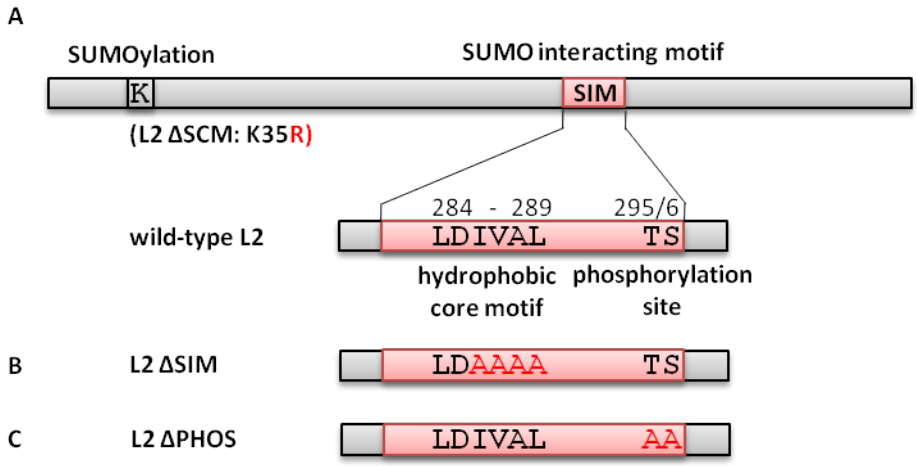

Fig. 3.4: Different L2 mutants for characterization of the L2 interaction with SUMO. ***A*** Wild-type protein sequence of HPV16 L2 with the lysine at position 35, which represents the target for SUMOylation, and the SUMO interacting motif at position 284-289. The extended SIM region contains the hydrophobic core region (LDIVAL, position 284-289) and a potential CK2 phosphorylation site (TS, position 295/6). In the L2 ΔSCM mutant, the lysine (K) at position 35 was replaced by arginine (R). ***B*** The L2 ΔSIM mutant was created by replacing the IVAL motif in the hydrophobic core with alanines. ***C*** The L2 ΔPHOS mutant comprises two alanines instead of the phosphorylation receptors threonine (T) and serine (S) at position 295/6.

To characterize interaction of the L2 mutants with SUMO2, again, immunoprecipitation experiments were performed. Therefore, wild-type L2, L2 ΔSIM, and L2 ΔPHOS were coexpressed together with GFP-SUMO2 and characterized by immunodetection (Fig. 3.5). After immunoprecipitation of GFP with a Jl-8 antibody, coprecipitation was observed for wild-type L2 (lane 6). Remarkably, there was almost no coprecipitation of L2 ΔSIM (lane7), as the L2 ΔSIM band intensity only reached the level of the negative control after coexpression of wild-type L2 and GFP (lane 5). Like wild-type L2, also L2

ΔPHOS was successfully detected after coprecipitation (lane 8) indicating that mutation of the potential phosphorylation site had no effect on the L2 interaction with GPF-SUMO2.

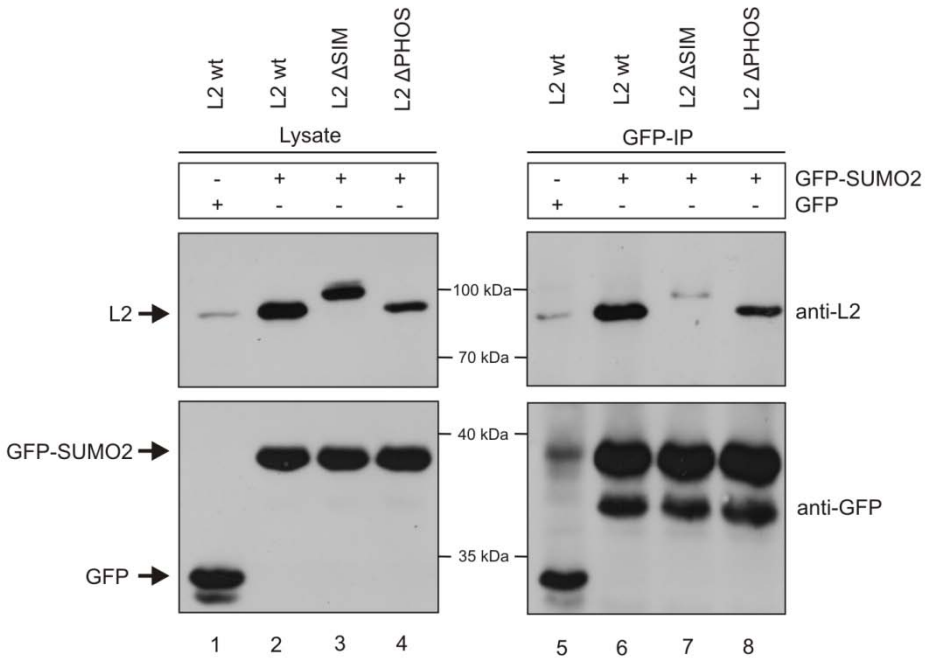

Fig. 3.5: No coprecipitation of L2 ΔSIM after coexpression with GFP-SUMO2. Wild-type L2, L2 ΔSIM, and L2 ΔPHOS were coexpressed together with GFP-SUMO2 for 24 h in HeLa cells and analyzed by immunodetection. After Jl-8 immunoprecipitation of the GFP proteins, coprecipitation of wild-type L2 (lane 6) and L2 ΔPHOS (lane 8) was observed. Almost no coprecipitation was detected for L2 ΔSIM (lane 7). The observed L2 ΔSIM band only reached background intensity comparable to the negative control with coexpressed wild-type L2 and GFP (lane 5). Note that again the amount of detectable L2 was significantly increased upon coexpression with GFP-SUMO2 compared to GFP alone.

In order to characterize a possible influence of SUMOylation on SIM-based L2 interaction with GFP-SUMO2, coprecipitation experiments were repeated with coexpression of GFP-SUMO2 together with wild-type L2 or L2 ΔSCM, which is SUMOylation deficient. After precipitation of GFP with a Jl-8 antibody, both, wild-type L2 and L2 ΔSCM, were co-precipitated (Fig. 3.6, A, lanes 3 and 4). Interestingly, for L2-precipitation with an L2-specific antibody (L2-1), no coprecipitation of GFP-SUMO2 was observed (Fig. 3.6, B, lanes 7 and 8), although L2-precipitation was successful. Remarkably, in none of the numerous experiments, a coprecipitation of GFP-SUMO constructs was observed after L2 precipitation based on the L2-specific L2-1 antibody.

To check the possible influence of SUMOylation of L2 interaction with SUMO, an additional precipitation experiment was performed. Therefore, wild-type 3xFLAG-L2 was coexpressed together with GFP-SUMO1/2 ΔGG mutants, which are SUMOylation deficient. In contrast to wild-type GFP-SUMO1/2 containing the full-length SUMO protein, the SUMO1/2-ΔGG proteins resemble C-terminally truncated SUMO isoforms. The shortened protein sequence of SUMO1-ΔGG (amino acids 1-95) ends before the double glycine motif, which is located at amino acid position 96/97 of wild-type SUMO1. In parallel, the protein sequence of SUMO2-ΔGG (amino acids 1-91) ends at position 91

just before the double glycine at amino acid position 92/93 of wild-type SUMO2. Theoretically, both SUMO1/2-ΔGG isoforms are not able to participate in SUMO modification of SUMO targets anymore, since the necessary double glycine, which serves as target for covalent binding of SUMO with SUMO-ligands, is missing. Finally, after coexpression of wild-type 3xFLAG-L2 together with GFP-SUMO1 ΔGG or GFP-SUMO2 ΔGG and precipitation of 3xFLAG-L2, no coprecipitation of GFP-SUMO1/2 ΔGG was observed (Fig. 3.5, C, lanes 5 and 6). Note that there is a comparable amount of detected L2 within the lysate controls (lanes 1-3) and IPs (lanes 3-6) after L2 coexpression with the SUMO1/2-ΔGG mutants and GFP alone, indicating that there is no L2 stabilization based on GFP-SUMO1/2 ΔGG as it was seen for L2 and wild-type SUMO1/2. Immunofluorecence microscopy with overexpressed SUMO1/2-ΔGG revealed an exclusively cytoplasmic localization of GFP-SUMO1/2 ΔGG with almost no GFP signal within the nucleus (data not shown).

We were also able to characterize L2 SUMOylation after simple coexpression of L2 together with SUMO1/2 (Fig. 3.6, D). While each one additional high molecular L2 band was detected for coexpression of wild-type L2 and SUMO1 or SUMO2, which run at the characteristic molecular weight of a L2-GFP-SUMO1/2 fusion protein (lanes 2 and 3), in line with the results obtained by Marusic *et al.* 2010, no high molecular L2 bands were detected after expression of L2 ΔSCM (lanes 5 and 6). Additionally, there were also no high molecular L2 bands detected for coexpression of wild-type L2 together with GFP-SUMO1/2 ΔGG (lanes 8 and 9).

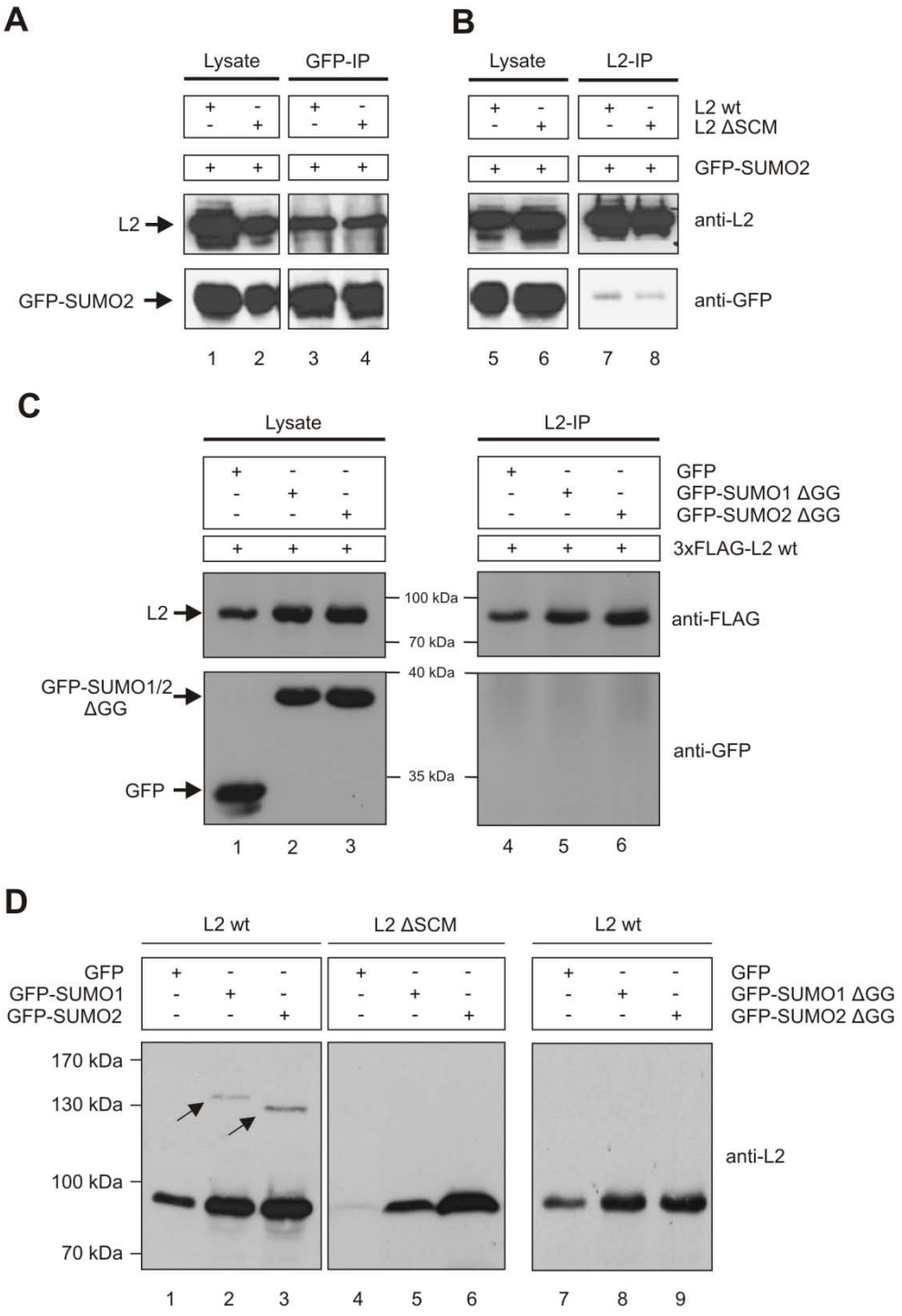

Fig. 3.6: Coprecipitation experiments including SUMOylation-deficient L2 ΔSCM or GFP-SUMO1/2 ΔGG. ***A*** Wild-type L2 was coexpressed with GFP-SUMO2 in HeLa cells for 24 h. After GFP precipitation, both wild-type L2 and L2 ΔSCM were successfully co-precipitated (lanes 3 and 4). ***B*** Again, wild-type L2 was coexpressed with GFP-SUMO2, but precipitation was performed based on an anti L2 antibody (L2-1). No significant coprecipitation of GFP-SUMO2 was observed (lanes 7 and 8). ***C*** Wild-type 3xFLAG L2 was coexpressed with GFP-SUMO1/2 ΔGG, which cannot be covalently linked to SUMO substrates. After precipitation of 3xFLAG L2 with an anti-FLAG antibody, no coprecipitation of GFP or GFP-SUMO1/2 ΔGG was observed (lanes 4-5). There was difference in the amount of L2 after coexpression of L2 with GFP or GFP-SUMO1/2 ΔGG in the lysate controls and IPs, indicating no L2-stabilization based on SUMO1/2 ΔGG. ***D*** Characterization of L2 SUMOylation after coexpression of wild-type L2 or L2 ΔSCM together with GFP, GFP-SUMO1, GFP-SUMO2 or together with GFP-SUMO1, -2 ΔGG. Arrows indicate SUMOylated L2 detected by anti-L2 antibodies.

3.1.5 Wild type L2 colocalizes with GFP-SUMO1/2 in PML NBs

After a SIM-based *in vitro* interaction of HPV16 L2 and SUMO2 was observed in immunoprecipitation experiments, overexpressed L2 and SUMO1/2 were characterized by immunofluorescence microscopy. Therefore, HPV16 L2 variants were coexpressed with GFP-SUMO1/2 and the cellular localization of the proteins was monitored. Wild-type L2 accumulated in the cell nucleus within larger aggregates and almost always colocalized with endogenous PML bodies (Fig. 3.7). For GFP-SUMO1 or -SUMO2, an almost 100% colocalization with L2 wt was observed for both SUMO isoforms. In general, the majority of overexpressed wild-type L2 colocalized with GFP-SUMO1 or GFP-SUMO2 at cellular PML bodies. PML-localization of wild-type L2, GFP-SUMO1, or GFP-SUMO2 was also observed in control experiments with separate overexpression of the respective proteins, showing that the PML-localization did not depend on coexpression.

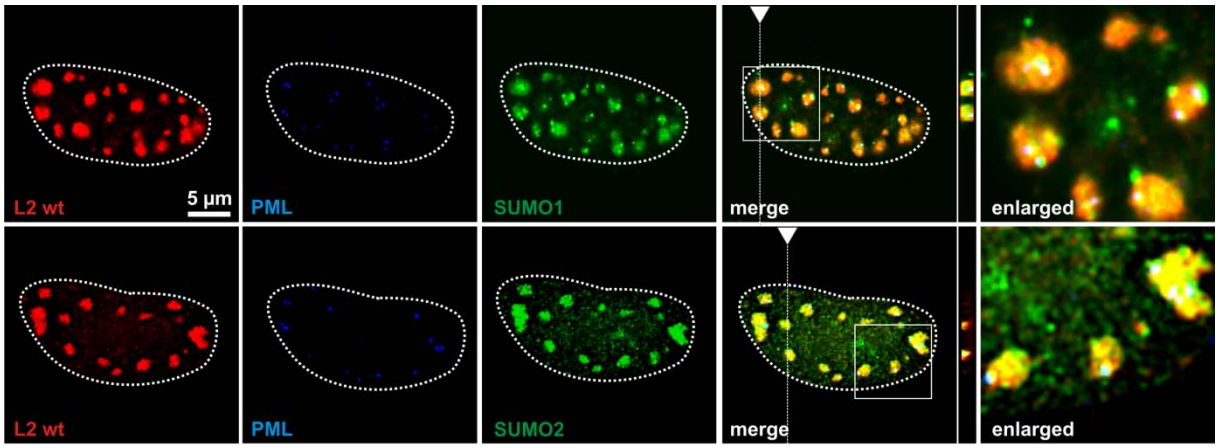

Fig. 3.7: Wild-type L2 accumulated in the nucleus and colocalized with GFP-SUMO1/2 at PML-NBs. After coexpression of wild-type L2 together with GFP-SUMO1 or GFP-SUMO2 for 48 h in HeLa cells, L2 accumulated in the nucleus and colocalized with GFP-SUMO1/2 within larger aggregates at the PML-NBs. PML-localization of L2, GFP-SUMO1, or GFP-SUMO2 was also observed after separate overexpression of the respective proteins, indicating that the observed PML-localization did not depend on coexpression.

3.1.6 No colocalization of L2 ΔSIM with SUMO1/2 or PML

Also the subcellular localization of L2 ΔSIM was characterized upon coexpression with GFP-SUMO1/2 (Fig. 3.8, A). Here, the L2 ΔSIM structures were less distinct and featured a rather diffuse distribution all over the cell nucleus compared with the wild-type L2 aggregates. Remarkably, there was almost no (or only random) colocalization of L2 ΔSIM with PML-NBs or GFP-SUMO1 or GFP-SUMO2. After coexpression of L2 ΔPHOS or L2 ΔSCM with GFP-SUMO1/2, a wild-type like localization of the L2 mutants was observed (Fig. 3.8, B and C). L2 ΔPHOS and L2 ΔSCM colocalized at PML-NBs together with GFP-SUMO1 or GFP-SUMO2. The same L2 localization pattern was observed after separate overexpression of L2 ΔPHOS or L2 ΔSCM without GFP-SUMO1/2.

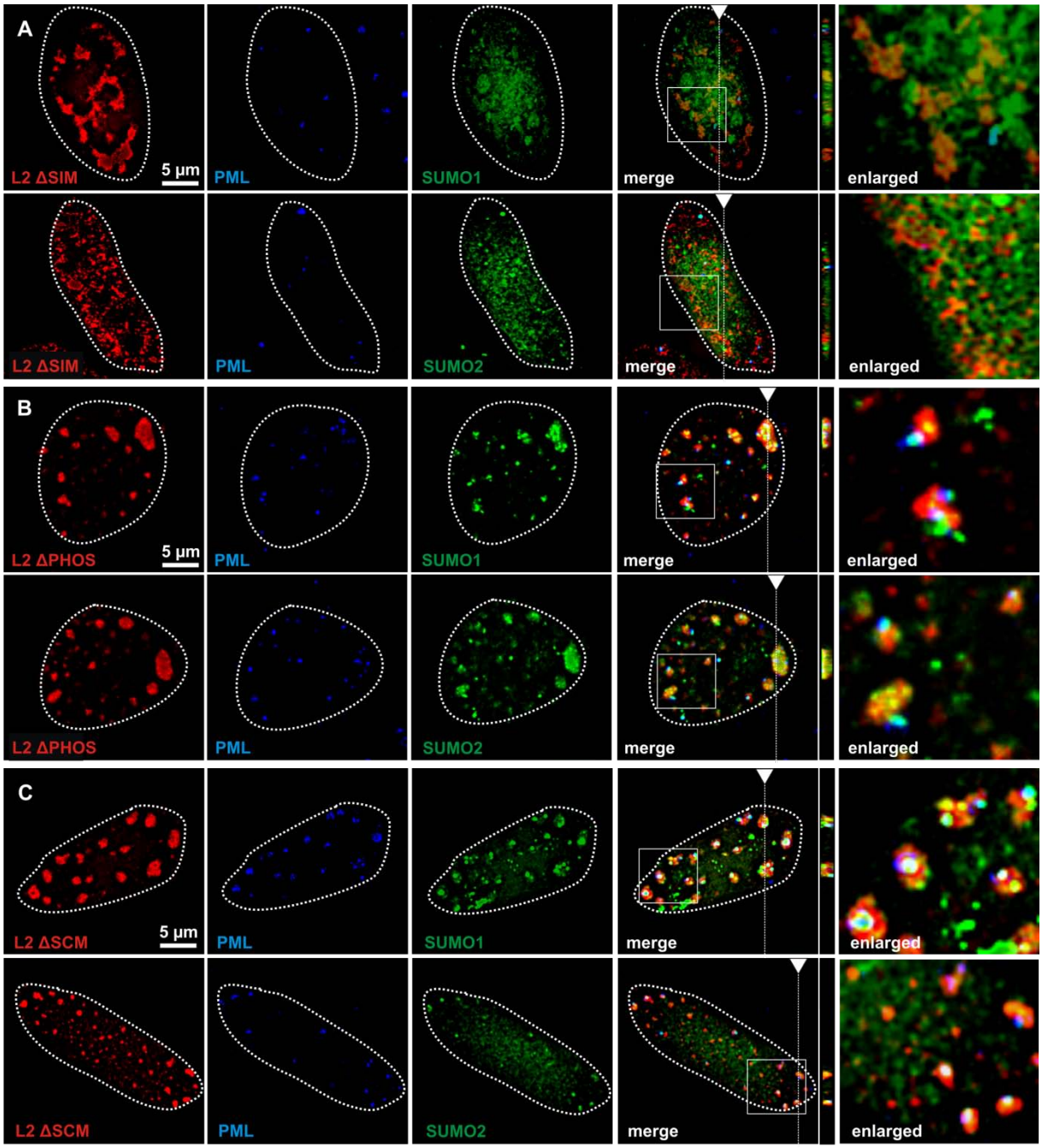

Fig. 3.8: No PML-NB localization of L2 ΔSIM. ***A*** After coexpression of L2 ΔSIM with GFP-SUMO1 or GFP-SUMO2 for 48 h in HeLa cells, a diffuse L2 distribution and no colocalization with GFP-SUMO1/2 or PML-NBs was observed. GFP-SUMO1 and GFP-SUMO2 still colocalized at the PML-NBs. ***B*** For coexpression of L2 ΔPHOS with GFP-SUMO1 or -2, a wild-type L2 distribution was observed. L2 ΔPHOS colocalized with GFP-SUMO1 or -2 at PML-NBs. ***C*** Also for coexpression of L2 ΔSCM, a wild-type L2 distribution was observed with colocalization of L2 ΔSCM with GFP-SUMO1/2 at the PML-NBs.

3.1.7 L2 wt and L2 ΔSCM are stabilized by SUMO1/2 after coexpression in HeLa cells

In several immunoprecipitations with overexpressed L2 and GFP-SUMO1/2, a significant L2 stabilization was observed after coexpression with GFP-SUMO1 and especially GFP-SUMO2. Based on these observations and previous publications reporting on SUMOylation-based L2 stabilization (Marusic 2010), L2 stabilization assays were performed. Therefore, L2 was coexpressed with GFP-SUMO1, GFP-SUMO2, or GFP for 24 h. Then, cycloheximide (CHX) was added to stop further protein synthesis and cell lysates were characterized by immunodetection after 0.5, 1, 2, and 4 hours (Fig. 3.9, A). Note that the zero time controls were prepared directly before CHX was added to the parallel samples. The L2 amounts were quantified by densitometry and plotted against the time (Fig. 3.9, B).

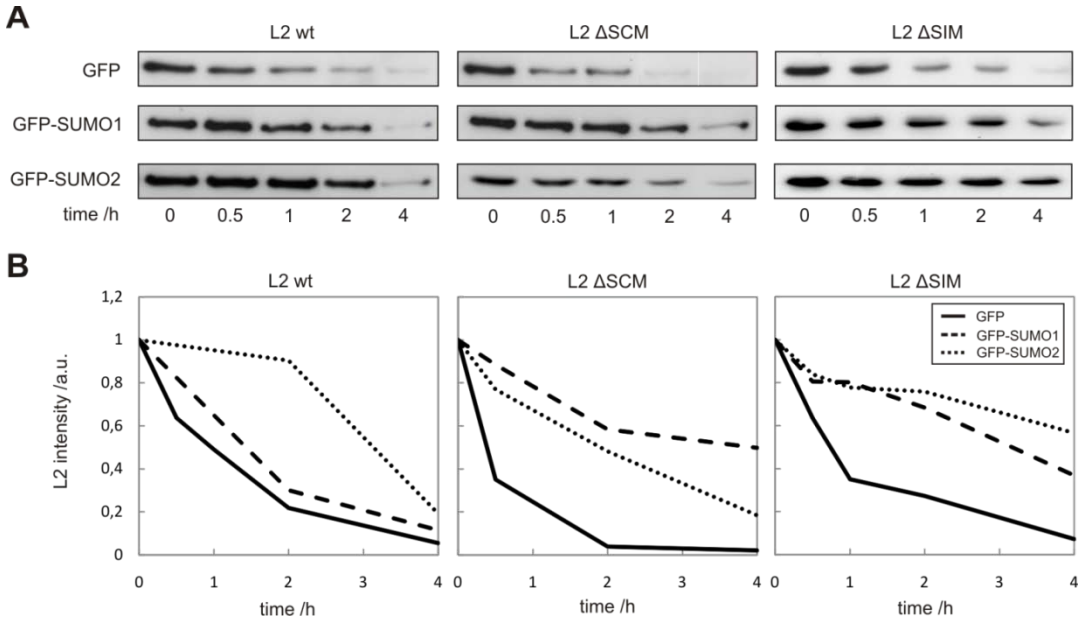

Fig. 3.9: L2 stabilization assay. ***A*** After coexpression of L2 together with GFP-SUMO1, GFP-SUMO2, or GFP protein synthesis was inhibited by addition of cycloheximide (CHX, 50 µg/ml). Lysates were prepared after 0.5, 1, 2, and 4 hours and characterized by immunodetection. The zero time control was prepared directly before addition of CHX to the parallel samples. For densitometrical quantification of L2, L2 blots with equal L2 zero time intensities were compared by variation of the exposure time during development of the films. ***B*** L2 bands were quantified densitometrically, normalized to the L2 amount of the zero-time controls (including β-actin correction) and plotted against the time. The protein half-life times of the different L2 mutants were determined by fitting of linear or exponential decay functions and were summarized in **Table 3.1**.

Without coexpression of GFP-SUMO proteins, the shortest L2 half-life time was detected for L2 ΔSCM (0.33 ± 0.2 h, Table 3.1). The half-life time for wild-type L2 was about 0.9 ± 0.2 h, for L2 ΔSIM about 1.4 ± 0.2 h. In general, coexpression of L2 together with GFP-SUMO1 or GFP-SUMO2 resulted in significantly prolonged L2 half-life times. Coexpression of GFP-SUMO2 extended half-life times of wild-type L2 and L2 ΔSIM to about 3.2 ± 0.2 h and 5.0 ± 0.2 h (GFP-SUMO1: 2.3 ± 0.2 h and 3.1 ± 0.2 h). For L2 ΔSCM, especially coexpression of GFP-SUMO1 resulted in a longer L2 half-life time of about 3.7 ± 0.2 h (GFP-SUMO2: 2.4 ± 0.2 h).

Table 3.1: L2 stabilization assay. L2 half-life times for coexpression of L2 with GFP-SUMO1, GFP-SUMO2, or GFP. The half-life times were determined by linear or exponential fitting of the L2 decay functions of **Figure 3.9, B**.

	L2 wt	L2 ΔSCM	L2 ΔSIM
GFP	0.9 ± 0.2	0.3 ± 0.2	1.4 ± 0.2
GFP-SUMO1	2.3 ± 0.2	3.7 ± 0.2	3.1 ± 0.2
GFP-SUMO2	3.2	2.4	5.0

3.1.8 No Interaction of L2 and SUMO1/2 in GST-SUMO or SUMO-his pulldowns

To characterize a possible interaction of purified SUMO1/2 with overexpressed L2, SUMO1/2 pulldown experiments were performed. Therefore, GST-SUMO1/2 or SUMO1/2-his_6 was immobilized on an affinity matrix followed by incubation with L2. Coprecipitation of L2 was characterized by immunodetection (Fig. 3.10). No coprecipitation of L2 was observed after incubation with GST, GST-SUMO1, or GST-SUMO2 (Fig. 3.10, A, lanes 2-4), although an adequate amount of the respective GST proteins was immobilized on the affinity matrix (see anti-GST Western Blot and Direct Red 81 protein staining, lanes 2-4). GST-pulldown and coprecipitation of L2 was repeated under different buffer and washing conditions, but no coprecipitation of L2 was observed. After immobilization of SUMO1/2-his_6 and incubation with L2, again, there was no coprecipitation of L2, since L2 band intensities in the lanes with L2 incubation with SUMO1/2-his_6 (Fig. 3.10, B, lanes 7 and 8) were comparable with the negative control after incubation of L2 with Ni-NTA beads without immobilized SUMO1/2 (lane 6). Nevertheless, anti-His Western Blots and Coomassie protein staining indicated immobilization of an adequate amount of highly pure SUMO1/2-his_6 (lanes 7 and 8).

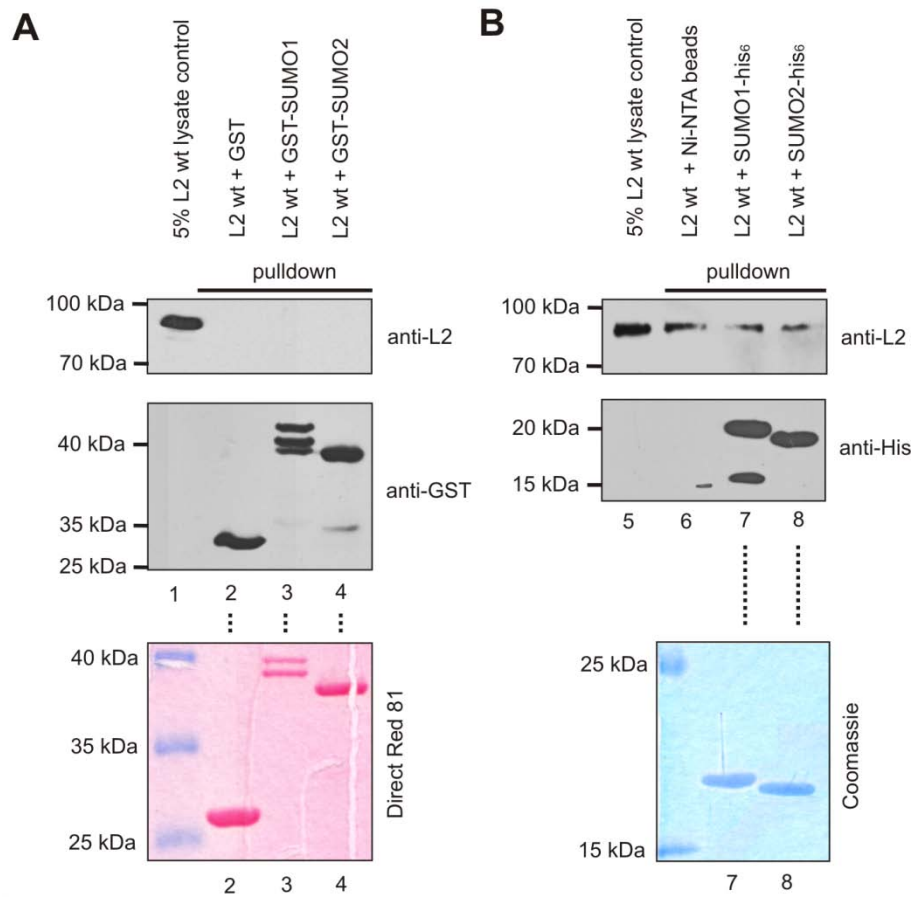

Fig. 3.10: No coprecipitation of L2 after SUMO1/2 immobilization. ***A*** GST-SUMO1 or GST-SUMO2 was overexpressed in *E.coli* and immobilized and purified on glutathione sepharose beads. L2 was overexpressed in HeLa cells and the L2 lysate was incubated with 8 µg of immobilized GST-SUMO1, GST-SUMO2, or GST. Immobilization of the GST proteins, as well as coprecipitation of L2, was characterized by immunodetection with anti-L2 or anti-GST antibodies. Although adequate amounts of L2 (lane 1) and GST-SUMO1/2 (lanes 3 and 4) were detected, no coprecipitation of L2 was observed. ***B*** SUMO1/2-his$_6$ was expressed in *E. coli* and immobilized and washed on Ni-NTA beads. L2 lysates were prepared after overexpression in HeLa cells and incubated with 8 µg of immobilized SUMO1-his$_6$, SUMO2-his$_6$, or Ni-NTA beads. Characterization of co-precipitated L2 by immunodetection revealed an equal amount of L2 after incubation with immobilized SUMO1 and SUMO2 (lanes 7 and 8), but a comparable L2 amount was also detected in the negative control after incubation of L2 with Ni-NTA beads without SUMO1/2 (lane 6). Therefore, the detected L2 bands only represent background precipitation of L2 on the Ni-NTA beads.

3.1.9 No interaction of L2 and SUMO in Mammalian-2-Hybrid screening

In addition to immunoprecipitation experiments, mammalian 2-Hybrid experiments were performed to monitor L2-SUMO interaction. Therefore, a bait fusion protein, containing a DNA binding domain (BD) and SUMO1/2, and a prey fusion protein, containing an activation domain (AD) and L2 as the potential interaction partner, were coexpressed in HeLa cells together with a luciferase reporter plasmid. After cell lysis, a luciferase-based reporter gene assay was performed to characterize transactivation of the luciferase gene by interaction of L2 with SUMO1 or SUMO2. Transactivation of the luciferase gene was only observed for the internal positive control, where a p53-BD fusion

protein interacts with a SV40-AD fusion protein (Fig. 3.11). For the combination of L2 fusion proteins with SUMO1 or SUMO2 fusion constructs, no transactivation of the luciferase gene was observed, as luciferase expression was comparable with the negative or blank controls. The experiment was repeated after a switch of L2 and SUMO1/2 within the bait and prey fusion proteins. However, also coexpression of BD-L2 together with AD-SUMO1 or AD-SUMO2 fusion proteins did not result in a transactivation of the luciferase reporter (data not shown).

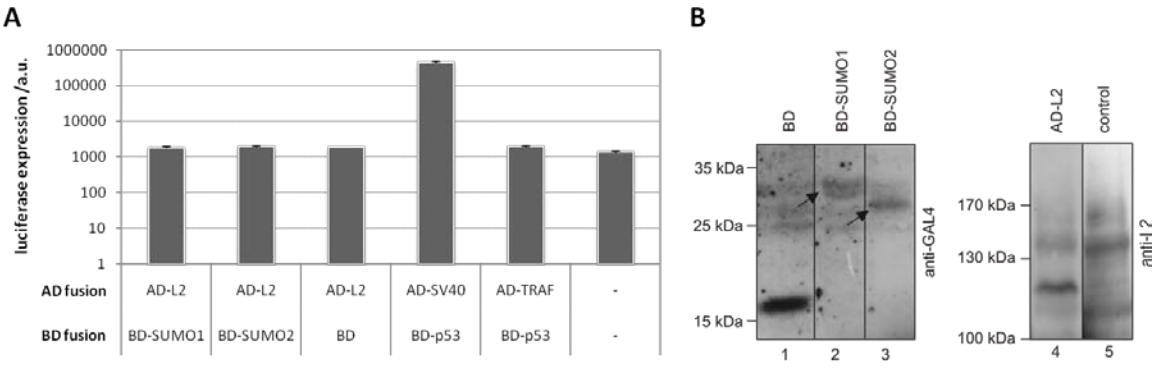

Fig. 3.11: No L2 interaction with SUMO1 or SUMO2 in mammalian 2-hybrid experiments. ***A*** AD-L2 was coexpressed with BD-SUMO1 or BD-SUMO2 in HeLa cells for 24 h followed by quantification of the luciferase expression upon transactivation of the luciferase reporter gene. There was no luciferase expression for coexpression of AD-L2 and BD-SUMO1/2, as detection levels were comparable to the negative controls (AD-L2 + BD, AD-TRAF + BD-p53) or the blank control without protein expression. Luciferase expression was only observed for the positive control of the 2-hybrid system, where coexpression of AD-SV40 and BD-p53 resulted in transactivation of the luciferase reporter. ***B*** The separate expression of the BD-SUMO1/2 and AD-L2 fusion proteins was characterized by immunodetection with an anti-GAL4 antibody for BD fusion proteins and anti-L2 for the AD-L2 fusion protein after overexpression for 24 h in HeLa cells.

3.1.10 The L2 SIM is also important for ubiquitin interaction of HPV16 L2

For the correct reproduction of viruses, a complex and well-regulated interaction with the host cell is absolutely necessary. Thereby, interaction with the cellular SUMO apparatus is regularly observed, but very often also ubiquitination or phosphorylation trigger the viral pathway. Based on these findings and the remarkable structural homology of SUMO proteins with ubiquitin, in the following experiment, a potential interaction of HPV16 L2 with ubiquitin was investigated by coprecipitation experiments with ubiquitin agarose beads. Therefore, cell lysates with overexpressed HPV16 L2 or L2 ΔSIM were incubated with ubiquitin-coupled agarose beads and incubated for 1.5 h at RT. After washing of the beads, potential co-precipitated L2 protein was characterized by immunodetection (Fig. 3.12). Only wild-type L2 was co-precipitated with ubiquitin agarose. There was no coprecipitation of L2 ΔSIM.

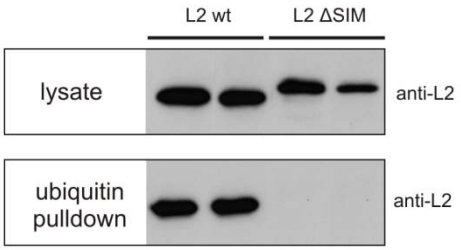

Fig. 3.12: No coprecipitation of L2 ΔSIM with ubiquitin agarose. Wild-type L2 and L2 ΔSIM were overexpressed for 24 h in HeLa cells in two parallels. L2 lysates were incubated with ubiquitin-coupled agarose beads and L2 coprecipitation was analyzed by immunodetection. While a strong L2 coprecipitation was observed for wild-type L2, there was no coprecipitation of L2 ΔSIM.

3.2 Structural and functional analysis of SUMO-interaction deficient L1/L2 ΔSIM PsVs

3.2.1 HPV16 L1/L2 ΔSIM PsVs are noninfectious

After characterizing the interaction of L2 with SUMO proteins after overexpression, the main focus was on the functional relevance of the L2 SIM in the context of HPV16 virions and infection. Therefore, wild-type L1/L2 PsVs and also L1/L2 ΔSIM PsVs were prepared. Infection of HeLa or HaCaT cells with L1/L2 wt, L1/L2ΔPHOS, or L1/L2 ΔSCM PsVs resulted in comparable luciferase expression levels (Fig. 3.13, A). Remarkably, luciferase expression was significantly decreased after infection with L1/L2 ΔSIM PsVs. Control infection with L1 VLPs did not result in significant luciferase expression.

To check whether the loss of infectivity of the L1/L2 ΔSIM PsVs was based on incorrect incorporation of L1 or L2 ΔSIM into the PsVs during capsid assembly, the L1 and L2 content of the PsV was quantified by immunodetection (Fig. 3.13, B). All PsV preparations contained an equal level of L1 and L2. For L1 VLPs, no L2 was detected, as L1 VLPs completely lack viral L2.

For comparable characterization of the infectivity of the different PsVs, the amount of PsVs was adjusted according to the DNA content of the respective PsV preparation to establish a constant level of reporter DNA for each PsV type. Reporter DNA quantification revealed an equal DNA level for all PsVs (Fig. 3.13, C). Thus, putative artifacts stemming from different reporter gene contents of the PsVs during infection assaying can be excluded.

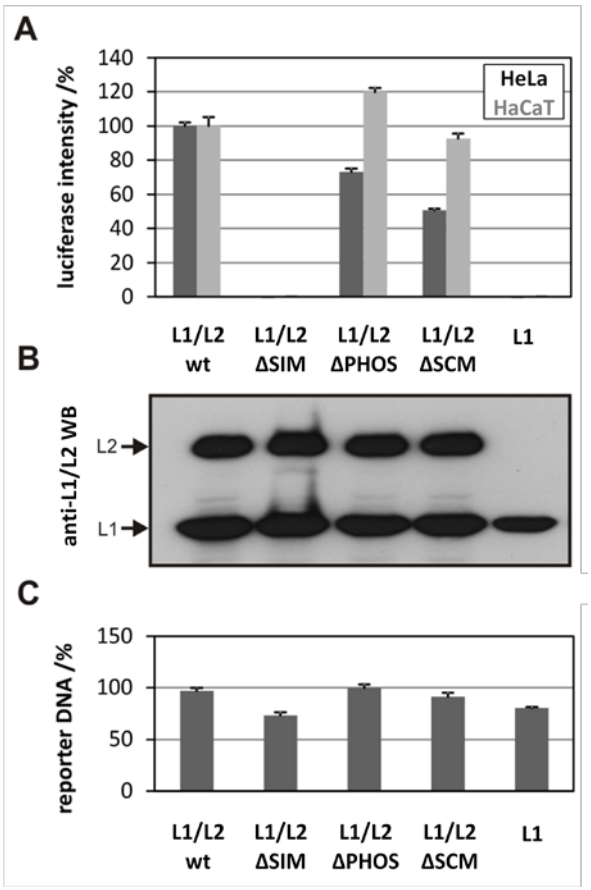

Fig. 3.13: L1/L2 ΔSIM PsVs are noninfectious. ***A*** HeLa or HaCaT cells were infected with L1/L2 PsVs or L1 VLPs for 24 h. Infectivity was characterized based on expression of a luciferase reporter gene, which was incorporated into the PsVs/VLPs during virus assembly. Infection with wild-type PsVs, as well as L1/L2 ΔPHOS or L1/L2 ΔSCM, resulted in comparable luciferase expressions. Remarkably, after infection with L1/L2 ΔSIM PsVs, no luciferase expression was detected. There was also no luciferase expression after infection with L1 VLPs. ***B*** Immunodection of L1 (anti-L1, 312F antibody) and L2 proteins (anti-L2, L2-1 antibody) revealed an equal amount of L1 and L2 for all PsVs/VLPs. ***C*** The reporter DNA content of the respective PsVs/VLPs was analyzed based on the Quant-iT^{TM} picogreen® DNA quantification kit (Invitrogen). All PsVs/VLPs contained comparable amounts of reporter DNA.

3.2.2 Correct assembly of L1/L2 ΔSIM PsVs

L1/L2 ΔSIM PsVs were subjected to an additional ultracentrifugation step on a 10-60% (w/v) sucrose gradient to analyze the content of larger L1/L2 aggregates, isolated capsomers, or nonassembled L1/L2 within the PsV preparation, which could cause loss of infectivity of L1/L2 ΔSIM PsVs preparations. Therefore, after ultracentrifugation, the PsV fractions were characterized by immunodetection (Fig. 3.14). All PsV gradients contained well detectable amounts of L1 and L2 protein (for L1 VLPs only L1 was detected). Maximum L1 and L2 intensity was detected for fractions 12-14, which represented the peak fractions for all PsV gradients depicting intact PsVs. Within the last fractions, there were no larger amounts of aggregated viral debris or L1/L2 aggregates. As for L1 VLP, the L1 maximum was not as distinct as for the other PsVs and also the bottom fraction 16 and 17 contained larger amounts of L1. This could be an indication that L1 VLPs were not as uniform in

size and structure as the other PsVs. Additionally, in all gradients, there was no L1 or L2 detected in one of the first fractions, which is a good mark that all L1 and L2 was incorporated into the PsVs. Infection assays with the pooled PsVs peak fractions after sucrose gradient ultracentifugation confirmed the results obtained before: Infection with wild-type PsVs and L1/L2 ΔSCM PsV led to comparable levels of luciferase expression, again, indicating full functionality and infectivity of the PsVs. No luciferase expression was detected for the L1/L2 ΔSIM PsVs and also for L1 VLPs (data not shown).

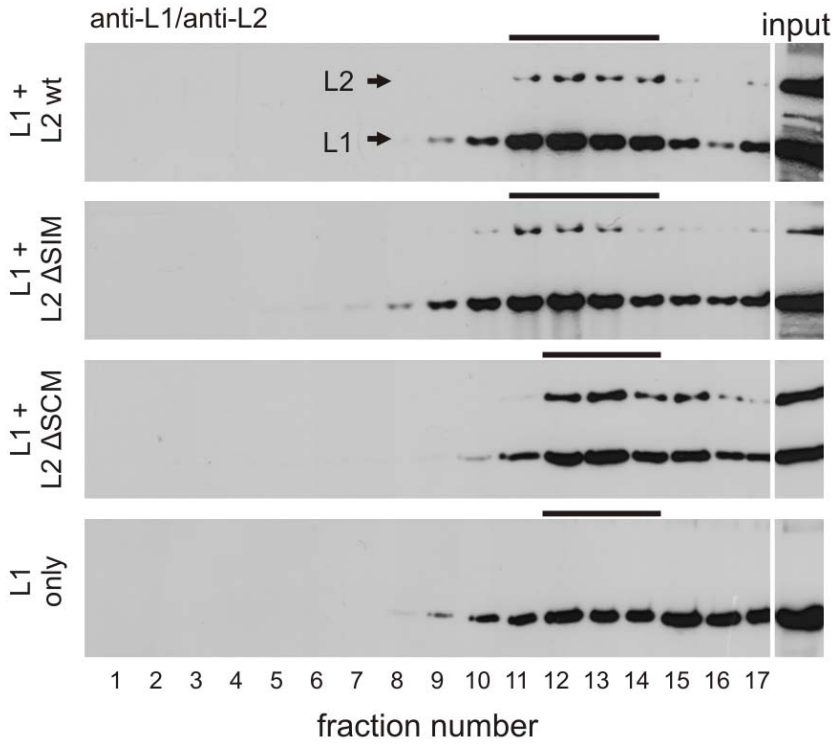

Fig. 3.14: Correct assembly of L1/L2 ΔSIM PsVs. To characterize the correct assembly of L1/L2 ΔSIM PsVs, the purified PsVs were subjected to an additional ultracentrifugation (150 min at 36,000 rpm and 4 °C) to detect possible L1/L2 aggregates, isolated capsomers, or non-assembled L1/L2, which could cause the loss of infectivity of L1/L2 ΔSIM PsVs preparations. The fractions were characterized by immunodetection with anti-L2 (L2-1) and anti-L1 (312F) antibodies. The highest L1/L2 amounts were detected in the peak fractions 12-14. There was no larger amount of non-assembled L1/L2, which would be detectable in the first fractions of the gradient. There were also no larger L1/L2 aggregates within the last fractions, indicating that the majority of PsVs within the respective preparation were intact and not disrupted allowing formation of even larger L1/L2 aggregates. There was no detection of any clear peak fractions for L1 VLPs, possibly indicating a larger polydispersity.

3.2.3 L1/L2 ΔSIM PsVs show a wild-type phenotype in electron microscopy

After characterization of PsV assembly by sucrose gradient ultracentrifugation, the PsVs were additionally characterized by Transmission Electron Microscopy (TEM) to directly visualize the capsid structure and to check for any defects for L1/L2 ΔSIM PsVs, which could cause loss of infectivity. All PsVs investigated here featured a wild-type phenotype with typical spherical capsids with a diameter

of about 55 nm (Fig. 3.15). In general, the mutations within the L2 capsid proteins (L2 ΔSIM, L2 ΔPHOS, L2 ΔSCM) did not lead to a visible defect of the capsid structure of the assembled L1/L2 PsVs. Additionally, also staining of the reporter DNA with 5-ethynyl-2´-deoxyuridine (EdU) during PsV preparation, which allows for a fluorescence microscopic characterization of PsV infection, did not visibly alter the capsid structure of the respective PsVs (data not shown).

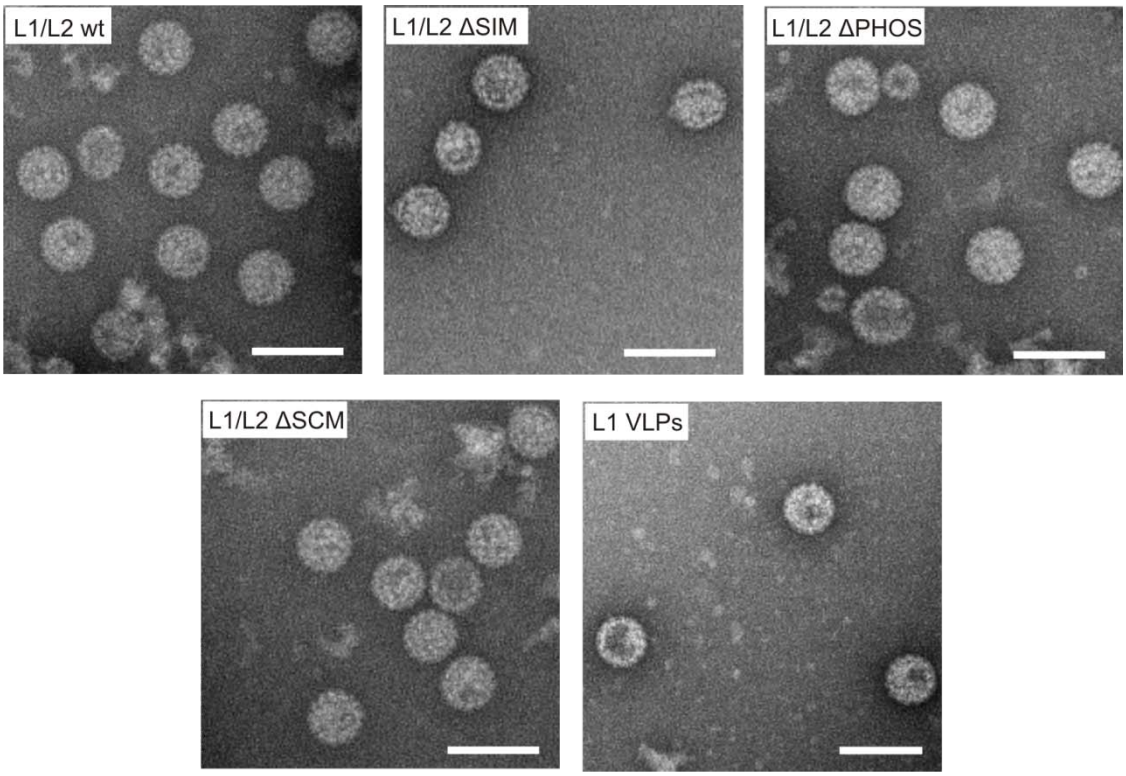

Fig. 3.15: L1/L2 ΔSIM PsVs show a wild-type capsid structure in electron microscopy. PsVs were streaked on copper grits, stained with uranylacetate, and washed with PBS. TEM pictures were made on a 300 kV *High Resolution Cryo-TEM*. A comparable amount of intact viral cpasids with diameters of about 55 nm were detected within all PsV/VLP preparations (scale bar: 100 nm). There were no visible structural defects of the viral capsids due to virus assembly based on L1 and L2 ΔSIM, L2 ΔPHOS, or L2 ΔSCM. The pictures were taken by Philip Arnold (AG Markl, Johannes Gutenberg University, Mainz).

3.2.4 L1/L2 ΔSIM PsVs bind to HeLa and HaCaT cells and are endocytosed

Loss of infectivity of L1/L2 ΔSIM PsVs could by provoked by several factors. To exclude aberrations during cell binding and endocytosis of L1/L2 ΔSIM PsVs, the attachment of the PsV onto target cells and viral uptake by endocytosis was characterized by flow cytometry. To test cell binding of PsVs, HeLa and HaCaT cells were infected with L1/L2 PsVs for 15 min. Then, the PsVs were labeled with an anti-L1 antibody in combination with an AlexaFluor488 secondary fluorescence antibody for detection in flow cytometry (Fig. 3.16, A and B).

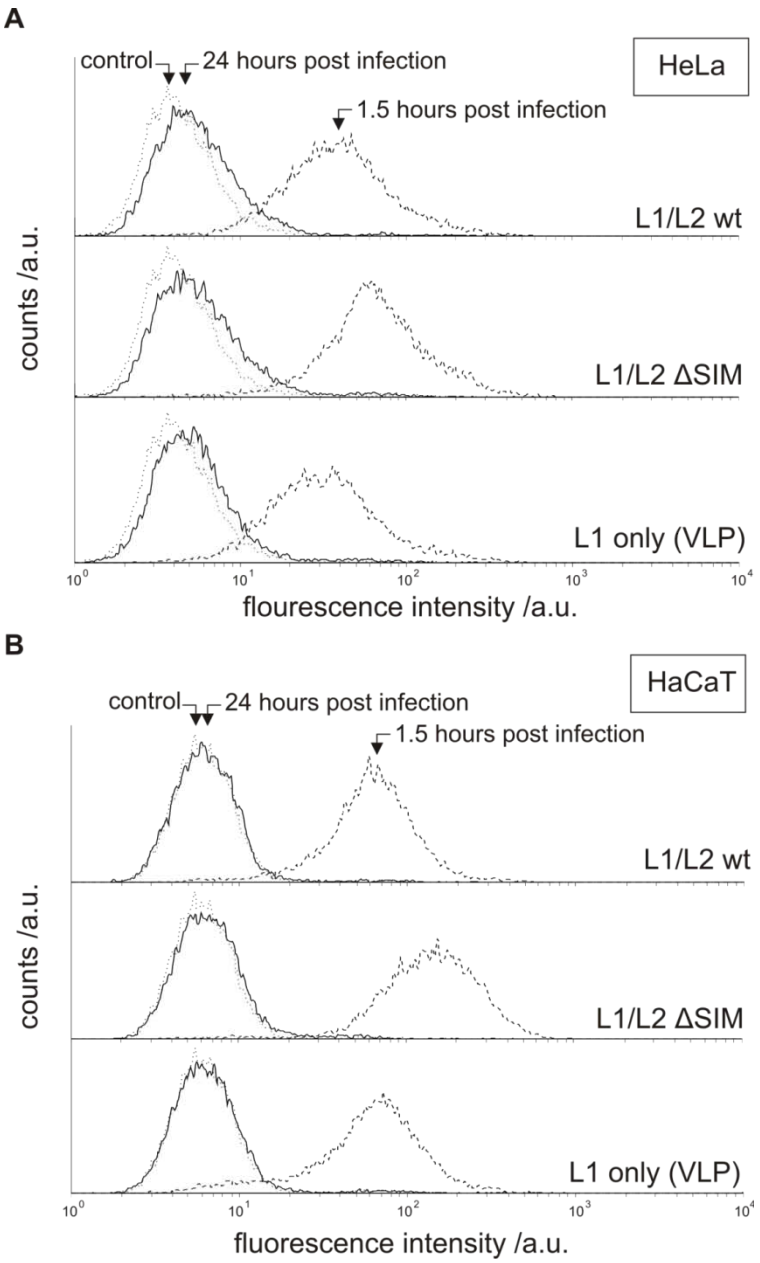

Fig. 3.16: Wild-type cell binding and endocytosis of L1/L2 ΔSIM PsVs. HeLa cells (***A***) or HaCaT cells (***B***) were infected with L1/L2 PsVs. Cell binding and endocytosis of the PsVs/VLPs was characterized by flow cytometry based on detection of viral L1 with a primary anti-L1 antibody (L1-7), which was coupled with a secondary fluorescence antibody (AF488). For characterization of cell binding, the target cells were incubated with PsVs/VLPs for 10 min, washed, and subsequently prepared for quantification of the L1 fluorescence by flow cytometry. Here, high L1 fluorescence intensities were reached for all PsVs/VLPs, indicating that equal amounts of viruses were able to bind to the target cells. To check whether cell-bound PsVs/VLPs were also able to be endocytosed, target cells were again infected for 10 min, but this time flow cytometry was performed after a 24 h incubation of the target cells with the cell-bound viruses to allow endocytosis. All PsVs/VLPs seemed to be endocytosed, as there was no L1 fluorescence stemming from residual surface-bound viruses. Here, the L1 fluorescence was at the same level as within negative controls with non-infected HeLa or HaCaT cells.

An equal level of L1 fluorescence was detected for all PsVs/VLPs, indicating that comparable amounts of PsVs/VLPs, including L1/L2 ΔSIM PsVs, were attached to the host cells. To analyze endocytosis of cell-bound PsVs/VLPs, again, HeLa and HaCaT cells were infected for 15 min. This time, the cells were

incubated for additional 24 h to allow endocytosis of the viruses. After fluorescence-labeling of L1, the L1 fluorescence was again characterized by flow cytometry. Fluorescence intensities were on a background level and comparable with negative controls without PsV/VLP infection of the target cells. This is a direct hint that all PsVs/VLPs, also L1/L2 ΔSIM PsVs, were successfully endocytosed after cell binding, since there was no detection of L1 fluorescence stemming from residual PsVs/VLPs on the cell surface.

In a novel attempt, the cell binding of PsVs/VLPs was also characterized by standard CW-EPR measurements. Therefore, PsVs/VLPs were incubated with Fremy's Salt (NDS, potassium nitrosodisulfonate) to allow electrostatic attachment of NDS to postitively charaged amino acid patches of L1 and L2. Then, the L1-/L2-coupled NDS molecules served as a sensor for monitoring the cell binding of the NDS-labeled viruses after incubation with target cells by measurement of the time-dependent decay of the NDS signal in CW EPR measurements. The NDS CW EPR spectra were not further analyzed according to spectral parameters, since variations in spectral breadth and/or mobility effects were only affected by the sample viscosity due to residual amounts of Optiprep® medium, which could not be maintained at exactly comparable levels during preparation of the different PsVs for CW EPR measurements but did not significantly interfere with EPR activity of the NDS molecules. However, EPR samples were comparable within the same PsV type, since the samples used for characterization of effects based on addition of cells or heparin originated from each one master sample for each type of PsVs containing PsVs and NDS. NDS within pure buffer solution featured highest half-life times. Whenever NDS molecules get in closer contact, like e.g. at the positively charged amino acid patches in L1/L2, the half-life time of the NDS molecules decreases. For NDS incubation with wild-type L1/L2 PsVs, NDS half-life times of about 45 ± 10 min were detected (Fig. 3.17, A). After addition of heparin to the NDS/PsV solution, extended half-life times of about 60 ± 10 min were detected, while addition of HaCaT cells led to decreased NDS half-life times of about 35 ± 10 min. These trends were also observed for L1/L2 ΔPHOS and L1/L2 ΔSCM PsVs. Experiments based on NDS incubation with L1/L2 ΔSIM PsVs and L1 VLPs resulted in slightly longer NDS half-life times, also for incubation with heparin or HaCaT cells. Incubation of the NDS/PsV solution with a larger amount of HaCaT cells lead to a drastic decrease of NDS half-life times without a greater change of the half-life times for samples without HaCaT cells (Fig. 3.17, B). Since addition of heparin lead to a stabilization of NDS in all samples, it was checked whether pre-incubation of the NDS/PsV mix with even higher amounts of heparin could inhibit the effect of strongly decreased NDS intensity provoked by addition of HaCaT cells (Fig. 3.17, C). In fact, after incubation of the NDS/PsVs mix with heparin, the NDS half-life times after addition of HaCaT cells were comparable with NDS half-life times before addition of HaCaT cells (about 70 ± 10 min).

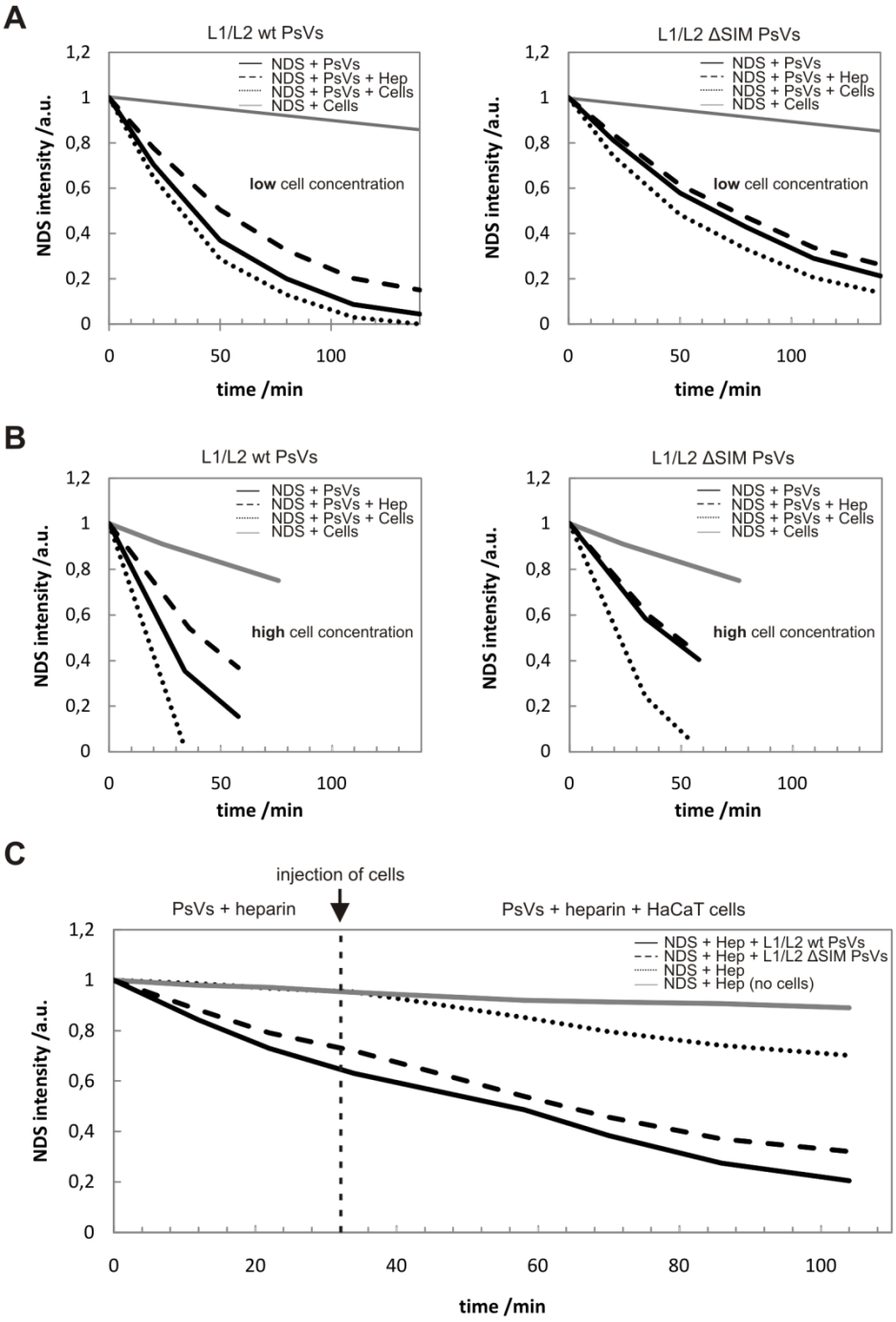

Fig. 3.17: Addition of HaCaT cell induces NDS dissociation in NDS/PsV samples in CW EPR measurements. Different PsVs/VLPs were incubated with NDS at equimolar levels of L1/L2 and NDS. The NDS EPR signal intensity was plotted against the time for the mixture of NDS and PsVs alone, or after addition of an excess amount of heparin or HaCaT cells. ***A*** Addition of about 10,000 HaCaT cells per sample lead to reduced NDS half-life times (35 min) when compared with the reference sample without cells (40 ± 10 min) or with the sample containing heparin (60 ± 10 min). The same trends were observed for L1/L2 ΔSIM PsVs, but here, in general, slightly prolonged NDS half-life times were deduced. ***B*** The NDS intensity vanished within several minutes when larger amounts of HaCaT cells (~200,000) were added to the NDS/PsV samples. Half-life times for the reference samples without HaCaT did not vary significantly from the previous experiment in **Fig. 3.17, A**. Also, the NDS half-life time of the negative control containing only NDS and a comparable amount of HaCaT cells was not shortened significantly, indicating only a small background interaction of NDS with the injected HaCaT cells. Again, slightly extended NDS half-life times were detected for samples containing L1/L2 ΔSIM PsVs (and L1 VLPs, data not shown). ***C*** It was also tested whether pre-incubation of PsVs/VLPs with heparin could inhibit the effect of shortened NDS half-life times after addition of HaCaT cells. Remarkably, NDS half-life times after addition of HaCaT cells were comparable to the half-life times of the mixture of NDS/PsVs with heparin before injection of cells (about 70 ± 10 min).

3.2.5 No PML-colocalization of DNA or L2 after infection with L1/L2 ΔSIM PsVs

Flow cytometry and CW-EPR measurements with Framy's Salt indicated a wild-type cell binding and endocytosis of L1/L2 ΔSIM PsVs. Here, fluorescence microscopy was performed to check for an influence of the L2 ΔSIM mutation on the nuclear transport or PML-localization of the L2-DNA complex, which could also lead to a loss of infectivity for L1/L2 ΔSIM PsVs. Therefore, L2 and the reporter DNA were labeled with different fluorescence dyes to characterize the cellular localization. After infection with L1/L2 wt, L1/L2 ΔPHOS, and L1/L2 ΔSCM PsVs, a very strong colocalization of viral DNA and L2 was found in the cytoplasm and in the cell nucleus (Fig. 3.18). In the nucleus, a strong colocalization of viral DNA and L2 with PML was observed. Remarkably, after infection with L1/L2 ΔSIM PsVs, no PML-localization of DNA or L2 was observed. Instead, there were large L2 aggregates, which were only detectable when focusing out of the plane of the cell nuclei (see arrows in Fig. 3.19).

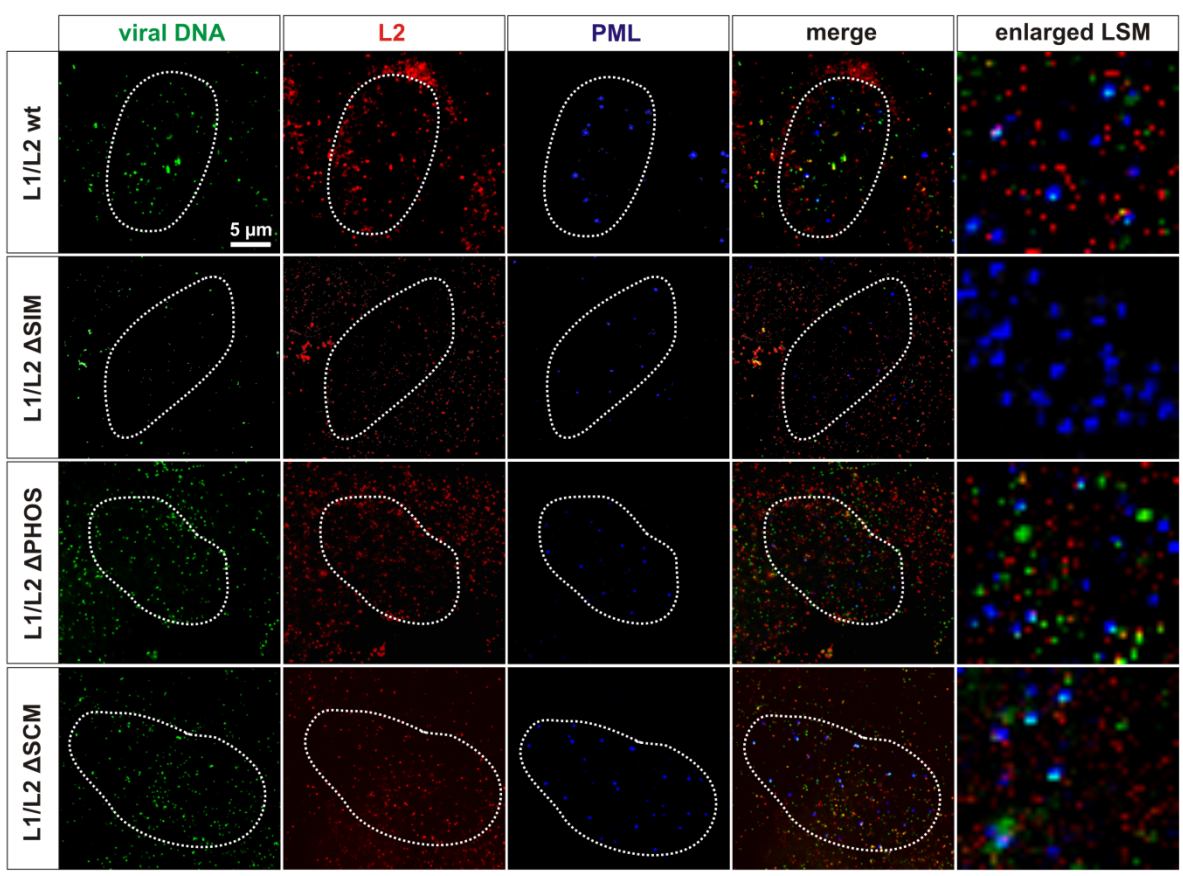

Fig. 3.18: No PML-localization of viral DNA or L2 after infection with L1/L2 ΔSIM PsVs. After infection of HeLa cells with L1/L2 wt, L1/L2 ΔPHOS, and L1/L2 ΔSCM PsVs, a strong colocalization of viral DNA and L2 was observed in the cytoplasm and in the nucleus (see also enlarged pictures of the cell nuclei taken with a laser scanning microscope, LSM). In the nucleus, a strong PML-localization of viral DNA and L2 was observed. After infection with L1/L2 ΔSIM PsVs, almost no PML-localization of viral DNA or L2 was detected. Viral DNA was labeled based on 5-ethynyl-2´-deoxyuridine (EdU) in combination with an AlexaFluor488 fluorescence dye. The last column shows an enlarged section of the cell nucleus taken by laser scanning microscopy (LSM).

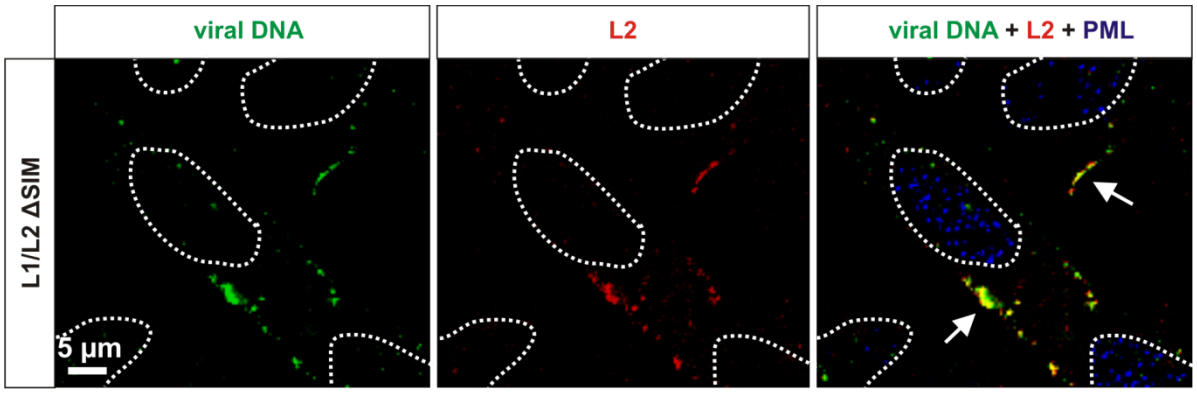

Fig. 3.19: L2 ΔSIM aggregates on the cell surface. L2 ΔSIM colocalized with the viral DNA in dense structures at the cellular surface after 24 h of infection. Almost no L2 ΔSIM was found within the nucleus (pictures taken on a laser scanning microscope, LSM).

In order to statistically quantify colocalization of L2 or viral DNA with endogenous PML, a pixel-by-pixel colocalization analysis was performed. Therefore, 80-100 nuclei were selected for each type of PsVs and PML-localization of L2 or viral DNA was determined. The PML-colocalizations after infection with wild-type viruses were used as 100% reference. Most PML-colocalized L2 was observed after infection with L1/L2 ΔSCM PsVs (160%) and wild-type PsVs (100%, Fig. 3.20, A). Almost no PML-localized L2 was detected after infection with L1/L2 ΔSIM PsVs (7%). Infection with L1/L2 ΔPHOS PsVs resulted in a medium colocalization level of L2 with PML (60%). With regard to the viral DNA, significant levels of PML-localized viral DNAs were only detected after infection with wild-type or with L1/L2 ΔPHOS PsVs (100 and 65%). Almost no PML-colocalization of viral DNA was detected after infection with L1/L2 ΔSIM (<1%) and L1/L2 ΔSCM PsVs (13%).

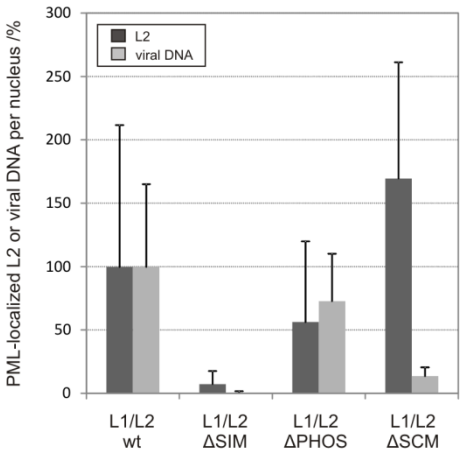

Fig. 3.20: No PML-colocalization of L2 and viral DNA after infection with L1/L2 ΔSIM PsVs. The PML-colocalization of L2 or viral DNA per nucleus is given in percent with respect to the colocalization levels detected after infection with wild-type PsVs (100% control). Almost no PML-colocalization of L2 or viral DNA was detected after infection with L1/L2 ΔSIM PsVs. Infection with L1/L2 ΔSCM PsVs lead to decreased levels of PML-localized viral DNA, but not L2.

3.2.6 No destabilization of L2 after infection with L1/L2 ΔSIM PsVs

To analyze differences in protein stability of viral L2 after infection with mutant L1/L2 ΔSIM PsVs, which could be indicative for the differences observed for the localization of L2 ΔSIM, L1 and L2 stability assays were performed after infection with L1/L2 PsVs. Therefore, the amount of L1 and L2 was quantified based on immunodetection of L1 and L2 at time points of 1, 8, 24, and 48 h post infection (Fig. 3.21, A).

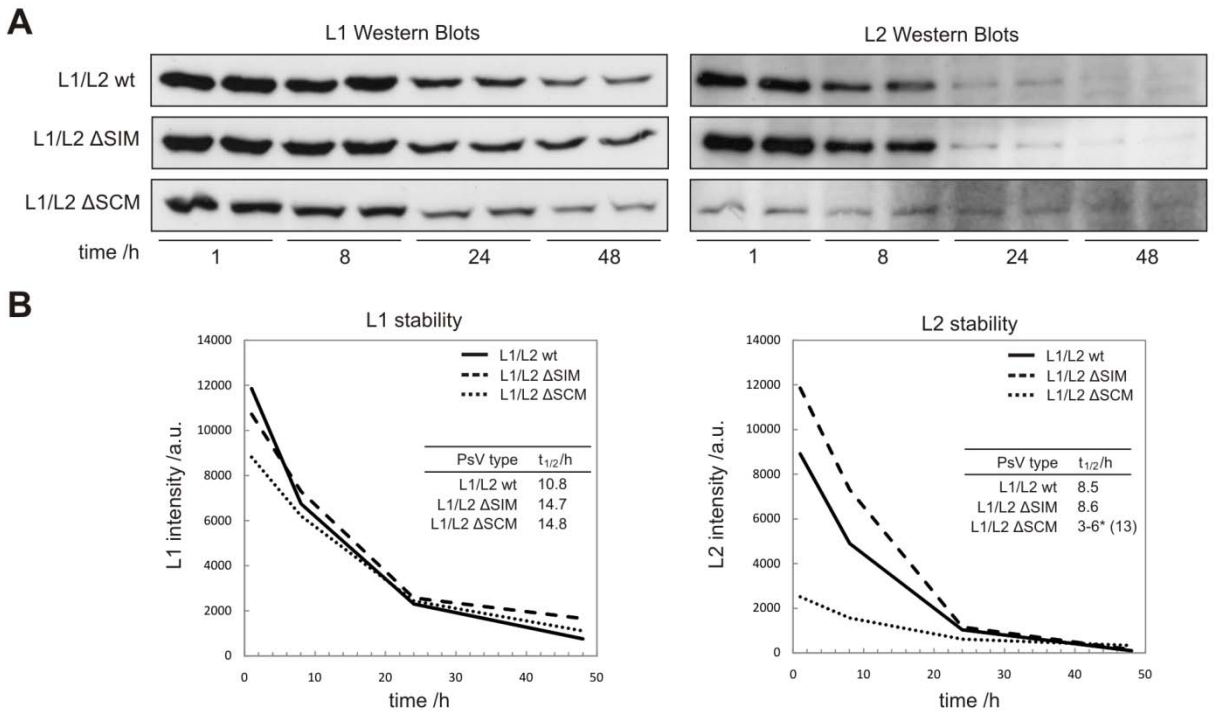

Fig. 3.21: No destabilization of L2 after infection with L1/L2 ΔSIM PsVs. ***A*** Comparable L1 amounts were detected after infection of HeLa cells with L1/L2 wt and L1/L2 ΔSIM PsVs for the given infection periods (1, 8, 24, and 48 hours, with two parallel experiments, each). Slightly less L1 was detected after infection with L1/L2 ΔSCM PsVs. A comparable amount of L2 was detected after infection with wild-type PsVs and L1/L2 ΔSIM PsVs. For infection with L1/L2 ΔSCM PsVs, L2 detection levels were significantly lower (about 20% of the wild-type L2). ***B*** The L1/L2 amounts were obtained by densitometrical analysis of the L1/L2 Western Blots, normalized according to the β-actin control, and plotted against the infection time. L1 and L2 half-life times were derived by exponential fitting of the L1/L2 decay curves (with $R^2 > 0.95$ for all fit functions). There were no significant differences of the L2 half-life times after infection with L1/L2 wt or L1/L2 ΔSIM PsVs (both about 9 hours). The small amount of L2, which was detected after infection with L1/L2 ΔSCM PsVs, had a very long half-life time of about 13 h. However, assumption of roughly comparable L2 levels at the beginning of infection gave rise to a corrected half-life time between 3 and 6 hours L2 ΔSCM, which seems to be more realistic due to comparable L1 amounts for infection with the different PsVs and normalization of the PsV amounts to gain a balanced L1 and L2 content. Remarkably, after 24 hours of infection, which also represents the standard infection time, the L2 content was at a comparable level for all PsVs.

The L1/L2 half-life times were determined by exponential fitting of the respective decay curves after densitometrical analysis of the L1/L2 bands (Fig. 3.21, B). Equal L1 amounts were detected after infection with wild-type and L1/L2 ΔSIM PsVs. A little less L1 was detected after infection with L1/L2 ΔSCM PsVs. L1 half-life times were almost comparable, but slightly expanded after infection with

L1/L2 ΔSIM and L1/L2 ΔSCM PsVs (about 15 h) when compared with wild-type PsVs (about 11 h). In contrast, the amounts of detected L2 varied significantly. After infection with wild-type and L1/L2 ΔSIM PsVs, comparable amounts of L2 were detected, while after infection with L1/L2 ΔSCM PsVs, the detectable L2 amount was only about 20% with respect to the wild-type PsVs. L2 half-life times were about 9 h for wild-type and L1/L2 ΔSIM PsVs. After infection with L1/L2 ΔSCM PsVs, the residual L2 seemed to feature a longer half-life time of about 14 h. However, since the amount of the different PsVs used for infection was normalized to guarantee a comparable L1/L2 amount at the starting point, a corrected half-life time for L2 ΔSIM was derived with a half-life time of 3-6 h implementing a very fast decay of L2 ΔSCM.

3.2.7 Overexpression of wild type L2 does not recover infectivity of L1/L2 ΔSIM PsVs

In order to check whether overexpression of wild-type L2 could restore infectivity of HPV16 L1/L2 ΔSIM PsVs, wild-type L2 was overexpressed before infection with L1/L2 wt or L1/L2 ΔSIM PsVs. There was no luciferase expression for infection with L1/L2 ΔSIM PsVs after overexpression of wild-type L2 (Fig. 3.22). Control experiments with transfection of an empty control plasmid before infection with wild-type PsVs led to the same luciferase expression as after overexpression of wild-type L2.

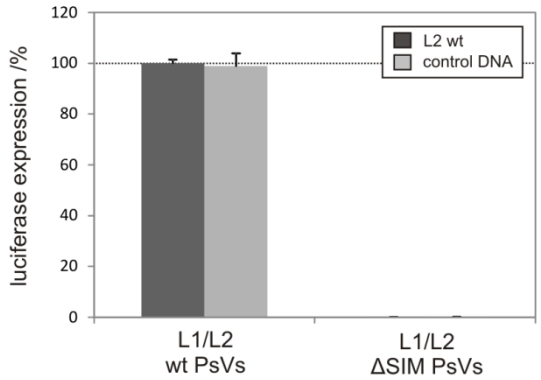

Fig. 3.22: Overexpression of wild-type L2 does not recover infectivity of L1/L2 ΔSIM PsVs. HeLa cells were transfected with wild-type L2 DNA or the same amount of an empty control plasmid. After 24 h, the cells were infected with either L1/L2 wt or L1/L2 ΔSIM PsVs for 24 h. Both, in the control experiment and after overexpression of wild-type L2, no luciferase expression was observed for infection with L1/L2 ΔSIM PsVs. With respect to wild-type PsVs, the same level of luciferase expression was observed after transfection of the control plasmid or wild-type L2 DNA.

3.2.8 Overexpression of GFP-SUMO1/2 enhances infectivity of HPV16 PsVs

To characterize the influence of a modified level of cellular SUMO proteins on HPV infection, different amounts of GFP-SUMO1, GFP-SUMO2, or GFP control DNA were transfected into HeLa cells. After protein expression for 24 hours, the cells were infected with L1/L2 wt PsVs (Fig. 3.23 A) or L1/L2 Δ SCM PsVs (Fig. 3.23, B). Interestingly, increasing luciferase expression was observed with increasing amounts of transfected GFP-SUMO1 or GFP-SUMO2 DNA for both PsVs types. It is noteworthy that especially expression of GFP-SUMO2 seems to increase infectivity of both PsVs types. Additional experiments showed that there were no additive effects due to coexpression of GFP-SUMO1 together with GFP-SUMO2 on infectivity of PsVs.

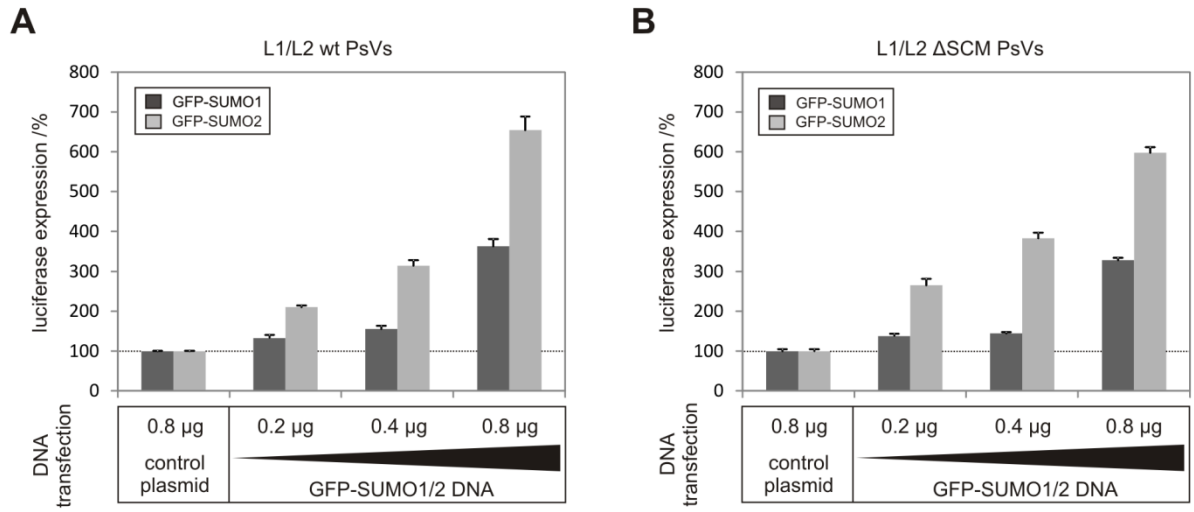

Fig. 3.23: GFP-SUMO1/2-dependent enhancement of HPV infection. HeLa cells were transfected with different amounts of GFP-SUMO1, GFP-SUMO2, or GFP DNA. The total amount of transfected DNA was kept constant by addition of an empty control plasmid. After 24 hours of protein expression, the cells were infected with L1/L2 wt (***A***) or L1/L2 ΔCM PsVs (***B***) for 24 hours. Luciferase expression was normalized according to the expression level for the control experiments without overexpression of GFP-SUMO1/2. Both, for infection with wild-type PsVs or L1/L2 ΔCM PsVs, a DNA dosis-dependent increase of luciferase expression was observed. Especially expression of GFP-SUMO2 led to a 5-7 fold increase of luciferase expression. Expression of GFP had no effect on luciferase expression, when compared with control transfections with an empty pcDNA 3.1 (+) vector.

3.2.9 SUMO2 siRNA knockdown strongly increases infectivity of HPV16 PsVs

After checking the effect of overexpression of SUMO proteins on infectivity of HPV16 PsVs, additional experiments based on depletion of SUMO proteins were performed. Therefore, endogenous SUMO1/2 was depleted by RNA interference after transfection with specific SUMO1/2 siRNAs. First, the knockdown of overexpressed GFP-SUMO1/2 was characterized by quantification of the GFP fluorescence to ensure functionality of the selected siRNAs (Fig. 3.24, A).

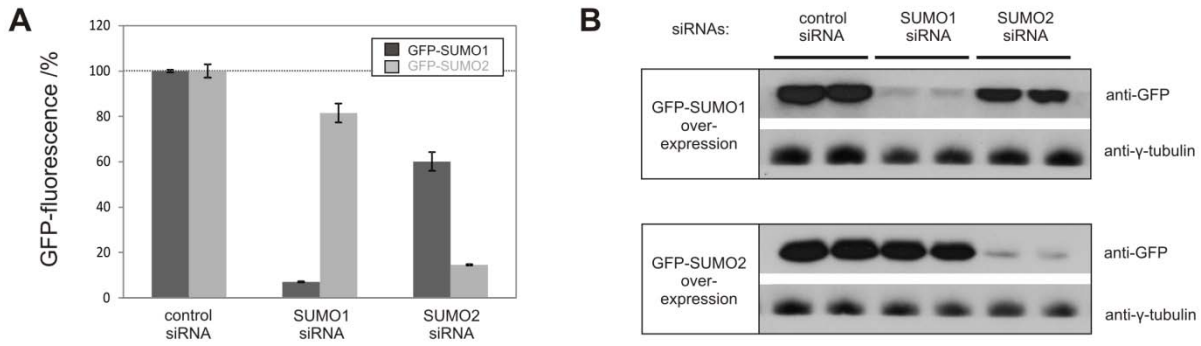

Fig. 3.24: Specific knockdown of GFP-SUMO1 or GFP-SUIMO2 by SUMO1/2 siRNAs. HeLa cells were transfected with SUMO1, SUMO2, or control siRNA for 24 h followed by transfection of GFP-SUMO1 or GFP-SUMO2 DNA. GFP-SUMO1/2 was overexpressed for additional 24 h before the cell lysate was characterized by quantification of the GFP fluorescence in a plate reader (***A***) or by immunodetection of GFP-SUMO1/2 with an anti-GFP (Jl-8) antibody (***B***). Transfection with SUMO1 siRNA lead to an almost complete depletion of GFP-SUMO1 while GFP-SUMO2 levels remained comparable to the controls with transfection of control siRNA. Transfection with SUMO2 siRNA resulted in a significant depletion of GFP-SUMO2 while GFP-SUMO1 levels were at about 60% when compared to transfection of control siRNA.

An almost total loss of GFP fluorescence was found for overexpression of GFP-SUMO1 after transfection of SUMO1 siRNA. Transfection of SUMO2 siRNA had almost no effect on GFP fluorescence of overexpressed GFP-SUMO1. *Vice versa*, an almost total loss of GFP fluorescence of GFP-SUMO2 was recorded after transfection with SUMO2 siRNA. Transfection with SUMO2 siRNA resulted in an about 40% reduction of GFP fluorescence for GFP-SUMO1. The depletion of the siRNA target molecules GFP-SUMO1 and GFP-SUMO2 was also characterized by immunodetection (Fig. 3.24, B). A significant depletion of overexpressed GFP-SUMO1 was detected after transfection of SUMO1 siRNA. Band intensities of GFP-SUMO1 remained almost unaltered for transfection with control siRNA and SUMO2 siRNA. As for overexpression of GFP-SUMO2, transfection with SUMO2 siRNA induced an almost complete loss of GFP-SUMO2 compared to transfections with control siRNA and SUMO1. Taken together, the two siRNAs selectively and efficiently depleted expression of the respective target proteins GFP-SUMO1 and GFP-SUMO2 after overexpression.

After the specific siRNA-mediated depletion of overexpressed GFP-SUMO1/2 was confirmed, the effect of depletion of endogenous SUMO proteins on infectivity of HPV16 PsVs was characterized (Fig. 3.25). Transfection with SUMO1 siRNA resulted in a significant reduction of luciferase expression after infection with wild-type and L1/L2 ΔSCM viruses (20 and 30% with respect to the control). Remarkably, luciferase expression exceeded the background detection level for infection with L1/L2 ΔSIM PsVs. Transfection with SUMO2 siRNA led to a strong enhancement of luciferase expression (about 600% and 800%) for wild-type and L1/L2 ΔSCM PsVs. However, also lucifease expression upon infection with L1/L2 ΔSIM PsVs was significantly increased.

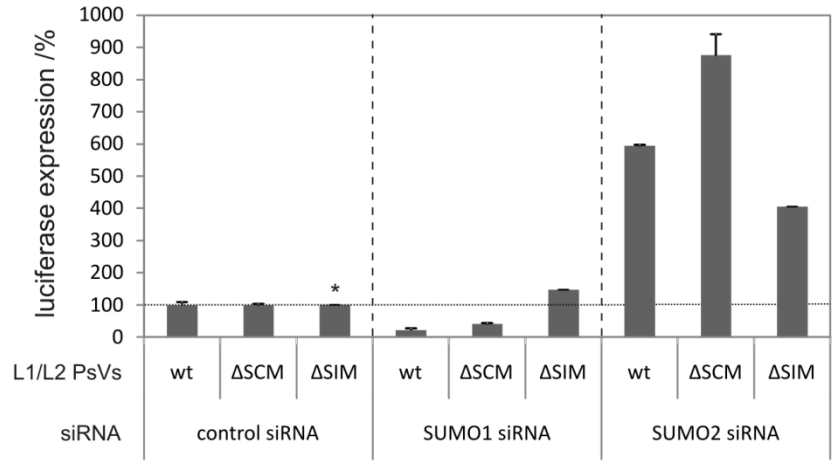

Fig. 3.25: SUMO2 depletion increased infectivity of HPV16 PsVs. HeLa or HaCaT cells were transfected with SUMO1, SUMO2, or control siRNA followed by infection with L1/L2 wt, L1/L2 ΔSCM, or L1/L2 ΔSIM PsVs for 24 h. Luciferase expression levels were corrected according to the LDH and normalized to the expression detected after transfection with control siRNA. Note that the 100% control for infection with L1/L2 ΔSIM PsVs (marked with a star) only represents the experimental background, since infection with L1/L2 ΔSIM PsVs did not lead to significant luciferase expression. Transfection with SUMO1 siRNA significantly reduced luciferase expression after infection with L1/L2 wt or L1/L2 ΔSCM PsV. Remarkably, for infection with L1/L2 ΔSIM PsVs, luciferase expression levels for the first time crossed the level of background detection. Transfection with SUMO2 siRNA resulted in strongly increased luciferase expression levels for all PsVs, including L1/L2 ΔSIM.

In a control experiment, the possible influence of the siRNA transfection procedure on the following expression of a transfected luciferase reporter gene was characterized (Fig. 3.26, A). Luciferase expression was at an equal level after transfection of control siRNA and SUMO2 siRNA. As for transfection with SUMO1 siRNA, the luciferase intensity was reduced to about 75%. In the positive control, transfection of luciferase siRNA successfully reduced luciferase expression to about 30% intensity.

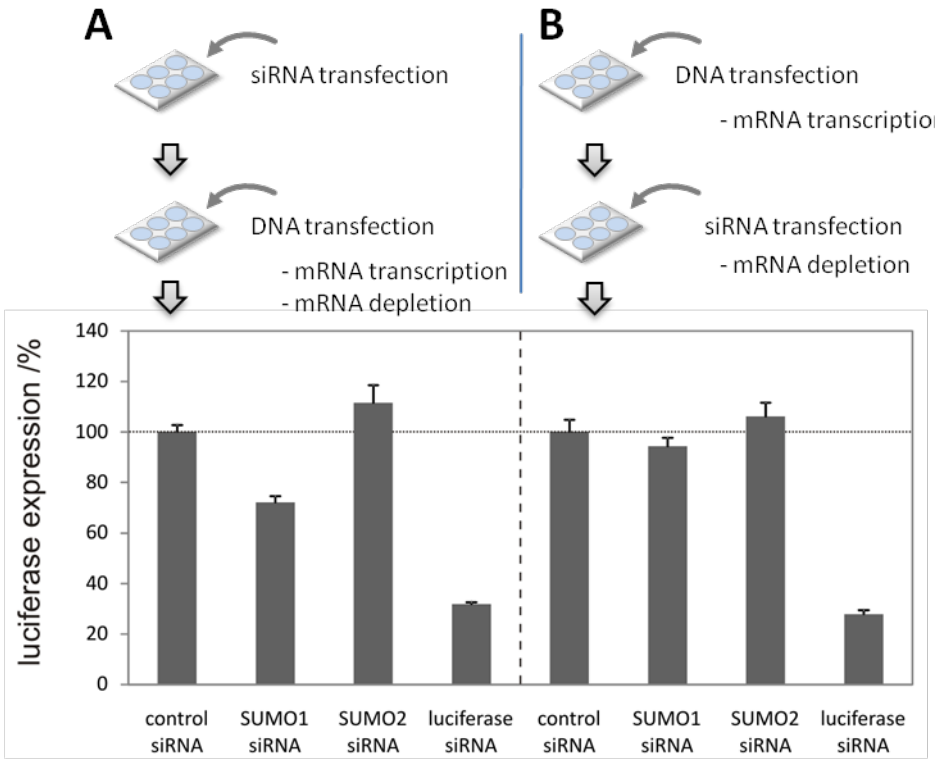

Fig. 3.26: Effects of siRNA transfection on transcription of the reporter luciferase gene. ***A*** HeLa cells were transfected with control siRNA, SUMO1 siRNA, SUMO2 siRNA, or luciferase siRNA for 24 h. Then, the cells were transfected with a standard luciferase reporter plasmid followed by expression for 24 h and detection of luciferase expression. Transfection with control siRNA and SUMO2 siRNA resulted in comparable luciferase expression. SUMO1 siRNA transfection led to slightly decreased luciferase expression (75%). Transfection of luciferase siRNA, as a positive control, led to decreased luciferase expression levels of about 30%. ***B*** HeLa cells were transfected with the luciferase reporter plasmid for 24 h followed by siRNA transfection. No changes of the luciferase expression were detected after transfection with SUMO1/2 siRNA when compared to transfection with the control siRNA. Transfection of luciferase siRNA in the positive control resulted in a luciferase expression of about 30%.

Additionally, to exclude potential artifacts based on a siRNA influence on transcription of the luciferase gene, the experiment was repeated in different order. This time, first, transfection with the luciferase reporter DNA was performed for 24 h allowing for a stable transcription and expression phase of the luciferase gene. This step was followed by siRNA transfection for 24 h (Fig. 3.26, B). Transfection of control siRNA and SUMO1/2 siRNA resulted in comparable luciferase expression levels. Luciferase expression was only reduced (30%) for the samples with luciferase siRNA transfection.

3.3 Biophysical interaction studies of HPV16 L2 with SUMO1/2

The interaction of the HPV16 capsid protein L2 with SUMO1 and SUMO2 was characterized by immunoprecipitation, 2-hybrid screening, and fluorescence microscopy as described in the previous chapters. To get further information about the interaction with SUMO proteins, additional interaction studies were performed using electron paramagnetic resonance (EPR) spectroscopy as the main method of this chapter, but also fluorescence correlation spectroscopy (FCS), isothermal titration calorimetry (ITC), fluorescence and circular dichroism spectroscopy, and also molecular dynamics (MD) simulations. Therefore, adequate amounts of SUMO1/2 and L2 proteins had to be produced.

3.3.1 Purification of SUMO1/2 protein by native his tag affinity purification

Purification of SUMO1 and SUMO2 was performed based on expression of SUMO1/2-his_6 fusion proteins in *E. coli* followed by Ni-NTA affinity purification under nondenaturing conditions. Quantification of the protein content was performed by Bradford Assaying. Standard protein yields were in the range of 1-2 mg SUMO1/2 protein for cell-pellets obtained from a 100 ml culture volume. Purified SUMO1/2 was characterized by Coomassie staining and immunodetection (Fig. 3.27).

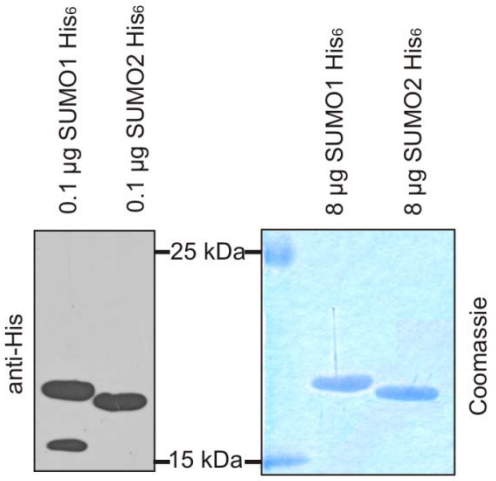

Fig. 3.27: Affinity purification of highly pure SUMO1/2-his_6. SUMO1/2-his_6 was overexpressed in *E. coli* (Rosetta 2 DE3) for 4 h at 30 °C. Then, the cells were harvested and stored in aliquots at -80 °C. After cell lysis in 20 mM Tris pH 8.0/500 mM NaCl/5 mM imidazole, SUMO1/2 his_6 was purified in gravity columns with Ni-NTA resin under native conditions. The column was washed with the same buffer containing 35 mM imidazole and final protein elution was done with 335 mM imidazole. 0.1 µg or 8 µg purified SUMO1/2-his_6 were characterized by immunodetection with anti-His antibodies or Coomassie protein staining. Each one clear band of SUMO1- or SUMO2-his_6 was observed without larger detection of background proteins.

In Coomassie stainings, each one clear protein band was detected for purified SUMO1- or SUMO2-his_6 without detectable contributions of background proteins.

3.3.2 Denaturing purification of HPV16 L2

3.3.2.1 Full-length and soluble L2 protein after expression in HEK293 cells

In a first attempt, the expression of HPV16 L2 protein from different protein expression systems was analyzed, since early L2 purification experiments did not result in noteworthy L2 amounts. First, specialized *E. coli* expression strains were used to express his_{10}-L2 and GST-L2 fusion proteins followed by characterization of the expressed proteins by immunodetection (Fig. 3.28). Despite of the well detectable bands for the full length HPV16 L2 proteins, there was a large amount of inaccurately expressed or disrupted L2 indicated by a large number of lower molecular weight bands. In additional experiments, expression temperature and time was modified to allow for a better expression of full-length L2, but did not result in significant improvements.

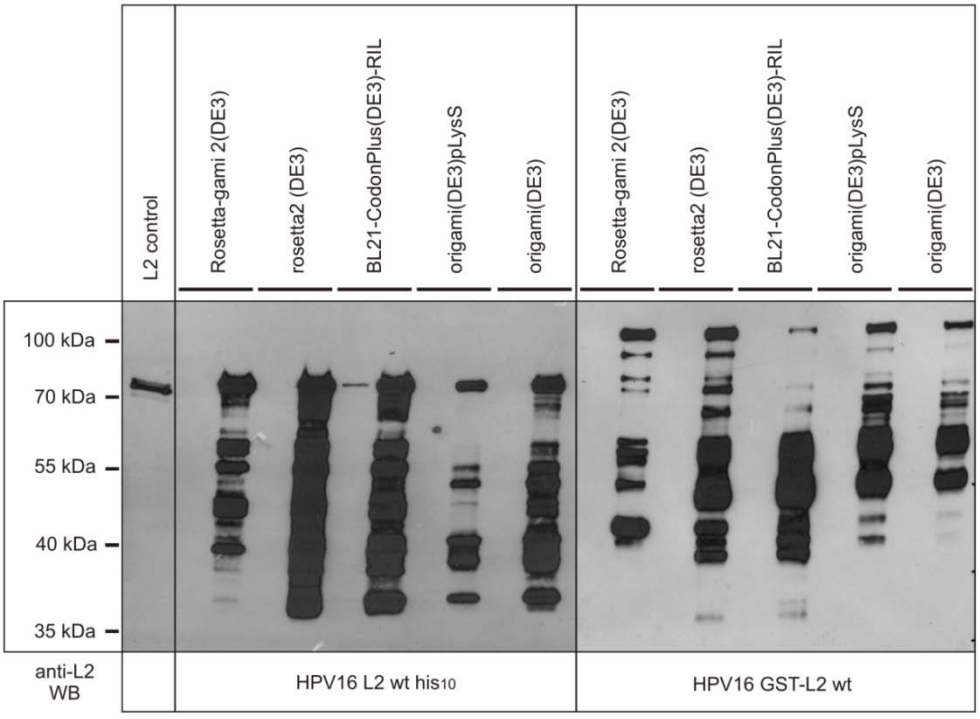

Fig. 3.28: No adequate expression of L2-his_{10} or GST-L2 fusion proteins in *E. coli*. Special *E. coli* expression strains were transformed with L2-his_{10} or GST-L2 expression vectors. Before induction of protein expression, the cultures were brought to an equal cell density. Expression was performed for 2 h at 37 °C. Normalized amounts of the cell suspensions were lysed in 2.5 x SDS-PAGE loading buffer and characterized by immunodetection with an anti-L2 (L2-1) antibody including also a non induced negative control (first lane for each cell type).

L2 was also expressed in *Leishmania tarentolae* and human HEK293T cells. Pilot experiments showed that in both systems significantly more full-length L2 protein was obtained. In order to guarantee highest purification performance, first, the solubility of L2 was checked for the different expression systems and under different buffer conditions. This was done by ultracentrifugation at 100,000 g and characterization of the content of soluble L2 in the supernatant or insoluble L2 in the pellet by immunodetection. After expression of L2 in *Leishmania tarentolae*, cell lysis, and ultracentrifugation, the synthesized L2 was in a rather water insoluble state. For none of the native lysis buffers, a significant amount of solubilized L2 was detected in the supernatant (Fig. 3.29).

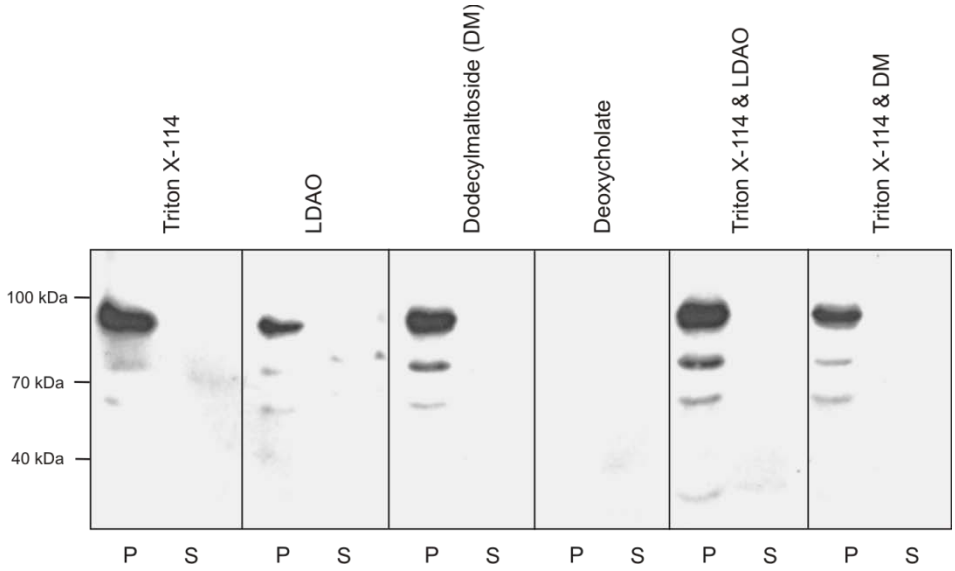

Fig. 3.29: L2 is insoluble after expression in *Leishmania tarentolae*. L2 expressing cells were resuspended in 1xPBS pH 7.5/ 500 mM NaCl/ 1mM DTT and the lysate was divided into several aliquots. Before sonification of cells, different detergents were added to cell suspension (2% (v/v), LDAO: Lauryldimethylamine-oxide). After incubation for 45 min at 4 °C, the lysates were centrifuged for 10 min at 10,000 g. The supernatant was subsequently subjected to ultra centrifugation at 100,000 g for 1 h at 4 °C. After centrifugation and resuspension of the pellet, an equal amount of pellet (P) and supernatant (S) was characterized by immunodetection. Almost the entire L2 signal corresponds to insoluble L2, which was located in the pellet.

L2 solubility was also checked after L2 expression in HEK293 cells (Fig. 3.29). In the presence of Triton X-100, Triton X-114, Dodecylmaltoside, or LDAO, a large amount of soluble L2 was detected (up to 50 % of the total L2, Fig. 3.30).

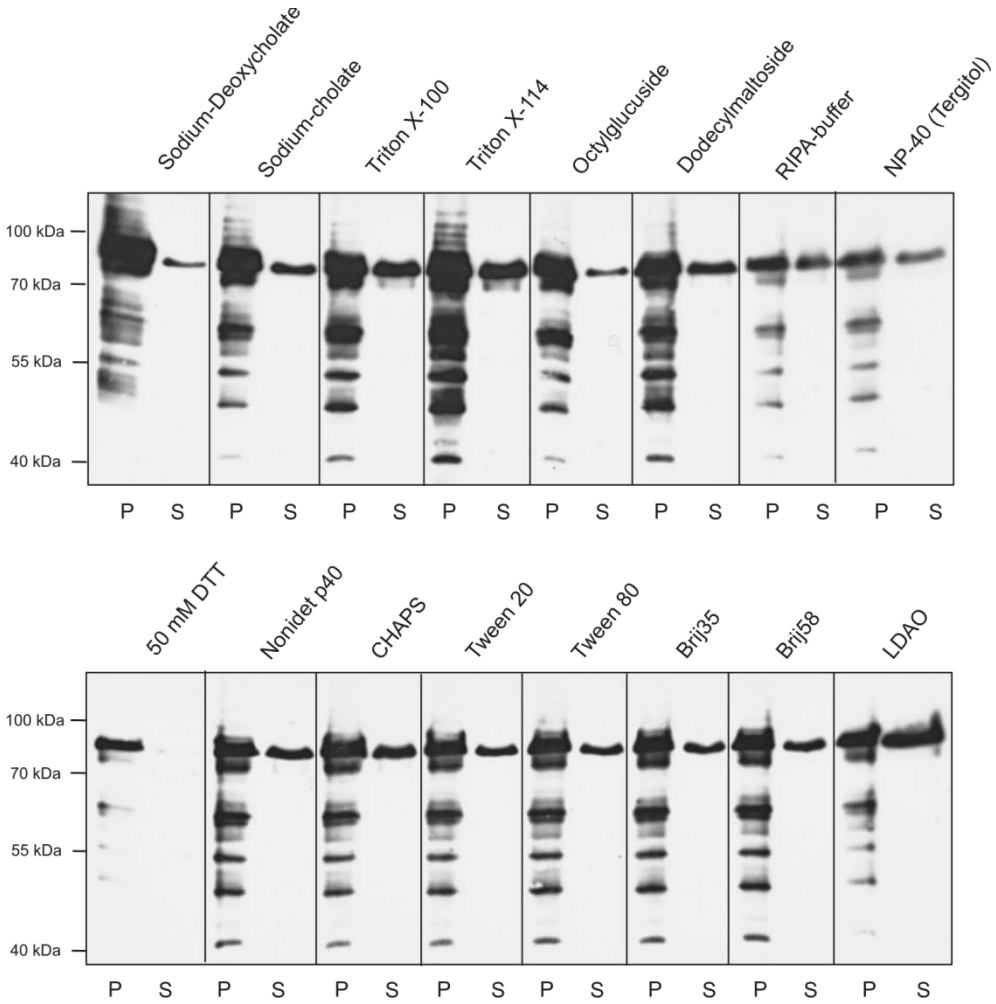

Fig. 3.30: High solubility of HPV16 L2 expressed in HEK293 cells. The cells containing HPV16 L2 protein were lysed in standard buffer (1xPBS pH 7.5/ 500 mM NaCl/ 1mM DTT) containing different detergents (1 % (v/v)), allowing for L2 solubilization. After sonification and incubation, the cell lysates were centrifuged at 100,000 x g for 1 h at 4 °C. The same amount of supernatant (S) and resuspended pellet solution (P) was characterized by immunodetection. The majority of the L2 signal corresponds to insoluble L2, but larger fractions of soluble L2 were detected after incubation with lysis buffers containing Triton X-100, Triton X-114, Dodecylmaltoside, or LDAO.

In addition to solubility screening with different detergents, also an influence of the pH on L2 solubility was checked (Fig. 3.31). There were no significant changes in the ratio of insoluble L2 in the resolubilized UZ pellet (P) and the soluble L2 in the supernatant (S) over the selected pH range (pH 4.5-10).

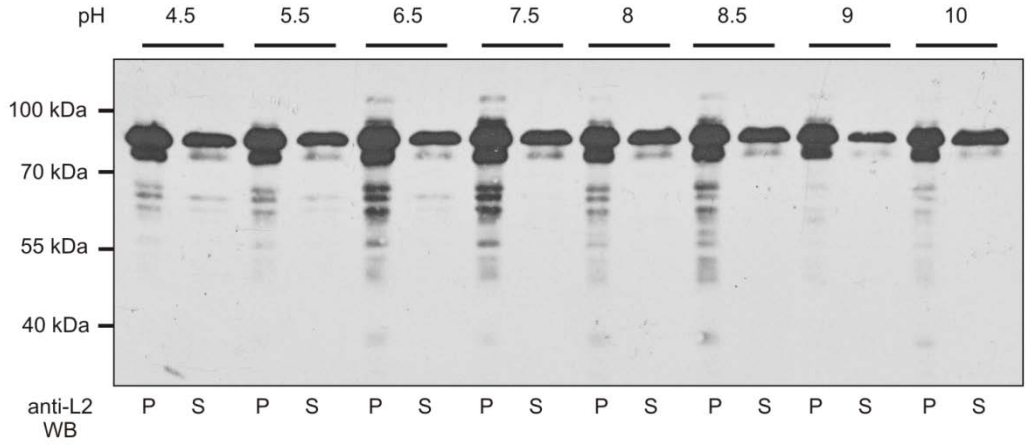

Fig. 3.31: No pH-dependence of L2 solubility. The L2 solubilization assay was performed with a standard lysis buffer containing 50 mM Tris HCl/350 mM NaCl/ 2% (v/v) Triton X-100/ 1 mM DTT in the pH range of pH 4.5-10. After ultracentrifugation at for 1 h at 100,000 g and 4 °C, comparable amounts of the supernatant and the resuspended pellet were characterized by immunodetection.

Even higher amounts of soluble L2 were achieved by using LMPG (lysomyristoylphosphatidylglycerol) as detergent. Additionally, it was checked whether the L2 solubility depends on the position of the polyhistidine affinity tag. Therefore, the solubilization assay was repeated with different composition of the lysis buffers. The, L2 solublility was analyzed densitometrically after immunodetection of L2 (Fig. 3.32). The highest L2 solubilization (50%) was achieved with Tris or phosphate buffers containing 2% (v/v) LMPG. In contrast, buffers containing Triton X-100 led to solubilization levels of 20-30%. In general, L2 fusion proteins containing a C-terminal polyhistidine tag featured slightly increased solubility. Taking into account the comparable accessibility of the tags for his antibodies (data not shown) and the fact that with the use of a C-terminal L2 his fusion protein, only full length L2 is purified in theory, only L2 his_6 was used for further experiments.

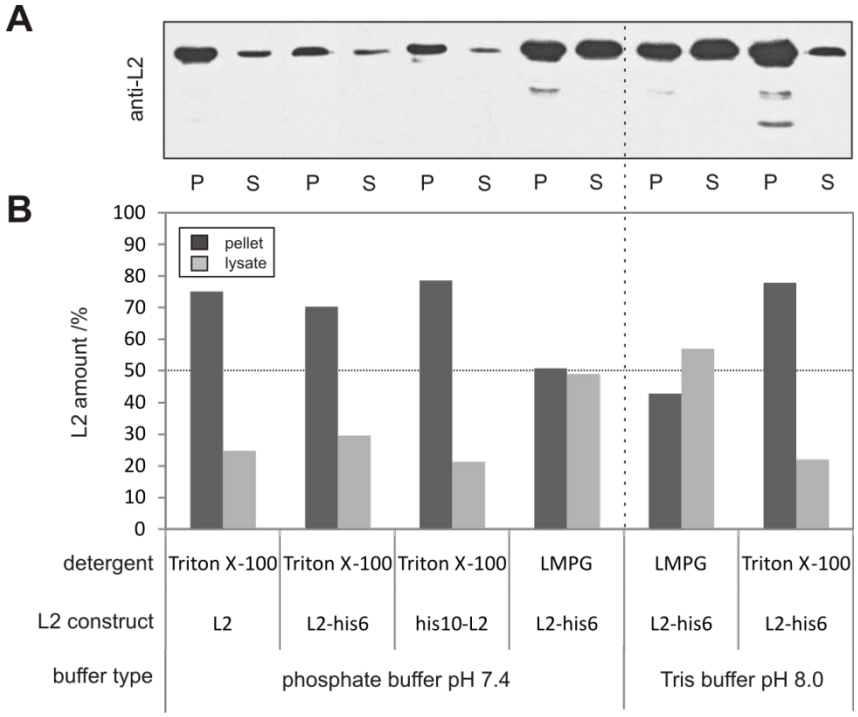

Fig. 3.32: High L2 solubilization with 2% (v/v) Triton X-100 or LMPG. L2 wt, his_{10}-L2, or L2-his_6 was expressed in HEK293 cells. L2 was solubilized either in phosphate buffer pH 7.5 (300 mM NaCl) or Tris buffer pH 8.0 (300 mM NaCl) containing 2% (v/v) Triton-X100 or LMPG. After incubation for 45 min at 4 °C, the lysate was centrifuged for 10 min at 13,000 g followed by ultracentrifugation of the supernatant for 1 h at 4 °C and 100,000 g. Equal amounts of supernatant and resuspended pellet were characterized by immunodetection (***A***) and densitometry (***B***). In general, higher total amounts of L2 and especially solubilized L2 in the UZ supernatant were found for cell lysis in LMPG containing buffers or for Tris buffers containing Triton X-100. The location of the polyhistidine affinity tag did not significantly affect L2 solubilization.

After optimization of L2 solubilization, purification under non-denaturing conditions was performed, but did not lead to adequate amounts of purified L2. Most obviously, the reasons for low-yield L2 purification were low affinity binding of L2 to the Ni-NTA affinity matrix and a yet too small fraction of soluble L2. Also adjustment of the imidazole concentration during purification or the use of alternative purification tags (e.g. Strep-Tag) did not improve purification results. Further non-denaturing purification attempts including expression of a maltose binding protein (MBP) fusion protein with L2 in *E. coli* or L2-his_6 expression and purification from inclusion bodies in *E. coli* resulted in expression and/or purification of highly fragmented L2, which was not suitable for further characterization.

3.3.2.2 High yield L2 purification under denaturing conditions

All attempts to produce highly pure L2 protein by non-denaturing purification did not result in adequate L2 amounts for biophysical characterization. The main problems were low solubility, no or very low selective binding of L2 to the His bead matrix (Ni-NTA resin), and fragmentation of L2 during

the purification process or the protein expression itself. However, in this work, a method for medium scale purification of HPV16 L2 based on his-tag affinity purification under denaturing conditions was established, offering adequate and highly pure L2 amounts for biophysical characterization of HPV16 L2 (100-400 µg L2 per 15 cm plate overexpressing HEK293 cells). Therefore, the L2 pellet was first resuspended in lysis buffer containing Triton X-100 to solubilize the maximum amount of cellular background proteins. The lysate was subjected to ultracentrifugation to collect the large fraction of insoluble L2 in the pellet, which was then denatured in guanidine buffer and purified based on Ni-NTA affinity purification. Purification of L2 fusion proteins with N- or C-terminal his tag led to well detectable L2 bands at about 80 kDa (Fig. 3.33, lanes 4-6).

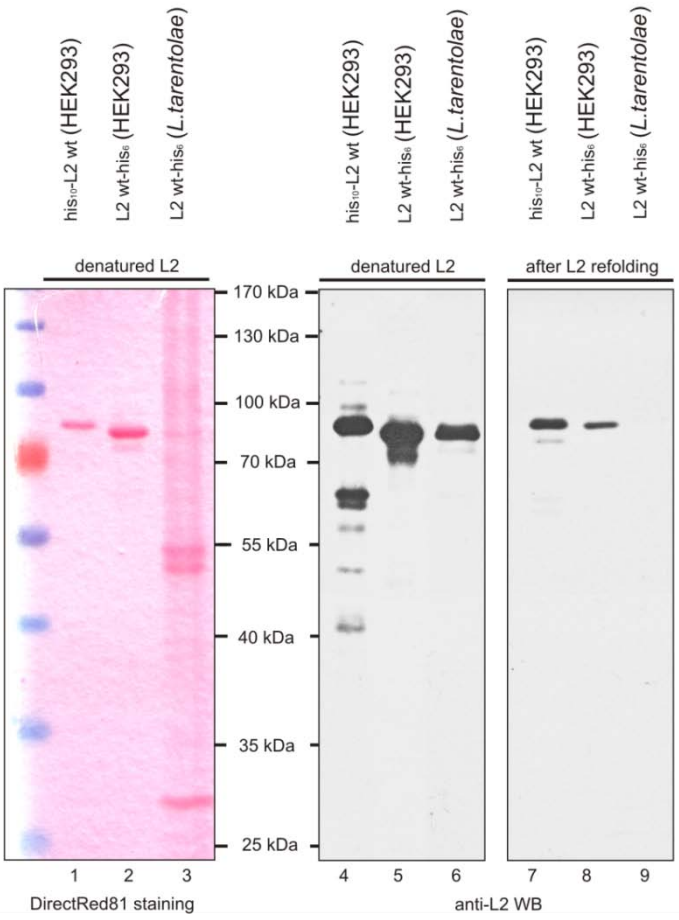

Fig. 3.33: Purification of HPV16 L2 under denaturing conditions. L2 was expressed in HEK293 or *L. tarentolae*. The L2 lysates were prepared in 50 mM Tris pH 8.0 350 mM NaCl, 1 mM DTT, 1% (v/v) Triton X-100. After sonication and incubation for 45 min at 4 °C, the lysate was centrifuged for 1 h at 100,000 g and 4 °C. The supernatant containing the soluble fraction of L2 and all soluble background protein was discarded. The pellet was resuspended in 6 M Guanidine HCl with one freeze-thaw cycle and sonication. The solution was incubated with Ni-NTA-beads for 30 min at RT in a gravity column. After washing and elution, the L2 protein was characterized by protein staining with Direct Red 81 and immunodetection (anti-L2, L2-1). Adequate amounts of purified L2-his_6 or his_{10}-L2 without larger contributions of background proteins were detected after L2 expression in HEK293 (lanes 1-2 and 4-5). For purification of L2 expressed *in L. tarentolae*, only a faint L2 band on an intense background of cellular proteins was detected after protein staining (lane 3). L2 refolding by ethanol precipitation resulted in well-detectable L2 bands after immunodetection for L2 purified from HEK293 (lanes 7-8, no detection of L2 purified from *L. tarentolae* after refolding).

For L2 purified from HEK293 cells, in Direct Red 81 stainings, only the major L2 bands were detectable with only very small contributions of background proteins (lanes 1 and 2). As for the purification of L2-his_6 from *L. tarentolae*, the major L2 band was hardly visible (lane 3) and there was a large level of background protein detection.

3.3.2.3 Characterization of affinity purified HPV16 L2 protein

After successful purification of HPV16 L2 from HEK293 cells by his affinity purification under denaturing conditions, L2 refolding was performed by dialysis in non-denaturing buffer or by ethanol precipitation of L2 followed by resolubilization of the L2 pellet in non-denaturing buffer. Subsequently, L2 refolding was characterized by immunodetection (Fig. 3.33, lanes 7-9). This led to well-detectable, non-fragmented bands for L2 purified from HEK293 cells (lanes 7-8), which were comparable to the samples with direct application of L2 in 6 M Guanidine HCl (lanes 4-6). Further L2 characterization was performed by optical photometry, fluorescence spectroscopy, circular dichroism (CD) spectroscopy, and dynamic light scattering (DLS).

A small but significant fraction of L2 seems to aggregate into larger particles during L2 refolding, which was visible in the large content of scattered light at higher wavelengths in UV/Vis spectroscopy (Fig. 3.34, A, see dashed marker line). Additional hints for L2 aggregation came from DLS measurements. Samples containing refolded L2 had a particle diameter of about 5-6 nm with a very high polydispersity index (PDI) of about 0.9, signaling the detection of particles of very different sizes. After centrifugation of the L2 sample and characterization of the supernatant, the mean diameter was significantly decreased (4 nm). Additionally, there was a higher uniformity for the particles within the sample, which was represented by a decreased PDI of about 0.3.

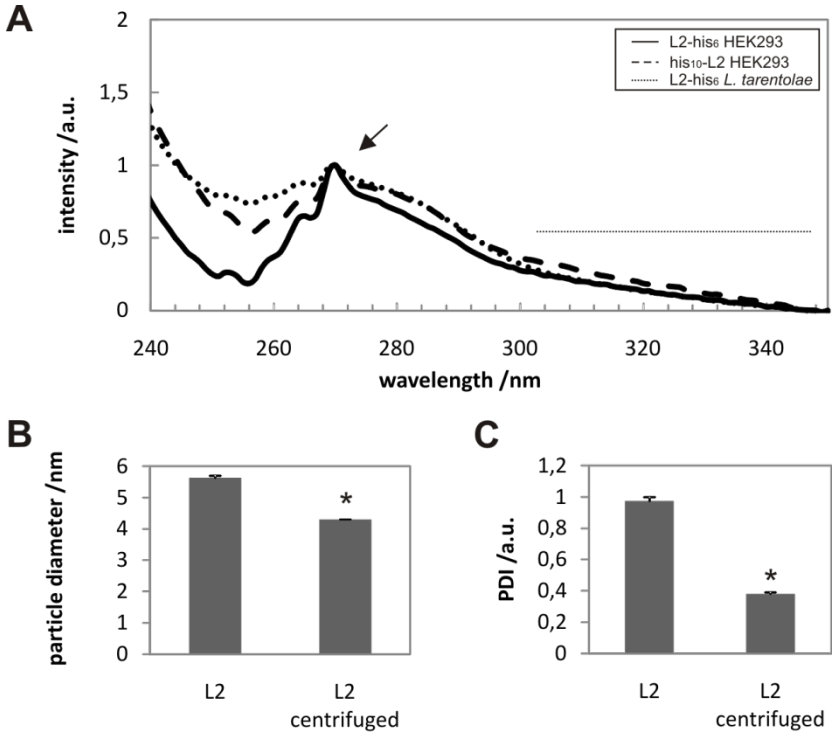

Fig. 3.34: L2 aggregation during refolding. ***A*** After ethanol precipitation, the L2 pellet was resuspended in Tris buffer and characterized by UV/vis spectroscopy. A significant contribution of scattered light at higher wavelengths indicated detection of aggregated structures within the sample (see spectral region under the dashed line). Interestingly, the maximum of light absorption was shifted toward the absorption maximum of phenylalanine (~275 nm, see arrow). ***B*** Dynamic light scattering with refolded L2 revealed an apparent L2 particle diameter between 5 and 6 nm. After centrifugation of the sample (20 min, 22,000 g, 4 °C) and characterization of the supernatant, a decreased mean particle diameter of about 4 nm was detected (marked with a star). ***C*** The polydispersity index (PDI) was very high for non-centrifuged L2, signaling the detection of a very broad distribution of particle diameters. After centrifugation, the PDI was significantly reduced, indicating a larger uniformity of detected particles (marked with a star).

Since there was no information about the level of background proteins, despite estimations based on desitometry performed with Coomassie stained SDS gels, the background level of proteins was additionally determined in a different way. Therefore, fluorescence spectroscopy was used. The L2 protein sequence comprises 22 tyrosines and 15 phenylalanines but no tryptophans. Thus, low trypthophan fluorescence (350 nm) together with high tyrosine (303 nm) and phenylalanine (282 nm) fluorescence intensities would indicate a low level of background proteins for highly pure L2 samples. In fact, for his_{10}-L2, and especially, L2-his_6 purified from HEK293 cells, the tryptophan contribution was significantly reduced (Fig. 3.35). The maximum fluorescence intensity clearly shifted towards the fluorescence maxima of tyrosines and phenylalanines, indicating a very low content of background protein for purification of L2 from HEK293 cells (marked with a star). For samples containing L2-his_6 stemming from *L. tarentolae,* the fluorescence maximum was clearly located at about 340-350 nm. Here, the fluorescence spectrum almost entirely consists of the tryptophan fluorescence of background proteins.

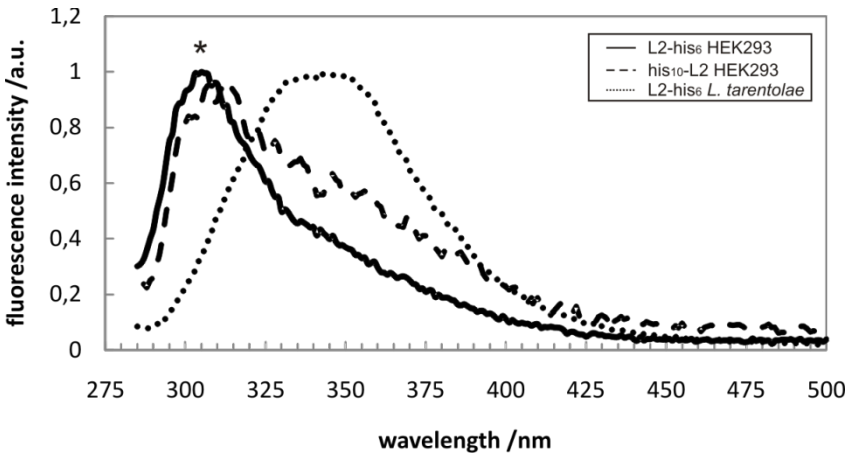

Fig. 3.35: Low level of background tryptophan fluorescence in purified and refolded L2 samples. The fluorescence intensity of tryptophans from background proteins at about 345 nm was significantly reduced for L2 expressed in HEK293 cells. Only the fluorescence maximum of the 22 tyrosines within the L2 proteins sequence was detected at about 305 nm (marked with a star) indicating a high purity of L2.

Additionally, CD spectra of the refolded L2 samples were recorded to obtain information about the content of secondary structure elements. The CD spectrum of the purest L2-his_6 preparation from HEK293 cells contained fractions of all secondary structure elements (Fig. 3.36). It was found that the spectrum contained about 55% random coil elements, 25% alpha helical elements, and 20% β-sheet elements. This fingerprint could serve as basis for interaction studies with SUMO proteins via the L2 SIM. The non covalent interaction with formation of induced β-sheet elements could lead to measurable changes within the CD spectrum.

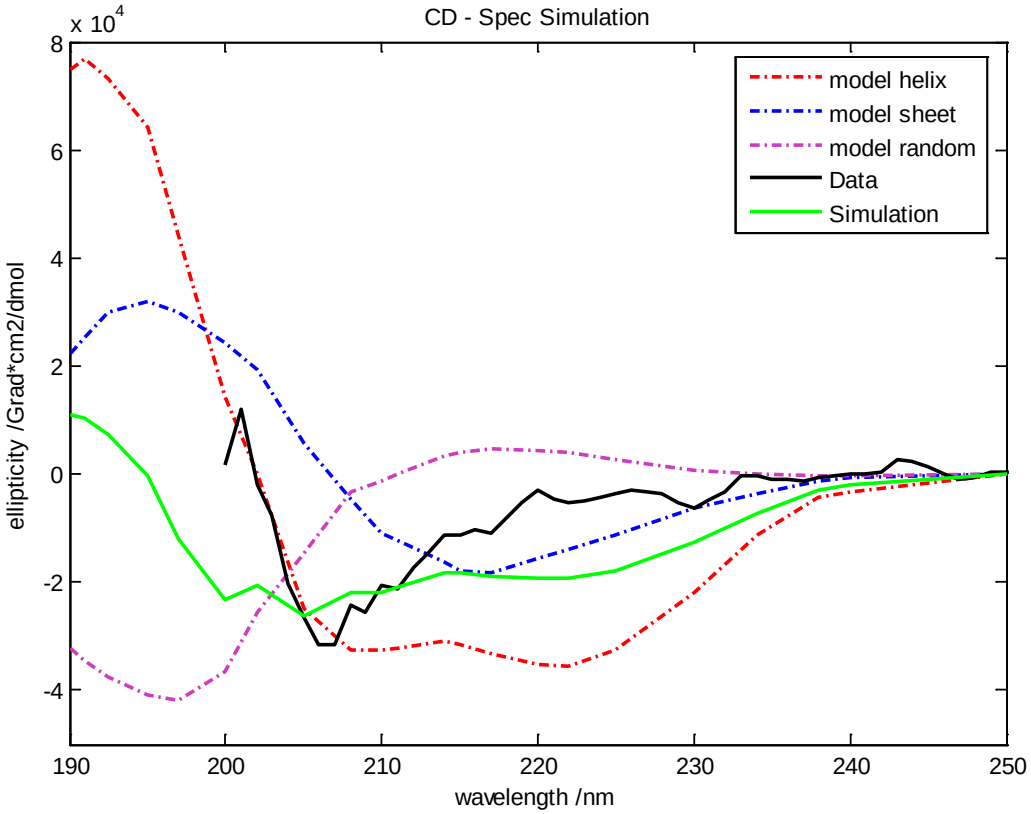

Fig. 3.36: CD spectrum of HPV16 L2. Simulation of the experimental CD data obtained for HPV16 L2 (black line) with model CD spectra based on with home-written MATLAB® software revealed a contribution of about 55 % random coil elements, 25 % alpha helical elements, and 20 % β-sheet elements.

3.3.3 Noncovalent interaction of HPV16 L2 and SUMO1/2 characterized by EPR

CW EPR measurements were performed to study the *in vitro* interaction of purified L2 with purified SUMO1 or SUMO2. For these experiments, only one of the interaction partners contains a spin label. The smaller SUMO protein was selected for site-directed spin labeling (SDSL), since potential interaction with the larger L2 molecule would result in a well detectable slow down of SUMO1/2 diffusion due to formation of larger SUMO-L2 complexes. Additionally, L2 interaction with SUMO should result in the detection of significant changes within the local vicinity of the EPR label attached to SUMO proteins. In order to measure distances between SUMO and L2 by DEER measurements, SDSL has to be performed for both interaction partners. Therefore, labeling experiments with both, purified SUMO1/2 and L2, were performed.

3.3.3.1 Highly efficient spin labeling of purified SUMO1/2

Site-directed spin labeling of the cysteine residue C52 (SUMO1) and C48 (SUMO2) was performed including reduction of the sulfhydryl groups with triscyanoethylphosphin (TCEP) and labeling with 3-(2-iodoacetamido)-PROXYL (PROXYL-IAA). Excess spin label was removed by buffer exchange with PD-10 columns or centricons. The protein containing fractions were pooled, concentrated in spin-concentrators (MWCO 5,000) and characterized by CW EPR measurements (Fig. 3.37).

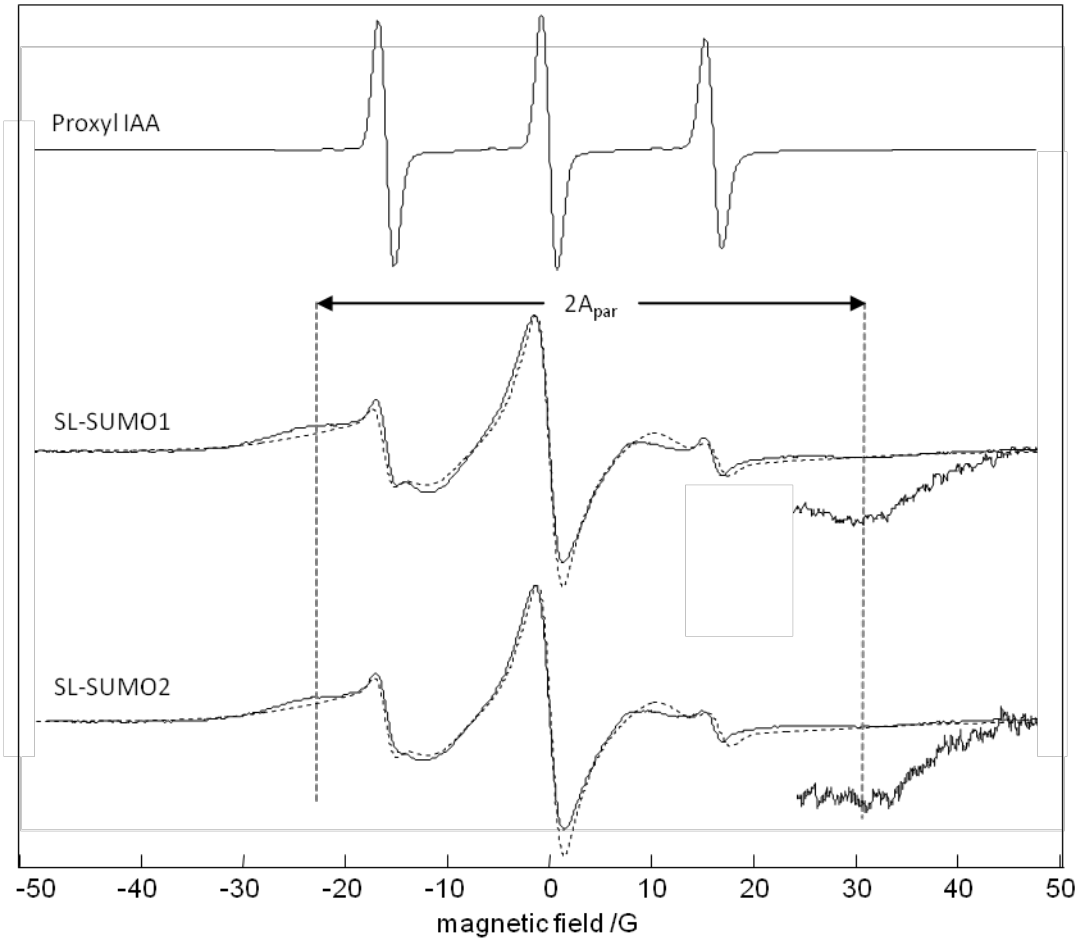

Fig. 3.37: Highly efficient spin-labeling of SUMO1/2. CW EPR spectra of the EPR samples after site-directed spin-labeling of SUMO1/2 were extremely broadened with respect to the control sample with Proxyl IAA. The separation between the resolved outer hyperfine extrema of the spectra ($2A_{par}$) was about 52.7 G for SL-SUMO1 and about 52.8 G for SL-SUMO2. Simulation of the experimental SL-SUMO1 and SL-SUMO2 CW EPR spectra (dashed magenta lines) revealed a content of about 3-5% free spin label within the EPR samples.

The CW EPR spectra obtained after site-directed spin-labeling of SUMO1/2 featured an extremely broadened line-shape indicating successful labeling of the SUMO1/2 molecules and immobilization of the spin labels. The separation between the well-resolved outer hyperfine extrema of the spectra

($2A_{par}$) was about 52.7 G for SL-SUMO1 and about 52.8 G for SL-SUMO2. Simulation of the recorded EPR spectra revealed a content of free spin label of only about 3-5 % and labeling efficiencies of about > 95% for SUMO1 and SUMO2, as well as rotation correlation times of about 11 ns (compared with 1 ns for the Proxyl IAA reference). Especially the shape and location of the low field line, which is most sensitive for immobilization effects of the label molecule, show the typical pattern of a label which is located close to or within an surface helix (Mchaourab 1996; Isas 2002). In fact, the labeling positions C52 (SUMO1) and C48 (SUMO2) are both located within a surface helical region (aa 45-55 for SUMO1, aa 41-51 for SUMO2).

3.3.3.2 SL-SUMO2 seems to self-arrange into SUMO oligomers

After purification and spin labeling, the SUMO1/2 proteins were again characterized by SDS-PAGE and immunodetection to detect possible degradation of SL-SUMO1/2, as well as potential oligomerization of SL-SUMO1/2 due to intermolecular disulfide bridging (Fig. 3.38). Especially for SDP-PAGE sample preparations of spin-labeled (SL-) SUMO1/2 without addition of reducing agents, an increased level of high molecular SUMO2 bands was observed. The number and intensity of the high molecular bands was slightly diminished by addition of DTT or TCEP, but only boiling of the SL-SUMO1/2 samples at 95 °C with addition of β-mercaptoethanol lead to an almost complete reduction of high molecular SUMO2 bands. In general, for purified SUMO2 (without SDSL), only the prominent band at about 36 kDa was detectable. SL-SUMO1 was not characterized by additional reduction assays so far, but standard sample preparation in 2.5 x SDS-PAGE loading buffer did not lead to significant detection of high molecular weight bands in immunodetections.

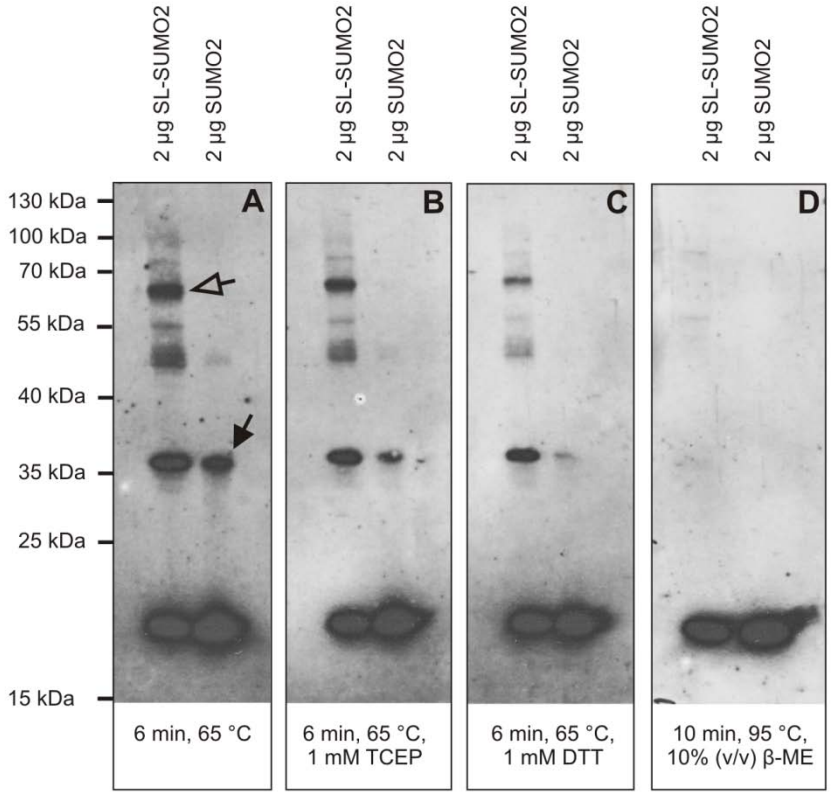

Fig. 3.38: High molecular (SL-) SUMO2 aggregates. ***A*** Incubation at 65 °C for 6 min resulted in the detection of the main SL-SUMO2 bands at about 18 kDa, but also in an additional band at about 36 kDa for labeled and nonlabeled SUMO2. These bands most obviously represented (SL-) SUMO2 dimers (see black arrowhead). Only for SL-SUMO2, an increased amount of additional bands appeared at even higher molecular weights. The most prominent band of the additional, high molecular bands was located at about 60 kDa and could represent SL-SUMO2 trimers (open arrow). To test stability of the oligomers in the presence of different reduction agents, the samples were also prepared with 1 mM TCEP (***B***), 1 mM DTT (***C***), and 10% (v/v) β-mercaptoethanol (***D***). The intensity of the bands at higher molecular weight decreased, especially for sample treatment with β-mercaptoethanol and incubation at 95 °C. Here, only very faint bands at 36, 55, and 75 kDa were detected. The band at about 60 kDa vanished completely. For sample preparation with TCEP or DTT and incubation at 65 °C, the pattern of higher molecular bands was comparable to that without reduction agents, but was less intense.

3.3.3.3 HPV16 L2 interacts with SL-SUMO1/2

Interaction studies with HPV16 L2 and SUMO1/2 were performed based on spin labeled SUMO1/2 (SL-SUMO1/2) and the full length L2 protein at different molecular ratios in the range of about 1:1 to 1:4 (L2:SUMO1/2). The samples were prepared by dissolving the appropriate amount of lyophilized or ethanol precipitated L2 in SL-SUMO1/2 solution and incubation for 45 min at RT. Then, CW EPR measurements were performed to detect a possible spectral broadening and slow down due to the L2 attachment to the labeled SUMO1 or SUMO2 molecules. In fact, a clear L2-dose dependent spectral broadening due to a shift of the outer hyperfine extrema was observed after incubation of SL-SUMO1 with L2 (Fig. 3.39).

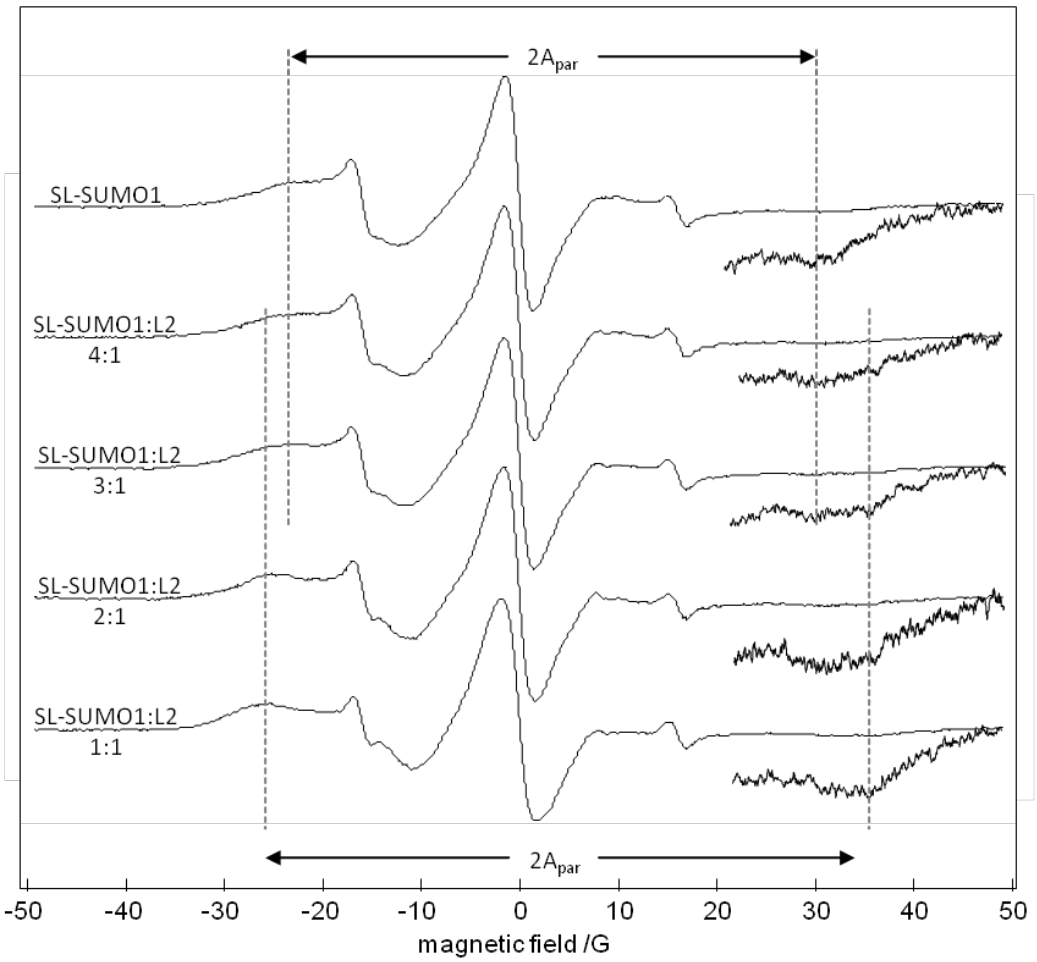

Fig. 3.39: L2 interacts with SL-SUMO1. CW EPR measurements were performed at 5 °C after incubation of SL-SUMO1 with different amounts of L2. L2 addition lead to the detection of an additional paramagnetic species featuring a significantly increased separation $2A_{par}$ between the outer hyperfine extrema (60.14 G compared with 52.72 G for SL-SUMO1, alone).

Detailed spectra analysis showed that addition of L2 lead to detection of a second species of spin labels with significantly enlarged separation between the outer hyperfine extrema with values about 60.14 G, a shift of 7.42 G with respect to the samples without L2 (52.72 G). The spectral shape clearly changed from that of a typical surface-helix bound label to that of a label bound to a helix at a protein interaction interface (Mchaourab, 1999; Isas, 2002). The L2 dose-dependent slow down of the spectrum clearly indicated an interaction of HVP16 L2 with SUMO1/2. The same trend was found for the measurements of SL-SUMO2 with increasing amounts of L2 (Fig. 3.40).

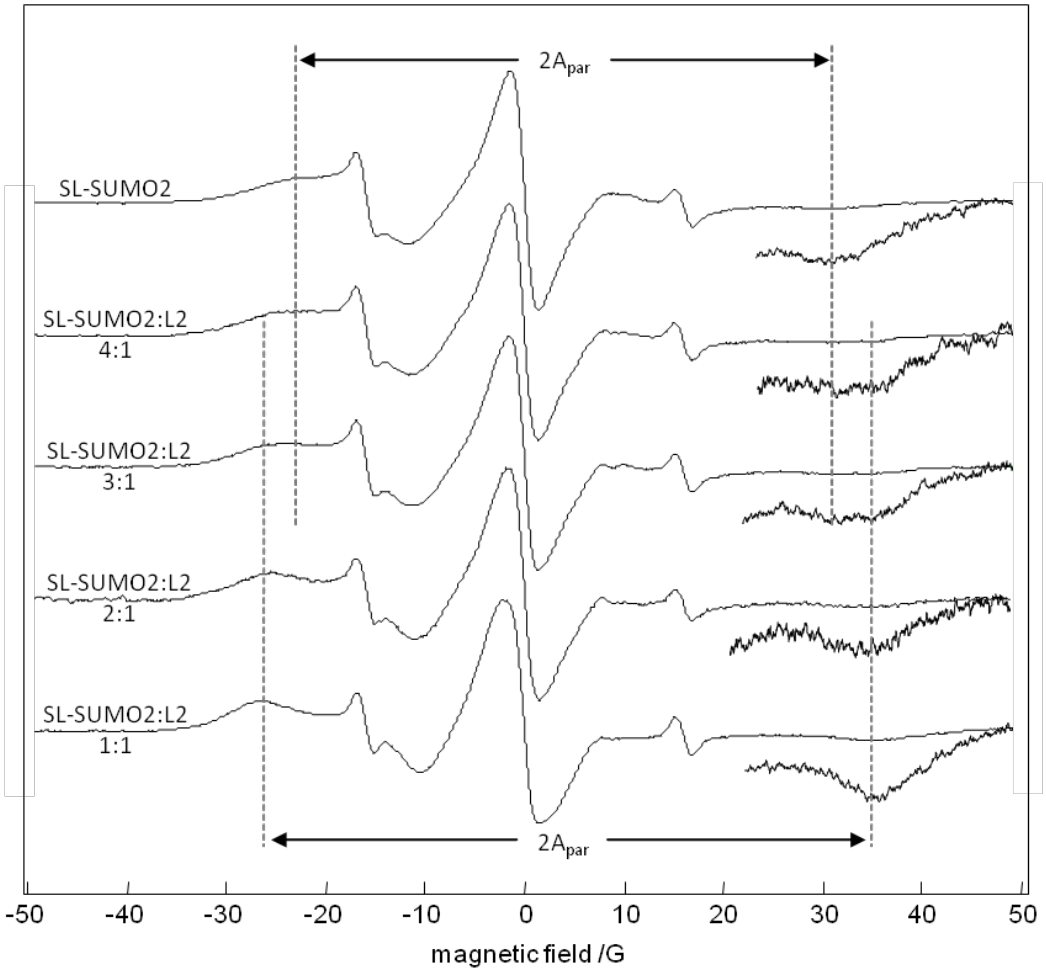

Fig. 3.40: L2 interacts with SL-SUMO2. CW EPR measurements were performed at 5 °C after incubation of SL-SUMO2 with different amounts of L2. Like it was shown for SL-SUMO1, also L2 addition to SL-SUMO2 led to the detection of an additional paramagnetic species. Interestingly, the separation $2A_{par}$ between the outer hyperfine extrema was even more pronounced (61.7 G compared with 52.83 G for SL-SUMO2, alone).

This time, the observed second EPR species featured $2A_{par}$ values of about 61.7 G, which were significantly larger than $2A_{par}$ values of about 52.83 G for SL-SUMO2 alone ($\Delta 2A_{par} \approx 8.87$ G).

With respect to the mobility of the spin label, a plot of the inverse of the second moment ($\langle H^2 \rangle^{-1}$) *vs.* the inverse of the central linewidth (ΔH_0^{-1}) gives a good empirical indication for the localization of the label within the secondary structure elements (Mchaourab 1996; Isas 2002). The inverse of the central linewidth (ΔH_0^{-1}) is a direct measure of the mobility of the nitroxide side chains and therefore also a measure of the mobility of the local labeling position. The inverse of the second moment ($\langle H^2 \rangle^{-1}$) also represents a measure for the mobility of the spin label, but with slightly more weight on immobile spectral components emphasizing contributions from the outer hyperfine extrema of the spectra. Utilizing both measures in a plot, it can be checked whether the label is positioned within buried, contact, or surface regions of the secondary structure elements. For assignment of the

labeling position of SL-SUMO1/2 in measurements together with L2, the inverse of the central linewidth was directly read from the spectra, while the inverse of the second moment was acquired by simulation of the spectra with home-written MATLAB® software. For measurements with SL-SUMO1/2 without L2, the data points were positioned directly within the region of standard spin labels attached at positions within helical surface structures of example proteins (Fig. 3.41). With increasing amounts of L2 within the sample, especially the inverse of the central linewidth was significantly smaller, so that the labels seemed to be positioned at a more immobile helical contact region.

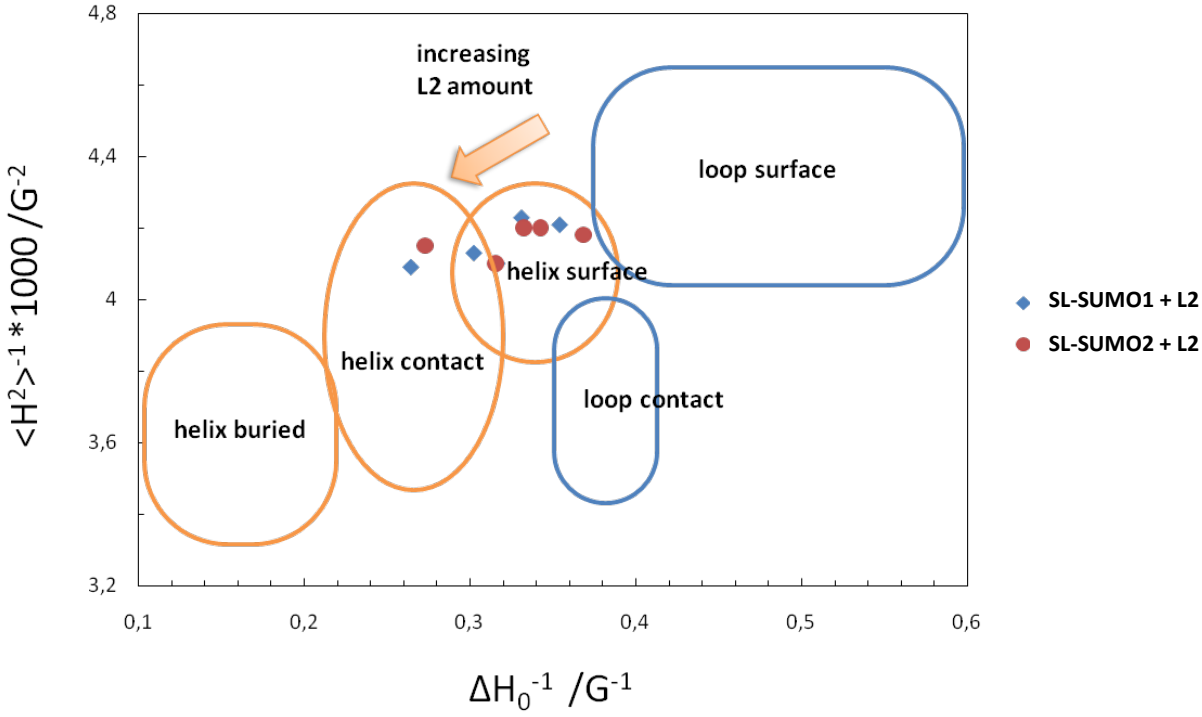

Fig. 3.41: L2 addition induces a contact helical surrounding for the spin labels attached to SL-SUMO1/2. The inverse of the second moment ($<H^2>^{-1}$) was plotted against the inverse of the central linewidth (ΔH_0^{-1}), allowing for a structural characterization of the region where the spin label is attached, based on empirical CW EPR data. The data points acquired for CW EPR spectra of SL-SUMO1/2 alone or with small amounts of L2 were located directly within a plot area, which is characteristic for a helix surface attachment of the spin label. For measurements with larger amounts of L2, the data points were positioned within the plot region characteristic for contact helical attachment of spin labels.

It was also tested whether the L2 single cysteine mutants were able to interact with SUMO1/2. This was of special interest, since for several physiologic L2 features, a formation of a disulfide bridge between the SH group C22 and the SH group at position C28 of the L2 amino acid sequence was reported to be necessary (Campos and Ozbun 2009; Conway 2009; Gambhira 2009). Both L2 C22S and L2 C28S were able to interact with SL-SUMO1 or SL-SUMO2 (Fig. 3.42). A significant loss of mobility was represented by large $2A_{par}$ values (53-59 G), which were comparable to the spectra of wild-type L2 with SL-SUMO1/2. The observed, marginal differences between the spectra stem from inaccuracies of protein quantification and normalization for these measurements.

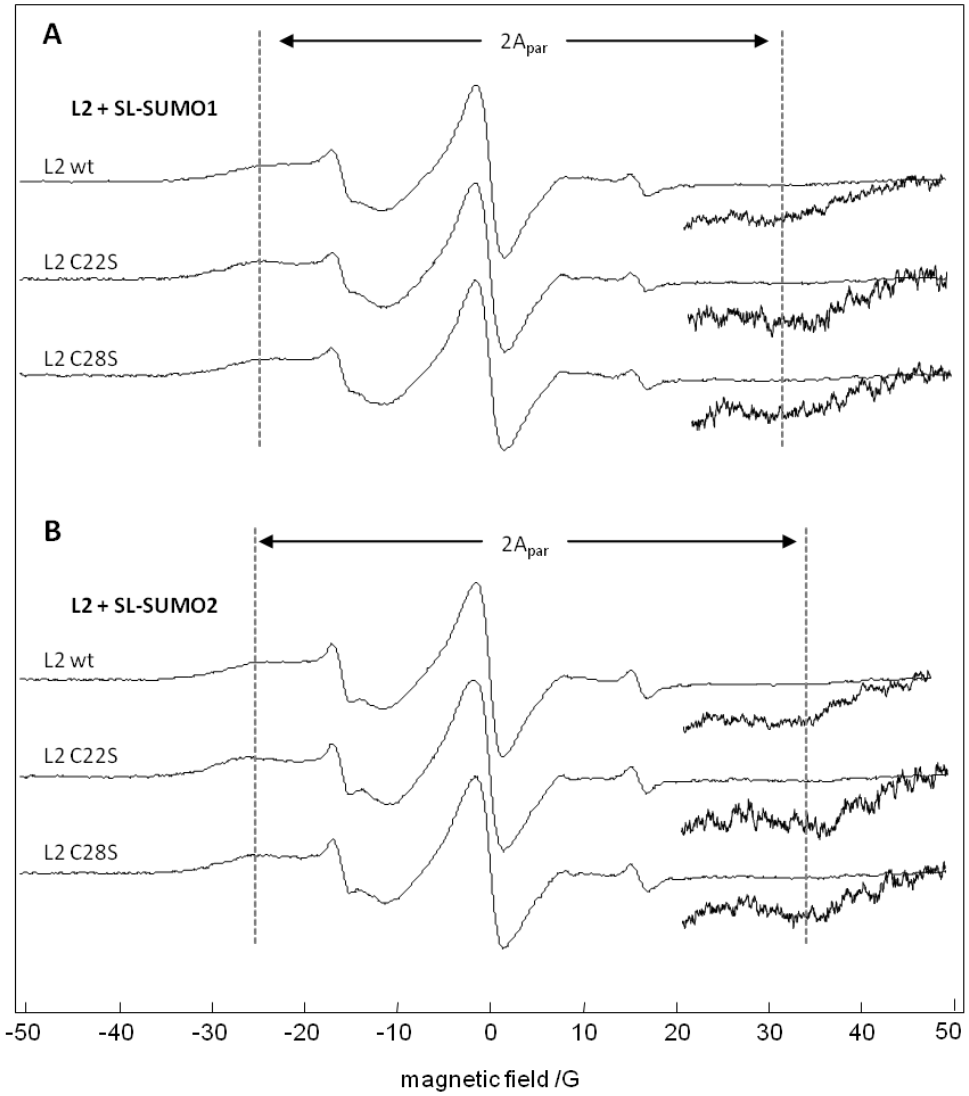

Fig 3.42: L2 cysteine mutants are able to interact with SL-SUMO1/2. CW EPR measurements were performed with wild-type L2, L2 C22S, and L2 C28S after incubation with SL-SUMO1 (***A***) or SL-SUMO2 (***B***) at about equimolar protein ratios. In all measurements, significantly enlarged separations $2A_{par}$ between the outer hyperfine extremas were observed, indicating protein interaction. The splitting was even more pronounced in samples containing L2 C22S or L2 C28S when compared with wild-type L2, which was most obviously due to a slightly higher L2 protein concentration.

3.3.3.4 The interaction of L2 with SL-SUMO1/2 is diminished by L2 antibodies

Furthermore, it was analyzed, whether the addition of a highly selective anti-L2 antibody could lead to even more immobilized spectra due to the binding of the larger L2-antibody complex by SL-SUMO1/2, or whether the antibody competes with the SL-SUMO1/2 proteins for L2 interaction. No further immobilization of the spin label was observed. In contrast, there was an increase of mobility of the spin label represented by smaller $2A_{par}$ values, which reached values detected for the SL-SUMO1/2 samples without L2 (Fig 3.43). This clearly is a sign that the interaction of L2 with SL-SUMO1/2 was canceled or at least strongly diminished by the competing L2 antibody.

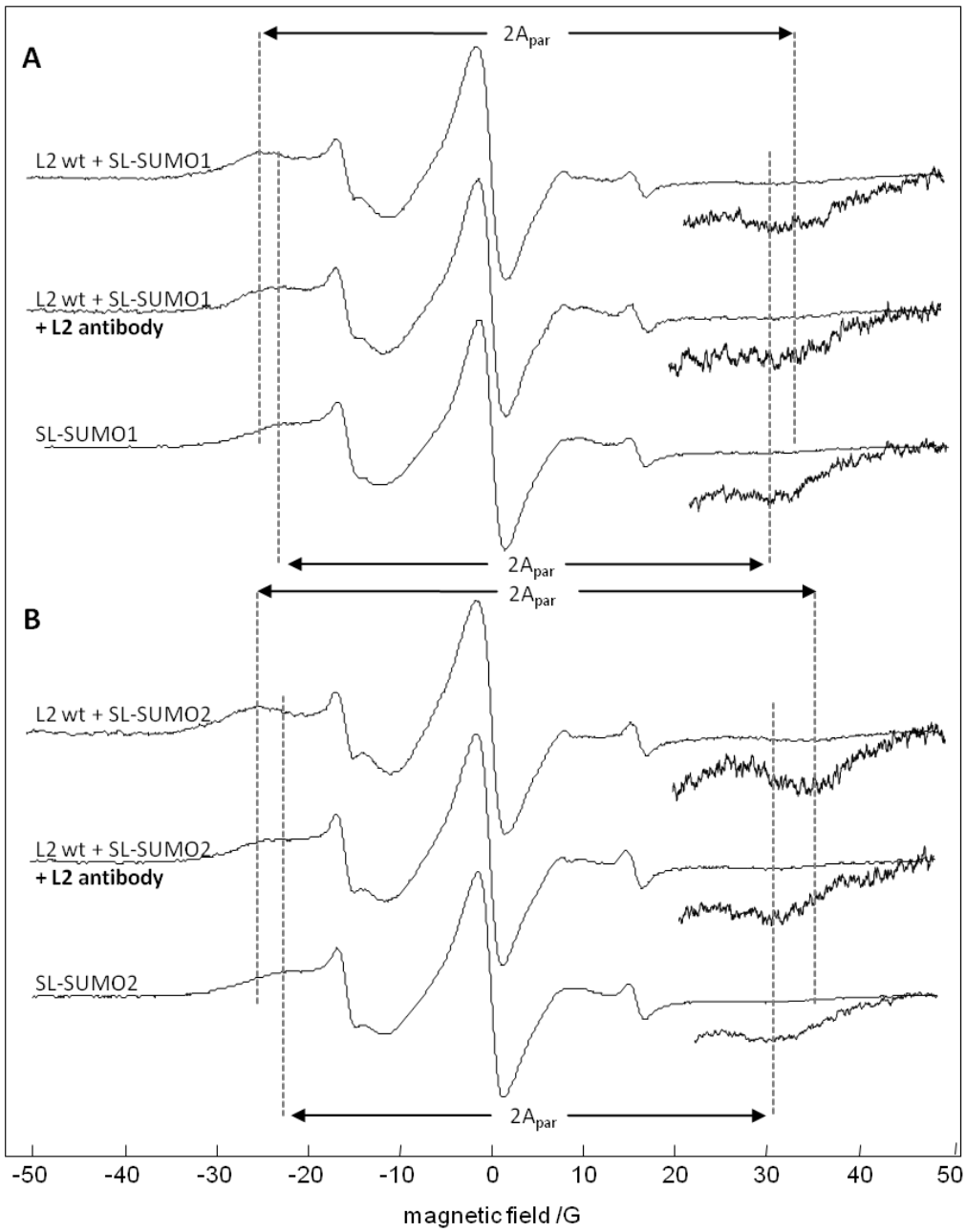

Fig. 3.43: L2-antibody-induced dissociation of L2 and SL-SUMO1/2. EPR samples containing equimolar amounts of L2 and SL-SUMO1 (***A***) or SL-SUMO2 (***B***) were incubated with a highly specific L2 antibody (L2-1). The CW EPR spectra obtained after L2 antibody addition featured significantly decreased $2A_{pat}$ values (52.8 - 54.5 G) when compared with $2A_{pat}$ values from spectra taken before antibody addition (56.9 – 60 G). In general, the spectra obtained after L2 antibody addition were comparable with spectra containing only SL-SUMO1/2, indicating an almost complete inhibition of L2 interaction with SUMO1/2.

3.3.3.5 The L2 labeling positions C22 and C28 are inaccessible for spin labeling

In order to gain more information about L2-SUMO1/2 interaction and to measure DEER distances between the interaction partners, in addition to SDSL of SUMO1/2, also HPV16 L2 was subjected to SDSL. Here, wild-type L2, as well as the L2 point mutants L2 C22S and L2 C28S, were used. All labeling

experiments were based on L2 which was His-affinity purified under denaturing conditions in 6 M guanidine HCl. Since first pilot labeling experiments based on the standard protocol, which was also used for labeling of SUMO1/2, did not lead to successful L2 labeling, a series of test labeling reactions was performed (Fig. 3.44). Here, the most important labeling parameters were modified, e.g. the labeling conditions (denaturing vs. non-denaturing), reduction, and final removal of excess spin label, as well as washing steps and sample concentration. Most possible combinations were tested with all available L2 types (wild-type, L2 C22S, L2 C28S). Additionally, labeling was performed in 4 M NaCl buffer to minimize potential electrostatic shielding of L2 structure elements, or in the presence of SUMO1/2. Taken together, none of the experiments resulted in correct labeling of L2 protein. The "best" labeling reaction resulted in a sample which eventually contained a labeled L2 fraction of about 5%. Spectral acquisition could also be complicated by extremely broad spectra due to strong immobilization of the label and potential spin-spin interaction for SL-L2 wt, which would theoretically contain two spin labels at a <2 nm distance (at L2 position C22 and C28).

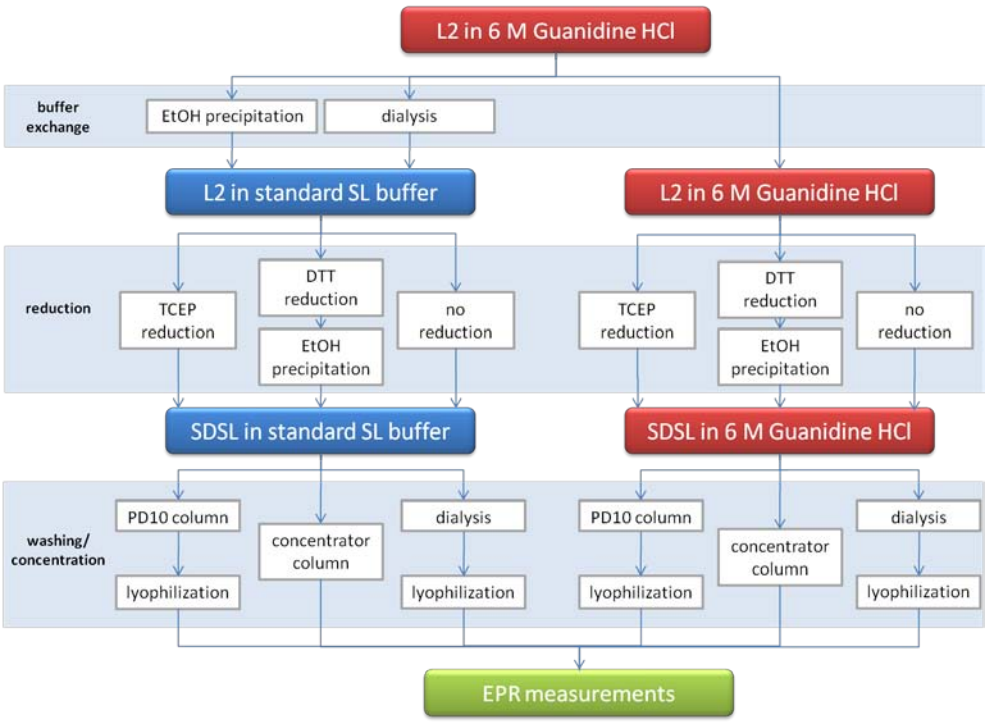

Fig. 3.44: Different protocols for L2 spin labeling. For efficient labeling of L2, a large set of protocols was tested including modification of the most important experimental parameters like refolding of L2 before labeling, L2 reduction, the general labeling conditions (denaturing or non-denaturing), as well as final washing and protein concentration steps. Finally, CW EPR measurements were performed to analyze L2 labeling efficiency.

3.3.4 No interaction of HPV16 L2 SIM peptides with SUMO1/2 in EPR

Since labeling of purified, full length HPV16 L2 was not successful, L2 peptides containing the HPV16 L2 SIM region were synthesized and used as a target for spin labeling. Labeling of the L2 SIM peptide would allow for interaction screening with nonlabeled SUMO1/2 in CW EPR measurements and additionally allow detection of DEER distances between the spin labels attached to the L2 SIM peptides and the labels attached to SUMO1 or SUMO2 if there is an interaction between the L2 SIM peptide with SUMO1 or SUMO2. Synthesis of two types of L2 peptides with different labeling position (L2 CysSIM and L2 SIMCys) theoretically allowed for discrimination of the orientation of the L2 SIM attachment to SUMO1 or SUMO2. Each peptide contained a single cysteine residue in a peripheral region, leaving the hydrophobic core of the SIM untouched (Fig. 3.45).

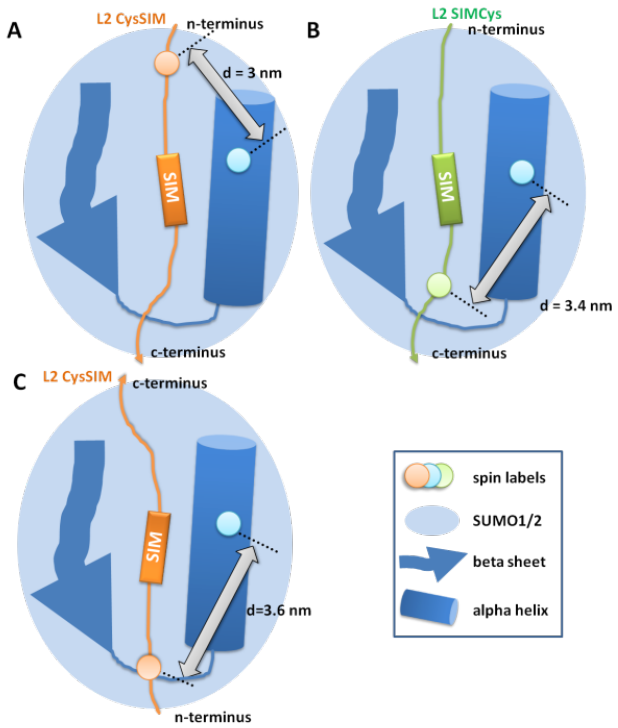

Fig. 3.45: Possible orientation discrimination of the L2 SIM peptide attachment on SUMO1/2. Two types of L2 peptides containing the SIM region at position 284-289 were synthesized (Genscript). The CysSIM peptide (amino acid sequence: I**C**PDPDF**LDIVAL**HRPALTSRRT, 23 amino acids) contains a cysteine, which is located near the N-terminus of the peptide. In contrast, the SIMCys peptide (amino acid sequence: APDPDF**LDIVAL**HRPA**C**TSRRT, 22 amino acids) comprises the cysteine near its C-terminus. Detection of different sets of DEER distances between spin labels attached to the L2 SIM peptides and the labels attached to SUMO1/2 allow for discrimination of parallel attachment (***A***) and (***B***), or anti-parallel attachment of the L2 SIM peptides with respect to the orientation of the neighbored beta sheet of the SUMO1/2 target (***C***).

Labeling of the L2 SIM peptides was performed based on reduction with TCEP and labeling with ProxyIAA. Before DEER measurements were performed, first, it was checked whether spin-labeled L2 SIM peptides would interact with nonlabeled SUMO1/2 in CW EPR measurements (Fig. 3.46).

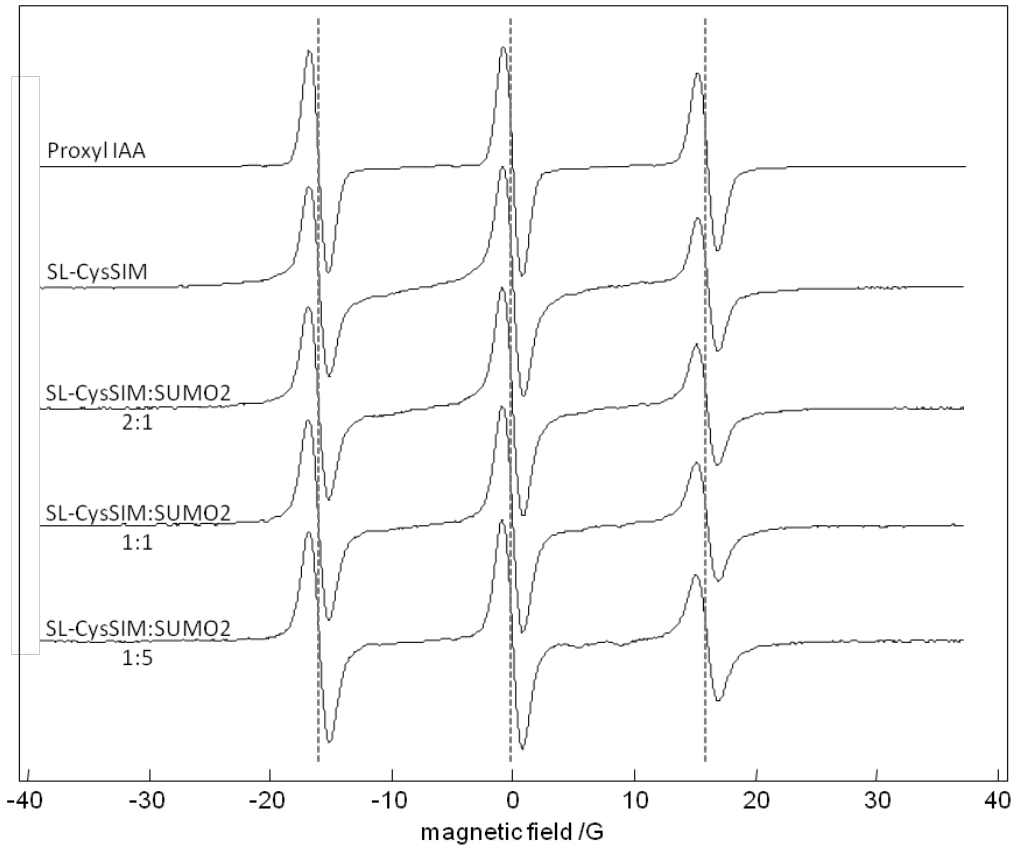

Fig. 3.46: No immobilization of spin-labeled L2 CysSIM peptides after SUMO2 addition. CW EPR measurements were performed at 5 °C. Spin-labeled CysSIM samples featured significantly immobilized spectra (rotational correlation times t_c~1.4 ns) when compared with control spectra with Proxyl-IAA (t_c~1 ps). Interestingly, after addition of increasing amounts of SUMO2, no effects of further immobilization caused by a potential interaction of the CysSIM peptide with SUMO2 were observed. In contrast, addition of increasing amounts of SUMO2 lead to a less broadened spectral line shape.

The spectra obtained for SL-CysSIM and SL-SIMCys samples without SUMO showed a significant reduction of mobility of the spin label as it was supposed after attachment of the spin labels to the L2 CysSIM peptide containing 23 amino acids. For g values of [2.0080 2.0049 2.0029] and A values (in Gauss) of [2.07 5.67 40.14], rotational correlation times of about 1.4 ns were calculated by simulation of the spectra (~1 ps for the Proxyl IAA reference). In a concentration row, the labeled L2 SL-CysSIM peptides were incubated with different amounts of nonlabeled SUMO2. An interaction of the short peptides with the larger SUMO1 or SUMO2 should result in significant changes of the spin label mobility. This was not observed here. Instead, the spectra obtained for SL-CysSIM after SUMO2 addition were almost identical to the reference spectra without SUMO2. The experiments were also performed with addition of SUMO1 and L2 SIMCys peptides (Fig. 3.47). There was no immobilization of the spin label due to addition of SUMO1/2 in any of the experiments when compared with the reference spectra without SUMO1/2 (dashed lines).

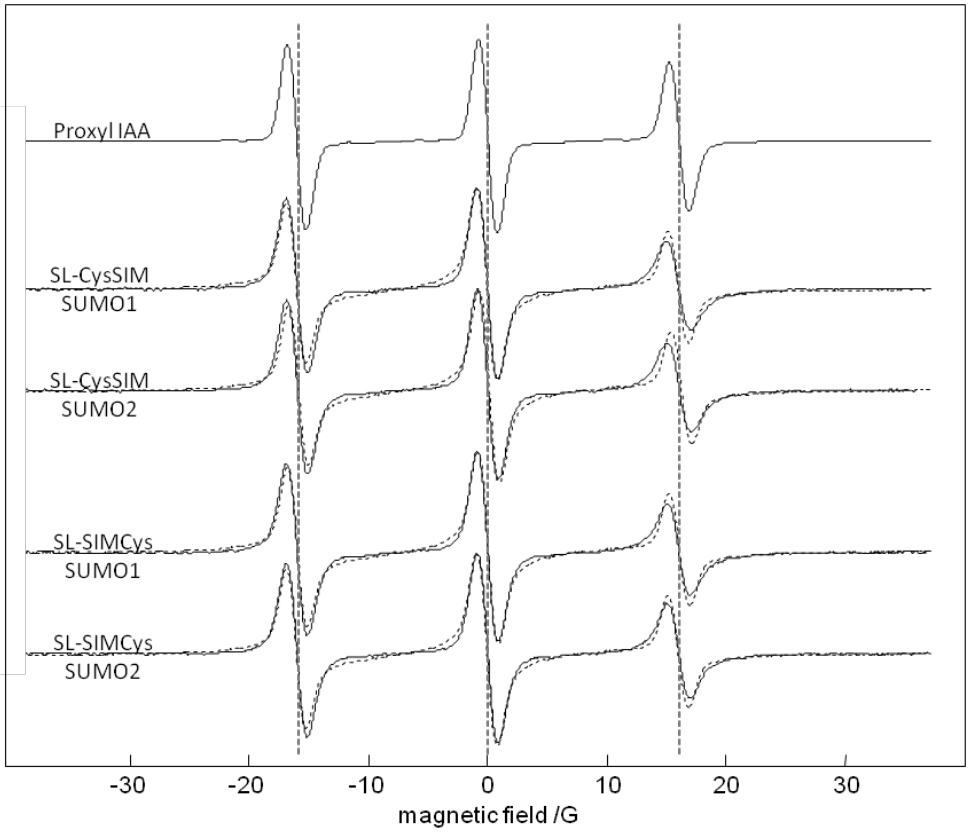

Fig. 3.47: SUMO1/2 addition does not induce immobilization of spin-labeled L2 SIM peptides. Spin-labeled SL-CysSIM or SL-SIMCys peptides were incubated with a fivefold excess of nonlabeled SUMO1 or SUMO2 and characterized by CW EPR measurements at 5 °C. Addition of SUMO1/2 lead to a less broadened line shape of the spectra when compared with control spectra without addition of SUMO1 or SUMO2 (dashed lines).

Interaction of SL-SUMO1/2 with L2 SL-CysSIM or SL-SIMCys peptides was additionally characterized by ESE-detected pulse EPR measurements and DEER. For ESE-detected EPR spectra, no significant differences between spectra containing only SL-SUMO1/2 and those containing SL-SUMO1/2 together with labeled L2 peptides were observed (Fig. 3.48). There was only a slight narrowing of the spectra detected for the labeled L2 CysSIM and SIMCys peptides without addition of SL-SUMO1/2 (marked with arrows).

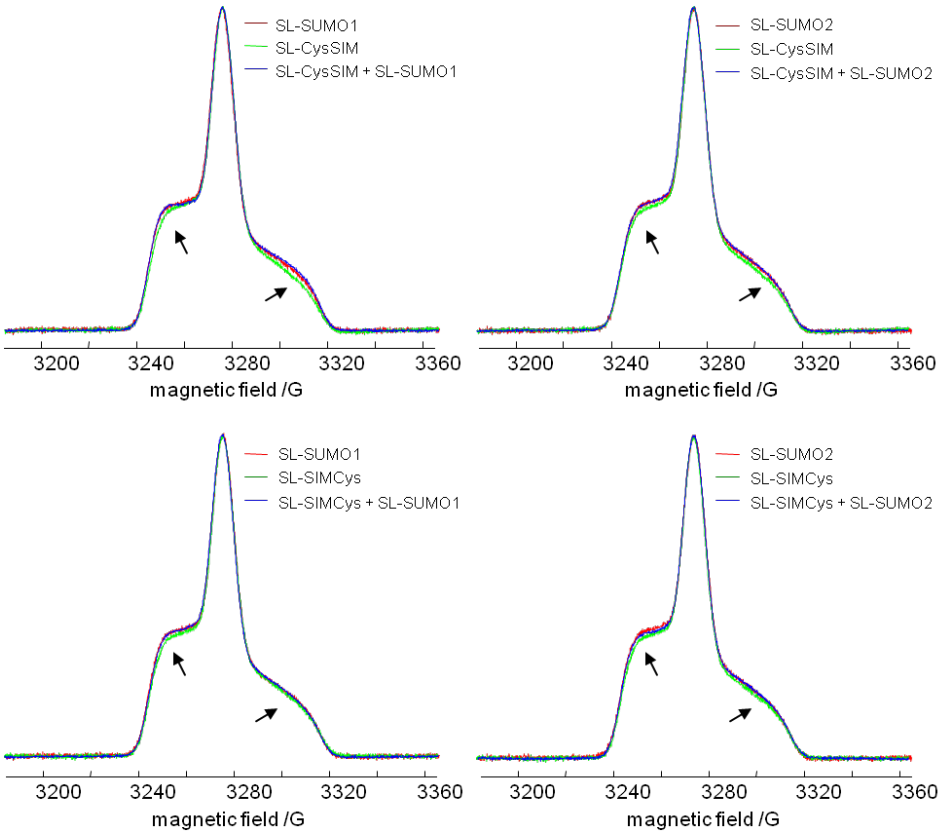

Fig. 3.48: ESE EPR experiments show no spectra changes upon incubation of spin-labeled L2 SIM peptides with SL-SUMO1/2. Spin-labeled CysSIM or SIMCys L2 peptides were characterized by ESE EPR measurements at 50 K with or without incubation with equimolar amounts of SL-SUMO1 or SL-SUMO2. Spectra with CysSIM or SIMCys alone were comparable with reference spectra containing Proxyl IAA and slightly narrowed when compared with spectra taken from SL-SUMO1/2 samples (see black arrows). There were no significant differences between SL-SUMO1 and SL-SUMO2 spectra. Also spectra of SL-CysSIM or SL-SIMCys samples were almost identical.

Samples were further subjected to more selective DEER measurements to check whether small fractions of L2 peptides and SUMO molecules interact with each other, leading to detection of DEER distances (Fig. 3.49).

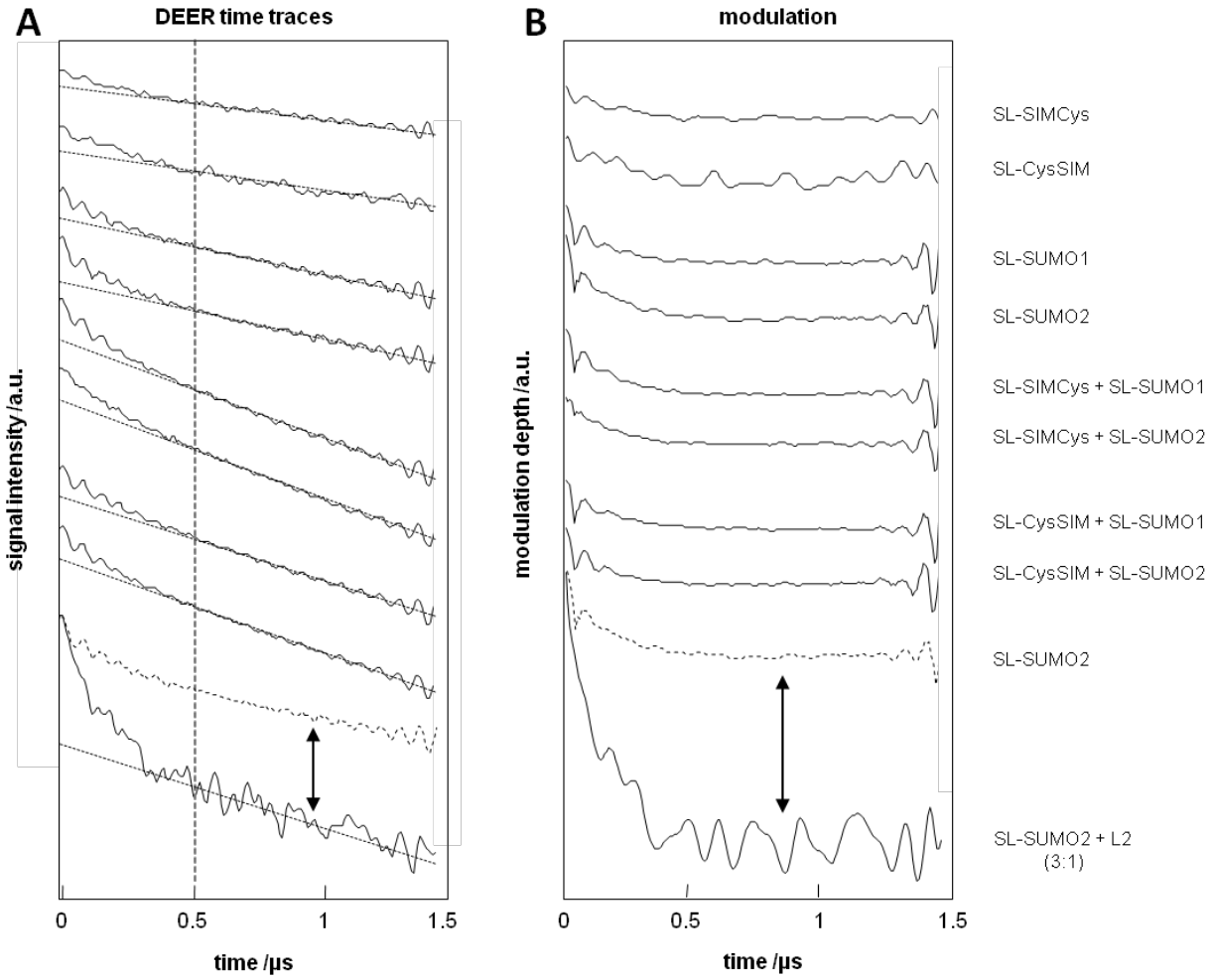

Fig. 3.49: No detection of DEER distances upon incubation of spin-labeled L2 SIM peptides with SL-SUMO1/2. DEER measurements were performed at 50 K with a d_2 time of 1.5 µs. ***A*** The original DEER time traces were plotted together with the respective background functions (dashed lines, homogeneous 3D background, background fitting from 0.5-1.5 µs). ***B*** After background correction, only one very broad and slight modulation with very small modulation amplitude was detected for samples containing SL-SUMO1 and especially SL-SUMO2 (modulation amplitudes 0.05 ± 0.02 and 0.08 ± 0.02). Samples including L2 SIM peptides together with SL-SUMO1/2 did not feature enhanced modulation depths or additional modulations upon interaction of the L2 peptides with SUMO protein. Remarkably, incubation of SL-SUMO2 with a threefold molar excess on nonlabeled L2 did result in a significant increase of modulation depth (0.27 ± 0.05) when compared with SL-SUMO2 alone (0.08 ± 0.02, see double arrow).

There were no dominant modulations in any of the original DEER time traces. The time traces obtained for SL-CysSIM or SL-SIMCys followed the experimental background (dashed lines) with only very small deviations. Analysis of the time traces obtained for SL-SUMO1 and especially SL-SUMO2 revealed one very broad modulation with very small modulation depth, which could be attributed to a very broad distribution of distances around 3.5 nm. Times traces obtained for samples containing spin-labeled L2 SIM peptides (SL-CysSIM, SL-SIMCys) together with SL-SUMO1 or SL-SUMO2 decayed slightly faster, but the modulation depths were comparable to the modulation depths of SL-SUMO1/2 samples without L2 SIM petides, indicating that L2 SIM addition did not result in an increase of detectable DEER distances between the L2 peptides and SUMO molecules. Most

interestingly, addition of a threefold molar excess of full-lenghth, nonlabeled L2 to SL-SUMO2 resulted in significantly increased modulation depths (0.27 ± 0.05 vs. 0.08 ± 0.02 for SL-SUMO2, alone).

3.3.5 Interaction of HPV16 L2 SIM peptides with SUMO1/2 in FCS

The potential interaction of the HPV16 L2 SIM peptide and SUMO1/2 was additionally characterized by Fluorescence Correlation Spectroscopy (FCS). In this method, the size of the smaller interaction partner (here the L2 SIM peptide) was determined by measurement of the diffusion rate of a fluorophor, which was coupled to the peptide before. Measurements were also performed with the addition of the interaction partner SUMO1 or SUMO2 to the L2 SIM. Lower diffusion rates would thereby indicate a larger size or hydrodynamic radius of the molecule with the attached fluorophor. This would be a direct hint for interaction of the L2 SIM peptide with SUMO1/2. First, the labeling of the peptides was performed and characterized. For FCS measurements, the HPV16 L2 SIM peptide SIMCys was reduced with TCEP and incubated with the BODIPY®507/545 IA fluorophor. The labeling efficiency was tested photometrically by detection of free sulfhydryl groups with Ellmann's reagent (5,5'-dithiobis-(2-nitrobenzoic acid) or DTNB). Absorption was only detected for the samples containing reduced CysSIM without addition of BODIPY®507/545 IA (A_{412nm} = 0.25), while for samples which were incubated with the fluorophor, no significant absorption was measured. Therefore, it can be concluded that almost all SH groups were labeled with BODIPY®507/545. For FCS measurements, the fluorescence labeled L2 CysSIM peptides were mixed with a 3-5 fold excess of SUMO1/2.

The autocorrelation curves for L2 CysSIM peptides together with SUMO1 (shown in red, Fig. 3.50, A) or SUMO2 (shown in red, Fig. 3.50, B) showed a significant shift towards higher diffusion times compared to the measurements with L2 CysSIM peptides (shown in black).

Multicomponent fitting of the experimentally detected autocorrelation curves was used for determination of the diffusion coefficients and hydrodynamic radii of the observed fluorescence species (Tab. 3.2).

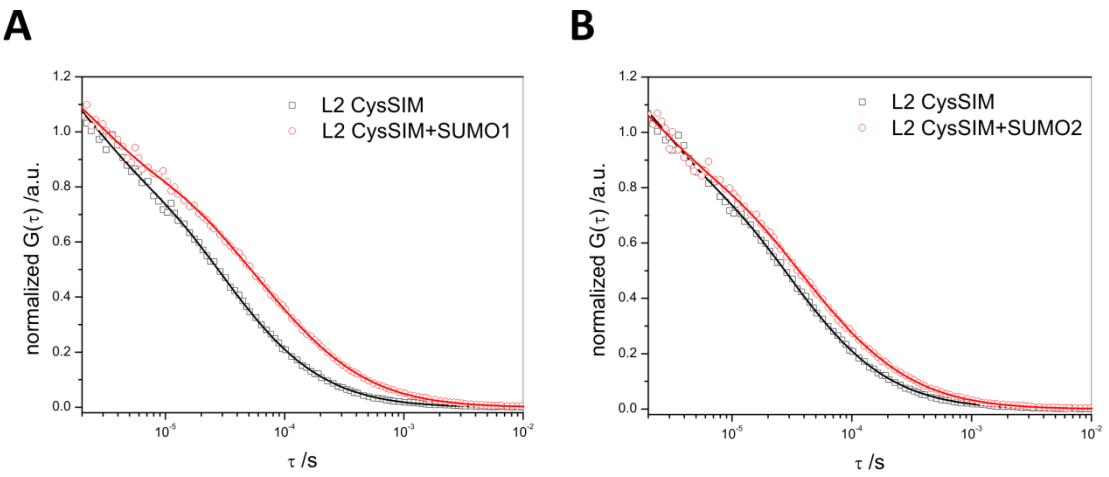

Fig. 3.50: SUMO1/2-induced shift of the autocorrelation curves obtained for FCS measurements with fluorescence labeled L2 CysSIM peptides. FCS measurements were performed at RT with BODIPY®507/545 labelded L2 CysSIM peptides with or without incubation with a 3-5 fold excess of SUMO1 (***A***) or SUMO2 (***B***). After addition of SUMO1 or SUMO2, a significant shift of the autocorrelation curves towards higher correlation times was observed (red lines/data points).

Tab. 3.2: FCS parameters for measurements with fluorescence labeled L2 CysSIM peptides with SUMO1 or SUMO2.

	τD /ns	Rh /nm	% high molecular weight
CysSIM	20	0.56	
CysSIM + SUMO1	104	1.9	50%
CysSIM + SUMO2	100	1.9	25%

Compared with diffusion times of the free L2 SIM molecules (20 ns), addition of SUMO1 or SUMO2 resulted in significantly slower diffusion rates (~100 ns). Also a remarkable increase of the hydrodynamic radius was observed after addition of SUMO1/2 (0.56 nm for CysSIM controls vs. 1.9 nm after SUMO1/2 addition). Further analysis showed that a fraction of about 50% of the fluorophors was bound in higher molecular complexes after addition of SUMO1, while the fraction was about 25% after addition of SUMO2.

3.3.6 No interaction of L2 with SUMO1/2 in isothermal titration calorimetry

In order to confirm the presented results for L2 interaction with SUMO1/2 and to determine binding affinities, isothermal titration calorimetry was performed (Fig. 3.51).

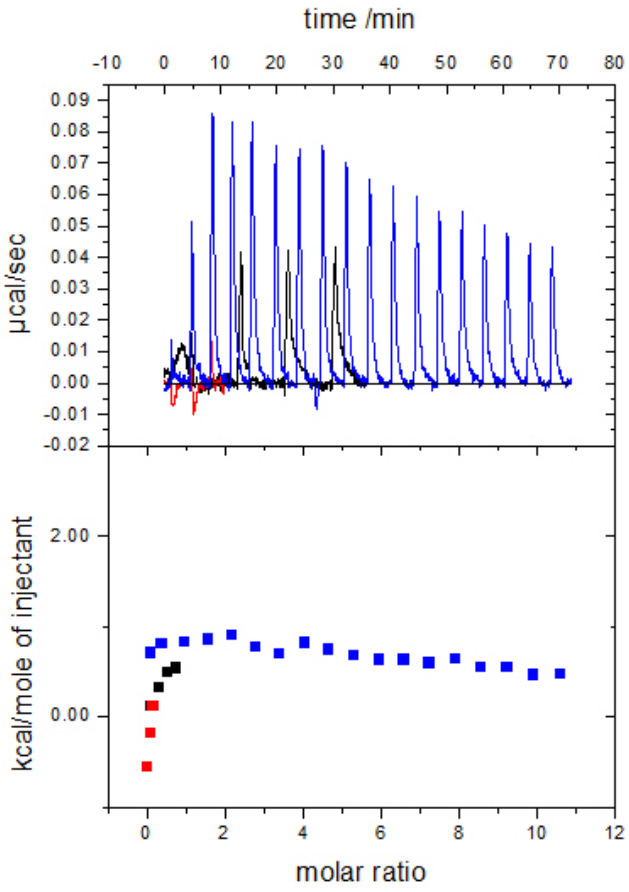

Fig. 3.51: Isothermal titration calorimetry (ITC) data for the interaction of full-length L2 with SUMO2 (blue) or L2 SIM peptides with SUMO1 (black). The top panel shows the ITC thermogram. The bottom panel shows the integrated heat of each injection after correction for the heat of dilution. Assuming binding at a molar 1:1 ration, the binding constant was about 1 KCa/mol for SUMO2 injection to L2, and about 0.5 KCa/mol for injection of SUMO1 to the L2 SIM peptide, which was comparable with the dilution heat upon injection of buffer solution in the control experiment (red).

For titration of SUMO2 into a sample solution containing full-length L2, a binding constant of about 1 kCa/mol was determined. For SUMO1 injection into a sample solution containing L2 SIM peptide, a binding constant of about 0.6 KCa/mol was obtained, which was comparable with background dilution artifacts (see red data points).

3.3.7 The L2 SIM peptide attaches to SUMO1 and SUMO2 in MD simulations

In order to reproduce L2-SUMO interaction data and to characterize the potential interaction interface of the L2 SIM region and the SUMO receptor, MD simulations were performed. Therefore, the L2 SIM peptide (amino acid sequence: APDPDF**L**D**IV**ALHRPALTSRRT) was modeled onto the potential SIM receptor grooves on SUMO1 or SUMO2 in parallel or anti-parallel orientation of the L2 SIM with respect to the sheet-helix motif of the SUMO receptors. After equilibration for several

nanoseconds, for each of the four simulations (L2 SIM-SUMO1, L2 SIM-SUMO2, each with parallel or anti-parallel orientation), simulation snapshots were taken and the orientation of the L2 SIM peptides on the SUMO surface was characterized. For each simulation, the root-mean-square deviation (RMSD) was determined to describe conservation of a potential, conserved L2 SIM structure, which could be characteristic for the interaction of the L2 SIM peptide with SUMO proteins.

Docking experiments of the L2 SIM peptide onto SUMO1 in parallel orientation resulted in a tight fitting of the hydrophobic core residues IVAL into the hydrophobic SUMO1 pocket located near the SUMO1 ARG54 (Fig. 3.52). Dipolar interactions were detected between the L2 SIM ASP3 and LYS37, ASP5 and LYS39 or ARG54, and ASP8 and ARG54 or LYS46. The RMSD of the L2 SIM peptide was about 5.6 Å, indicating no significant stabilization of the L2 SIM structure on the SUMO1 surface. For anti-parallel orientation, the L2 SIM region only very superficially attached to the SUMO1 surface. The RMSD of the L2 SIM was 6.7 Å, indicating no interaction with SUMO2 under these conditions. A potential dipolar interaction was only detected between the L2 SIM ASP5 and LYS35. In contrast, after docking of the L2 SIM peptide on SUMO2 in parallel orientation, the peptide was tightly associated within the hydrophobic SUMO2 acceptor groove. Also, the directly neighboring peptide regions were in close contact to characteristic side chains of SUMO2 surface residues (see black arrows). Dipolar interactions were identified between ASP3 of the L2 SIM and LYS33, as well as ASP5 with ARG50, and ASP8 with LYS35, but also the C-terminal ARG14 with ASP16. Especially the SIM core amino acids IVAL were directly located with a hydrophobic surface grove of the SUMO2 receptor directly located beneath the SUMO2 ARG50. This characteristic orientation of the L2 SIM was significantly stabilized indicated by a low RMSD of the L2 SIM peptide of about 2.2 Å. Docking of the L2 SIM peptide to SUMO2 in anti-parallel orientation did not result in a stabilized attachment of the peptide on the surface of SUMO2. With increasing simulation time, the L2 peptide moved further away from the SUMO2 surface also represented by an increased RMSD of the L2 Sims of about 4.4 Å. Additionally, there were only two dipolar interactions of the L2 SIM ASP5 with LYS35 and L2 SIM ASP8 with LYS42, which were not present in all simulation snapshots.

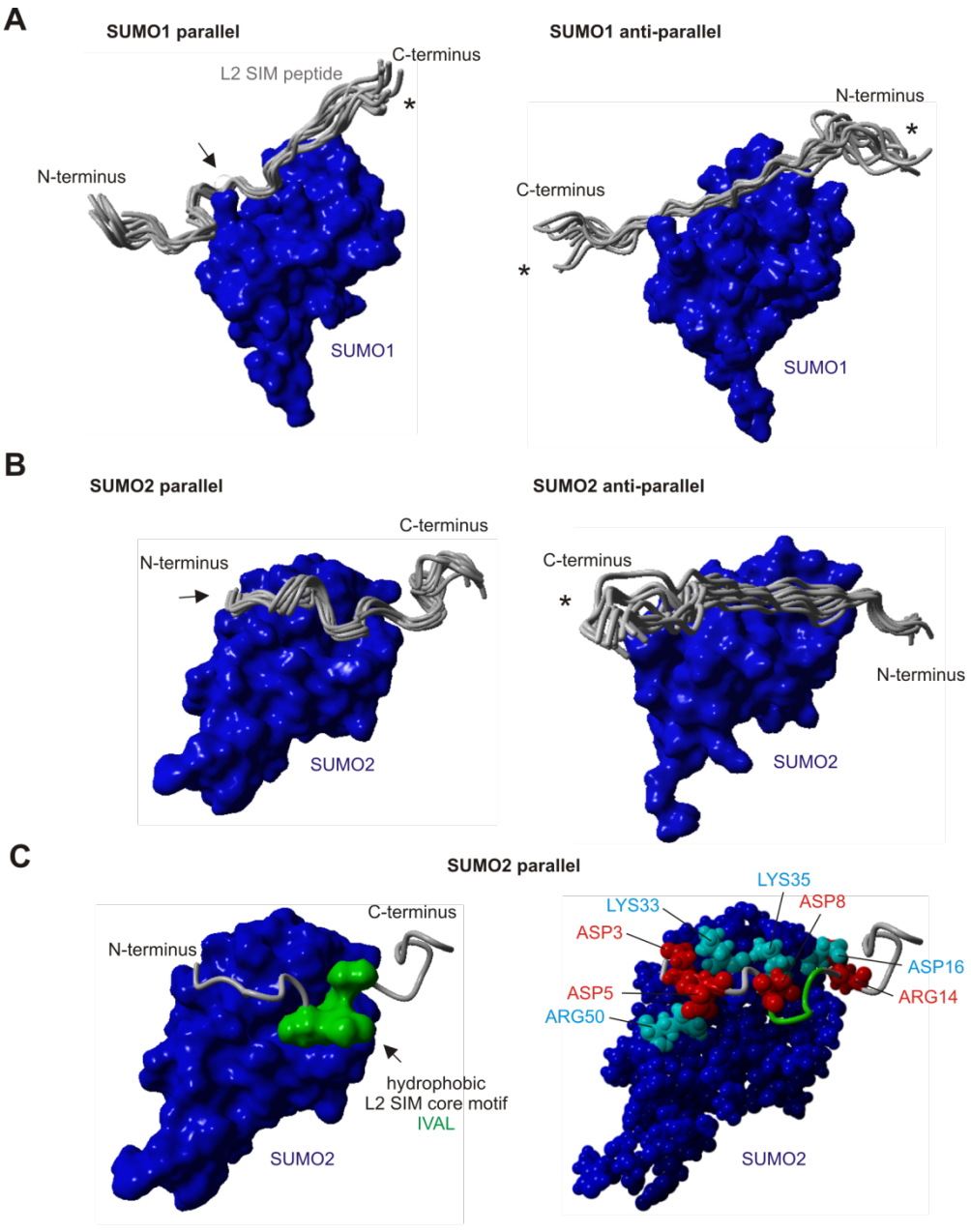

D

acceptor molecule	L2 SIM orientation	root-mean-square distance (RMSD)
SUMO1	parallel	5.65 ± 3.25 Å
	anti-parallel	6.72 ± 2.85 Å
SUMO2	parallel	2.23 ± 1.12 Å
	anti-parallel	4.41 ± 2.24 Å

E

acceptor molecule	L2 SIM residue	SUMO acceptor residue	central L2 SIM region
SUMO1 (parallel)	ASP3	LYS37	IVAL
	ASP5	LYS39/ARG54	
	ASP8	LYS46/ARG54	
SUMO2 (parallel)	ASP3	LYS33	IVAL
	ASP5	ARG50	
	ASP8	LYS35	
	ARG14	ASP16	

Fig. 3.52: MD simulations of the L2 SIM peptide interaction with SUMO1/2. ***A*** Superposition of L2 SIM structures after parallel or anti-parallel docking of the L2 SIM peptide onto SUMO1. Black arrows indicate tight surface attachment of the L2 peptide. Asterisks denote significant flexibility of the peptide termini. ***B*** Superposition of L2 SIM structures after parallel or anti-parallel docking of the L2 SIM peptide onto SUMO2. ***C*** View on the hydrophobic core of the L2 SIM peptide (amino acids IVAL, green) within the hydrophobic groove (left) and the amino acid residues involved in ionic interaction after docking to SUMO2 in parallel orientation (right). ***D*** RMSD values for the different L2 SIM-SUMO1/2 interaction modi. ***E*** Amino acids involved in ionic interactions and determination of the central hydrophobic core motif of the L2 SIM.

4. Discussion

Human papillomaviruses (HPVs) are a family of nonenveloped DNA viruses, which mostly account for benign papillomas. However, several high-risk HPVs, such as HPV16, also cause cervical cancer or other epithelial tumors (Walboomers and Snijders 1999; Parkin 2006). After infection of basal cells, the life cycle of HPVs fundamentally depends on the differentiation of keratinocytes including genome amplification and production of new viruses in fully differentiated epithelial cells. The HPV capsid is composed of the major capsid protein L1 and the minor capsid protein L2, which plays a key role in several steps during HPV infection, including nuclear transport of the L2-DNA complex, and assembly of new viruses (Florin, Sapp et al. 2002a; Florin 2002b; Florin, Becker et al. 2006; Kämper, Day et al. 2006; Buck, Cheng et al. 2008; Schneider 2011). For functional regulation of these processes, L2 exploits different cellular mechanisms. There is strong evidence that pathogens and viruses frequently use the cellular apparatus of small ubiquitin-like modifiers (SUMOs) for regulation and establishment of persistent infection (Wimmer 2012). Multiple viral proteins which are functionally related to L2 thereby interact with SUMO proteins by both covalent SUMO modification (also termed SUMOylation) but also noncovalent interaction based on SUMO interacting motifs (SIMs) (Wimmer 2012). It was shown before that also the HPV16 L2 protein is SUMOylated and that especially L2 SUMOylation with SUMO2/3 significantly increased L2 stability upon coexpression (Marusic 2010). In this context, it was of highest importance to characterize the unknown physiologic relevance of L2 SUMOylation, but also to elucidate whether L2 is able to interfere with the cellular

SUMO apparatus via SUMO interacting motifs (SIMs) by noncovalent interaction and to characterize possible consequences for HPV infection.

This study provides the first direct evidence that HPV16 L2 directly interacts with SUMO proteins via a conserved SIM (amino acids 286-289: IVAL). Incorporation of L2 lacking the SIM region (L2 ΔSIM) led to an almost complete loss of infectivity for HPV16 L1/L2 ΔSIM pseudobiruses (PsVs), while incorporation of SUMOylation deficient L2 did not influence infectivity of HPV16 L1/L2 PsVs. The lack of the L2 SIM had no effect on virus binding and endocytosis, but almost entirely abolished colocalization of L2 or the viral DNA with promyelocytic leukemia bodies (PML bodies or ND-10) after infection with L1/L2 ΔSIM PsVs, which is characteristic for wild-type L1/L2 PsVs (Day 1998; Florin 2002b; Schneider 2011). After cellular L2 expression, the lack of the L2 SIM had no effect on nuclear import, but led to an inhibition of L2 colocalization with PML. However, since generation of L1/L2 PsVs also succeeded with L2 lacking the SIM, SIM-based SUMO interaction does not seem to be crucial for morphogenesis of new viral particles.

4.1 Covalent SUMOylation has no effect on assembly and infectivity of L1/L2 PsVs

There is a manifold of examples showing that viral proteins counteract the viral defense system of infected target cells by exploiting the cellular SUMO apparatus (Wimmer 2012). Thereby, both SUMOylation of viral proteins, but also SIM-based interaction with SUMO, leads to modification, delocalization, or even destruction of cellular PML bodies, which are regarded as antiviral centers featuring an especially high level of SUMOylated anti-viral proteins like PML, Sp100, DAXX, or ATRX. Also the HPV16 L2 protein interacts with components of the PML-NBs, leading to modification and reorganization of PML-NBs (Florin 2002b). First, we characterized the ability of L2 to be SUMO modified by covalent SUMOylation. After overexpression of L2 together with GFP-SUMO1 or GFP-SUMO2, clear high molecular weight bands featuring the theoretical weight of GFP-SUMO1/2 modified L2 were found for wild-type L2, while no such bands were identified after expression of SUMOylation deficient L2 lacking the SUMO conjugation motif (L2 ΔSCM). We were additionally able to identify a preference of L2 SUMOylation for GFP-SUMO2, while less L2 SUMOylation was observed for GFP-SUMO1. Most interestingly, L2 SUMOylation led to stabilization of L2, as half-life times of overexpressed L2 ΔSCM were significantly decreased when compared with wild-type L2 after coexpression with GFP (0.3 h vs. 0.9 h). This was in line with previous results reporting SUMOylation of wild-type L2, especially by SUMO2/3, but not L2 ΔSCM, which had a stabilizing effect on L2 (Marusic 2010). In this work, the effect of L2 SUMOylation on L2 stability was additionally characterized by measuring L2 turn over/degradation after coexpression together with GFP-SUMO1

or GFP-SUMO2. As a general trend, coexpression of GFP-SUMO1 or GFP-SUMO2 resulted in significantly extended L2 half-life times and enhanced stabilization of all L2 mutants when compared with GFP-L2 coexpression without SUMO1/2. There are several possible explanations for L2 stabilization. First, L2 half-life times could be directly affected by SUMOylation due to altered molecular structure and interaction activity of the modified L2. Second, it is plausible that enhanced SUMOylation levels due to GFP-SUMO1/2 overexpression could lead to enhanced SUMOylation of transcription factors, resulting in increased expression levels. However, this assumption may be disqualified at least in some part due to the fact that the stability assay was based on addition of cycloheximide (CHX) just before characterization of L2 stability, which represents an inhibitor of eukaryotic translation and allows for determination of L2 turnover without artifact stemming from transcription or translation. An additional explanation could be that the coexpressed GFP-SUMO1/2 fusion proteins are dominant-negative for formation of fully-functional anti-viral and L2 degrading PML-NBs, which in turn leads to extended L2 half-life times. A further reason for increased L2 stability could be, that the lysine at position 35, which serves as acceptor during L2 SUMOylation, can not longer be targeted by ubiquitin, which could induce L2 degradation.

By L2 overexpression experiments, also the influence of L2 SUMOylation on morphogenesis of new HPV16 PsVs was investigated. Previously, a diffuse L2 localization pattern all over the nucleus for wild-type L2 and L2 ΔSCM was reported in immunofluorescence microscopy in the presence of endogenous SUMO (Marusic 2010). Conversely, our experiments showed a well defined colocalization of L2 with PML and SUMO1/2 at the PML-NBs for wild-type L2 and L2 ΔSCM in HeLa and HaCaT cells with or without coexpression of GFP-SUMO1 or GFP-SUMO2. In addition, it was reported that SUMOylated L2 does not interact with L1 in pulldown experiments, which could have important effects on HPV morphogenesis. In our studies, L2 ΔSCM had no influence on L2-incorporation into HPV16 L1/L2 PsVs and the mutant L1/L2 ΔSCM PsVs featured a wild-type level of incorporated viral DNA and a typical capsid structure.

This study provides the first results for unraveling the consequences of L2 SUMOylation on HPV infection including cellular localization of viral proteins and DNA after infection. SUMOylation is obviously not required for the typical localization of the L2-DNA complex at PML bodies after HPV16 infection, as immunofluorescence experiments showed a clear localization of both, L2 and viral DNA, at PML NBs after infection with wild-type HPV16 L1/L2 PsVs or L1/L2 ΔSCM PsVs. Additionally, SUMOylation deficiency of L2 had only a slight effect on infectivity. The infection level of L1/L2 ΔSCM PsVs was decreased to about 50-70% in many infection experiments when compared with wild-type PsVs. This could indicate a small but measureable influence of L2 SUMOylation on HPV infectivity,

which could be caused by the lower L2 stability and the decreased half-life time of SUMOylation deficient L2 ΔSCM observed after infection and overexpression.

4.2 Two highly conserved SUMO interaction motifs (SIMs) in HPV16 L2

SUMOylation does not represent the only way for proteins to interact with the cellular SUMO apparatus. As a second mechanism, also a noncovalent interaction of proteins with SUMO via SUMO interacting motifs (SIMs) was frequently observed (Minty 2000; Song 2004; Hannich 2005; Kerscher 2007). Since SUMOylation is also linked with SIM-based SUMO interaction, as it was already observed for PML-NB associated proteins like DAXX and Sp100 (Johnson 2004) but also during regulation of SUMOylation by SIM-containing E3 ligases (Gareau 2010), we searched for potential SIMs within the L2 protein sequence, which could allow for noncovalent L2 interaction with SUMO. A total number of nine potential SIMs was identified by sequence analysis within the HPV16 L2 sequence, which all followed the classical (V/I/L)-(V/I/L)-X-(V/I/L) or (V/I/L)-X-(V/I/L)-X-(V/I/L) consensus motif of a SIM (Minty 2000; Song 2004; Hannich 2005; Song 2005; Kerscher 2007). From the nine identified potential L2 SIMs, only the first six featured significant sequence conservation of the hydrophobic core region of the SIM in sequence alignments of high risk HPV16 L2 proteins. Additional conserved flanking, positively or negatively charged amino acids and phosphorylation sites, which are important for first surface binding of the SIM-containing proteins with SUMO (Gareau 2010), were observed for the SIMs at amino-acid positions 105-109, 235-238, and 284-289. Two of these SIMs represented double SIM motifs, in which each two SIMs lie directly on top of each other in parallel orientation (SIM 105-109, IVSLV) or antiparallel orientation (SIM 284-289, LDIVAL).

In order to better specify the respective sequence positions of the SIMs, the L2 sequence was additionally characterized by bioinformatic tools. L2 structure predictions indicate that there is only a small content of helical regions (9%), which are especially located towards the N-terminus. Beta strand regions (23%) seem to be distributed all over the primary protein sequence of L2. In general, most of the primary sequence seems to feature random coil character (65%) with a tendency towards special disorder in several regions, including the foremost parts of the n-terminus and the region containing the potential SIM at position 284-289. These results roughly match the data obtained from simulation of circular dichroism spectra obtained for purified HPV16 L2 (25% helix, 20% sheet, 55% random coil). The N-terminus seems to be highly accessible, which can be seen in a hydrophobicity/hydrophilicity plot of the L2 protein sequence, and confirms experimental data obtained for L2 after binding of HPV to the primary receptor, where the L2 N-terminus is cleaved by furin enabling infectious endocytosis (Richards, Lowy et al. 2006). The rest of the protein sequence

shares medium values for hydrophilicity/hydrophobicity, but there are smaller exceptions. Thus, for the region of aa 43-57, a significantly increased hydrophobicity was predicted, which overlaps with a transmembrane region predicted for the same part of the L2 sequence. The region of the potential double-SIM at the L2 sequence position 284-289 and eventually also the double SIM region at position 105-109 represent additional spots of locally high hydrophobicity, eventually to better fit into the hydrophobic pocket on the SUMO surface. Especially, the double-SIM at position 284-289 is additionally flanked by stretches of high hydrophilicity on both sides, perhaps to optimize first contact of L2 and SUMO by electrostatic interaction. The double SIM at position 105-109 is located directly after the N-terminal cyclophilin B interaction site (aa 97-103) involved in exposition of the L2 N-terminus after cell binding (Bienkowska-Haba 2009; Bienkowska-Haba, Williams et al. 2012) and directly before an L2 interaction site for the annexin A2 heterotetramer (A2t, L2 sequence position 108-120) proposed as potential secondary receptor facilitating HPV infection (Woodham, Da Silva et al. 2012). However, it is unlikely that the L2 SIM is involved in this very early step of infection by regulation or competition to the cyclophilin/A2t interaction, as SUMO proteins are mainly localized in the nucleus and the cytoplasm and may only be present in endosomes in the context of (poly)-SUMOylated target proteins involved in their regulation pathways. However, the close neighborhood of the SIM to the cyclophilin/A2t interaction site could affect mutation experiments for dissection of the functionality of the SIM and interfere with functions based on cyclophilin/A2t binding.

Taken together, L2 sequence analysis provided direct hints for the existence of more than one SIM in the L2 sequence. There are at least two sequence regions containing double SIMs (105-109 and 284-298) with highest levels of sequence conservation and fulfilling all hallmarks of a classical SIM including the hydrophobic core region and flanking negatively charged amino acids important for long range electrostatic interaction involved in SIM-based SUMO interaction. In our studies, we focused on the L2 SIM at position 284-289.

4.3 L2 directly interacts with SUMO1/2 proteins

Subsequently, L2 interaction studies with SUMO1/2 were performed. For clarity, all interaction results are summarized in **Table 4.1**. In 3xFLAG-L2 precipitation experiments, a clear coprecipitation of GFP-SUMO2 was observed after coexpression of wild-type 3xFLAG-L2 together with GFP-SUMO1 or GFP-SUMO2. One may only speculate why wild-type L2 only interacts with GFP-SUMO2 in immunoprecipitation. One explanation could be the well-known target specificity of SUMO proteins, which is not only reported for SUMOylation but also for SIM-based SUMO interaction (Meulmeester 2008; Gareau 2010) and could be induced by the availability and localization of L2 interaction

partners, which are covalently modified by SUMO2, as there is no molecular basis for SUMO isoform specifity exclusively based on the SIM sequence, so far (Gareau 2010). The importance of the selective interaction of L2 with GFP-SUMO2 could be based on the known situation that SUMO2 and the almost identical SUMO3 play key roles in cellular regulation mechanism after cell stress in formation of poly-SUMO2/3 chains, which are directly linked with SUMO targeted protein degradation by the cellular proteasome (Saitoh 2000; Johnson 2004; Loftus 2009; Vertegaal 2010; Wadosky 2011). SUMO1 plays a role as potential chain end of poly-SUMO2/3 chains, but also in several more uncommon regulation mechanisms of SUMO1 targets.

Evidence for a direct L2 interaction with SUMO proteins came from electron paramagnetic resonance (EPR) measurements based on affinity purified and spin labeled SUMO1-his$_6$ or SUMO2-his$_6$ together with affinity-purified L2-his$_6$. Purified SUMO1 or SUMO2 was efficiently labeled with the EPR spin label Proxyl IAA at the helical position C52 (SUMO1) and C48 (SUMO2) by site-directed spin labeling (SDSL), incubated with different amounts of purified L2, which was refolded in the presence of SL-SUMO1/2-his$_6$, and characterized by continuous wave (CW) EPR. In the EPR spectra, a clear L2 dose dependent loss of mobility was observed in spectra of SL-SUMO1 and SL-SUMO2, indicating SUMO interaction with L2. While the labeling position was characterized as a region of a surface helix for SUMO1/2 samples without L2 addition, with increasing L2 amount, the mobility was even more limited and the labeling position was classified as a region of a contact helix typical for interaction surfaces. Also the L2 mutants C22S and L2 C28S were able to interact with SUMO1/2, indicating that the disulfide bridge, which is formed between both cysteines under physiological conditions (Campos 2009), is not necessary for *in vitro* interaction of L2 with SUMO1/2. Interestingly, incubation of the L2 SUMO1/2 samples with an L2 (L2-1) antibody, which recognizes the L2 epitope FTDPSVL (aa 163-170), led to enhanced mobility of the labeled SUMO1/2 region, indicating a reduction of L2 interaction with SUMO1/2 because of a higher affinity of the L2 antibody. This is possible due to a sterical inhibition of the L2-SUMO interaction based on close vicinity of the L2-1 epitope and the SIM in the native L2 protein structure. This could also explain why no coprecipitation of SUMO proteins was found after the numerous precipitations of L2 with L2 (L2-1) antibodies.

For reproduction of the interaction data, additional His- or GST-pulldown experiments were performed based on precipitation of GST-SUMO1/2 or SUMO1/2-his$_6$ and coprecipitation of L2, but no L2 interaction with SUMO1/2 was observed. The negative interaction results for pulldown experiments were most obviously caused by a strong formation of L2 aggregates in the presence of PML-containing components in the cell lysates prior to incubation of the separate L2 sample with precipitated and purified GST-SUMO1/2 or SUMO1/2-his$_6$, which possibly inhibited L2 interaction with SUMO. In contrast, in immunoprecipitation experiments with GFP-SUMO1/2, overexpressed L2

was able to interact with coexpressed GFP-SUMO1/2 directly after protein synthesis and before potential aggregation of L2 with PML-proteins. Additionally, there was no interaction of L2 with SUMO1/2 in mammalian 2-hybrid screening. In these experiments, L2 and SUMO1/2 were overexpressed as fusion proteins together with relatively large activation- or DNA binding-domains (both about 20 kDa), which could possibly interfere with protein interaction, albeit correct expression of fusion proteins. Another possible explanation could be that L2 features an inhibitory effect on transactivation due to transcriptional repression, as it is known that L2 also interact with factors like DAXX and Tbx, which act as transcription repressors (Wimmer 2012, Schneider 2012).

Tab. 4.1: Summary of L2/SUMO interaction data. L2 interaction with SUMO1/2 was characterized by different methods based on full-length L2 or L2 peptides containing a 22 or 23 amino acid sequence of L2 containing the L2 SIM at position 296-289. "+++", "++", "+" denote a grading for positive interaction of L2 with SUMO, "--" denotes no interaction, "ND": not determined. Abbreviations for the methods used: IP: immunoprecipitation, IF: immunofluorescence microscopy, EPR: Electron Paramagnetic Resonance spectroscopy, PD: pulldown experiments with purified/immobilized SUMO1/2, ITC: Isothermal titration calorimetry, FCS: Fluorescence Correlation Spectroscopy, MD: molecular dynamics simulation.

full-length L2					L2 SIM peptide	
method	GFP-SUMO1	GFP-SUMO2	GST-SUMO1/2	SUMO1/2-his$_6$	**method**	SUMO1/2-his$_6$
IP	--	+++	ND	ND	**FCS**	++
IF	+++	+++	ND	ND	**EPR**	--
EPR	ND	ND	ND	+++	**ITC**	--
PD	ND	ND	--	--	**MD**	++(+)
ITC	ND	ND	ND	--		

4.4 The L2 SIM is crucial for L2 interaction with SUMO proteins

To check whether the identified L2 SIM at sequence position 284-289 is responsible for L2 interaction with SUMO, immunoprecipitation experiments were repeated with mutant L2 lacking the hydrophobic core of the SIM (L2 ΔSIM, IVAL286-289AAAA). Remarkably, no interaction of the deletion mutant, L2 ΔSIM, with GFP-SUMO2 was observed in immunoprecipitation, indicating that the SIM region was directly involved in SUMO interaction. For characterization of the influence of SUMOylation on L2 interaction with GFP-SUMO2, also L2 ΔSCM mutants were included in immunoprecipitation experiments. The lack of the SUMO conjugation motif did not abrogate L2 interaction with GFP-SUMO2. Additional hints for L2 interaction with GFP-SUMO proteins came from immunofluorescence microscopy after overexpression of L2 together with GFP-SUMO1/2. Here, overexpressed wild-type L2, L2 ΔSCM, or L2 ΔPHOS showed the known and characteristic L2 wild-type phenotype and colocalized at PML-NBs, where also the majority of GFP-SUMO1/2 was located. These observations confirmed already published results for wild-type L2 colocalization with PML (Day 1998; Florin 2002b) and highlight the importance of L2 to locate at the PML-NBs, which represent regulation centers for viral defense but also viral transcription and replication and are mainly composed of DAXX, Sp100, and PML (Swindle 1999; Day 2004; Wimmer 2012)(Tavalai 2008; Tavalai

and Stamminger 2009; Wimmer 2012). All of them are controlled by SUMOylation in multifactorial ways, as stabilization, activation, and localization of these SUMO targets is directly affected by SUMOylation also explaining the high abundance of SUMO proteins at these sites. Most remarkably, L2 lacking the SIM did not localize at PML-NBs. Albeit, after coexpression of GFP-SUMO1/2 and L2, SUMO still localized at the PML-NBs, L2 ΔSIM featured a very diffuse localization pattern throughout the entire cell nuclei. The missing colocalization of L2 ΔSIM with GFP-SUMO1/2 at PML NBs is an additional clear sign that L2 interaction with GFP-SUMO1/2 directly depends on the L2 SIM at position 284-289.

Taken together, interaction studies suggested that the L2 SIM is important for L2 interaction with SUMO1/2 featuring a special preference for interaction with SUMO2, which could be induced by interaction with L2 targets, which are covalently modified by SUMO2. This also offers an explanation why SUMO specificity was readily observed in immunoprecipitations featuring a physiological protein context, but was not observed in *in vitro* interaction studies with purified proteins.

4.5 Flanking sequences around the L2 SIM trigger SUMO interaction of L2

In a set of biophysical interaction experiments, the interaction of short L2 peptides containing the L2 SIM at position 284-289 with purified SUMO1 or SUMO2 was characterized. In EPR measurements, synthetically L2 SIM peptides containing 22 or 23 amino acids with each one cysteine at a selected position, were labeled by site-directed spin labeling and incubated with different amounts of nonlabeled SUMO1-his_6 or SUMO2-his_5. There was no change in mobility for the labeled position within the L2 SIM peptide after addition of SUMO proteins indicating no interaction of the L2 SIM peptides with SUMO. There was also no interaction in DEER measurements, where both L2 SIM peptides and SUMO proteins were spin-labeled, but did not lead to detection of intermolecular DEER distances between the labels. It is most likely that the small sequence part around the L2 SIM selected for peptide synthesis does not allow for a stable *in vitro* interaction with SUMO1/2, since important flanking positively and negatively charged amino acids are only partially implemented. From literature it is known that especially negative charges located on the side chains of these residues might modulate SUMO-SIM interaction through long range electrostatic interactions with basic residues in the closer vicinity of the hydrophobic pocket of SUMO (Minty 2000; Song 2004; Kerscher 2007). The L2 sequence around the SIM at position 284-289 comprises a total number of eight negatively and ten positively charged amino acids with partly very high sequence conservation in high risk L2 types, from which only each three amino acids were also present in the selected L2 SIM peptides investigated here. It is plausible that under *in vitro* conditions, only a significantly

enlarged part of the structure region of L2 around the SIM containing a larger amount of charged residues is able to bring the SIM together with the hydrophobic interaction pocket of the SUMO proteins, as it was seen for full-length L2 and SUMO1/2 in CW EPR.

Further support for this thesis came from isothermal titration calorimetric (ITC) measurements based on the same L2 SIM peptides after titration with nonlabeled SUMO1. The binding constants determined by assuming one binding site per SUMO1/2 molecule were only slightly larger than the dilution heat indicating no or only very weak interaction of the L2 SIM peptide with SUMO1/2 under these conditions. However, it has to be stated that positive interaction of SIM peptides from other SUMO targets containing only 9-13 amino acids were able to interact with SUMO under comparable experimental conditions yielding dissociation constants of about 3-12 µM (Sekiyama 2008).

Conversely, positive interaction results for the interaction of the L2 SIM peptide with SUMO1 and SUMO2 came from fluorescence correlation spectroscopy (FCS). Here, a large fraction of fluorescence labeled L2 SIM peptides (25 - 50%) was able to interact with SUMO1 or SUMO2 to form significantly larger L2 SIM-SUMO1 or L2 SIM-SUMO2 complexes with slower diffusion times (about 100 ns) and a higher hydrodynamic radius (about 1.9 nm) when compared with the fluorescence labeled L2 SIM peptide alone (diffusion time: 20 ns, hydrodynamic radius: 0.56 nm). Control measurements showed that there was no nonspecific attachment of free fluorescence labels on SUMO1 or SUMO2, which could distort interaction parameters. One reason for this situation could be that the complex of L2 SIM peptide and SUMO is based on a very weak and unstable interaction, which was only detectable by the highly sensitive (to the global aggregates) FCS experimental setup, but not with CW EPR, where the local mobility dominates (which might not have changed after complex formation) or ITC, which cannot discriminate very short-lived protein interactions. It is plausible that only a larger L2 structure context would lead to a more stable association of the L2 SIM with SUMO detectable by EPR or ITC.

4.6 The putative L2-SUMO interaction complex based on MD simulation

In this thesis, an MD approach was used to characterize the possible structure of a potential L2 SIM-SUMO interaction complex. Thereby, both parallel and antiparallel orientation of the L2 SIM peptide with respect to the acceptor beta sheet of SUMO1/2, which is extended by the SIM upon interaction, were taken into account and compared with each other. Highest specificity of the L2 SIM attachment was found for parallel orientation of the L2 SIM peptide on the interaction surface of SUMO2. Here, a total number of four amino acid residues of the L2 SIM peptide was involved in formation of ionic interactions with acceptor residues on the SUMO2 surface. The L2 SIM residues ASP3, ASP5, ASP8

were in close proximity of the SUMO2 surface residues LYS33, ARG50, and LYS35, which are part of a field of positively charged acceptor molecules around the central hydrophobic groove between the helix and the beta sheet of SUMO2. Additionally, there was an ionic interaction between ARG14 of the L2 SIM peptide and ASP16 on SUMO2. This led to a very stable conformation of the L2 SIM peptide with a very low RMSD throughout the entire MD simulation. Especially the hydrophobic core region of the SIM including the residues IVAL was deeply buried within a hydrophobic groove on the SUMO2 surface. A comparable conservation of the L2 SIM-SUMO interaction complex was observed after parallel docking of the L2 SIM peptide onto SUMO1. Here, the L2 SIM residues ASP3 were in close proximity of the surface acceptor LYS37, ASP5 in the proximity of LYS39/ARG54, and ASP8 in the proximity of LYS46/ARG54. In general, the SUMO surface residues which seemed to be involved in attachment of the SIM in these MD simulations also function as acceptors in known SIM-SUMO1 or SIM-SUMO2 structures (PDB structures for comparison: 2ASQ, 1Z5S, 2KQS, 2LAS for SUMO1 and 2RPQ for SUMO2/3).

Interestingly, two observations indicate that one L2 molecule could potentially interact with more than one SUMO molecule at the same time (Fig. 4.1). First, DEER measurements based on spin-labeled SUMO2 (SL-SUMO2) and L2 in a molar ratio of 3:1 revealed significantly increased modulation depths when compared with reference measurements with SL-SUMO2 alone. There is a significant contribution of distances around 3.2 nm indicating that at least two SL-SUMO2 molecules are orientated next to each other at a fixed orientation with an intermolecular distance of about 3.2 nm. Since there were no DEER distances in SL-SUMO2 samples, the only plausible reason is that two SUMO2 molecules interact with one L2 molecule at the same time via more than one L2 SIM, and that the distance between the spin-labels of the L2-bound SL-SUMO2 molecules is about 3.2 nm. This theory is in line with the observation that the L2 SIM at L2 position 105-109 was also able to attach to SUMO2 in MD simulations. There was a stable conformation of the L2 $SIM_{105-109}$ peptide after parallel attachment (RMSD ≈ 2.8 Å). The conformation was stabilized by dipolar interaction of the L2 $SIM_{105-109}$ GLU17 and GLU16 residues with basic LYS35 and LYS45 acceptor residues on the SUMO2 surface. As a result, this could indicate that L2 may interact with more than one SUMO protein at the same time and could also allow L2 interaction with poly-SUMO2/3 chains via multiple L2 SIMs, which is often observed for SUMO or ubiquitin E3 ligase enzymes (Yang and Sharrocks 2010; Boutell 2011). However, as the lack of the major L2 SIM at L2 position 286-289 completely inhibits L2 interaction with GFP-SUMO2 in immunoprecipitations, it seems that the second SIM does not act independently as a SIM, but instead might act as a functional module together with the major SIM at L2 position 289-289 and could have a potentiating effect on SUMO interaction, as it was also observed for the SUMO E3 ligase PC2 (Yang and Sharrocks 2010). In turn, since CW EPR measurements were performed with an about 1:1 molar ratio of L2 and SL-SUMO1 or SL-SUMO2, this means that a

further increase of SL-SUMO1/2 in CW EPR could lead to even more immobilized CW EPR spectra or detection of mix spectra, which contain contributions of a SL-SUMO species bound to the first L2 SIM and a SL-SUMO species bound to the second L2 SIM.

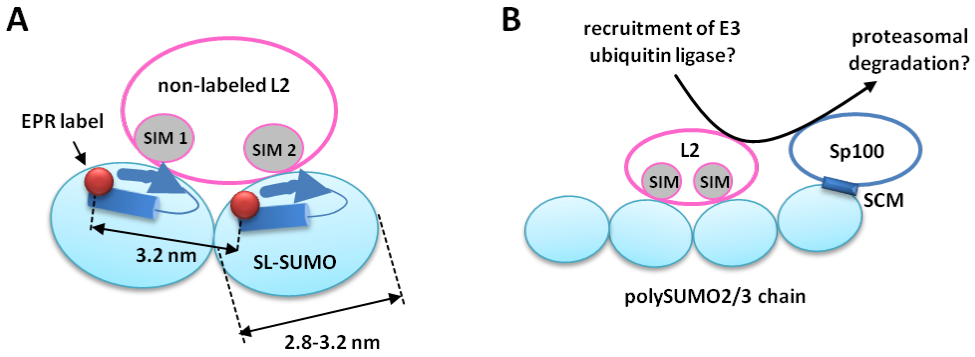

Fig. 4.1: The interaction of L2 with SUMO targets. ***A*** Schematic view on the putative interaction complex of non-EPR-labeled L2 with two spin labeled SL-SUMO molecules. A broad distance distribution around 3.2 nm was detected in DEER EPR measurements after incubation of nonlabeled L2 with an about threefold molar excess of spin-labeled SUMO2, which was not based on random interaction of SL-SUMO molecules, as no DEER distances were measured in reference samples containing only SL-SUMO2. This implies that at least two SL-SUMO2 molecules are located next to each other at a fixed orientation and with an intermolecular distance of about 3.2 nm between the SUMO2 labeling positions at cysteine 48 within the SUMO2 helix. One plausible reason explaining the fixed orientation of the SUMO proteins next to each other is the interaction of two or more SUMO molecules with one L2 via multiple L2 SIMs. ***B*** The L2 ability to interact with more than one SUMO molecule in *in vitro* interaction assays could allow L2 interaction with polySUMO chains of SUMOylated target proteins like e.g. Sp100, which could allow for proteasomal degradation of the SUMOylated L2 targets after recruitment of E3 ubiquitin ligases.

Thus, our results indicate that L2 accumulates at PML-NBs mediated by the L2 SIM and may interact with SUMO or with with (poly-)SUMOylated PML-components under ongoing infection. As a speculation, L2 could further target these components for proteasomal degradation, as it was already suggested for Sp100 (Florin 2002b). L2 could thereby facilitate degradation of antiviral PML-components by recruitment of an ubiquitin E3 ligase complex to the polySUMOylated antiviral target proteins.

4.7 The challenge of L2 purification and refolding

With respect to the biophysical characterization of HPV16 L2, it can be summarized that the most crucial experimental step is represented by L2 refolding, which had tremendous effects on all follow-up experiments. Since L2 purification was only possible under denaturing conditions based on his affinity purification, so far, L2 refolding had to be performed. This was done by L2 transfer into non-denaturing buffers after L2 precipitation or by gradual buffer exchange by dialysis or in proteins concentrator columns. For all of the protocols, a strong trend of HPV16 L2 for formation of large

aggregates was observed. Additional hints for a strong tendency of L2 for aggregation came from earlier studies reporting the presence of high molecular weigh L2 aggregates after ultracentrifugation of HPV PsV preparations (Becker 2003; Florin 2004) and own observation of L2 aggregation leading to extreme stickiness and loss of L2 upon L2 exposition to purification matrixes, like e.g. size exclusion columns or centricons. It seems that L2 aggregation can be minimized by L2 refolding in the presence of SUMO1 or SUMO2, which was also used as experimental setup for EPR measurements. However, in ITC experiments, the L2 and SUMO1/2 solution had to be prepared separately, leading to strong L2 aggregation levels. Although it was possible to re-dissolve the L2 aggregates by adjustment of the buffer salt concentration, no interaction was detected in ITC experiments, indicating that L2 folding is not trivial and requires further analysis. Improvement for this situation could be based on promising efforts in L2 purification under non-denaturing conditions based on a SUMOstar-L2 fusion protein and L2 expression in HEK293 cells, which yielded significantly improved L2 solubility and purification levels >65%. Most interestingly, the fusion protein used in this purification was designed based on the tertiary structure of SUMO, which could explain the positive stabilizing and chaperoning effects observed. Perhaps, L2 purification following this protocol could allow for large levels interaction screening based on EPR, CD, FCS, and ITC measurements and replace denaturing L2 purification performed here.

4.8 L1/L2 ΔSIM PsVs are non infectious despite correct assembly of the L1/L2 capsid

In order to characterize a possible effect of SIM-based SUMO interaction on HPV infection, L1/L2 ΔSIM PsV were prepared and infectivity of the PsVs was characterized. Remarkably, the mutant L1/L2 ΔSIM PsV were not able to infect HeLa or HaCaT cells. Thus, the lack of the L2 SIM had tremendous effects on HPV16 physiology. Now it was checked which SIM-dependent factors could influence loss of infectivity of L1/L2 ΔSIM PsVs and at which point of HPV16 infection the phenotype of L1/L2 ΔSIM PsVs diverged from that of wild-type PsVs due to the lack of the L2 SIM. First, the assembly of L1/L2 ΔSIM PsVs from L1 and mutant L2, as well as DNA incorporation into the mutant PsVs, was analyzed. It was not clear whether L2 ΔSIM would be correctly assembled into L1/L2 capsomers and final L1/L2 capsids or whether the L2 ΔSIM mutation would affect reporter DNA packaging into the PsVs. In general, after standard preparation of PsVs for infection assays, it is possible that there is still a larger amount of non-assembled L1 or L2 in the PsV peak fractions, non-incorporated L2, or possibly also high molecular capsomeric aggregates, which would finally ead to a decreased amount of infectious PsVs in the preparation. To analyze this, sucrose gradient ultra centrifugation and immunodetection of L1/L2 proteins was performed based on the peak fraction of standard purified PsVs (Becker, Florin et al. 2004; Florin 2004). Clear L1 and L2 peaks were identified in the same UZ fractions for all PsV

and with comparable band intensity. Additionally, there was no L1 or L2 detection in any of the high or low density edge fractions, indicating that the majority of the L1 and L2 protein in the standard PsVs preparations was in fact assembled into L1/L2 capsids, also for L1/L2 ΔSIM PsVs. For virus-like particles (VLPs), which only contain L1, the L1 bands were distributed over a larger number of fractions indicating larger polydispersity of the capsids perhaps due to the lack of L2, which features a stabilizing effect on HPV capsid structure. After identification of the peak fractions of the PsVs by sucrose gradient purification, the peak fractions were pooled and subjected to infection assays to reproduce infection data obtained for standard PsV preparations. Again, comparable levels of infectivity were found for wild-type and L1/L2 ΔSCM PsVs (50-75% infectivity compared with wild-type PsVs), while L1/L2 ΔSIM PsVs and L1 VLPs were noninfectious. Also the amount of incorporated reporter DNA (luciferase expression plasmid) was quantified, on the one hand to check the general ability of the different PsV types for DNA incorporation during PsV preparation, on the other hand to exclude artifacts of different reporter DNA levels in infection assays which could bias infection results. All PsVs and also the VLPs contained comparable amounts of reporter DNA. Thus, we were not able to reproduce a decreased level of DNA incorporation in VLPs, which was reported to be based on the lack of L2 in L1 VLPs (Stauffer, Raj et al. 1998; Buck 2004). Furthermore, it can be concluded that the L2 ΔSIM mutation did neither affect incorporation of L2 into L1/L2 PsVs nor incorporation of reporter DNA.

The peak fractions were additionally characterized by transmission electron microscopy (TEM) to detect possible aberrations of the L1/L2 capsid structure due to the L2 ΔSIM mutation. There were no changes of structure and size of L1/L2 ΔSIM PsVs when compared with wild-type PsVs. Also L1 VLPs and L1/L2 ΔPHOS PsVs showed a wild-type capsid structure with diameters of about 52-55 nm. There were no visible structural abnormalities of L1/L2 capsids after assembly from L1 and the selected L2 mutants. Also incorporation of 5-ethynyl-2´-deoxyuridine (Edu) as marker molecule, allowing staining of viral DNA in PsVs after infection of PsV in fluorescence microscopy, did not result in detectable changes of the capsid structure in TEM.

4.9 The L2 SIM is not involved in the early steps of HPV16 infection

After confirmation of the correct capsid assembly of L1/L2 ΔSIM PsVs, the cell binding properties of the mutant PsVs were investigated in flow cytometry. No change of the amount of mutant L1/L2 ΔSIM PsVs attached to the surfaced of HaCaT or HeLa target cells was observed when compared to the amount of wild-type PsVs after cells were incubated with comparable amounts of the different PsVs. Thus, the L2 ΔSIM mutation, albeit its location in a L2 sequence region declared as solvent

accessible (Kawana 1998), does not seem to significantly influence cell binding of the mutant PsVs. These results were also confirmed by passive monitoring of the PsV binding to HaCaT target cells with Fremy's Salt (NDS) in CW EPR measurements (Fig. 4.2).

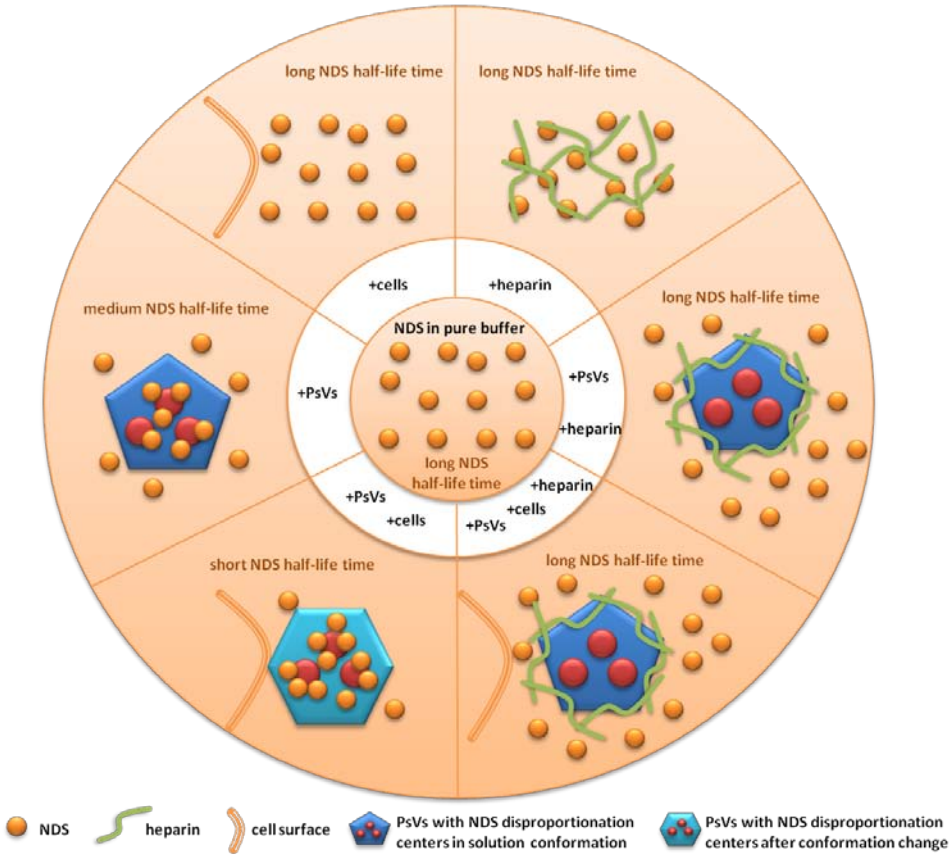

Fig. 4.2: NDS as a passive sensor for viral cell binding/capsid rearrangement of HPV16 in CW EPR measurements. While EPR-active NDS molecules share very long half-life times in standard buffers or after addition of cells or heparin, half-life times were significantly reduced after addition of PsVs, most obviously due to a dissociation of NDS molecules at the positively charged L1/L2 amino acid patches further referred to as NDS dissociation centers (NDCs). Incubation of the NDS/PsV mix with HaCaT cells leads to detection of very short NDS half-life times, most obviously based on even better accessibility of the NDCs due to a conformational change of the viral capsid upon binding to the surface of HaCaT cells. However, incubation of the NDS/PsV solution with heparin led to extended NDS half-life times, indicating that heparin prevents NDS molecules from localization at NDCs and most obviously does not lead to a conformation change of the capsid. Even after addition of HaCaT cells, no shortening of NDS half-life times was observed, confirming the ability of heparin to inhibit cell binding of PsVs.

While NDS half-life times and the corresponding EPR activity were maximal for NDS incubation in pure buffer solutions or solution containing heparin or HaCaT cells, shortened NDS half-life times were observed for incubation of the same amount of NDS with PsVs. This is most obviously due to a higher local concentration of NDS molecules at positively charged amino acid patches of L1 and L2 within the PsVs, which led to a disproportionation reaction of always two NDS molecules and loss of the EPR activity of the NDS molecules. Interestingly, incubation of the NDS/PsV solution with HaCaT cells resulted in even shorter NDS half-life times. Since incubation of NDS with the same amount of HaCaT cells did not result in comparable NDS decay levels, one reasonable explanation would be that

the strongly diminished NDS half-life times are caused by an increased accessibility of the centers facilitating NDS disproportionation (NDCs) within the PsVs allowed by structural rearrangement of the L1/L2 capsid upon cell binding. Thus, this experiment could allow for a systematic characterization of the early HPV infection steps, including L1 rearrangement upon L1-driven and L2 independent PsV binding to heparan sulfate proteoglycans (HSPGs) as the first receptor, followed by interaction with cyclophilin B inducing exposure of the L2 N-terminus, which is then cleaved by furin (Selinka 2003; Schelhaas 2008; Day 2008a; Day 2008b; Bienkowska-Haba 2009; Bienkowska-Haba, Williams et al. 2012).

At the current state of knowledge, it remains elusive to speculate which L1/L2 rearrangement step leads to the well accessible NDCs after cell attachment. However, with the use of cyclophilin or furin inhibitors, the effect of the respective PsV processing steps could be dissected systematically. In this context, remarkably, incubation of the PsV/NDS solution with the PsV cell binding inhibitor heparin (Joyce 1999; Giroglou, Florin et al. 2001; Schelhaas, Shah et al. 2012) results in significantly increased NDS half-life times, indicating that the positively charged L1/L2 patches are obviously not accessible for NDS molecules in the presence of heparin. One may speculate that the PsV attachment to heparin, which mimics the heparan sulfate molecules on the cell surface, was not sufficient to induce the L1/L2 conformation change, which leads to the fast decay of NDS molecules upon cell binding. In this context, our results are in line with recent reports, arguing that heparin binding of PsVs does not lead to obvious changes of the capsid structure of HPV16 *in vitro* (Dasgupta 2011). Based on this, one remaining plausible explanation is that the extremely prolonged NDS half-life times may be caused by an attachment of the PsVs to the polyanion heparin, which coats the PsVs within several seconds and renders the NDCs, which are positioned within the PsVs, inaccessible for the NDS molecules. As a consequence, the NDS molecules reside evenly distributed in the residual buffer volume with NDS decay levels comparable with those for NDS in pure buffer. Addition of HaCaT cells to PsVs preincubated with heparin did not lead to decreased NDS half-life times, which is a direct confirmation of the inhibitory effect of heparin on cell binding proposed before. It seems plausible that the heparin coating of the PsVs blocks both, penetration of NDS molecules into the PsVs and structural rearrangement of the L1/L2 capsid due to the lack of cell binding. Otherwise, L1/L2 rearrangement should at least result in a somewhat better accessibility of the NDCs to the NDS molecules and in slight reduction of NDS half-life times, which was not observed here.

In addition, there were no significant differences between NDS half-life times after incubation with wild-type L1/L2 PsVs, L1/L2 ΔSIM PsVs, or even L1 VLPs with HaCaT cells, indicating that cell binding happened in an equal manner for all virus types in the presence of target cells and did not depend on L2, as it was reported before (Selinka 2003; Day, Lowy et al. 2003b; Kämper, Day et al. 2006), or the

L2 SIM. Also the relative changes of half-life times after addition of heparin or HaCaT cells to the PsV/NDs solution revealed no significant differences between the different viruses. Thus, the first binding steps and subsequent conformational changes of the PsV seem to occur L2-independently.

The CW EPR approach with NDS as paramagnetic sensor molecule represents a very promising biophysical method for characterization of PsV binding and subsequent rearrangement of the HPV capsid. This method, for the first time, allows to directly measure effects of HPV inhibitors on L1/L2 conformation during early steps of infection.

Next, endocytosis of L1/L2 ΔSIM PsVs was characterized by flow cytometry. After 24 h of infection, no PsVs were detected on the surface of the target cells, indicating that, analogous to wild-type PsVs, also L1/L2 ΔSIM PsVs were taken up by endocytosis in a comparable time scale. Although it seems that the L2 ΔSIM mutation does not visibly seem to alter L1/L2 processing on the cell surface or the endocytosis step itself and all signs suggest that it develops its influence after disassembly of PsVs in the endosomes, it is still possible that the L2 SIM features undiscovered regulatory functions in the early steps of infection, which regulate later steps, like e.g. L2 furin cleavage on the cell surface was reported to allow endosomal escape of the L2-DNA complex in a much later step (Day 2009). In general, such rather small modifications could lead to slight but important conformational changes affecting transport from the primary to the secondary receptor and modulate the composition of the bio-active high-molecular compounds, which are attached to the incoming PsV after ECM binding as it is observed e.g. for cyclophilin B (Bienkowska-Haba 2009). These compounds influence whether PsVs are taken up via infectious or non infectious endocytosis pathways and trigger disassembly of PsVs in endosomes (Bienkowska-Haba 2009; Bienkowska-Haba, Williams et al. 2012; Surviladze, Dziduszko et al. 2012). Unfortunately, experimental setups of the cell binding and endocytosis experiments presented here were not able to discriminate between infectious or noninfectious binding/endocytosis of PsVs, so we were only able to verify that also L1/L2 ΔSIM PsVs were taken up into the cell by any kind of endocytosis.

4.10 No PML-colocalization of L2 or viral DNA after infection with L1/L2 ΔSIM PsVs

As there were no detectable differences in PsV structure, cell binding, and endocytosis of L1/L2 ΔSIM PsVs when compared with wild-type viruses, next, the cellular localization of L2 and viral DNA was characterized by immunofluorescence microscopy after PsV infection. Colocalization analysis revealed a high level of PML-associated L2 and viral DNA after infection with wild-type PsVs like it was also reported before (Schneider 2011). In contrast, almost no L2 or DNA colocalization with PML

was observed after infection with L1/L2 ΔSIM PsVs. 24 h post infection with L1/L2 ΔSIM PsVs, almost no L2 or viral DNA was located within the cell nuclei. The majority of L2 and viral DNA was located in larger aggregates outside of the nucleus. Exact determination of the cellular localization of the L2 ΔSIM aggregates requires additional experiments and was not further characterized at this point. Interestingly, SIM-dependent loss of nuclear translocation of viral proteins was already reported for the E3 protein of vaccinia viruses, which also features PML-disruptive functions comparable with the HPV L2 protein (Gonzalez-Santamaria, Campagna et al. 2011). Here, additionally, the stability of the E3 ΔSIM mutants, as well as E3 SUMOylation, was drastically decreased by lack of the SIM. As for HPV16 L2, no significant destabilization of L2 ΔSIM was observed, which could possibly be due to L2 localization in relatively isolated and large aggregates. However, for overexpressed L2 ΔSIM, which was able to locate within the nucleus, but with significantly decreased intensity when compared with wild-type L2, no L2 SUMOylation was observed. The reason could be that L2 SUMOylation only takes place in the nucleus, which was only reachable for a reduced fraction of L2 ΔSIM after overexpression and for almost no L2 ΔSIM after PsV infection with L1/L2 ΔSIM PsVs. However, L2 ΔSIM still comprises three potential nuclear localization sites, one at the N-terminus (nNLS), one at the C-terminus (cNLS), and an additional one in the central L2 region near the L2 SIM (mNLS) (Becker, Florin et al. 2004; Darshan, Lucchi et al. 2004; Mamoor, Onder et al. 2012). In fact, the mNLS seems to be relevant for nuclear localization of L2 and should allow nuclear transport of L2 ΔSIM. Most interestingly, the mNLS was also characterized as nuclear retention signal (Mamoor, Onder et al. 2012). Thus, it is possible that, although there is indeed nuclear localization of L2 ΔSIM, the lack of L2 interaction with SUMO based on the SIM near the mNLS nuclear retention signal could lead to the loss of nuclear localization of the majority of L2 ΔSIM molecules and result in nuclear export based on a leucine-rich export signal (aa 462-473)(Mamoor, Onder et al. 2012). Thus, the L2 SIM might be important for L2 interaction with SUMOylated proteins in PML-NBs, which prevents L2 from nuclear export.

4.11 The L2 SIM at position 284-289 is not regulated by CK2 phosphorylation

Interestingly, L1/L2 ΔPHOS PsVs lacking a potential CK2 phosphorylation site near the L2 SIM at position 295/6 (TS) showed no aberrations in infectivity when compared with wild-type PsVs, including also cell binding and endocytosis. These results confirmed the wild-type phenotype of overexpressed L2 ΔPHOS also observed in immunofluorescence or immunoprecipitation, where the L2 ΔPHOS mutation did not influence L2 localization or L2 interaction with GFP-SUMO2. Thus, there is either no phosphorylation at this highly conserved L2 sequence motif or potential phosphorylation does not lead to increased SIM-based SUMO interaction, as it was shown for a number of SUMO

interaction partners in different studies. For example, phosphorylation of the SIMs of DAXX or PIAS1 by casein kinase 2 (CK2) enhanced binding to SUMO targets (Naik ; Shih 2007; Stehmeier 2009). However, to the best of our knowledge, there are no examples of phosphorylation regulated SIMs in viral proteins reported so far.

4.12 SUMO siRNA knockdown affects HPV16 infectivity

Infectivity of PsVs was also characterized by siRNA-mediated knockdown of SUMO1/2 proteins. Interestingly, knockdown of intrinsic SUMO1 or SUMO2 had diverse effects on infectivity of PsVs. While knockdown of SUMO1 resulted in a decreased infectivity for L1/L2 wild-type and L1/L2 ΔSCM PsVs, knockdown of SUMO2 drastically increased infection levels for the same PsVs. One plausible explanation would be that SUMO2 directly affects antiviral functions by modification and interaction with cellular antiviral regulation factors such as DAXX, PML, or Sp100. Under normal conditions, (poly)SUMOylation and SUMO interaction of PML-components leads to a complex SUMO network interconnecting the PML-component to form functional and antiviral PML-NBs (Boutell 2011). Especially SUMO2 and SUMO3 are involved in cellular regulation mechanisms including polySUMO chains after cell stress (Wadosky 2011) and might regulate proteasomal degradation of (poly)SUMOylated target proteins and also viral proteins in the context of PML-NBs. It is plausible that SUMO knockdown and the lack of the SUMO network leads to non-functional PML-NBs, a situation which could significantly increase half-life times of viral proteins. However, the contribution of SUMO1 to infectivity of HPV PsVs remains elusive. Perhaps SUMO1 siRNA knockdown induces DAXX to reside in its state of transcription repression by preventing DAXX SUMOylation by SUMO1, which could otherwise enable PML-NB localization of DAXX and attenuation of its repressing function (Jang, Ryu et al. 2002; Lin, Huang et al. 2006; Hwang and Kalejta 2009). One might also speculate that the effect of SUMO1 knockdown could also be the result of transcription regulation by SUMO1 siRNA transfection, as a slight decrease of luciferase expression was detected in control experiments after siRNA transfection and overexpression of luciferase.

Even more remarkably, siRNA-mediated knock down of SUMO1 or SUMO2 led to a partial reactivation of infectivity of L1/L2 ΔSIM viruses, but also L1 VLPs. Reasons for this could be that L2 and finally the viral DNA, which also reaches the cell nucleus in background levels (Selinka 2007), regains its infectivity by knockdown of cellular SUMO1/2 and de-functionalization of PML-NBs, which would otherwise completely inhibit infectivity by recruitment of antiviral PML-components like DAXX and Sp100. Without the complex of L2 with viral DNA, the DNA seems to be entirely blocked for transcription explaining noninfectivity of L1/L2 ΔSIM PsVs and L1 VLPs under normal levels of

endogenous SUMO1/2. These assumptions were additionally strengthened by the observation that DAXX knockdown also allowed medium level infectivity of L1/L2 ΔSIM PsVs and L1 VLPs, and underlines the antiviral function of DAXX during HPV infection (data not shown).

Overexpression of GFP-SUMO1/2 led to a GFP-SUMO1/2 dose-dependent increase of infectivity of L1/L2 wild-type and L1/L2 ΔSCM PsVs. As SUMO proteins normally establish functional and antiviral PML-NBs by interaction with a manifold of the more than 70 PML-NB associated cell factors by (poly-) SUMOylation or SUMO interaction, a positive effect of increased levels of cellular and functional SUMO proteins on viral infectivity appears to be rather doubtful. Also, stabilization of SUMO targets by SUMOylation induced by higher cellular SUMO levels would also affect cellular proteins and would not per se favor viral proteins. In contrast, it seems clearly more credible that the overexpressed GFP-SUMO proteins are not able to establish the characteristic network of antiviral proteins needed for antiviral defense. Most obviously, the GFP-SUMO proteins feature a dominant-negative character, allowing interaction of SUMO with some of their interaction partners, but without formation of the intact antiviral defense barrier by dose-dependent suppression of the residual and fully-functional cellular SUMO proteins. Thus, overexpression of GFP-SUMO seems to support the reported effect of L2 to increase SUMOylation of cellular proteins (Marusic 2010), perhaps allowing for a better recognition of the polySUMOylated L2 targets by L2, but could additionally lead to formation of non-functional PML-NBs.

Remarkably, overexpression of wild-type L2 was not able to recover infectivity of L1/L2 ΔSIM PsVs. One reason could be that the complex of L2 ΔSIM and DNA after L1/L2 ΔSIM PSV infection could not even enter the nucleus, where the majority of overexpressed, wild-type L2 is located and therefore cannot interfere in infection. There is some experimental evidence that overexpression of a modified form of L2 (L2 Δ1-12) lacking the N-terminal part, which is normally removed by furin cleavage upon cell binding of PsVs, increases infectivity of wild-type PsVs, but not of L1/L2 ΔSIM PsVs. Interestingly, wild-type L2 overexpression did not enhance infectivity of wild-type L1/L2 PsVs. One could speculate that only the truncated L2 form represents active L2 and is able to influence/enhance infectivity.

4.13 Tentative model for regulation of the intrinsic antiviral resistance by HPV16 L2

Based on the reported data, the following mechanistical hypothesis of HPV infection may be drawn (Fig. 4.3). All characterized HPV16 PsVs and VLPs are able to bind to the host cells and are endocytosed regardless of any L2 mutations influencing L2 SUMOylation or SIM-based SUMO interaction. However, after endocytosis and viral disassembly in the endosomes, which was not characterized here, the complex of L2 and viral DNA was only able to reach PML-NBs after infection

with L1/L2 wild-type and L1/L2 ΔSCM PsVs and not for infection with L1/L2 ΔSIM PsVs and L1 VLPs (Fig. 4.3 A). This means that the L2 SIM is absolutely indispensable for the correct nuclear transport of the L2/DNA complex from endosomes to PML-NBs. As for infection with L1/L2 wild-type and L1/L2 ΔSCM PsVs, the next important challenge to gain HPV infectivity is the establishment of the viral replication centers in the close vicinity of the PML-NBs or recruitment of the PML-components to the L2-DNA complexes (Fig. 4.3, B). On the one hand, the presence of the PML-NBs seems to be crucial for HPV replication (Day 2004), on the other hand, for other DNA viruses, PML-NBs and especially their constituent DAXX induce repression of viral transcription most obviously by surrounding the incoming viral DNA with a network of cellular factors and associated chromatin remodeling factors, leading to a quiescence of the viral DNA (Boutell 2011). The direct colocalization of viral DNA with L2 seems to block transcriptional repression of cellular factors like DAXX, while it activates viral transcription based on additional factors (shown in blue in Fig. 4.3). It is already known that overexpressed L2 induces Sp100 release from PML-NBs and degradation, while DAXX is recruited to the PML-NBs (Florin 2002b), which could lead to a net attenuation of the inhibitory functions of DAXX (Li, Leo et al. 2000), which, remarkably, was also observed after overexpression of HPV16 L2 in HCMV infection (Schreiner 2012) . The SUMOylation of L2 thereby enhances L2 half-life time and could improve L2 linkage with the network of highly (poly-)SUMOylated cellular proteins, facilitating viral gene expression (Fig. 4.3 C). L2 ΔSCM is degraded much faster than wild-type L2 after PsV infection and results in reduced HPV infectivity due to L2 degradation and quiescence of the residual viral DNA based on interaction with the PML NBs (Fig. 4.3, D). Thereby, SUMOylation and SUMO interaction of the PML-NB associated proteins seem to play important roles for formation of functional anti-viral PML-NBs. Especially loss of SUMO2 by siRNA knockdown results in significantly increased HPV infectivity, possibly due to the loss of function of the PML-NBs (Fig. 4.3, E). This is interesting, as especially SUMO2/3 is supposed to participate in polySUMOylation of several cellular substrates during cell stress as it is also provoked by income of foreign DNA. Also DAXX knockdown leads to increased HPV infectivity, indicating a direct antiviral function of DAXX.

Remarkably, the knockdown of SUMO2 also seems to restore some infectivity to L1/L2 ΔSIM and L1 VLPs. A reason for that could be that viral DNAs, which enter the nucleus also after noninfectious endocytosis at background levels, but are normally targeted and deactivated by intact PML-NBs, regain infectivity by loss of function of the antiviral PML-NBs without the presence of SUMO2. Overexpression of GFP-SUMO1/2 could possibly have a comparable effect on HPV infection as SUMO2 knockdown, since the combination of SUMO1/2 with GFP could interfere with the formation of a SUMO network between cellular proteins and render most of the PML-NBs nonfunctional.

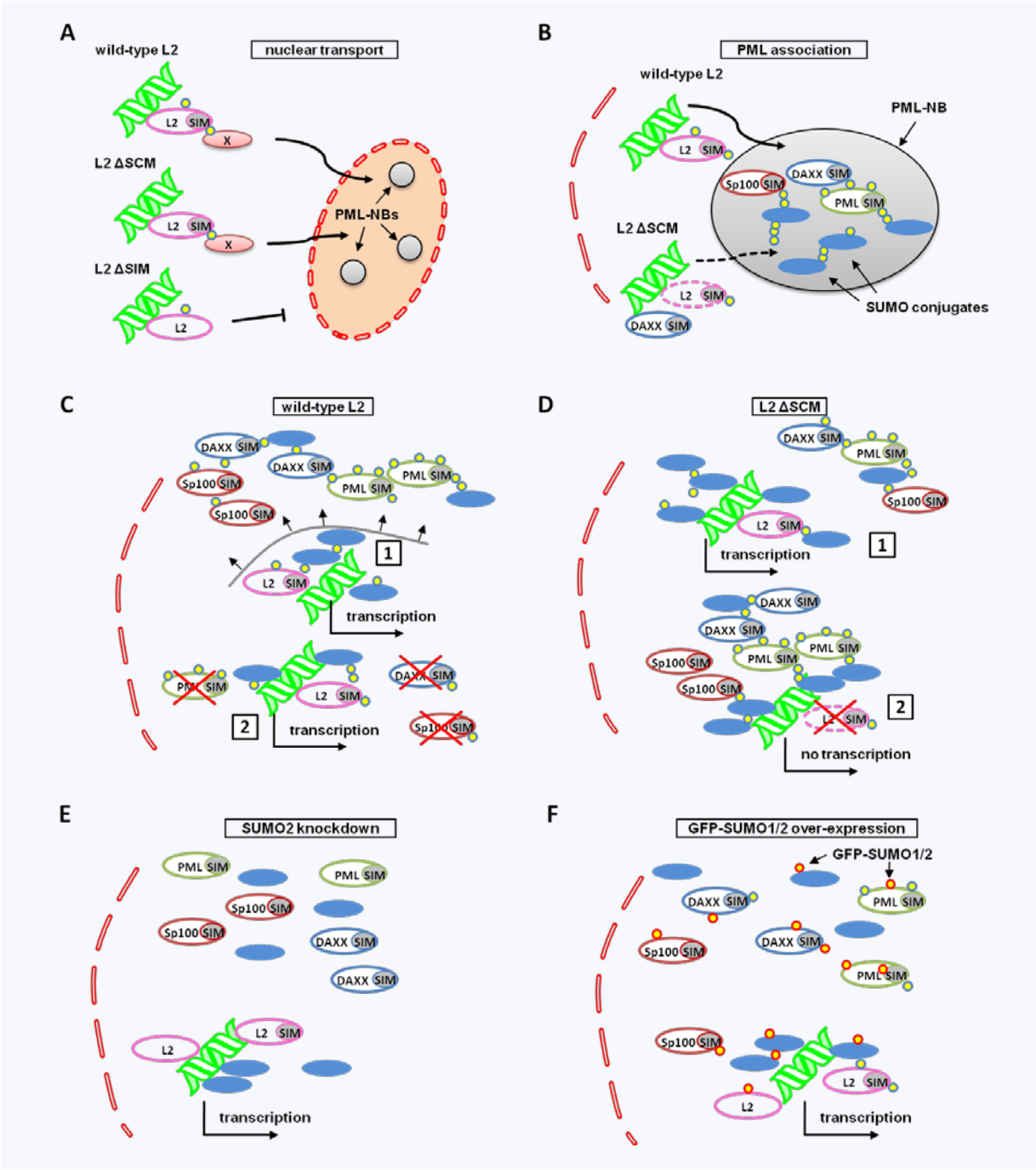

Fig. 4.3: Model depicting regulation of the intrinsic antiviral defense to HPV16 infection. ***A*** Only L2 containing the SIM is able to direct the L2-DNA complex into the cell nucleus, most obviously by interaction with a yet unknown factor. ***B*** While wild-type L2 is able to position most L2-DNA complexes in close vicinity to PML-NBs, a smaller amount of viral DNA reaches the PML-NBs in the presence of SUMOylation-deficient L2 ΔSCM. This could be caused by destabilization of L2 ΔSCM due to the lack of SUMOylation. The PML-NBs thereby represent the hot spot of the intrinsic antiviral defense by bundling active forms of the antiviral, SIM-containing and highly SUMOylated PML, DAXX, and Sp100, but at the same time allow for viral replication in the presence of L2. ***C*** Wild-type L2 mediates viral replication by deregulation of the antiviral activity of PML, DAXX, and Sp100 and enables viral transcription. In a first mechanism, L2 could shield the viral DNA from the PML-NB components to prevent quiescence of the DNA (1). It is also plausible that L2 targets some of the (poly)SUMOylated PML-NB components for degradation (2). ***D*** In the presence of L2 ΔSCM, the antiviral factors are shielded from the viral DNA enabling transcription (1) but a part of the L2 ΔSCM is rapidly degraded resulting in the quiescene of a large fraction of viral DNA upon interaction PML-NB components (2). SUMO2 siRNA knockdown ***E*** or GFP-SUMO1/2 overexpression ***F*** results in the formation of non-functional PML-NBs lacking the SUMO interaction network and lacking antiviral activity, allowing transcription of viral DNA which entered the nucleus even after noninfectious endocytosis of L1 VLPs or L1/L2 ΔSIM PsVs.

The mechanism by which L2 modulates activity of the PML-NBs and/or induces even their disruption, as it is sometimes observed for HPV, still remains elusive. As our results show only a subordinate role of L2 SUMOylation on HPV16 infection, the focus clearly is on SIM-based interaction of L2. It is plausible that L2 could fulfill important functions in proteasomal degradation of cellular target proteins as suggested by the observed loss of Sp100 after L2 overexpression (Florin 2002b). As there were direct hints that L2 could be able to interact with more than one SUMO2 molecules at the same time in *in vitro* assays, in a speculation, also interaction with polySUMO2/3 chains would be possible. This could be a link to a possible SUMOylation targeted ubiquitin ligase function of L2 targeting polySUMOylated proteins for degradation. Especially interaction with poly-SUMO2/3 chains is one of the hallmarks of RING-finger containing SUMO-targeted ubiquitin ligases (StUbLs), which target poly-SUMOylated cellular proteins for proteasomal degradation by polyubiquitination, as it was also suggested for the L2 analogue structure protein ICP0 of HSV-1 (Boutell 2011). Since HPV16 L2 does not seem to represent an StUbL itself, as it does not contain a RING or HECT domain itself, but in general is to be able to interact with multiple SUMOylated PML-components, L2 could possibly target known E3 ubiquitin ligases with known SUMOylated L2 interaction partners, inducing transfer of (poly-)ubiquitin from E2 ubiquitin ligases to the SUMOylated target molecules to enable proteasomal degradation. There are two major E3 ubiquitin ligase families: HECT (homology to E6-assiciated protein carboxyl terminus) and RING (Really Interesting New Gene) E3 ubiquitin ligases. Cullin-RING ubiquitin ligases (CRLs) represent the largest class containing cullin, a RING finger protein, and a substrate recognition unit. It was already shown that HPV viruses utilize the system of ubiquitin ligases for proteasomal degradation of cellular target proteins and thus, also L2 interaction with ubiquitin E3 ligases may be possible. For example, the HPV16 E6 protein interacts with a group of cellular E6-AP E3 ubiquitin ligase, inducing binding and ubiquitin-mediated proteolysis of the tumor suppressor protein p53 (Huibregtse, Scheffner et al. 1995; Tomaic, Pim et al. 2011). In another example, the HPV E7 protein binds to pRb and recruits the cullin 2 ubiquitin ligase for ubiquitination and subsequent proteosomal degradation of pRb (Barrow-Laing, Chen et al. 2010).

Based on the E3 ubiquitin ligase function of ICP0 and the interaction of a large group of viral proteins with components involved in proteasomal degradation (Tavalai and Stamminger 2009; Wimmer 2012), we checked whether L2 would be able to interact with ubiquitin. Interestingly, we were able to observe a SIM-dependent L2 interaction with ubiquitin in ubiquitin pulldown experiments. However, since L2 does not contain characteristic RING or HECT domains important for interaction with ubiquitin E2 ligases for transfer of (poly)ubiquitin, it is most likely that L2 only represents a recognition element for identification of potential targets and is probably part of a larger E3 ligase complex including L2 interaction with further elements featuring E3 ligase function. Interestingly, in yeast 2-hybrid screening, obscurin-like 1 (OBSL1) was identified as an L2 interaction partner

(Schneider 2011). OBSL1 functions as cytoskeletal linker, contains at least seven bona fide SIMs, and regulates the activity of the cullin7 E3 ubiquitin ligase (Geisler, Robinson et al. 2007; Hanson, Murray et al. 2009). One may speculate that the L2 interaction with OBSL1 could represent one possibility of L2 to mediate activity of cellular E3 ubiquitin ligases. As also the E3 SUMO ligase RanBP9 (Ran binding protein 9) is a ligand of the Rho-GEF domain of obscurin (Bowman, Catino et al. 2008). Therefore, the characterization of the interplay of L2, OBSL1, and potential ubiquitin or SUMO ligases could reveal important hints for functionality of HPV infection, since obscurins and cullins seem to play important roles in several cancer tissues also triggering apoptosis (Haagenson, Tait et al. 2012; Perry, Shriver et al. 2012). Finally, HPV16 L2 may join the group of viral proteins, in which SUMO interaction and SUMOylation may influence viral infectivity by disruption/modification of PML-NBs, as it was already observed for many viral proteins including ICP0 of the Herpes Simplex Virus 1, ORF61p of the Vaccinia Zoster Virus, IE1/2 and pp71 of the Human Cytomegalovirus, BZLF-1, EBNA-LP, and EBNA1 from Epstein-Barr Virus, LAN2 of the Kaposi's Sarcoma-associated Herpesvirus, E3L of the Vaccinia Virus, and ORF75c of the Mouse Hepatitis *Virus* 68 (Tavalai and Stamminger 2009; Wimmer 2012), from which direct effects of viral SIMs on infection were identified for ICP0 (Boutell 2011), ORF61 (Wang, Oliver et al. 2011), IE2 (Kim 2010), and E3L (Gonzalez-Santamaria, Campagna et al. 2011) partially also containing SIM-based interaction with components involved in ubiquitination.

5. Conclusions

Here, we report for the first time that the minor capsid protein L2 of the human papillomavirus (HPV) type 16, is able to interact with SUMO, not only by SUMOylation, as it was reported before, but also by noncovalent SIM-based SUMO interaction. The direct L2 interaction with SUMO proteins, which represent one of the most important key players in modulating activity of anti-viral proteins bundled in PML-NBs, is closely correlated with the presence of at least one bona fide and highly conserved SIM at L2 sequence position 286-289. HPV16 pseudoviruses (PsVs) lacking the SIM are noninfectious. Cell binding and endocytosis were not visibly interfered by the lack of the SIM. These results were also confirmed by a novel CW EPR attempt, which passively measures the cell binding ability of PsVs and, in addition, features selectivity for structural rearrangement of the L1/L2 capsid after successful attachment to the target cells. Additionally, the inhibitory effect of heparin on cell binding and structural L1/L2 rearrangement was confirmed, which also elucidated the potential of this method to study early steps of HPV infection occurring on the cell surface, such as e.g. inhibition of interaction with cyclophilin, furin, the annexin A2 heteroteteramer, or MMP/ADAM proteases with the respective inhibitors. The L2 SIM seems to be closely entangled with the fate of the L2-DNA complex, which is transported to the PML-NBs in the nucleus for wild-type viruses but cannot be detected in the nucleus or at PML-NBs after infection with L1/L2 ΔSIM PsVs. However, it is possible that the L2 SIM mediates L2 interaction with SUMO-modified proteins and could thereby participate in regulatory functions modulating the activity of transcription factors and the antiviral defense at the PML-NBs. The L2 SIM could also posses some influence on HPV morphogenesis, since overexpressed

L2 ΔSIM, which was localized within the nucleus, was not able to colocalize with PML-NBs indicating multiple functions of the L2 SIM. However, preparation of correctly assembled PsVs was also possible based on mutant L2 lacking the SIM, which could indicate that PML-localization of L2 is not needed for HPV morphogenesis. Speculations about the viral mechanism which counteracts antiviral defense are beyond the scope of this work. Nevertheless, we were able to collect several hints providing the following tentative picture which is in line with the general trends observed during infection of other viruses: *i)* The L2 SIM could be be crucial for nuclear transport of the L2-DNA complex and also for its association with PML-NBs facilitating viral transcription and replication. *ii)* L2 possibly facilitates interaction with SUMO and most obviously (poly-)SUMOylated cellular proteins, including the transcription co-repressor DAXX and Sp100, which could lead to modulation of their antiviral activity: e.g. attenuation of the repressive function of DAXX upon L2-induced PML-localization of DAXX, which otherwise induces quiescence of incoming viral DNA in remote nuclear regions or degradation of Sp100. *iii)* an possible E3 ubiquitin ligase function of L2 could lead to modulation and/or degradation of antiviral cellular proteins, which could be based on the L2 ability to identify (poly)SUMOylated cellular factors with its multiple SIMs and concomitant interaction with E3 ubiquitin-ligase complexes, like e.g. cullin inducing proteasomal degradation, as it was already observed for p53 and pRb degradation by HPV16 E6 and E7. It is possible that L2 plays a major role in escape from or in enduring intrinsic antiviral defense for HPVs, facilitating productive infection.

Acknowledgements

I would like to express my deepest gratitude to the friends and colleagues who enabled me to do this Dissertation and especially to my family. First and foremost, I would like to thank PD Dr. Dariush Hinderberger for his everlasting and enthusiastic interest and support of my work, for his patience and numerous ideas and suggestions, which completed this work, and Dr. Gilles Spoden, my daily mentor and guidance, sharing all his skills, know-how, and energy to overcome nearly all problems one can face with in science.

I am especially grateful to Dr. Luise Florin for giving me the possibility to work in her lab and for continuous assistance in all possible questions, and to Dr. Carsten Lambert enabling me to work in the exciting field of HPV research.

I am also especially grateful to Prof. Wolfgang Spiess, who gave me all thinkable support during the start of the dissertation.

I would also like to thank Prof. apl. Nadja Hellmann and Prof. Harald Paulsen for fruitful discussions and experimental support whenever needed.

I am also much indebted to Dr. Kaloian Koynov and Philipp Arnold for their excellent experimental support in FCS and TEM.

Of course, I am especially obliged to my coworkers and friends, who made this dissertation come true. I thank Dennis Kurzbach for instantaneous experimental support during all day (and night) times, Marc Schneider and Konstanze Scheffer for their permanent help and Fatima Boukhallouk and Christian Bauer for technical support and regenerating discussions.

Special thanks also go to Kristina Hüttinger for her help and motivation in all situations and scientific cooperation.

I would also like to thank Jens Stieler featuring Chuck Norris-like skills in solving all imaginable (and non-imaginable) problems during every-day lab life and Carolin Velte, Mareli Allmeroth, Sabine Füser, and Carsten Dietz for their help and support.

I would especially like to thank you, Louisa, for giving me energy and motivation whenever needed. Without you, this thesis would not exist in this form.

References

Achilonu, I. and J. P. Goldring (2010). "Direct red 81 and amido black stain proteins in polyacrylamide electrophoresis gels within 10 min." Anal Biochem **400**(1): 139-141.

Adamson, A. L., Kenney, S. (2001). "Epstein-Barr virus immediate-early protein BZLF1 is SUMO-1 modified and disrupts promyelocytic leukemia bodies." J Virol **75**: 2388 –2399.

Akogbe, G. O., A. Ajidahun, et al. (2012). "Race and prevalence of human papillomavirus infection among men residing in Brazil, Mexico and the United States." International Journal of Cancer **131**(3): E282-E291.

André, M., Le Caer, J.-P., Greco, C., Planchon, S., Nemer, E.l.W., Boucheix, C., Rubinstein, E., Chamot-Rooke, J., Le Naour, F. (2006). "Proteomic analysis of the tetraspanin web using LC-ESI-MS/MS and MALDI-FTICR-MS." Proteomics **6**: 1437-1449.

Antinore, M. J., M. J. Birrer, et al. (1996). "The human papillomavirus type 16 E7 gene product interacts with and trans-activates the AP1 family of transcription factors." EMBO J **15**(8): 1950-1960.

Arroyo, M., S. Bagchi, et al. (1993). "Association of the human papillomavirus type 16 E7 protein with the S-phase-specific E2F-cyclin A complex." Mol Cell Biol **13**(10): 6537-6546.

Atherton, N. M. (1993). Principles of Electron Spin Resonance, Ellis Horwood.

Auvinen, E., Crusius, K., Steuer, B. and Alonso, A. (1997). "Human papillomavirus type 16 E5 protein (review)." Int J Oncol **11**: 1297-1304.

Baker, C. C., W. C. Phelps, et al. (1987). "Structural and transcriptional analysis of human papillomavirus type 16 sequences in cervical carcinoma cell lines." J Virol **61**(4): 962-971.

Baker, T. S., W. W. Newcomb, et al. (1991). "Structures of bovine and human papillomaviruses. Analysis by cryoelectron microscopy and three-dimensional image reconstruction." Biophys J **60**(6): 1445-1456.

Barrow-Laing, L., W. Chen, et al. (2010). "Low- and High-Risk Human Papillomavirus E7 Proteins Regulate p130 Differently." Virology **400**(2): 233-239.

Bayer, P. e. a. (1998). "Structure determination of the small ubiquitin-related modifier SUMO-1." J. Mol. Biol. **280**: 275–286.

Becker, K. A., L. Florin, et al. (2004). "Nuclear localization but not PML protein is required for incorporation of the papillomavirus minor capsid protein L2 into virus-like particles." Journal of Virology **78**(3): 1121-1128.

Becker, K. A., Florin, L., Sapp, C., Sapp, M. (2003). "Dissection of human papillomavirus type 33 L2 domains involved in nuclear domains (ND) 10 homing and reorganization." Virology **314**: 161–167.

Beier, C. and H. J. Steinhoff (2006). "A structure-based simulation approach for electron paramagnetic resonance spectra using molecular and stochastic dynamics simulations." Biophys J **91**(7): 2647-2664.

Belnap, D. M., Olson, N. H., Cladel, N. M., Newcomb, W. W., Brown, J. C., Kreider, J. W., and N. D. Christensen, and Baker, T. S. (1996). "Conserved features in papillomavirus and polyomavirus capsids." J Mol Biol **259**(2): 249-263.

Berliner, L. J., Grunwald,J., Hankovszky,H.O., and Hideg,K. (1982). "A novel reversible thiol-specific spin label: Papain active site labeling and inhibition." Analytical Biochemistry, **119**(450-455).

Bernard, H.-U., Burk, R.D., Chen, Z., van Doorslaer, K., Hausen, H., and de Villiers, E.M. (2010). "Classification of papillomaviruses (PVs) based on 189 PV types and proposal of taxonomic amendments." Virology **401**: 70-79.

Bernardi, R. P., P. P. (2007). "Structure, dynamics and functions of promyelocytic leukaemia nuclear bodies." Nature Rev. Mol. Cell Biol **8**: 1006–1016.

Bernier-Villamor, V., Sampson, D. A., Matunis, M. J. & Lima, C. D. (2002). "Structural basis for E2-mediated SUMO conjugation revealed by a complex between ubiquitinconjugating enzyme Ubc9 and RanGAP1." Cell **108**: 345–356.

Bienkowska-Haba, M., Patel, H.D., Sapp, M. (2009). "Target cell cyclophilins facilitate human papillomavirus type 16 infection." PLoS Pathog **5**: e1000524.

Bienkowska-Haba, M., C. Williams, et al. (2012). "Cyclophilins Facilitate Dissociation of the HPV16 Capsid Protein L1 from the L2/DNA Complex Following Virus Entry." J Virol.

Bird, G., O'Donnell, M., Moroianu, J. and Garcea, R.L. (2008). "Possible role for cellular karyopherins in regulating polyomavirus and papillomavirus capsid assembly." J Virol **82**: 9848-9857.

Blom, N., Gammeltoft, S., and Brunak, S. (1999). "Sequence- and structure-based prediction of eukaryotic protein phosphorylation sites." Journal of Molecular Biology **254**(5): 1351-1362.

Boddy, M. N., Howe, K., Etkin, L. D., Solomon, E. &Freemont, P. S. (1996). "PIC1, a novel ubiquitin-like protein which interacts with the PML component of a multiprotein complex that is disrupted in acute promyelocytic leukaemia." Oncogene **13**: 971-982.

Boshart, M., L. Gissmann, et al. (1984). "A new type of papillomavirus DNA, its presence in genital cancer biopsies and in cell lines derived from cervical cancer." EMBO J **3**(5): 1151-1157.

Bossis, I., Roden, R.B.S., Gambhira, R., Yang, R., Tagaya, M., Howley, P.M., Meneses, P.I. (2005). "Interaction of tSNARE syntaxin 18 with the papillomavirus minor capsid protein mediates infection." J Virology **79**: 6723-6731.

Bottomley, M. J., M. W. Collard, et al. (2001). "The SAND domain structure defines a novel DNA-binding fold in transcriptional regulation." Nat Struct Biol **8**(7): 626-633.

Boukamp, P., R. T. Petrussevska, et al. (1988). "Normal keratinization in a spontaneously immortalized aneuploid human keratinocyte cell line." J Cell Biol **106**(3): 761-771.

Bousarghin, L., Touze, A., Combita-Rojas, A., Coursaget, P. (2003). "Positively charged sequence of human papillomavirus type 16 capsid proteins are sufficient to mediate gene transfer into target cells via the heparan sulphate receptor." J Gen Virol **84**: 157-164.

Boutell, C., Cuchet-Lourenco, D., Vanni, E., Orr, A., Glass, M., McFarlane, S., and Everett, R. D. (2011). "A Viral Ubiquitin Ligase Has Substrate Preferential SUMO Targeted Ubiquitin Ligase Activity that Counteracts Intrinsic Antiviral Defence." PLoS pathogens **7**: e1002245.

Bouvard, V., Matlashewski, G., Gu, Z.M., Storey, A. and Banks, L. (1994). "The human papillomavirus type 16 E5 gene cooperates with the E7 gene to stimulate proliferation of primary cells and increases viral gene expression." Virology **203**: 73-80.

Bowman, A. L., D. H. Catino, et al. (2008). "The Rho-Guanine Nucleotide Exchange Factor Domain of Obscurin Regulates Assembly of Titin at the Z-Disk through Interactions with Ran Binding Protein 9." Mol Biol Cell **19**(9): 3782-3792.

Brehm, A., Nielsen, S. J., Miska, E. A., McCance, D. J., Reid, J. L., Bannister, A. J., and Kouzarides, T. (1999). "The E7 oncoprotein associates with Mi2 and histone deacetylase activity to promote cell growth." Embo J **18**(9): 2449-2458.

Broutian, T. R., Brendle, S.A., Christensen, N.D. (2010). "Differential binding patterns to host cells associated with particles of several human alphapapillomavirus types." J Gen Virol **91**: 531–540.

Buck, C. B., N. Cheng, et al. (2008). "Arrangement of L2 within the Papillomavirus Capsid▽." J Virol **82**(11): 5190-5197.

Buck, C. B., Day, P.M., Thompson, C.D., Lubkowski, J., Lu, W., Lowy, D.R., Schiller, J.T. (2006). "Human alpha-defensins block papillomavirus infection." Proc Natl Acad Sci USA **103**: 1516-1521.

Buck, C. B., Pastrana, D.V., Lowy, D.R. and Schiller, J.T. (2004). "Efficient intracellular assembly of papillomaviral vectors." J Virol **78**: 751-757.

Buck, C. B., Thompson, C. D., Pang, Y. Y., Lowy, D. R., and Schiller, J. T. (2005). "Maturation of papillomavirus capsids." J Virol **79**(5): 2839-2846.

Bund, T., J. M. Boggs, et al. (2010). "Copper uptake induces self-assembly of 18.5 kDa myelin basic protein (MBP)." Biophys J **99**(9): 3020-3028.

Buschmann, T., Fuchs, S. Y., Lee, C. G., Pan, Z. Q. & Ronai, Z. (2000). "SUMO-1 modification of Mdm2 prevents its selfubiquitination and increases Mdm2 ability to ubiquitinate p53." Cell **101**: 753–762.

Calle, C. e. a. (2006). "Pulse EPR Methods for Studying Chemical and Biological Samples Containing Transition Metals." Helv. Chim. Acta **89**: 2495-2521.

Calleja-Macias, I. E., M. Kalantari, et al. (2005). "Papillomavirus Subtypes Are Natural and Old Taxa: Phylogeny of Human Papillomavirus Types 44 and 55 and 68a and -b." J Virol **79**(10): 6565-6569.

Campos, S. K., J. A. Chapman, et al. (2012). "Opposing effects of bacitracin on human papillomavirus type 16 infection: enhancement of binding and entry and inhibition of endosomal penetration." J Virol **86**(8): 4169-4181.

Campos, S. K. and M. A. Ozbun (2009). "Two Highly Conserved Cysteine Residues in HPV16 L2 Form an Intramolecular Disulfide Bond and Are Critical for Infectivity in Human Keratinocytes." PLoS ONE **4**(2).

Capili, A. D. L., C. D. (2007). "Taking it step by step: mechanistic insights from structural studies of ubiquitin/ubiquitin-like protein modification pathways." Curr. Opin. Struct. Biol **17**: 726–735.

Chang, T. H., Kubota, T., Matsuoka, M., Jones, S., Bradfute, S. B., Bray, M., and Ozato, K. (2007). "Ebola Zaire virus blocks type I interferon production by exploiting the host SUMO modification machinery." PLoS pathogens **5**: 1000493.

Chen, E. Y., Howley, P.M., Levinson, A.D., Seeburg, P.H. (1982). "The primary structure and genetic organization of the bovine papillomavirus type 1 genome." Nature **299**: 529-534.

Chen, S. C., Chang, L. Y., Wang, Y. W., Chen, Y. C., Weng, K. F., Shih, S. R., and Shih, H. M. (2011). "Sumoylation-promoted enterovirus 71 3C degradation correlates with a reduction in viral replication and cell apoptosis." J Biol Chem **286**: 31373-31384.

Chen, S. L., Huang, C.H., Tsai, T.C., Lu, K.Y. and Tsao, Y.P. (1996). "The regulation mechanism of c-jun and junB by human papillomavirus type 16 E5 oncoprotein." Arch Virol **141**: 791-800.

Chiang, C. M., M. Ustav, et al. (1992). "Viral E1 and E2 proteins support replication of homologous and heterologous papillomaviral origins." Proc Natl Acad Sci U S A **89**(13): 5799-5803.

Chiocca, S., Kurtev, V., Colombo, R., Boggio, R., Sciurpi, M.T., Brosch, G., Seiser, C., Draetta, G.F., and Cotten, M. (2002). "Histone deacetylase 1 inactivation by an adenovirus early gene product." Current Biology **CD12**: 594-598.

Chiu, M. W., Shih, H.M., Yang, T.H., Yang, Y.L. (2007). "The type 2 dengue virus envelope protein interacts with small ubiquitin-like modifier-1 (SUMO-1) conjugating enzyme 9 (Ubc9)." J. Biomed. Sci **14**: 429–444.

Chow, L. T., and Broker, T. R. (1994). "Papillomavirus DNA replication." Intervirology **37**(3-4): 150-158.

Citro, S., Chiocca, S. (2010). "Listeria monocytogenes: a bacterial pathogen to hit on the SUMO pathway." Cell Res. **20**: 738 –740.

Colombo, R., Boggio, R., Seiser, C., Draetta,G. F., and Chiocca, S. (2002). "The adenovirus protein Gam1 interferes with sumoylation of histone deacetylase1." EMBO Reports **3**: 1062-1068.

Conrad, M., V. J. Bubb, et al. (1993). "The human papillomavirus type 6 and 16 E5 proteins are membrane-associated proteins which associate with the 16-kilodalton pore-forming protein." J Virol **67**(10): 6170-6178.

Conway, M. J., Alam, S., Christensen, N.D., Meyers, C. (2009). "Overlapping and independent structural roles for human papillomavirus type 16 L2 conserved cysteines." Virology **393**: 295–303.

Cornelis, G. R., Denecker, G. (2001). "Yersinia lead SUMO attack." Nature Med **7**: 21-23.

Culp, T. D., L. R. Budgeon, et al. (2006). "Human papillomaviruses bind a basal extracellular matrix component secreted by keratinocytes which is distinct from a membrane-associated receptor." Virology **347**(1): 147-159.

Culp, T. D., Christensen, N.D. (2004). "Kinetics of in vitro adsorption and entry of papillomavirus virions." Virology **319**: 152–161.

Cutts, F. T., S. Franceschi, et al. (2007). "Human papillomavirus and HPV vaccines: a review." Bull World Health Organ **85**(9): 719-726.

Danos, O., M. Katinka, et al. (1982). "Human papillomavirus 1a complete DNA sequence: a novel type of genome organization among papovaviridae." EMBO J **1**(2): 231-236.

Darshan, M. S., J. Lucchi, et al. (2004). "The L2 minor capsid protein of human papillomavirus type 16 interacts with a network of nuclear import receptors." Journal of Virology **78**(22): 12179-12188.

Dasgupta, J., Bienkowska-Haba, M., Ortega, M.E., Patel, H.D., Bodevin, S., Spillmann, D., Bishop, B., Sapp, M., Chen, X.S. (2011). "Structural basis of oligosaccharide receptor recognition by human papillomavirus." J Biol Chem **286**(2617-2624).

Davy, C. E., D. J. Jackson, et al. (2005). "Human Papillomavirus Type 16 E1ΛE4-Induced G2 Arrest Is Associated with Cytoplasmic Retention of Active Cdk1/Cyclin B1 Complexes." J Virol **79**(7): 3998-4011.

Day, P. M., Baker, C. C., Lowy, D. R., and Schiller, J. T. (2004). "Establishment of papillomavirus infection is enhanced by promyelocytic leukemia protein (PML) expression." Proc Natl Acad Sci U S A **101**(39): 14252-14257.

Day, P. M., Gambhira, R., Roden, R.B., Lowy, D.R. and Schiller, J.T. (2008a). "Mechanisms of human papillomavirus type 16 neutralization by l2 cross-neutralizing and l1 type-specific antibodies." J Virol **82**: 4638-4646.

Day, P. M., D. R. Lowy, et al. (2003b). "Papillomaviruses infect cells via a clathrin-dependent pathway." Virology **307**(1): 1-11.

Day, P. M., Lowy, D.R. and Schiller, J.T. (2008b). "Heparan sulfate-independent cell binding and infection with furin-precleaved papillomavirus capsids." J Virol **82**: 12565-12568.

Day, P. M., Roden, R.B., Lowy, D.R. and Schiller, J.T. (1998). "The papillomavirus minor capsid protein, L2, induces localization of the major capsid protein, L1, and the viral transcription/replication protein, E2, to PML oncogenic domains." J Virol **72**: 142-150.

Day, P. M. a. S., J.T. (2009). "The role of furin in papillomavirus infection." Future Microbiol **4**: 1255-1262.

de Villiers, E. M., L. Gissmann, et al. (1981). "Molecular cloning of viral DNA from human genital warts." J Virol **40**(3): 932-935.

de Villiers, E. M., Gunst, K., Stein, H. and Scherubl, H. (2004). "Esophageal squamous cell cancer in patients with head and neck cancer: Prevalence of human papillomavirus DNA sequences." Int J Cancer **109**: 253-258.

Dell, G., Wilkinson, K. W., Tranter, R., Parish, J., Leo Brady, R., and Gaston, K. (2003). "Comparison of the structure and DNA-binding properties of the E2 proteins from an oncogenic and a non-oncogenic human papillomavirus." J Mol Biol **334**(5): 979-991.

Demeret, C., Goyat, S., Yaniv, M., and Thierry, F. (1998). "The human papillomavirus type 18 (HPV18) replication protein E1 is a transcriptional activator when interacting with HPV18 E2." Virology **242**(2): 378-386.

Desterro, J. M., Rodriguez, M. S. & Hay, R. T. (1998). "SUMO-1 modification of IκBα inhibits NF-κB activation." Mol. Cell **2**: 233–239.

Deyrieux, A. F., Rosas-Acosta, G., Ozbun, M. A., and. Wilson, V. G (2007). "Sumoylation dynamics during keratinocyte differentiation." J Cell Sci **120**: 125-136.

Doorbar, J. (2006). "Molecular biology of human papillomavirus infection and cervical cancer." Clin Sci (Lond) **110**: 525-541.

Dürst, M., L. Gissmann, et al. (1983). "A papillomavirus DNA from a cervical carcinoma and its prevalence in cancer biopsy samples from different geographic regions." Proc Natl Acad Sci U S A **80**(12): 3812-3815.

Duncan, J. S. L., D. W. (2008). "Too much of a good thing: the role of protein kinase CK2 in tumorigenesis and prospects for therapeutic inhibition of CK2." Biochim. Biophys. Acta **1784**: 33–47.

Eckert, L. O., D. H. Watts, et al. (1999). "A matched prospective study of human immunodeficiency virus serostatus, human papillomavirus DNA, and cervical lesions detected by cytology and colposcopy." Infect Dis Obstet Gynecol **7**(3): 158-164.

Eckert, R. L., Crish, J.F. and Robinson, N.A. (1997). "The epidermal keratinocyte as a model for the study of gene regulation and cell differentiation." Physiol Rev **77**: 397-424.

Einstein, M. H., Baron, M., Levin, M.J., Chatterjee, A., Edwards, R.P., Zepp, F., et al. (2009). "Comparison of the immunogenicity and safety of Cervarix and Gardasil human papillomavirus (HPV) cervical cancer vaccines in healthy women aged 18-45 years." Hum Vaccin **5**: 705-719.

Endter, C., Hartl, B., Spruss, T., Hauber, J., Dobner, T. (2005). "Blockage of CRM1-dependent nuclear export of the adenovirus type 5 early region 1B 55-kDa protein augments oncogenic transformation of primary rat cells." Oncogene **24**: 55-64.

Endter, C., Kzhyshkowska, J., Stauber, R., Dobner, T. (2001). "SUMO-1 modification required for transformation by adenovirus type 5 early region 1B 55-kDa oncoprotein." Proc. Natl. Acad. Sci. U. S. A. **98**: 11312–11317.

Etter, D. J., G. D. Zimet, et al. (2012). "Human papillomavirus vaccine in adolescent women: a 2012 update." Curr Opin Obstet Gynecol.

Evander, M., I. H. Frazer, et al. (1997). "Identification of the alpha6 integrin as a candidate receptor for papillomaviruses." J Virol **71**(3): 2449-2456.

Everett, R. D. (2001). "DNA viruses and viral proteins that interact with PML nuclear bodies." Oncogene **29**: 7266-7273.

Everett, R. D., and M. K. Chelbi-Alix. (2007). "PML and PML nuclear bodies: implications in antiviral defence." Biochimie **89**: 819-830.

Fay, A., Yutzy, W.H., Roden, R.B., Moroianu, J. (2004). "The positively charged termini of L2 minor capsid protein required for bovine papillomavirus infection function separately in nuclear import and DNA binding." J Virol **78**: 13447-13454.

Finnen, R. L., K. D. Erickson, et al. (2003). "Interactions between Papillomavirus L1 and L2 Capsid Proteins." J Virol **77**(8): 4818-4826.

Flores, E. R., Allen-Hoffmann, B.L., Lee, D., Sattler, C.A. and Lambert, P.F. (1999). "Establishment of the human papillomavirus type 16 (HPV-16) life cycle in an immortalized human foreskin keratinocyte cell line." Virology **262**: 344-354.

Florin, L., K. A. Becker, et al. (2006). "Identification of a Dynein Interacting Domain in the Papillomavirus Minor Capsid Protein L2." J Virol **80**(13): 6691-6696.

Florin, L., Becker, K.A., Sapp, C., Lambert, C., Sirma, H., Müller, M., Streeck, R.E., Sapp, M. (2004). "Nuclear translocation of papillomavirus minor capsid protein L2 requires Hsc70." J Virol **78**: 5546–5553.

Florin, L., C. Sapp, et al. (2002a). "Assembly and Translocation of Papillomavirus Capsid Proteins." J Virol **76**(19): 10009-10014.

Florin, L., Schafer, F., Sotlar, K., Streeck, R.E. and Sapp, M. (2002b). "Reorganization of nuclear domain 10 induced by papillomavirus capsid protein l2." Virology **295**: 97-107.

Funk, J. O., Waga, S., Harry, J. B., Espling, E., Stillman, B., and Galloway, D. A. (1997). "Inhibition of CDK activity and PCNA-dependent DNA replication by p21 is blocked by interaction with the HPV-16 E7 oncoprotein." Genes Dev **11**(16): 2090-1200.

Gambhira, R., Jagu, S., Karanam, B., Day, P.M., Rode,n R. (2009). "Role of L2 cysteines in papillomavirus infection and neutralization." Virol J **6**: 176.

Ganguly, N. (2012). "Human papillomavirus-16 E5 protein: oncogenic role and therapeutic value." Cellular Oncology **35**(2): 67-76.

Gareau, J. R., and Lima, C.D. (2010). "The SUMO pathway: emerging mechanisms that shape specificity, conjugation and recognition." Nature Molcellbio **11**: 861-871.

Geisler, S. B., D. Robinson, et al. (2007). "Obscurin-like 1, OBSL1, is a novel cytoskeletal protein related to obscurin." Genomics **89**(4): 521-531.

Geiss-Friedlander, R. M., F. (2007). "Concepts in sumoylation: a decade on." Nature Rev. Mol. Cell Biol **8**: 947–956.

Giroglou, T., L. Florin, et al. (2001). "Human Papillomavirus Infection Requires Cell Surface Heparan Sulfate." J Virol **75**(3): 1565-1570.

Goldman, S. A., Bruno, G. V., Polnaszek, C. F., Freed, J. H. (1972). "An ESR Study of Anisotropic Rotational Reorientation and Slow Tumbling in Liquid and Frozen Media " J Chem Phys **56**: 716-726.

Gong, L., Millas, S., Maul, G. G. & Yeh, E. T. (2000). "Differential regulation of sentrinized proteins by a novel sentrinspecific protease." J. Biol. Chem. **275**: 3355–3359.

Gonzalez-Santamaria, J., M. Campagna, et al. (2011). "Regulation of vaccinia virus E3 protein by small ubiquitin-like modifier proteins." J Virol **85**(24): 12890-12900.

Goujon, M., McWilliam, H., Li, W., Valentin, F., Squizzato, S., Paern, J., Lopez, R. (2010). "A new bioinformatics analysis tools framework at EMBL-EBI " Nucleic acids research **38**: Suppl: W695-699.

Graham, F. L., J. Smiley, et al. (1977). "Characteristics of a human cell line transformed by DNA from human adenovirus type 5." J Gen Virol **36**(1): 59-74.

Graham, S. V. (2008). "Papillomavirus 3' UTR regulatory elements." Front Biosci **13**: 5646-5663.

Grassmann, K., B. Rapp, et al. (1996). "Identification of a differentiation-inducible promoter in the E7 open reading frame of human papillomavirus type 16 (HPV-16) in raft cultures of a new cell line containing high copy numbers of episomal HPV-16 DNA." J Virol **70**(4): 2339-2349.

Gu, Z. a. M., G. (1995). "Effect of human papillomavirus type 16 oncogenes on MAP kinase activity." J Virol **69**: 8051-8056.

Guo, D. e. a. (2004). "A functional variant of SUMO4, a new IκBα modifier, is associated with type 1 diabetes." Nature Genet **36**: 837-841.

Gurer, C., Berthoux, L., Luban, J. (2005). "Covalent modification of human immunodeficiency virus type 1 p6 by SUMO-1." J Virol **79**: 910 –917.

Haagenson, K. K., L. Tait, et al. (2012). "Cullin-3 protein expression levels correlate with breast cancer progression." Cancer Biol Ther **13**(11).

Hagemeier, S. R., Dickerson, S. J., Meng, Q., Yu, X., Mertz, J. E., and Kenney, S.C. (2010). "Sumoylation of the Epstein-Barr virus BZLF1 protein inhibits its transcriptional activity and is regulated by the virus-encoded protein kinase." J Virol **84**: 4383-4394.

Haimann, M. M., Y. Akdogan, et al. (2011). "Conformational changes of the chaperone SecB upon binding to a model substrate--bovine pancreatic trypsin inhibitor (BPTI)." Biol Chem **392**(10): 849-858.

Hanania, U., Furman-Matarasso, N., Ron, M. & Avni, A. (1999). "Isolation of a novel SUMO protein from tomato that suppresses EIX-induced cell death." Plant J. **19**: 533-541.

Hannich, J. T. e. a. (2005). "Defining the SUMO-modified proteome by multiple approaches in Saccharomyces cerevisiae." J. Biol. Chem. **280**: 4102–4110.

Hanson, D., P. G. Murray, et al. (2009). "The primordial growth disorder 3-M syndrome connects ubiquitination to the cytoskeletal adaptor OBSL1." Am J Hum Genet **84**(6): 801-806.

Hateboer, G., Hijmans,E. M., Nooij, J. B., Schlenker, S., Jentsch, S. and Bernards, R. (1996). "mUBC9, a novel adenovirus E1A-interacting protein that complements a yeast cell cycle defect." J Biol Chem **271**: 25906-25011.

Heino, P., Zhou, J., Lambert, P.F. (2000). "Interaction of the papillomavirus transcription/replication factor, E2, and the viral capsid protein, L2." Virology **276**: 304-314.

Hietakangas, V. e. a. (2003). "Phosphorylation of serine 303 is a prerequisite for the stress-inducible SUMO modification of heat shock factor 1." Mol. Cell. Biol **23**: 2953–2968.

Hines, C. S., Meghoo, C., Shetty, S., Biburger, M., Brenowitz, M., and Hegde, R. S. (1998). "DNA structure and flexibility in the sequence-specific binding of papillomavirus E2 proteins." J Mol Biol **276**(4): 809-818.

Ho, G. Y., Studentsov, Y., Hall, C.B., Bierman, R., Beardsley, L., Lempa, M. and Burk, R.D. (2002). "Risk factors for subsequent cervicovaginal human papillomavirus (HPV) infection and the protective role of antibodies to HPV-16 virus-like particles." J Infect Dis **186**: 737-742.

Hochstrasser, M. (1996). "Ubiquitin-dependent protein degradation." Annu. Rev. Genet **30**: 405-439.

Hochstrasser, M. (2000). "Evolution and function of ubiquitin-like protein-conjugation systems." Nature Cell Bio **2**: E151-E157.

Hoeller, D. e. a. (2007). "E3-independent monoubiquitination of ubiquitin-binding proteins." Mol. Cell **26**: 891–898.

Höfer, P., Grupp, A., Nebenführ, H. ,Mehring, M. (1986). "Hyperfine sublevel correlation (hyscore) spectroscopy: a 2D ESR investigation of the squaric acid radical." Chem. Phys. Lett **132**: 279-282.

Hofmann, K., and Falquet., L. (2001). "A ubiquitin-interacting motif conserved in components of the proteasomal and lysosomal protein degradation systems." TRENDS in Biochemical Sciences **26**(6): 347-350.

Hollenbach, A. D., C. J. McPherson, et al. (2002). "Daxx and histone deacetylase II associate with chromatin through an interaction with core histones and the chromatin-associated protein Dek." J Cell Sci **115**(Pt 16): 3319-3330.

Holmgren, S. C., N. A. Patterson, et al. (2005). "The Minor Capsid Protein L2 Contributes to Two Steps in the Human Papillomavirus Type 31 Life Cycle." J Virol **79**(7): 3938-3948.

Homchaudhuri L., D. A., M., Nilsson, S.B., Bamm, V.V., Musse, A. A., Smith, G.S.T., Harauz, G., and Boggs, J.M. (2010). "SDSL-EPR study of a C-terminal segment of myelin basic protein in a myelin mimetic environment." Biophys. J. **98**: 232a-233a.

Howley, P. M., Knipe, D. M., and Fields, B. N. (2007). Fields Virology, Lippincott Williams & Wilkins.

Hubbell, W. L., Cafiso, D. S., Altenbach, C. (2000). "Identifying conformational changes with site-directed spin labeling." Nature Struct. Biol **7**: 735-739.

Huibregtse, J. M., M. Scheffner, et al. (1995). "A family of proteins structurally and functionally related to the E6-AP ubiquitin-protein ligase." Proc Natl Acad Sci U S A **92**(7): 2563-2567.

Hummel, M., J. B. Hudson, et al. (1992). "Differentiation-induced and constitutive transcription of human papillomavirus type 31b in cell lines containing viral episomes." J Virol **66**(10): 6070-6080.

Hwang, J. and R. F. Kalejta (2009). "Human cytomegalovirus protein pp71 induces Daxx SUMOylation." J Virol **83**(13): 6591-6598.

Hwang, J. S., Mason, R. P., Hwang, L. P., Freed, J. H. (1975). "ESR Studies of Heisenberg Spin Exchange. II. Effects of Radical Charge and Size." J Chem Phys **52**: 2511-2523.

Isas, J. M., Langen, R., Haigler, H.T. & Hubbell, W.L. (2002). "Structure and dynamics of a helical hairpin and loop region in annexin 12: a site-directed spin labeling study." Biochemistry **41**(1464-1473).

Ishii, Y., K. Tanaka, et al. (2010). "Inhibition of nuclear entry of HPV16 pseudovirus-packaged DNA by an anti-HPV16 L2 neutralizing antibody." Virology **406**(2): 181-188.

Ishov, A. M., O. V. Vladimirova, et al. (2004). "Heterochromatin and ND10 are cell-cycle regulated and phosphorylation-dependent alternate nuclear sites of the transcription repressor Daxx and SWI/SNF protein ATRX." J Cell Sci **117**(Pt 17): 3807-3820.

Izumiya, Y., Ellison, T. J., Yeh, E. T., Jung, J. U., Luciw, P. A., and Kung, H. J. (2005). "Kaposi's sarcoma-associated herpesvirus K-bZIP represses gene transcription via SUMO modification." J Virol **79**: 9912-9925.

Jaber, T., Bohl, C. R. Lewis, G. L. Wood, C. West, Jr., J. T., and Weldon, Jr., R. A. (2009). "Human Ubc9 contributes to production of fully infectious human immunodeficiency virus type 1 virions." J Virol **83**: 10448-10459.

Jang, M. S., S. W. Ryu, et al. (2002). "Modification of Daxx by small ubiquitin-related modifier-1." Biochem Biophys Res Commun **295**(2): 495-500.

Jentsch, S. P., G. (2000). "Ubiquitin and its kin: how close are the family ties?" Trends Cell Biol. **10**: 335-342.

Jeschke, G. (2002). "Determination of the Nanostructure of Polymer Materials by Electron Paramagnetic Resonance Spectroscopy." Macromolecular Rapid Communications **23**: 227-246.

Jiang, M. X. and M. J. Imperiale (2012). "Design stars: how small DNA viruses remodel the host nucleus." Future Virology **7**(5): 445-459.

Johansson, C., M. Somberg, et al. (2012). "HPV-16 E2 contributes to induction of HPV-16 late gene expression by inhibiting early polyadenylation." EMBO J.

Johnson, E. S. (2004). "PROTEIN MODIFICATION BY SUMO." Annu. Rev. Biochem **73**: 355–382.

Johnson, K. M., Kines, R.C., Roberts, J.N., Lowy, D.R., Schiller, J.T., Day, P.M. (2009). "Role of heparan sulfate in attachment to and infection of the murine female genital tract by human papillomavirus." J Virol **83**: 2067-2074.

Joyce, J., Tung, J., Przysiecki, C., Cook, J., Lehman, E., Sands, J., Jansen, K., Keller, P. (1999). "The L1 major capsid protein of human papillomavirus type 11 recombinant virus-like particles interacts with heparin and cell-surface glycosaminoglycans on human keratinocytes." Journal of Biological Chemistry **274**.

Junk, M. J., U. Jonas, et al. (2008). "EPR spectroscopy reveals nanoinhomogeneities in the structure and reactivity of thermoresponsive hydrogels." Small **4**(9): 1485-1493.

Kamitani, T., Kito, K., Nguyen, H. P., Fukuda-Kamitani, T. & Yeh, E. T. (1998). "Characterization of a second member of the sentrin family of ubiquitin-like proteins." J. Biol. Chem **273**: 11349–11353.

Kämper, N., P. M. Day, et al. (2006). "A Membrane-Destabilizing Peptide in Capsid Protein L2 Is Required for Egress of Papillomavirus Genomes from Endosomes." J Virol **80**(2): 759-768.

Kang, D., Gho, J. S., Suh, M., and Kang, C. (2002). "Highly Sensitive and Fast Protein Detection with Coomassie Brilliant Blue in Sodium Dodecyl Sulfate-Polyacrylamide Gel Electrophoresis." Bull. Korean Chem. Soc **23**: 1511-1512.

Karanam, B., Peng, S., Li, T., Buck, C., Day, P.M., Roden, R.B. (2010). "Papillomavirus infection requires gamma secretase." J Virol **84**: 10661-10670.

Kattnig, D. R., T. Bund, et al. (2012). "Lateral self-assembly of 18.5-kDa myelin basic protein (MBP) charge component-C1 on membranes." Biochim Biophys Acta.

Kaukinen, P., Vaheri, A., Plyusnin, A. (2003). "Noncovalent interaction between nucleocapsid protein of Tula hantavirus and small ubiquitinrelated modifier-1, SUMO-1." Virus Res **92**: 37-45.

Kawana, K., Matsumoto, K., Yoshikawa, H., Taketani, Y., Kawana, T., Yoshiike, K., Kanda, T. (1998). "A surface immunodeterminant of human papillomavirus type 16 minor capsid protein L2." Virology **245**: 353-359.

Kawana, K., Yoshikawa, H., Taketani, Y., Yoshiike, K., Kanda, T. (1999). "Common neutralization epitope in minor capsid protein L2 of human papillomavirus types 16 and 6." J Virol **73**: 6188-6190.

Kawana, Y., K. Kawana, et al. (2001). "Human Papillomavirus Type 16 Minor Capsid Protein L2 N-Terminal Region Containing a Common Neutralization Epitope Binds to the Cell Surface and Enters the Cytoplasm." J Virol **75**(5): 2331-2336.

Kerscher, O., Felberbaum, R. & Hochstrasser, M. (2006). "Modification of proteins by ubiquitin and ubiquitin-like proteins." Annu. Rev. Cell Dev. Biol **22**: 159-180.

Kerscher, O., Felberbaum, R. & Hochstrasser, M. (2007). "SUMO junction-what's your function? New insights through SUMO-interacting motifs." EMBO Rep **8**: 550–555.

Kfoury, Y., N. Setterblad, et al. (2011). "Tax ubiquitylation and SUMOylation control the dynamic shuttling of Tax and NEMO between Ubc9 nuclear bodies and the centrosome." Blood **117**(1): 190-199.

Kim, E. T., Kim, Y.E., Huh, Y.H., Ahn, J.H. (2010). "Role of noncovalent SUMO binding by the human cytomegalovirus IE2 transactivator in lytic growth." J Virol **84**: 8111– 8123.

Kim, K. I. e. a. (2000). "A new SUMO-1-specific protease, SUSP1, that is highly expressed in reproductive organs." J. Biol. Chem **275**: 14102–14106.

Kines, R. C., Thompson, C.D., Lowy, D.R., Schiller, J.T., Day, P.M. (2009). "The initial steps leading to papillomavirus infection occur on the basement membrane prior to cell surface binding." Proc Natl Acad Sci USA **106**: 20458-20463.

Klingelhutz, A. J., Foster, S. A., and McDougall, J. K. (1996). "Telomerase activation by the E6 gene product of human papillomavirus type 16." Nature **380**(6569): 79-82.

Knappe, M., Bodevin, S., Selinka, H.C., Spillmann, D., Streeck, R.E., Chen, X.S., et al. (2007). "Surface-exposed amino acid residues of HPV16 L1 protein mediating interaction with cell surface heparan sulfate." J Biol Chem **282**: 27913-27922.

Kocherginsky, N., Swartz, H. M. (1995). Nitroxide Spin Labels – Reactions in Biology and Chemistry, CRC Press.

Kondo, K., Ishii, Y., Ochi, H., Matsumoto, T., Yoshikawa, H., Kanda, T. (2007). "Neutralization of HPV16, 18, 31, and 58 pseudovirions with antisera induced by immunizing rabbits with synthetic peptides representing segments of the HPV16 minor capsid protein L2 surface region." Virology **358**: 266–272.

Kraus, I., Molden, T., Holm, R., Lie, A.K., Karlsen, F., Kristensen, G.B., Skomedal, H. (2006). "Presence of E6 and E7 mRNA from human papillomavirus types 16, 18, 31, 33, and 45 in the majority of cervical carcinomas." J Clin Microbiol **4**: 1310-1317.

Kyratsous, C. A., Silverstein, S.J. (2009). "Components of nuclear domain 10 bodies regulate varicella-zoster virus replication." J Virol **83**: 4262– 4274.

Laemmli, U. K. (1970). "Cleavage of structural proteins during the assembly of the head of bacteriophage T4." Nature **227**(5259): 680-685.

Lambert, P. F. (1991). "Papillomavirus DNA replication." J Virol **65**: 3417-3420.

Lamsoul, I., J. Lodewick, et al. (2005). "Exclusive ubiquitination and sumoylation on overlapping lysine residues mediate NF-kappaB activation by the human T-cell leukemia virus tax oncoprotein." Mol Cell Biol **25**(23): 10391-10406.

Lancaster, W. D., C. Olson, et al. (1977). "Bovine papilloma virus: presence of virus-specific DNA sequences in naturally occurring equine tumors." Proc Natl Acad Sci U S A **74**(2): 524-528.

Laniosz, V., Nguyen, K.C., Meneses, P.I. (2007). "Bovine papillomavirus type 1 infection is mediated by SNARE syntaxin 18." J Virol **81**: 7435–7448.

Larkin, M. A., Blackshields, G., Brown, N.P., Chenna, R., McGettigan, P.A., McWilliam, H., Valentin, F., Wallace, I.M., Wilm, A., Lopez, R., Thompson, J.D., Gibson, T.J., and Higgins, D.G. (2007). "ClustalW and ClustalX version 2." Bioinformatics **23**: 2947-2948.

Lazo, P. A. (2007). "Functional implications of tetraspanin proteins in cancer biology." Cancer Sci **98**: 1666–1677.

Le, X. F., P. Yang, et al. (1996). "Analysis of the growth and transformation suppressor domains of promyelocytic leukemia gene, PML." J Biol Chem **271**(1): 130-135.

Lee, B. H., Yoshimatsu, K., Maeda, A., Ochiai, K., Morimatsu, M., Araki, K., Ogino, M., Morikawa,S., and Arikawa, J. (2003). "Association of the nucleocapsid protein of the Seoul and Hantaan hantaviruses with small ubiquitin-like modifier-1-related molecules." Virus Research **98**: 83-91.

Lee, D., Sohn, H., Kalpana, G.V. and Choe, J. (1999). "Interaction of E1 and hSNF5 proteins stimulates replication of human papillomavirus DNA." Nature **399**: 487-491.

Li, F. Q., Xiao, H., Tam, J.P., Liu, D.X. (2005). "Sumoylation of the nucleocapsid protein of severe acute respiratory syndrome coronavirus." FEBS Lett **579**: 2387–2396.

Li, H., C. Leo, et al. (2000). "Sequestration and inhibition of Daxx-mediated transcriptional repression by PML." Mol Cell Biol **20**(5): 1784-1796.

Lin, D. e. a. (2002). "Identification of a substrate recognition site on Ubc9." J. Biol. Chem. **277**: 21740–21748.

Lin, D. Y., Y. S. Huang, et al. (2006). "Role of SUMO-interacting motif in Daxx SUMO modification, subnuclear localization, and repression of sumoylated transcription factors." Mol Cell **24**(3): 341-354.

Lindahl, U., Kusche-Gullberg, M. and Kjellen, L. (1998). "Regulated diversity of heparan sulfate." J Biol Chem **273**: 24979-24982.

Liu, W. J., Gissmann, L., Sun, X.Y., Kanjanahaluethai, A., Müller, M., Doorbar, J., Zhou, J. (1992). "Sequence close to the N-terminus of L2 protein is displayed on the surface of bovine papillomavirus type 1 virions." Virology **227**: 474–483.

Loftus, L. T., Gala, R., Yang, T., Jessick, V.J., Ashley, M.D., Ordonez, A.N., Thompson, S.J., Simon, R.P., Meller, R. (2009). "Sumo-2/3-ylation following in vitro modeled ischemia is reduced in delayed ischemic tolerance." Brain Res **1272**: 71–80.

Longworth, M. S., Wilson, R., and Laimins, L. A. (2005). "HPV31 E7 facilitates replication by activating E2F2 transcription through its interaction with HDACs." Embo J **24**(10): 1821-1830.

Loo, Y. M. and T. Melendy (2004). "Recruitment of Replication Protein A by the Papillomavirus E1 Protein and Modulation by Single-Stranded DNA." J Virol **78**(4): 1605-1615.

Maeda, A., Lee, B. H., Yoshimatsu, K., Saijo, M., Kurane I., Arikawa, J., and Morikawa, S. (2003). "The intracellular association of the nucleocapsid protein (NP) of hantaan virus (HTNV) with small ubiquitin-like modifier-1 (SUMO-1) conjugating enzyme 9 (Ubc9." Virology **305**: 288-297.

Mamoor, S., Z. Onder, et al. (2012). "The high risk HPV16 L2 minor capsid protein has multiple transport signals that mediate its nucleocytoplasmic traffic." Virology **422**(2): 413-424.

Mantovani, F., and Banks, L. (1999). "The interaction between p53 and papillomaviruses." Semin Cancer Biol **9**(6): 387-395.

Mantovani, F., Banks, L. (2001). "The human papillomavirus E6 protein and its contribution to malignant progression." Oncogene **20**: 7874-7887.

Martin, R. E., Pannier, M., Diederich, F., Gramlich, V., Hubrich, M., Spiess, H. W. (1998). "Bestimmung der Länge von bis zu 2.8 nm langen TEMPO-Diradikalen mit einem neuen Vier-Puls-Doppel-Elektron-Elektron- Resonanz-Experiment." Angew Chem **110**: 2993-2998.

Marusic, M. B., Mencin, N., Licen, M., Banks, L., and Grm, H. S. (2010). "Modification of human papillomavirus minor capsid protein L2 by sumoylation." J Virol **84**: 11585-11589.

Marusic, M. B., M. A. Ozbun, et al. (2012). "Human Papillomavirus L2 Facilitates Viral Escape from Late Endosomes via Sorting Nexin 17." Traffic **13**(3): 455-467.

Matunis, M. J., Coutavas, E. & Blobel, G. (1996). "A novel ubiquitinlike modification modulates the partitioning of the Ran-GTPase-activating protein RanGAP1 between the cytosol and the nuclear pore complex." J. Cell Biol. **135**: 1457–1470.

Maytin, E. V., Lin, J.C., Krishnamurthy, R., Batchvarova, N., Ron, D., Mitchell, P.J. and Habener, J.F. (1999). "Keratin 10 gene expression during differentiation of mouse epidermis requires transcription factors C/EBP and AP-2." Dev Biol **216**: 164-181.

McBride, A. A., Oliveira, J.G., McPhillips, M.G., (2006). "Partitioning viral genomes in mitosis." Cell Cycle **5**: 1499-1502.

Mchaourab, H. S., Lietzow, M.A., Hideg, K. & Hubbell, W.L. (1996). "Motion of spin-labeled side chains in T4 lysozyme. Correlation with protein structure and dynamics." Biochemistry **35**: 7692-7704.

McIntyre, M. C., Ruesch, M. N., and Laimins, L. A. (1996). "Human papillomavirus E7 oncoproteins bind a single form of cyclin E in a complex with cdk2 and p107." Virology **215**(1): 73-82.

Merrill, J. C., T. A. Melhuish, et al. (2010). "A role for noncovalent SUMO interaction motifs in Pc2/CBX4 E3 activity." PLoS ONE **5**(1): e8794.

Meulmeester, E., Kunze, M., Hsiao, H. H., Urlaub, H. & Melchior, F. (2008). "Mechanism and consequences for paralogspecific sumoylation of ubiquitin-specific protease 25." Mol Cell **30**: 610–619.

Meyers, C., Frattini, M.G., Hudson, J.B. and Laimins, L.A. (1992). "Biosynthesis of human papillomavirus from a continuous cell line upon epithelial differentiation." Science **257**: 971-973.

Milligan, S. G., T. Veerapraditsin, et al. (2007). "Analysis of novel human papillomavirus type 16 late mRNAs in differentiated W12 cervical epithelial cells." Virology **360**(1): 172-181.

Milov, A. D., Ponomarev, A. B., Tsvetkov, Y. D. (1984). "Electron-electron double resonance in electron spin echo: Model biradical systems and the sensitized photolysis of decalin." Chem. Phys. Lett **110**: 67-72.

Minty, A., Dumont, X., Kaghad, M. & Caput, D. (2000). "Covalent modification of p73α by SUMO-1. Two-hybrid screening with p73 identifies novel SUMO-1-interacting proteins and a SUMO-1 interaction motif." J. Biol. Chem **275**: 36316–36323.

Mohideen, F. e. a. (2009). "A molecular basis for phosphorylation-dependent SUMO conjugation by the E2 UBC9." Nature Struct. Mol. Biol **16**: 945–952.

Mole, S., S. G. Milligan, et al. (2009). "Human papillomavirus type 16 E2 protein transcriptionally activates the promoter of a key cellular splicing factor, SF2/ASF." J Virol **83**(1): 357-367.

Müller, M., L. Gissmann, et al. (1995). "Papillomavirus capsid binding and uptake by cells from different tissues and species." J Virol **69**(2): 948-954.

Mukhopadhyay, D. D., M. (2007). "Modification in reverse: the SUMO proteases." Trends Biochem. Sci **32**: 286–295.

Muller, M., Y. Jacob, et al. (2012). "Large scale genotype comparison of human papillomavirus e2-host interaction networks provides new insights for e2 molecular functions." PLoS Pathog **8**(6): e1002761.

Munger K, H. H., Nguyen CL, Melquiot NV, Duensing A, Duensing S. (2006). "Viral carcinogenesis and genomic instability." EXS **96**: 179-199.

Munger, K., Howley, P.M. (2002). "Human papillomavirus immortalization and transformation functions." Virus Res **89**: 213-228.

Murata, T., Hotta, N., Toyama, S., Nakayama, S., Chiba, S., Isomura, H., Ohshima, T., Kanda, T., and Tsurumi, T. (2010). "Transcriptional repression by sumoylation of Epstein-Barr virus BZLF1 protein correlates with association of histone deacetylase." J Biol Chem **285**: 23925-23935.

Muromoto, R., K. Sugiyama, et al. (2004). "Physical and functional interactions between Daxx and DNA methyltransferase 1-associated protein, DMAP1." J Immunol **172**(5): 2985-2993.

Musse, A. A., J. M. Boggs, et al. (2006). "Deimination of membrane-bound myelin basic protein in multiple sclerosis exposes an immunodominant epitope." Proceedings of the National Academy of Sciences of the United States of America **103**(12): 4422-4427.

Naik, M. T., Huang, T., Shih, H. "Phosphorylation of SUMO-interacting motif by CK2 enhances Daxx SUMO binding activity." To be published.

Nelson, L. M., Rose, R. C., and Moroianu, J. (2002). "Nuclear import strategies of high risk HPV16 L1 major capsid protein." J Biol Chem **277**(26): 23958-23964.

Nielsen, A., T. Iftner, et al. (2012). "The importance of low-risk HPV infection for the risk of abnormal cervical cytology/histology in more than 40 000 Danish women." Sex Transm Infect.

Nishida, T., Tanaka, H. & Yasuda, H. (2000). "novel mammalian Smt3-specific isopeptidase 1 (SMT3IP1) localized in the nucleolus at interphase." Eur. J. Biochem **267**: 6423–6427.

Odintsova, E., Voortman, J., Gilbert, E., Berditchevski, F. (2003). "Tetraspanin CD82 regulates compartmentalisation and ligand-induced dimerization of EGFR." J Cell Sci **116**: 4557-4566.

Ohsumi, Y. (2001). "Ubiquitin and proteasomes: Molecular dissection of autophagy: two ubiquitin-like systems " Nature Reviews Molecular Cell Biology **2**: 211-216.

Okun, M. M., P. M. Day, et al. (2001). "L1 Interaction Domains of Papillomavirus L2 Necessary for Viral Genome Encapsidation." J Virol **75**(9): 4332-4342.

Okura, T. e. a. (1996). "Protection against Fas/APO-1- and tumor necrosis factor-mediated cell death by a novel protein, sentrin." J. Immunol **157**: 4277–4281.

Ouyang, J., Shi, Y., Valin, A., Xuan, Y. & Gill, G. (2009). "Direct binding of CoREST1 to SUMO-2/3 contributes to gene-specific repression by the LSD1/CoREST1/HDAC complex." Mol. Cell **34**: 45–154.

Owerbach, D., McKay, E. M., Yeh, E. T., Gabbay, K. H. & Bohren, K. M. (2005). "A proline-90 residue unique to SUMO-4 prevents maturation and sumoylation." Biochem. Biophys. Res. Commun **337**: 517–520.

Paintsil, J., Müller, M., Picken, M., Gissmann, L., and Zhou, J. (1996). "Carboxyl terminus of bovine papillomavirus type-1 L1 protein is not required for capsid formation." Virology **223**(1): 238-244.

Pal, S., Rosas, J.M., Rosas-Acosta, G. (2010). "Identification of the nonstructural influenza A viral protein NS1A as a bona fide target of the Small Ubiquitin-like MOdifier by the use of dicistronic expression constructs." J. Virol. Methods **163**: 498-504.

Pal, S., Santos, A., Rosas, J.M., Ortiz-Guzman, J., Rosas-Acosta, G. (2011). "Influenza A virus interacts extensively with the cellular SUMOylation system during infection." Virus Res **158**: 12-27.

Palacios, S., Perez, L. H., Welsch, S., Schleich, S., Chmielarska, K., Melchior, F., and Locker, J. K. (2005). "Quantitative SUMO-1 modification of a vaccinia virus protein is required for its specific localization and prevents its self-association." Mol Biol Cell **16**: 2822-2835.

Pannier, M., Veit, S., Godt, A., Jeschke, G., Spiess, H. W. (2000). "Dead-Time Free Measurement of Dipole–Dipole Interactions between Electron Spins." J. Magn. Reson **142**: 331-340.

Park, P., Copeland, W., Yang, L., Wang, T., Botchan, M.R. and Mohr, I.J. (1994). "The cellular DNA polymerase alpha-primase is required for papillomavirus DNA replication and associates with the viral E1 helicase." Proc Natl Acad Sci U S A **91**: 8700-8704.

Parkin, D. M. (2006). "The global health burden of infection-associated cancers in the year 2002." Int J Cancer **118**: 3030-3044.

Pear, W. S., G. P. Nolan, et al. (1993). "Production of high-titer helper-free retroviruses by transient transfection." Proc Natl Acad Sci U S A **90**(18): 8392-8396.

Perry, N. A., M. Shriver, et al. (2012). "Loss of giant obscurins promotes breast epithelial cell survival through apoptotic resistance." FASEB J **26**(7): 2764-2775.

Pichler, A., Gast, A., Seeler, J. S., Dejean, A. & Melchior, F. (2002). "The nucleoporin RanBP2 has SUMO1 E3 ligase activity." Cell **108**: 109-120.

Plato, M., Steinhoff, H.J., Wegener, C., Torring, J.T., Savitsky, A., Möbius, K. (2002). "Molecular Orbital Study of Polarity and Hydrogen Bonding Effects on the G and Hyperfine Tensors of Site Directed NO Spin Labeled Bacteriorhodopsin." Mol Phys **100**: 3711-3721.

Rangasamy, D., and Wilson, V. G. (2000a). "Bovine papillomavirus E1 protein is sumoylated by the host cell Ubc9 protein." J Biol Chem **275**: 30487-30495.

Rangasamy, D., Woytek, K., Khan, S.A., Wilson, V.G. (2000b). "SUMO-1 modification of bovine papillomavirus E1 protein is required for intranuclear accumulation." J. Biol. Chem. **275**: 37999 –38004.

Reichelt, M., Wang, L., Sommer, M., Perrino, J., Nour, A. M., Sen, N., Baiker, A., Zerboni, L., and Arvin, A. M. (2011). "Entrapment of viral capsids in nuclear PML cages is an intrinsic antiviral host defense against varicella-zoster virus." PLoS pathogens **7**: e1001266.

Reverter, D. L., C. D. (2005). "Insights into E3 ligase activity revealed by a SUMO-RanGAP1-Ubc9-Nup358 complex." Nature **435**: 687–692.

Ribet, D., M. Hamon, et al. (2010). "Listeria monocytogenes impairs SUMOylation for efficient infection." Nature **464**(7292): 1192-1195.

Richards, R. M., D. R. Lowy, et al. (2006). "Cleavage of the papillomavirus minor capsid protein, L2, at a furin consensus site is necessary for infection." Proc Natl Acad Sci U S A **103**(5): 1522-1527.

Roden, R. B., R. Kirnbauer, et al. (1994). "Interaction of papillomaviruses with the cell surface." J Virol **68**(11): 7260-7266.

Roden, R. B. S., Yuty, W., Fallon, R., Inglis, S., Lowy, D., Schiller, J.T. (2000). "Minor capsid protein of human genital papillomavirus contains subdominant, cross-neutralizing epitopes." Vaccine **270**: 254-257.

Rodriguez, M. S., Dargemont, C. & Hay, R. T. (2001). "SUMO-1 conjugation in vivo requires both a consensus modification motif and nuclear targeting." J. Biol. Chem **278**: 12654–12659.

Rogan, S., Heaphy, S. (2000). "The vaccinia virus E3L protein interacts with SUMO-1 and ribosomal protein L23a in a yeast two hybrid assay." Virus Genes Cells **21**: 93–195.

Ryan, A. K. a. R., M.G. (1997). "POU domain family values: flexibility, partnerships, and developmental codes." Genes Dev **11**: 1207-1225.

Rytinki, M. M., Kaikkonen, S., Pehkonen, P., Jaaskelainen, T. & Palvimo, J. J. (2009). "PIAS proteins: pleiotropic interactors associated with SUMO." Cell. Mol. Life Sci **66**: 3029–3041.

Sadanari, H., Yamada, R., Ohnishi, K., Matsubara, K., Tanaka, J. (2005). "SUMO-1 modification of the major immediate-early (IE) 1 and 2 proteins of human cytomegalovirus is regulated by different mechanisms and modulates the intracellular localization of the IE1, but not IE2, protein." Arch. Virol. **150**: 1763–1782.

Saitoh, H., Hinchey, J. (2000). "Functional heterogeneity of small ubiquitin-related protein modifiers SUMO-1 versus SUMO-2/3." J Biol Chem **275**: 6252-6258.

Sampson, D. A., Wang, M. & Matunis, M. J. (2001). "The small ubiquitin-like modifier-1 (SUMO-1) consensus sequence mediates Ubc9 binding and is essential for SUMO-1 modification." J. Biol. Chem **267**: 21664–21669.

Sapp, M. and M. Bienkowska-Haba (2009). "Viral entry mechanisms: human papillomavirus and a long journey from extracellular matrix to the nucleus." FEBS J **276**(24): 7206-7216.

Sapp, M., C. Fligge, et al. (1998). "Papillomavirus assembly requires trimerization of the major capsid protein by disulfides between two highly conserved cysteines." J Virol **72**(7): 6186-6189.

Schäfer, F., Florin, L., and Sapp, M. (2002). "DNA binding of L1 is required for human papillomavirus morphogenesis in vivo." Virology **295**(1): 172-181.

Scheffner, M., Werness, B.A., Huibregtse, J.M., Levine, A.J. and Howley, P.M (1990). "The E6 oncoprotein encoded by human papillomavirus types 16 and 18 promotes the degradation of p53." Cell **63**: 1129-1136.

Schelhaas, M., Ewers, H., Rajamäki, M.-L., Day, P.M., Schiller, J.T., Helenius, A. (2008). "Human papillomavirus type 16 entry: retrograde cell surface transport along actin-rich protrusions." PLoS Pathog **4**: e1000148.

Schelhaas, M., B. Shah, et al. (2012). "Entry of human papillomavirus type 16 by actin-dependent, clathrin- and lipid raft-independent endocytosis." PLoS Pathog **8**(4): e1002657.

Scherer, W. F., J. T. Syverton, et al. (1953). "Studies on the propagation in vitro of poliomyelitis viruses. IV. Viral multiplication in a stable strain of human malignant epithelial cells (strain HeLa) derived from an epidermoid carcinoma of the cervix." J Exp Med **97**(5): 695-710.

Schiemann, O., P. Cekan, et al. (2009). "Relative orientation of rigid nitroxides by PELDOR: beyond distance measurements in nucleic acids." Angew Chem Int Ed Engl **48**(18): 3292-3295.

Schiemann, O., N. Piton, et al. (2007). "Spin labeling of oligonucleotides with the nitroxide TPA and use of PELDOR, a pulse EPR method, to measure intramolecular distances." Nat Protoc **2**(4): 904-923.

Schiemann, O. and T. F. Prisner (2007). "Long-range distance determinations in biomacromolecules by EPR spectroscopy." Q Rev Biophys **40**(1): 1-53.

Schiller, J. T., Day, P.M., Kines, R.C. (2010). "Current understanding of the mechanism of HPV infection." Gynecol Oncol **118**: 12-17.

Schmitz, M., C. Driesch, et al. (2012). "Loss of gene function as a consequence of human papillomavirus DNA integration." International journal of cancer. Journal international du cancer **131**(5): E593-602.

Schneider, D. J., Freed, J. H. (1989). Biological Magnetic Resonance, Plenum Press.

Schneider, M. A. (2011). Identifizierung und Charakterisierung zellulärer Interaktionspartner des minoren Kapsidproteins L2 des

Humanen Papillomvirus 16. Biological Department. Mainz, Johannes Gutenberg-University Mainz.

Schneider, M. A., Spoden, G.A., Florin, L., Lambert, C. (2011). "Identification of the dynein light chains required for human papillomavirus infection." Cellular Microbiology **13**(1): 32-47.

Schreiner, S., Martinez, M., Groitl, P., Rayner, F., Vaollant, R., Wimmer, P., Bossis,. G., Sternsdorf, T., Marcinowski, L., Ruzsics, Z., Dobner, T., Wodrich., H. (2012). "Transcriptional Activation of the Adenoviral Genome is Mediated by Capsid Protein VI." PLOS pathogens **8**(2):e 1002549.

Schwartz, S. (2008). "HPV-16 RNA processing." Front Biosci **13**: 5880-5891.

Schwarz, E., M. Dürst, et al. (1983). "DNA sequence and genome organization of genital human papillomavirus type 6b." EMBO J **2**(12): 2341-2348.

Schwarz, E., Freese, U.K., Gissmann, L., Mayer, W., Roggenbuck, B., Stremlau, A. and zur Hausen, H. (1985). "Structure and transcription of human papillomavirus sequences in cervical carcinoma cells." Nature **314**: 111-114.

Schweiger, A., Jeschke, G. (2001). Principles of Pulse Electron Paramagnetic Resonance, Oxford University Press.

Seeler, J.-S., Dejean, A. (2003). "Nuclear and unclear functions of SUMO." nature molcellbio **4**: 690-699.

Seeler, J. S., A. Marchio, et al. (1998). "Interaction of SP100 with HP1 proteins: a link between the promyelocytic leukemia-associated nuclear bodies and the chromatin compartment." Proc Natl Acad Sci U S A **95**(13): 7316-7321.

Seitz, C. S., Q. Lin, et al. (1998). "Alterations in NF-κB function in transgenic epithelial tissue demonstrate a growth inhibitory role for NF-κB." Proc Natl Acad Sci U S A **95**(5): 2307-2312.

Sekiyama, N. e. a. (2008). "Structure of the small ubiquitin-like modifier (SUMO)-interacting motif of MBD1-containing chromatin-associated factor 1 bound to SUMO-3." J. Biol. Chem **283**: 35966–35975.

Selinka, H.-C., Florin, L., Patel, H.D., Freitag, K., Schmidtke, M., Makarov, V.A., Sapp, M. (2007). "Inhibition of transfer to secondary receptors by heparan sulfate-binding drug or antibody induces noninfectious uptake of human papillomavirus." J Virol **81**: 10970–10980.

Selinka, H. C., Giroglou, T. and Sapp, M. (2002). "Analysis of the infectious entry pathway of human papillomavirus type 33 pseudovirions." Virology **299**: 279-287.

Selinka, H. C., Giroglou, T., Nowak, T., Christensen, N.D. and Sapp, M. (2003). "Further evidence that papillomavirus capsids exist in two distinct conformations." J Virol **77**: 12961-12967.

Shafti-Keramat, S., A. Handisurya, et al. (2003). "Different Heparan Sulfate Proteoglycans Serve as Cellular Receptors for Human Papillomaviruses." J Virol **77**(24): 13125-13135.

Shalizi, A. e. a. (2006). "A calcium-regulated MEF2 sumoylation switch controls postsynaptic differentiation." Science **311**: 1012–1017.

Shih, H.-M., Chang, C.-C., Kuo, H.-Y., Lin, D.-Y. (2007). "Daxx mediates SUMO-dependent transcriptional control and subnuclear compartmentalization." Biochem Soc Trans **35**: 1397–1400.

Shope, R. E. and E. W. Hurst (1933). "INFECTIOUS PAPILLOMATOSIS OF RABBITS : WITH A NOTE ON THE HISTOPATHOLOGY." J Exp Med **58**(5): 607-624.

Sichero, L., J. S. Sobrinho, et al. (2012). "Identification of novel cellular transcription factors that regulate HPVs 18 and 16 early promoters." J Infect Dis.

Slupetzky, K., Gambhira, R., Culp, T.D., Shafti-Keramat, S., Schellenbacher, C., Christensen, N.D., Roden, R.B.S., Kirnbauer, R. (2007). "A papillomavirus-like particle (VLP) vaccine displaying HPV 16 L2 epitopes induces cross-neutralizing antibodies to HPV 11." Vaccine **25**: 2001-2010.

Smith, J. L., Campos, S.K., Wandinger-Ness, A., Ozbun, M.A. (2008b). "Caveolin-1-Dependent Infectious Entry of Human Papillomavirus Type 31 in Human Keratinocytes Proceeds to the Endosomal Pathway for pH-Dependent Uncoating." J Virol **82**: 9505–9512.

Song, J., Durrin, L. K., Wilkinson, T. A., Krontiris, T. G. & Chen, Y. (2004). "Identification of a SUMO-binding motif that recognizes SUMO-modified proteins." Proc. Natl Acad. Sci. USA **101**: 4373–14378.

Song, J., Zhang, Z., Hu, W. & Chen, Y (2005). "Small ubiquitinlike modifier (SUMO) recognition of a SUMO binding motif: a reversal of the bound orientation." J. Biol. Chem **280**: 40122–40129.

Spengler, M. L., Kurapatwinski, K., Black, A.R., Azizkhan-Clifford, J. (2002). "SUMO-1 modification of human cytomegalovirus IE1/IE72." J Virol **76**: 2990–2996.

Spoden, G., K. Freitag, et al. (2008). "Clathrin- and Caveolin-Independent Entry of Human Papillomavirus Type 16—Involvement of Tetraspanin-Enriched Microdomains (TEMs)." PLoS ONE **3**(10).

Spoden, G. A., Besold, K., Krauter, S., Plachter, B., Hanik, N., Kilbinger, A.F.M., Lambert, C., Florin, L. (2011). "Polyethylenimine Is a Strong Inhibitor of Human Papillomavirus and Cytomegalovirus Infection." Antimicrobial Agents and Chemotherapy **56**: 75-82.

Spoden, G. A., Sapp, M., Florin, L. (2012 (submitted)). "Host cell factors involved in papillomavirus entry."

Stanley, M. A. (2012). "Epithelial Cell Responses to Infection with Human Papillomavirus." Clinical Microbiology Reviews **25**(2): 215-222.

Stauffer, Y., K. Raj, et al. (1998). "Infectious human papillomavirus type 18 pseudovirions." J Mol Biol **283**(3): 529-536.

Steger, G. and S. Corbach (1997). "Dose-dependent regulation of the early promoter of human papillomavirus type 18 by the viral E2 protein." J Virol **71**(1): 50-58.

Stehmeier, P. M., S. (2009). "Phospho-regulated SUMO interaction modules connect the SUMO system to CK2 signaling." Mol. Cell **33**: 400–409.

Sterk, L. M., Geuijen, C.A., Oomen, L.C., Calafat, J., Janssen, H., Sonnenberg, A. (2000). "The tetraspan molecule CD151, a novel constituent of hemidesmosomes, associates with the integrin alpha6beta4 and may regulate the spatial organization of hemidesmosomes." J Cell Biol **149**: 969–982.

Straight, S. W., B. Herman, et al. (1995). "The E5 oncoprotein of human papillomavirus type 16 inhibits the acidification of endosomes in human keratinocytes." J Virol **69**(5): 3185-3192.

Stubenrauch, F. a. L., L.A. (1999). "Human papillomavirus life cycle: active and latent phases." Semin Cancer Biol **9**: 379-386.

Sun, D., Xu, P., He, B. (2011). "Sumoylation of the P protein at K254 plays an important role in growth of parainfluenza virus 5." J Virol **85**: 10261–10268.

Surviladze, Z., A. Dziduszko, et al. (2012). "Essential roles for soluble virion-associated heparan sulfonated proteoglycans and growth factors in human papillomavirus infections." PLoS Pathog **8**(2): e1002519.

Swindle, C. S., Zou, N., Van Tine, B.A., Shaw, G.M., Engler, J.A., Chow, L.T. (1999). "Human papillomavirus DNA replication compartments in a transient DNA replication system." J Virol **73**: 1001–1009.

Tavalai, N., and Stamminger, T. (2008). "New insights into the role of the subnuclear structure ND10 for viral infection." Biochim Biophys Acta **1783**: 207-2221.

Tavalai, N. and T. Stamminger (2009). "Interplay between Herpesvirus Infection and Host Defense by PML Nuclear Bodies." Viruses **1**(3): 1240-1264.

Thierry, F. (2009). "Transcriptional regulation of the papillomavirus oncogenes by cellular and viral transcription factors in cervical carcinoma." Virology **384**: 375-379.

Tiwari, V., E. Maus, et al. (2012). "Role of heparan sulfate in sexually transmitted infections." Glycobiology.

Tomaic, V., D. Pim, et al. (2011). "Regulation of the human papillomavirus type 18 E6/E6AP ubiquitin ligase complex by the HECT domain-containing protein EDD." J Virol **85**(7): 3120-3127.

Valle, G. F. a. B., L. (1995). "The human papillomavirus (HPV)-6 and HPV-16 E5 proteins co-operate with HPV-16 E7 in the transformation of primary rodent cells." J Gen Virol **76**(5): 1239-1245.

Van Damme, E., and Van Ostade, X. (2011). "Crosstalk between viruses and PML nuclear bodies: a network-based approach." Frontiers in bioscience **17**: 2910-2920.

Van Damme, E., Laukens, K., Dang, T.H., Van Ostade, X. (2010). "A manually curated network of the PML nuclear body interactome reveals an important role for PML-NBs in SUMOylation dynamics." Int. J. Biol. Sci **6**: 51–67.

Vertegaal, A. C. (2010). "SUMO chains: polymeric signals." Biochem Soc Trans **38**: 46-49.

Volkov, A., C. Dockter, et al. (2009). "Pulsed EPR determination of water accessibility to spin-labeled amino acid residues in LHCIIb." Biophys J **96**(3): 1124-1141.

Volpers, C., Sapp, M., Snijders, P.J., Walboomers, J.M. and Streeck, R.E. (1995). "Conformational and linear epitopes on virus-like particles of human papillomavirus type 33 identified by monoclonal antibodies to the minor capsid protein L2." J Gen Virol **76**(11): 2661-2667.

Wadosky, K. M. a. W., M. S. (2011). "The story so far: post-translational regulation of peroxisome proliferator-activated receptors by ubiquitination and SUMOylation." Am J Physiol Heart Circ Physiol **302**: H515–H526.

Walboomers, J. M., Jacobs, M. V., Manos, M. M., Bosch, F. X., Kummer, J. A., Shah, K. V., and P. J. Snijders, Peto, J., Meijer, C. J., and Munoz, N. (1999). "Human papillomavirus is a necessary cause of invasive cervical cancer worldwide." J Pathol **189**(1): 12-19.

Wang, L., S. L. Oliver, et al. (2011). "Disruption of PML nuclear bodies is mediated by ORF61 SUMO-interacting motifs and required for varicella-zoster virus pathogenesis in skin." PLoS Pathog **7**(8): e1002157.

Waterhouse, A. M., J. B. Procter, et al. (2009). "Jalview Version 2--a multiple sequence alignment editor and analysis workbench." Bioinformatics **25**(9): 1189-1191.

Weissman, A. M., Shabek, N., Ciechanover, A. (2011). "The predator becomes the prey: regulating the ubiquitin system by ubiquitylation and degradation." Nature Reviews Molecular Cell Biology **12**: 605-620.

Wilson, R., F. Fehrmann, et al. (2005). "Role of the E1ΛE4 Protein in the Differentiation-Dependent Life Cycle of Human Papillomavirus Type 31." J Virol **79**(11): 6732-6740.

Wimmer, P., Schreiner, S., and Dobner, T. (2012). "Human pathogens and the host cell SUMOylation system." J Virol **7**: 211-225.

Woodham, A. W., D. M. Da Silva, et al. (2012). "The S100A10 Subunit of the Annexin A2 Heterotetramer Facilitates L2-Mediated Human Papillomavirus Infection." PLoS ONE **7**(8): e43519.

Wu, C. Y., Jeng, K.S., Lai, M.M. (2011). "The SUMOylation of matrix protein M1 modulates the assembly and morphogenesis of influenza A virus." J Virol **85**: 6618–6628.

Wu, Y. C., Bian, X. L., Heaton, P. R., Deyrieux, A. F., and Wilson, V. G. (2009). "Host cell sumoylation level influences papillomavirus E2 protein stability." Virology **387**: 176-183.

Wu, Y. C., Deyrieux, A. F., and Wilson, V. G. (2007). "Papillomaviruses and the host SUMOylation system." Biochemical Society Transactions **35**: 1433-1435.

Xu, K., C. Klenk, et al. (2011). "Modification of nonstructural protein 1 of influenza A virus by SUMO1." J Virol **85**(2): 1086-1098.

Xue, Y., R. Gibbons, et al. (2003). "The ATRX syndrome protein forms a chromatin-remodeling complex with Daxx and localizes in promyelocytic leukemia nuclear bodies." Proc Natl Acad Sci U S A **100**(19): 10635-10640.

Yamashita, D. e. a. (2004). "The transactivating function of peroxisome proliferator-activated receptor gamma is negatively regulated by SUMO conjugation in the amino-terminal domain." Genes Cells **9**: 1017–1029.

Yang, R., P. M. Day, et al. (2003a). "Cell Surface-Binding Motifs of L2 That Facilitate Papillomavirus Infection." J Virol **77**(6): 3531-3541.

Yang, R., Yutzy, W., Viscidi, R., Roden, R. (2003b). "Interaction of L2 with β-actin directs intracellular transport of papillomavirus and infection." Journal of Biological Chemistry **278**.

Yang, S. H., Galanis, A., Witty, J. & Sharrocks, A. D. (2006). "An extended consensus motif enhances the specificity of substrate modification by SUMO." EMBO J **25**: 5083–5093.

Yang, S. H. and A. D. Sharrocks (2010). "The SUMO E3 ligase activity of Pc2 is coordinated through a SUMO interaction motif." Mol Cell Biol **30**(9): 2193-2205.

Yang, X. H., Richardson, A.L., Torres-Arzayus, M.I., Zhou, P., Sharma, C., Kazarov, A.R., Andzelm, M.M., Strominger, J.L., Brown, M., Hemler, M.E. (2008). "CD151 accelerates breast cancer by regulating alpha 6 integrin function, signaling, and molecular organization." Cancer Res **68**: 3204–3213.

Yang, X. J. G., S. (2006). "A recurrent phospho-sumoyl switch in transcriptional repression and beyond." Mol. Cell **23**: 779-786.

Yasugi, T., Vidal, M., Sakai, H., Howley, P. M., and Benson, J. D. (1997). "Two classes of human papillomavirus type 16 E1 mutants suggest pleiotropic conformational constraints affecting E1 multimerization, E2 interaction, and interaction with cellular proteins." J Virol **71**: 5942-5951.

You, J., Croyle, J.L., Nishimura, A., Ozato, K. and Howley, P.M. (2004). "Interaction of the bovine papillomavirus E2 protein with Brd4 tethers the viral DNA to host mitotic chromosomes." Cellular Microbiology **117**: 349-360.

Yousef, A. F., Fonseca, G. J., Pelka, P., Ablack, J. N., Walsh, C., Dick, F. A., Bazett-Jones, D. P., Shaw, G. S., and Mymryk, J. S. (2010). "Identification of a molecular recognition feature in the E1A oncoprotein that binds the SUMO conjugase UBC9 and likely interferes with polySUMOylation." Oncogene **29**: 4693-4704.

Yu, Y. and K. Munger (2012). "Human papillomavirus type 16 E7 oncoprotein engages but does not abrogate the mitotic spindle assembly checkpoint." Virology.

Yunus, A. A. L., C. D. (2006). "Lysine activation and functional analysis of E2-mediated conjugation in the SUMO pathway." Nature Struct. Mol. Biol **13**: 491–499.

Zamborlini, A., A. Coiffic, et al. (2011). "Impairment of human immunodeficiency virus type-1 integrase SUMOylation correlates with an early replication defect." J Biol Chem **286**(23): 21013-21022.

Zerfass-Thome, K., Zwerschke, W., Mannhardt, B., Tindle, R., Botz, J. W., and Jansen-Durr, P. (1996). "Inactivation of the cdk inhibitor p27KIP1 by the human papillomavirus type 16 E7 oncoprotein." Oncogene **13**(11): 2323-2330.

Zerfass, K., A. Schulze, et al. (1995). "Sequential activation of cyclin E and cyclin A gene expression by human papillomavirus type 16 E7 through sequences necessary for transformation." J Virol **69**(10): 6389-6399.

Zhang, W., Y. Tian, et al. (2012). "A postulated role of p130 in telomere maintenance by human papillomavirus oncoprotein E7." Med Hypotheses **79**(2): 178-180.

Zhao, K. N., Hengst, K., Liu, W. J., Liu, Y. H., Liu, X. S., McMillan, N. A., and Frazer, I. H. (2000). "BPV1 E2 protein enhances packaging of full-length plasmid DNA in BPV1 pseudovirions." Virology **272**(2): 382-393.

Zhong, S., Muller, S., Ronchetti, S.,. Freemont, P.S, Dejean, A., Pandolfi, P.P. (2000a). "Role of SUMO-1-modified PML in nuclear body formation." Blood **95**: 2748-2752.

Zhong, S., Salomoni, P., Ronchetti, S., Guo, A., Ruggero, D., Pandolfi, P.P. (2000b). "Promyelocytic leukemia protein (PML) and Daxx participate in a novel nuclear pathway for apoptosis." J. Exp. Med. **191**: 631–640.

zur Hausen, H. (2000). "Papillomaviruses causing cancer: evasion from host-cell control in early events in carcinogenesis." J Natl Cancer Inst **92**: 690-698.

List of Abbreviations and Symbols

τ	rotational correlation time
(T)EM	(transmission) electron microscopy
a.u.	arbitrary units
aa	amino acid
AB	antibody
AD	activation domain
a_{iso}	isotropic hyperfine coupling constant
Amp	ampicillin
Aqua dest	distilled water
ATP	adenosine triphosphatee
BD	DNA binding domain
BODIPY IA	BODIPY® 507/545 IA, *N*-(4,4-Difluoro-1,3,5,7-Tetramethyl-4-Bora-3a,4a-Diaza-*s*-Indacene-2-yl)Iodoacetamide
bp	base pair
BPV	Bovine Papillomavirus
BSA	bovine serum albumin
C22S	denotes a mutation of cysteine at amino acid position 22 to serine
CD	circular dichroism (spectroscopy)

CMV	Cytomegalovirus
CRPV	Cottontail Rabbit Papillomavirus
C-terminus	carboxyterminus
CW	Continuous Wave
DEER	Double Electron Electron Resonance
DMEM	Dulbecco´s Modified Eagle´s Medium
DMSO	dimethylsulfoxid
DNA	desoxyribonucleic acid
DNase	desoxyribonuclease
DTT	dithiothreitol
DYNLT1	Cytoplasmatic Dynein Tctex-1 Light Chain
DYNLT3	Cytoplasmatic Dynein rp3 Light Chain
E	early expressed protein (HPV context)
E	ubiquin ligase protein (E1/2/3 ubiquin ligase context)
E. coli	Escherichia coli
ECL	enhanced chemiluminescence
EDTA	ethylendiamintetraacetate
EPR	Electron paramagnetic Resonance
ESE	Electron Spin Echo
et al.	*lat*. for et alteri
FCS	fetal calf serum
Fig.	figure
FLAG-tag	affinity tag (amino acid sequence N-DYKDDDDK-C)
g	gravitational acceleration (9.80665 m x s^{-1})
GFP	green fluorescent protein
GST	glutathione-S-transferase
h	hour
HECT	homology to E6-assiciated protein carboxyl terminus, E3 ligase family

HEPES	4-(2-hydroxyethyl)-1-piperazinethansulfonic acid
HIV	Humanes Immunodefiency Virus
HPV	Human Papillomavirus
HSPG	heparansulfate proteoglycan
HSV	Herpes Simplex Virus
IF	immunofluorescence
IP	immunpräzipitation
IPTG	isopropyl-ß-D-1-thiogalactopyranosid
Kan	Kanamycin
kb	kilobase pairs
kDa	kilodalton
L	late expressed protein
LCR	Long Control Region
LDH	lactate dehydrogenase
M	molarity (mol / l)
min	minute
mRNA	messanger-RNA
MTSSL	[1-oxyl-2,2,5,5-tetramethyl-D-pyrroline-3-methyl]methanethiosulfonat spin label
mw	microwave
NaF	sodium fluoride
ND10	Nuclear Domain 10
NDS	nitroso disulfonate
NLS	Nuclear Localization Signal
nt	nucleotide
N-terminus	aminoterminus
OD	optical density
ORF	Open Reading Frame
Ori	Origin of Replication

p670	late HPV16 promotor
p97	early HPV16 promotor
PAGE	polyacrylamid-gel-electrophoresis
PBS	Phosphate Buffered Saline
PCR	Polymerase Chain Reaction
PFA	paraformaldehyd
PML	protein identified in promyelocytic leukemia
PMSF	phenylmethylsulfonylfluorid
pRb	retinoblastom-tumor suppressor protein
Proxyl-IA	Proxyl-3-(2-iodoacetamido)
PsV	pseudovirus (containing an L1/L2 capsid and a reported DNA)
PV	Papillomavirus
RING	Really Interesting New Gene, E3 ligase family
RMSD	root-mean-square distance/deviation
RNA	ribonucleic acid
rpm	rounds per minute
RT	room temperature
s	second
SDS	sodium dodecyl sulphate
SDSL	site directed spin labeling
siRNA	small interfering RNA
ß-Gal	ß-galaktosidase
ß-ME	ß-mercaptoethanol
T	absolute temperature in Kelvin
Tab.	table
TCEP	triscyanoethylphosphin
TE	Tris-EDTA
TRIS	tris(hydroxymethyl)aminomethane

v/v	volume per volume
VLP	virus-like particle (virus particles composed of a L1 capsid and reporter DNA)
w/v	weight per volume
WB	Western Blot
wt	wild-type
X-band	microwave frequency range of ~9.1 GHz to ~9.8 GHz

Tab. I: Symbols for nucleic acids.

symbol	significance	nucleic acid	symbol	significance
A	A	adenine	W	A or T
C	C	cytosine	S	C or G
G	G	guanine	Y	C or T
T	T	thymine	K	G or T
U	U	uracile	V	A, C, or G
N	G, A, T, C		H	A, C, or T
M	A or C		D	A, G, or T
R	A or G		B	C, G, or T

Tab. II: Single letter and three letter code for amino acids.

signe letter code	three letter code	amino acid
A	Ala	alanine
B	Asx	aspartatic acid or asparagine
C	Cys	cysteine
D	Asp	aspartate
E	Glu	glutamic acid
F	Phe	phenylalanine
G	Gly	glycine
H	His	histidine
I	Ile	isoleucine
K	Lys	lysine
L	Leu	leucine
M	Met	methionine
N	Asn	asparagine
P	Pro	proline
Q	Gln	glutamine
R	Arg	arginine
S	Ser	serine
T	Thr	threonine
V	Val	valine
W	Trp	Trypthophan
X	Xaa	unknown or any amino acid
Y	Tyr	tyrosine
Z	Glx	glutamic acid or glutamine

Conferences and Meetings

The 5th EF-EPR Summer School on Advanced EPR Spectroscopy, 5th – 12th of September 2010, University of Constance (poster presentation).

The annual meeting of the European Magnetic Resonance Community (EUROMAR), 21th – 25th of August 2011, Frankfurt am Main (poster presentation).

Meeting of the Gesellschaft deutscher Virologen (GdV), 14th – 17th of March 2012, Essen (poster presentation)

11th workshop on the "Cell biology of viral infections 2012" of the Gesellschaft für Virologie (GfV), 19th-21th of September 2012, Deidesheim (scientific talk).

Publications

Pulsed EPR determination of water accessibility to spin-labeled amino acid residues in LHCIIb., Volkov, A., Dockter, C., Bund, T., Paulsen, H., Jeschke, G., Biophys. Journal, Volume 96 February 2009 1124-41.

Copper Uptake Induces Self-Assembly of 18.5 kDa Myelin Basic Protein (MBP)., Bund, T., Boggs, J.M., Harauz, G., Hellmann, N., Hinderberger, D., Biophys. Journal, Volume 99 October 2010 1–9.

Stereochemical consequences of oxygen atom transfer and electron transfer in imido/oxido molybdenum(IV, V, VI) complexes with two unsymmetric bidentate ligands, Hüttinger, K., Förster,C., Bund, T., Hinderberger, D., Heinze, K., Inorganic Chemistry volume 51(7) March 2012 4180-4192.

Lateral self-assembly of 18.5-kDa myelin basic protein (MBP) charge component-C1 on membranes., Kattnig, D. R., Bund, T., Boggs, J.M., Harauz, G., Hinderberger, D., Biochimica et Biophysica Acta – Biomembranes 1818(11) June 2012 2636-47.

The Transcription Factors TBX2 and TBX3 interact with HPV16 L2 and repress the Long Control Region of Human Papillomaviruses., Schneider, M., Scheffer, K., Bund, T., Lambert, C., Cotarelo, C., Pflugfelder, G., Florin, L., and Spoden, G., Journal of Virology, 2012 (in revision).

Timo Bund - Albert-Schweitzer-Straße 17A - 55128 Mainz - phone: +49 176 322 50 111
Email: bund@mpip-mainz.mpg.de

Curriculum Vitae

Personal Information

Name:	Timo Bund
Address:	Albert-Schweitzer-Straße 17A, 55128 Mainz
Phone:	+49 176 322 50 111
Email:	bund@mpip-mainz.mpg.de
Birthday & -place:	Oct. 19, 1983, Frankenthal (Pfalz), Germany
Nationality:	German
Family status:	Single, no children

Doctorate

2009 – 2012 (expected): Doctorate student at the Institute for Medical Microbiology and Hygiene (Dr. Luise Florin) and the Max Planck Institute for Polymer Research (Department of Polymer Spectroscopy, Prof. Dr. Hans W. Spiess/PD Dr. Dariush Hinderberger).
Stipendiary at the Max Planck Graduate Center (MPGC) in cooperation with the Johannes Gutenberg University, Mainz.

"Characterization of Human Papillomavirus (HPV) Type 16 Capsid-Cell Interactions During Viral Cell Entry"

Specifications:
- Writing of scientific publications/preparation of scientific presentations/posters
- Instruction and support for young scientists in practical internships
- Scientific exchange in interdisciplinary cooperations and scientific conferences
- Soft skill training courses: Time management, organization skills, scientific presentation and publication, application seminars
- Experimental methods: Circular Dichroism Spectroscopy, Dynamic Light Scattering, Electron Microscopy, Electron Paramagnetic Resonance Spectroscopy, Flow Cytometry, Fluorescence Spectroscopy, Immunofluorescence Microscopy, Isothermal Titration Calorimetry, microbiological and moleculargenetical standard procedures, Molecular Dynamics simulation, standard biochemical and virological assays

Studies of Biology

2008 - 2009	Diploma thesis (graded 1.0):
	"Studies of Membrane-bound, Spin-labeled Myelin Basic Protein (MBP) Using EPR Spectroscopy"
	Max Planck Institute for Polymer Research, Department of Polymer Spectroscopy, Prof. Dr. Hans W. Spiess/PD Dr. Dariush Hinderberger
2006 – 2009:	Diploma Studies of Biology at the Johannes Gutenberg University, Mainz
	Specialization: - Protein-biochemistry, Institute for General Botany - Molecular Genetics, Institute for Molecular Genetics - Biophysics, Institute for Biophysics - Nuclear Chemistry, Institute for Nuclear Chemistry - Magnetic Spectroscopy, Max Planck Institute for Polymer Research
	Oral examinations in Botany, Biophysics, Molecular Genetics, and Nuclear Chemistry (final grade: 1.7).

Education

1990 – 1994:	Albrecht-Dürer-Grundschule, Beindersheim
1994 – 2003:	Albert-Einstein Gymnasium Frankenthal (Pfalz)
	Abitur granted in March 2003 (final grade: 1.3)
	Main subjects: Mathematics, Physics, English
Sept. 2000:	Student exchange program USA (Madison, WI), German-American-Partnership Program (GAP)
2003 – 2004	community service: Die Johanniter, Frankenthal (Pfalz) Disposition and organization of daily schedules Management of the blood alert and emergency center

Industrial Activities

June 2000	Internship at the BASF AG, chromatographic quality control and analysis
Jul. - Aug. 2001	Student trainee at KSB AG, section "Konzerninformatik"
Sept. - Oct. 2002	Student trainee at KBA AG, section "Network administration and IT service"
Mar. - Apr. 2005	Student trainee at KBA AG, section "Network administration and IT service"

Core Capabilities

Profound knowledge in Protein-biochemistry, Microbiology, Molecular Genetics, Biophysics, Nuclear Chemistry, Bio-chemistry, Physical Chemistry, Developmental Genetics, and Virology.

Additional experience in computer-based protein modeling/visualization, molecular dynamics simulations, genome/phylological research methods.

Profound knowledge in continuous wave (CW) and (pulsed) electron paramagnetic resonance (EPR) spectroscopy.

Additional Capabilities

Languages:	English: business fluent French: fluent Latin
Software/PC:	MatLab, LaTeX, Origin, Sigma Plot; specific software applications: RasMol, PhyMol, SwissPDBViewer, ChemBioOffice, YASARA
Teaching activities:	Tutor at several teaching courses at the Johannes Gutenberg University, Institute for Special Botany
Other activities:	Catering at Mercator GmbH Member of the Deutsche Physikalische Gesellschaft (DPG) Member of the Stadtkapelle Frankenthal Member of the TSG 1848 Mainz- Bretzenheim e. V.

Hobbies

Sports:	Running (full and half-marathon distances), volleyball, badminton, tennis, table tennis, soccer
Additional activities:	friends, cooking, music (clarinet, keyboard), dancing, travelling, billiard and snooker

Mainz, 9/14/2012

Declaration

I hereby declare that I wrote the dissertation submitted without any unauthorized external assistance and used only sources acknowledged in the work. All textual passages which are appropriated verbatim or paraphrased from published and unpublished texts as well as all information obtained from oral sources are duly indicated and listed in accordance with bibliographical rules. In carrying out this research, I complied with the rules of standard scientific practice as formulated in the statutes of Johannes Gutenberg-University Mainz to insure standard scientific practice.

Mainz, ……..2012

……

(Timo Bund)